THESIS FOR THE DEGREE OF DOCTOR OF PHILOSOPHY

# Neutron monitoring based on the higher order statistics of fission chamber signals

ZSOLT ELTER

Division of Subatomic and Plasma Physics
Department of Physics
S-412 96 Göteborg, Sweden 2016

Division of Subatomic and Plasma Physics
Department of Physics
Chalmers University of Technology
S-412 96 Göteborg
Sweden
Telephone +46 (0)31 772 1000

Cover: "Kandinsky lost in a fission chamber" – Various simulated heavy ion trajectories in a fission chamber and related pulse shapes illustrated in a minimalist plot.

Neutron monitoring based on the higher order statistics of fission chamber signals
ZSOLT ELTER
Division of Subatomic and Plasma Physics
Department of Physics
Chalmers University of Technology

**ABSTRACT**

The work in this thesis corresponds to the safety aspect of Generation IV nuclear systems. One of the safety aspects concerns the enhancement of the performance of the in-vessel on-line core monitoring with neutron flux measurements. It was concluded earlier that fission chambers are the best candidate to provide in-vessel measurements in sodium cooled fast reactors.

This thesis focuses on the performance of signal processing methods in order to unfold the count rate of fission chambers. The main goal is to investigate the possible application of processing methods based on the higher order statistics of the signal in order to provide accurate count rate estimation over a wide range both for stationary and transient signals. The work also consists of the study of self-monitoring capabilities in order to detect fission chamber malfunctions at an early stage. The investigation is based on analytic assessments, on simulation of fission chamber responses and signals, and on experimental application of processing methods.

The thesis covers five main studies. The first part presents the theoretical description of fission chamber signals. The second part investigates the performance of the traditionally applied methods (pulse and Campbelling mode) through simulations. It is shown that these methods are not capable to cover the whole count rate range of the chamber. Therefore, the third part studies the possible application of methods based on higher order statistics of the signal through simulations and experiments. It is shown that these methods can provide accurate estimations over a wide count rate range. The fourth part covers the theoretical background of self-monitoring capabilities based on the spectral properties of the signal. Finally, the fifth part presents the implementation of the methods in a real-time neutron monitoring system based on a System on a Chip, which embeds a field-programmable gate array.

By the methods elaborated in this thesis, a faster, more effective and more accurate monitoring of the reactor power is possible than with the methods used so far, even when the normal operating state is changing.

*Keywords*: Neutron flux monitoring, Fission chamber, Filtered Poisson process, Experiment, Simulation, High order, Campbelling mode

**Appended papers**

This thesis is an introduction to and a summary of the work published in the following papers

PAPER I

L. Pál, I. Pázsit, and Zs. Elter. "Comments on the Stochastic Characteristics of Fission Chamber Signals". In: *Nuclear Instruments and Methods in Physics Research, Section A: Accelerators, Spectrometers, Detectors and Associated Equipment* 763 (2014), pp. 44–52
*The first author carried out the analytic work, and wrote the manuscript. The second author was involved in the derivations and the writing of the manuscript. The third author was involved in the verification of derivations and writing of the manuscript.*

PAPER II

Zs. Elter, I. Pázsit, and C. Jammes. "Remark on the applicability of Campbelling techniques for transient signals". In: *Nuclear Instruments and Methods in Physics Research, Section A: Accelerators, Spectrometers, Detectors, and Associated Equipment* 813 (2016), pp. 10–12
*The first author carried out the analytic work, performed the simulations, and wrote the manuscript. The second author was involved in the evaluation of results and the technical aspects of the manuscript. The third author was involved in the proof reading.*

PAPER III

Zs. Elter, C. Jammes, I. Pázsit, L. Pál, and P. Filliatre. "Performance investigation of the pulse and Campbelling modes of a fission chamber using a Poisson pulse train simulation code". In: *Nuclear Instruments and Methods in Physics Research Section A: Accelerators, Spectrometers, Detectors and Associated Equipment* 774 (2015), pp. 60–67
*The first author performed all simulations, parts of the programming needed, the analysis and wrote the manuscript. The second author was involved in the programming and the technical aspects of the manuscript. The third, fourth and fifth authors were involved in the proof reading and outline of the manuscript.*

PAPER IV

Zs. Elter, M. Bakkali, C. Jammes, and I. Pázsit. "Performance of Higher Order Campbell methods, Part I: review and numerical convergence study". In: *Nuclear Instruments and Methods in Physics Research Section A: Accelerators, Spectrometers, Detectors and Associated Equipment* 821 (2016), pp. 66–72
*The first author performed all simulations, the main part of the analysis and wrote the manuscript. The second author was involved in the analysis. The third author was involved in the technical aspects of the manuscript. The fourth author was involved in the proof reading and outline of the manuscript.*

PAPER V

Zs. Elter, G. de Izarra, P. Filliatre, C. Jammes, and I. Pázsit. "Performance of Higher Order Campbell methods, Part II: calibration and experimental application". In: *Nuclear Instruments and Methods in Physics Research, Section A: Accelerators, Spectrometers, Detectors, and Associated Equipment* 835 (2016), pp. 86–93
*The first author performed all the experiments and simulations, the post-processing, the main part of the analysis and wrote the manuscript. The second author was involved in the experiments and the technical aspects of the manuscript. The third author was involved in the simulations and the technical aspects of the manuscript. The fourth and fifth authors were involved in the proof reading and outline of the manuscript.*

PAPER VI

Zs. Elter, P. Filliatre, G. de Izarra, I. Pázsit, and C. Jammes. "Self-monitoring fission chamber: theoretical groundwork". In: *PHYSOR - International Conference on the Physics of Reactors, (Peer-reviewed).* Idaho Falls, USA: American Nuclear Society, May 2016
*The first author performed all simulations, the programming needed, the main part of the analysis and wrote the manuscript. The second and third authors were involved in the analysis and the technical aspects of the manuscript. The fourth and fifth authors were involved in the proof reading and outline of the manuscript.*

PAPER VII

G. de Izarra, Zs. Elter, and C. Jammes. "Design of a higher order Campbelling mode measurement system using open source hardware". In: Submitted to *Nuclear Instruments and Methods in Physics Research, Section A: Accelerators, Spectrometers, Detectors, and Associated Equipment* (2016)
*The first author performed the implementations, the programming needed, the experiments, the main part of the analysis and wrote the manuscript. The second author was involved in the experiments, the analysis, the writing and the technical aspects of the manuscript. The third author was involved in the proof reading and outline of the manuscript.*

**Related work not included in this thesis**

Zs. Elter. *pyFC: a TRIM-based fission chamber pulse shape simulator*. Tech. rep. CTH-NT-318. Chalmers University of Technology, 2015

Zs. Elter, C. Jammes, and P. Filliatre. "Simulation of stochastic processes in fission chambers". In: *International Youth Nuclear Congress*. 2014

C. Jammes et al. "Progress in the development of the neutron flux monitoring system of the French GEN-IV SFR: Simulations and experimental validations". In: *2015 4th International Conference on Advancements in Nuclear Instrumentation Measurement Methods and their Applications (ANIMMA)*. 2015, pp. 1–8

Zs. Elter. and I. Pázsit. "Energy Correlation of Prompt Fission Neutrons". In: *EPJ Web of Conferences* 111 (2016)

# CONTENTS

# Abbreviations

| | |
|---|---|
| **ADC** | Analog-to-Digital Converter |
| **CEA** | Commissariat à l'Energie Atomique et aux Energies Alternatives |
| **CPU** | Central Processing Unit |
| **DAC** | Digital-to-Analog Converter |
| **FPGA** | Field-programmable gate array |
| **FWHM** | Full width at half maximum |
| **HOC** | High Order Campbelling |
| **HTFC** | High temperature fission chamber |
| **PSD** | Power spectral density |
| **SFR** | Sodium cooled fast reactor |
| **SoC** | System on a chip |
| **SPND** | Self-powered neutron detector |
| **TTL** | Transistor-Transistor Logic |

# CHAPTER 1

## Introduction

The topic of this thesis is neutron monitoring, which had a major role in the safe operation of nuclear reactors since the earliest days of reactor technology. Neutron monitoring has been an active research topic at CEA (Commissariat à l'énergie atomique et aux énergies alternatives) for more than 40 years. This thesis contains the work that the author has performed during the last four years, from which 2.5 years were spent at CEA Cadarache. Neutron monitoring, based on fission chamber signal processing with the Campbelling technique is treated in this thesis through numerical simulations and experiments. The main concepts of neutron monitoring and the outline of this thesis is introduced in this chapter.

## 1.1 Neutron monitoring

Our society highly relies on nuclear fission power. Although, the tendency to build new units has fallen back, many predict that nuclear fusion reactors will be built in the foreseen future. For both the fission and fusion based technologies the safety is a major issue. As far as safety is concerned, instrumentation and control plays a key role in keeping the reactor within its operational limits. Since the released power in the reactor is directly related to the neutron density, the real-time measurement of the neutrons in the system provides a sound way of estimating the released power.

Therefore, neutron monitoring has been an important part of reactor instrumentation and control since the beginning of reactor physics. In the Chicago Pile-1, Fermi was using neutron counters, in order to verify whether the neutron flux was at a safe level [1].

The heart of any neutron monitoring system is the neutron detector. Detecting neutrons is a non-trivial task, since neutrons do not ionize matter. Hence, low energy neutrons are typically detected indirectly through absorption reactions, in which a certain isotope reacts with the neutron by emitting a high energy ionized particle. Commonly used isotopes and reactions include $^3He(n,p)$, $^{10}B(n,\alpha)$ and the fission of uranium or plutonium. Applying fission isotopes is advantageous, because higher energy neutrons (having a few MeV energy) can be detected as well. The neutron detector provides an electric current, and the task of the additional

parts of the neutron monitoring system is to process this signal in order to unfold the intensity of the detected neutrons. There are several ways to process the signal, but most methods have certain limitations: they usually either work accurately at low neutron fluxes or at high neutron fluxes. Thus, the neutron monitoring system has to incorporate several independent units to cover the whole flux range of the reactor, which increases the complexity of the system [2]. Hence, it is important to investigate the possibility to apply a processing method, which can provide accurate neutron flux estimation over the whole range. By the methods elaborated in this thesis, a faster, more effective and more accurate monitoring of the reactor power is possible than with the methods used so far, even when the normal operating state is changing.

The motivation of this work was to contribute to the development of a novel neutron flux monitoring system for the French Generation IV programme. Sodium-cooled fast reactors (SFR) are among the advanced reactors selected by the Generation IV International Forum. In Europe, the development of an innovative pool-type SFR is under way, led by the French CEA and its industrial partners [3].

## 1.2 Outline

This thesis is divided into five chapters. First, Chapter 2 describes the main characteristics of fission chambers, fission chamber signals, the applied software and experimental tools, and introduces the general Campbelling technique based on Paper I and Paper II. Then, Chapter 3, which is based on Paper III, reviews and studies the limitations of the traditionally applied neutron monitoring methods, the pulse and second order Campbell mode, through numerical simulations. Chapter 4 investigates the possible application of the higher order generalization of the Campbell technique in stationary and transient reactor phases. This part, based on Paper IV and Paper V, covers the numerical and experimental verification of the reliability of the higher order Campbell mode. Then, Chapter 5, which summarizes Paper VI, numerically investigates the possibility of detecting fission chamber failure based on the spectral properties of the signal. Finally, Chapter 6 presents the implementation of both the higher order Campbelling mode and the failure detection method on an FPGA based board to achieve real-time monitoring. This part, based on Paper VII, reviews the challenges of the implementation to realize real-time measurements, and presents some of the experimental results obtained during the tests of the device.

One major objective during the work included in this thesis was to investigate the feasibility of applying higher order Campbelling methods for real-time monitoring. Therefore, it is essential to have a proper knowledge on the accuracy of such methods, and to optimize the required measurement length in order to achieve an acceptable uncertainty, but still be able to perform as short measurements as possible. First, the random and systematic errors were assessed through

simulations, where one has an exact knowledge of the signal being processed. Second, the method was tested on experimental data, where the signal analysis was performed as post-processing, in order to verify that an accurate application is possible. Finally, the real-time feasibility of these methods had to be verified, therefore it was necessary to implement the methods on a device, which is capable to process the measured data on-line.

Most of the work in the thesis has been done by the author. However, in Paper I the application of the backward Master equation formalism, and the derivations were proposed and done by the first author of that paper, whereas in Paper VII the implementation of the Campbelling and self-monitoring methods on an FPGA based system was mainly done by the first author of that paper.

# Fission Chamber signal as filtered Poisson process

The main focus of this thesis is on the application of fission chambers in neutron monitoring systems. The development of neutron detectors based on fissile isotopes started at the early years of the nuclear era, and has continued ever since. The research of fission chambers for neutron monitoring is still an active topic having as focus areas: to optimize detectors for high temperature applications (high temperature fission chambers, HTFC) [4], to achieve regenerative fission chamber coatings for an expanded lifetime [5], and to develop fission chamber signal processing methods for wide flux range measurements [6]. This chapter gives a short introduction on fission chambers, the theoretical background of the related signal processing methods based on Paper I and Paper II, and the tools applied in this thesis to study fission chamber signals.

## 2.1  Fission chambers

Fission chambers are nuclear detectors that are widely used to deliver online neutron flux measurements [7]. This type of detector is an ionization chamber containing fissile material in order to detect neutrons. The most common design consists of one or more electrode pairs, at least one electrode is coated with a fissile layer from a few micrograms to a few grams depending on the application. The type of the enriched fissile isotope in the fissile layer depends on the neutron energy range of interest of the neutron environment. The spacing between each anode and cathode goes from tens of microns to a few millimeters. The chamber itself is filled with pressurized gas. The body of the chamber is sealed and an insulating material insures the electrical separation between the electrodes. A schematic illustration of a simple (only one electrode coated) fission chamber is shown in Fig. 2.1. The processes leading to a current pulse after a neutron entering the chamber are the following:

(a) When a neutron reaches the fissile coating, it is likely to induce a fission event which generates (usually) two heavily charged ions, the fission products emitted in two nearly opposite directions.

(b) The heavy ion which is emitted out of the fissile layer ionizes the filling gas
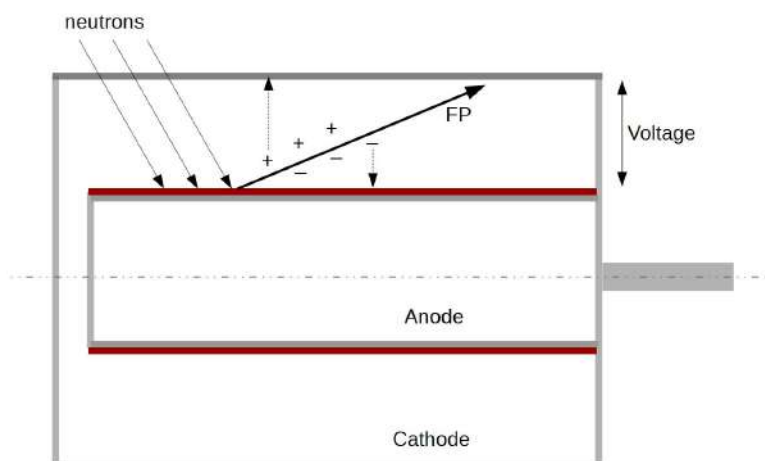
**Figure 2.1:** Schematic illustration of a fission chamber.

along its trajectory (therefore creates electron/ion pairs).

(c) A DC-voltage of a few hundred volts is applied between the electrodes, therefore the electrons and positive ions drift across the filling gas in opposite direction towards the anode and cathode respectively.

(d) During the drift both the electrons and the gas ions induce a current pulse (named in this thesis as electronic and ionic pulses) in the electrodes.

The DC-voltage between the electrodes must be high enough to collect all the charges, and low enough to prevent the production of secondary ionization pairs. If both conditions are fulfilled, the fission chamber operates in the so-called saturation regime, for which the neutron-induced current signal is proportional to the fission rate and nearly insensitive to the DC-voltage. In addition, one can note that the gamma particles and alpha particles that directly ionize the filling gas also generate a signal.

### 2.1.1 Fissile layer

The fission rate of the detector is given by

$$s(t) = N(t) \int \sigma_f \phi(E) dE \tag{2.1}$$

where $N(t)$ is the number of the fissionable isotope present in the fissile deposit at time $t$ (evolving with time), $\sigma_f$ is the microscopic fission cross-section of the isotope and $\phi(E)$ is the neutron spectra seen by the coating of the detector [8]. Eq. (2.1) neglects the count rate contribution of alpha particles.

The isotope of choice is determined by the application and the neutron environment. The most common deposits applied in fission chambers used for
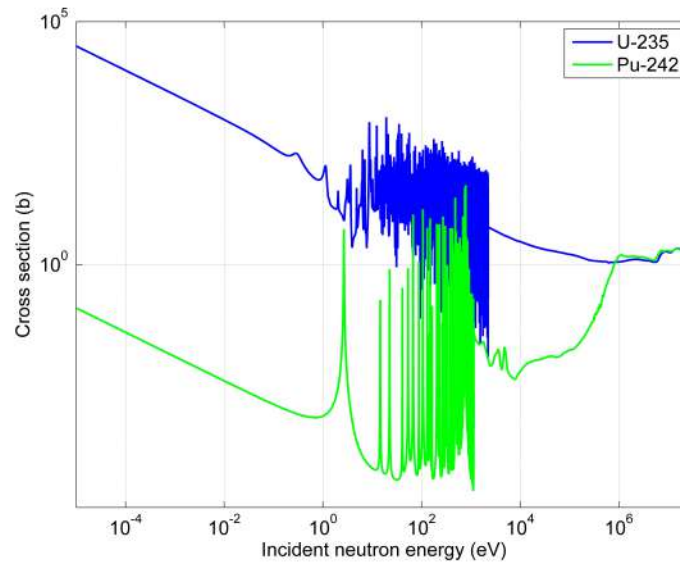
**Figure 2.2:** Microscopic fission cross sections of U-235 and Pu-242 from the JEFF 3.2 library [9].

neutron flux monitoring are made from enriched or natural uranium. Also, recently there is a novel interest in applying Pu-242 based coatings. Fig. 2.2 gives the microscopic fission cross-sections of U-235 and Pu-242. One can see that U-235 is rather sensitive to thermal neutrons. However, Pu-242 is a threshold isotope, which is sensitive to neutron energies above 1 MeV, therefore it is suitable for fast neutron measurements. Nevertheless, the fission cross-section of Pu-242 also has a significant thermal component. The joint estimation of the thermal and fast component is possible with combining the two types of fission chambers, in order to distinguish the count rate of thermal and fast neutrons [10].

As Eq. (2.1) shows, the fission rate evolves with time due the the depletion of the fissile deposit. This evolution strongly depends on the neutron fluence and spectrum (the characteristic time of the evolution can be hours or decades in different reactors). But in the applications and with the measurement times considered in this thesis (from a few ms to a few hours), the change of the fission rate due to depletion is negligible compared to the investigated count rate changes (such as control rod movement). Two possible methods are considered to overcome the problem of the time evolution: fission chambers containing regenerable fissile deposit [5, 8] and measurment systems coupled with depletion codes [11].

## 2.1.2  Filling gas

The application of monoatomic noble gas is preferred as filling gas, since the material of the electrode and the filling gas must not interact chemically and since the gamma radiation should not break up molecular bounds. The most common choice is an argon-based gas pressurized at a few bars.
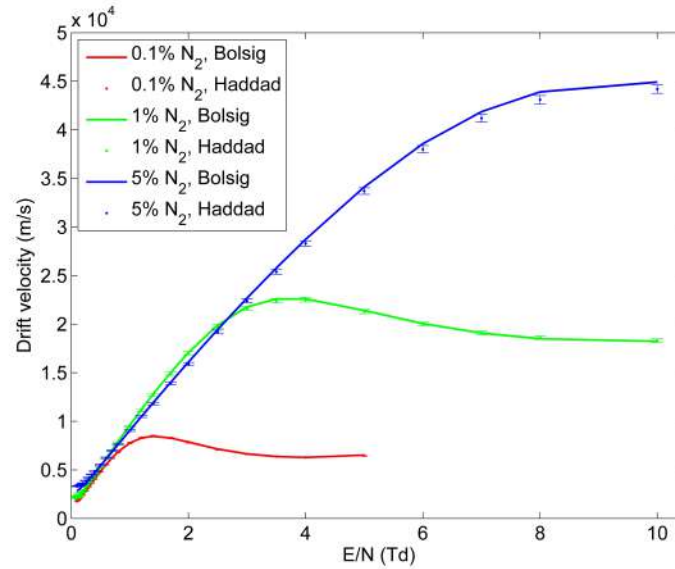
**Figure 2.3:** Electron drift velocity in Ar-$N_2$ mixtures (experimental results of Haddad [13] and BOLSIG [14] results with Biagi-v8.9 libraries [15]).

As shown later in this thesis, it is usually favorable to decrease the electron collection time and hence the width of the individual current pulses triggered by the incoming neutrons. A well-known solution to decrease the charge collection time is to add a few percents of polyatomic gas such as nitrogen [12]. Fig. 2.3 shows the drift velocity of a gas mixture as a function of the reduced electric field (which is the ratio $E/N$, where $E$ is the electric field and $N$ is the concentration of neutral particles). One can see that the electron drift velocity can be increased by a factor of four by introducing 1 % of nitrogen into the mixture. However, it was observed that nitrogen molecules disappear under irradiation at high temperature of an SFR [4], therefore increasing the nitrogen content is not favorable for HTFCs.

### 2.1.3   Why fission chambers in Astrid?

Astrid will be the demonstrator prototype of the fourth generation Sodium cooled Fast Reactor technology. Generation IV systems aim to deliver advances in four broad areas: sustainability, economics, safety and reliability, and proliferation resistance. The work in this thesis corresponds to the safety aspect: an important goal is that the operation of Generation IV nuclear energy systems has to excel in safety and reliability. As far as safety is concerned, the enhancement of in-vessel on-line core monitoring is required.

The instrumentation has to fulfill the following requirements in a Generation IV fast reactor in order to detect any abnormal change in the neutron flux:

- The data acquisition system has to deliver measurements continuously and quickly.

- The measured signals have to be easy to interpret.

- The detector has to have a long lifetime (at least three operating cycles).

- The detector has to be able to provide information about both the fast and the thermal parts of the neutron spectrum.

- The measurement system has to be able to monitor the reactor over a wide power range.

- The detector has to be able to operate at high temperatures (around $600\,^\circ$C).

Based on these aspects, Ref. [8] gives a detailed comparison of the performance of the most widely used neutron detectors in the existing research and power reactors: fission chambers, boron-lined counters and self-powered neutron detectors (SPND). The investigation shows that fission chambers have the longest lifetime. By using different deposits, the different parts of the spectrum can be investigated. The signal processing is relatively simple (no delayed contribution is present as in case of SPNDs), and the signal contribution of gamma radiation is relatively low. To achieve a large dynamic range one needs to combine different operating modes. The current work addresses the possibility of unifying these modes in order to further simplify the instrumentation.

Therefore, it was concluded that fission chambers are the best candidate to provide in-vessel measurements in Sodium cooled Fast Reactors.

## 2.2 Filtered Poisson process

As described earlier, a single incoming fission event in the fissile deposit triggers a detector response, a current pulse. Although, the shape of the response may vary for each event (as studied in Paper V), the impact of neglecting this variation is small when calibrating a fission chamber. Therefore, here the shape of an individual pulse is assumed to be

$$\varphi(x,t) = x \cdot f(t), \tag{2.2}$$

where $f(t)$ is a deterministic, normalized pulse shape (defined by the actual fission chamber characteristics), and $x$ is a random variable representing the amplitude of the pulse, characterized with an amplitude distribution $w(x)$.

The detector signal $\eta(t)$ is a superposition of pulses of the form

$$\eta(t) = \sum_{k=1}^{N(t)} x_k \cdot f(t - t_k) \tag{2.3}$$

where $t_k$ are the neutron arrival times in the detector, $x_k$ are the random pulse amplitudes, and $N(t)$ is the number of pulses having arrived until time $t$.

The fission chamber signal can be idealized as a filtered Poisson process (or shot noise). For such a stochastic process, the time interval between each pair of consecutive events has an exponential distribution with an intensity parameter. Therefore, in Eq. (2.3), $t_k - t_{k-1}$ is assumed to be exponentially distributed with an intensity parameter (discussed later). As a consequence, the number of events, or detected pulses at time $t$, $N(t)$, is a Poisson distributed random variable.

As described earlier, after the ionization of the filling gas by the fission fragments, both the electrons and the ions induce current pulses. This implies that the pulse function (2.2) is a composition of the electronic and ionic pulses (since by definition the ionic signal has the same count rate as the electronic signal, and the corresponding pulses arrive at the same time instant since the negative and positive charge creation is simultaneous). Although the total charge of the ions is approximately equal to the charge of the created electrons, the mobility of ions is three orders of magnitude lower in gases. Therefore, the width of ionic pulses is around three order of magnitude larger than that of the electronic pulses [16].
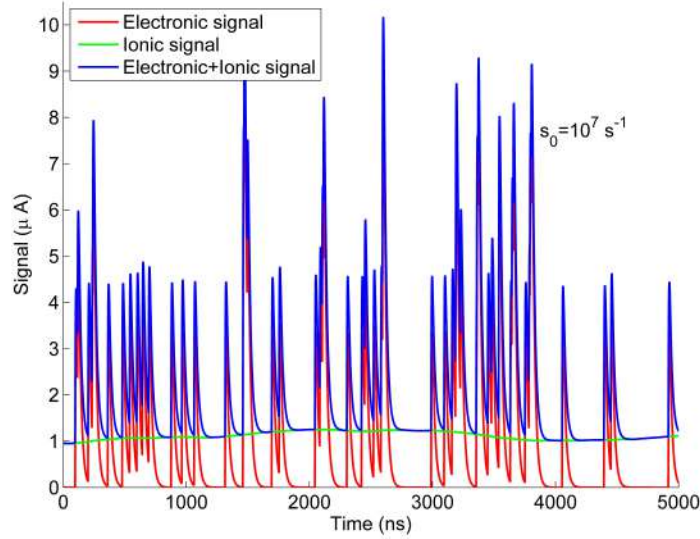


**Figure 2.4:** Illustration of a filtered Poisson process with constant intensity $s_0 = 10^7 \text{ s}^{-1}$.

Fig. 2.4 illustrates the filtered Poisson process as a composition of the electronic and ionic signals.

The power spectral density

$$PSD(f) = \frac{F^*[\eta(t)] \cdot F[\eta(t)]}{T_m} \qquad (2.4)$$

of such an idealized filtered Poisson process (containing pulses with realistic parameters) is illustrated in Fig. 2.5 ($F$ and $F^*$ stand for the Fourier transformation

and the conjugate of the Fourier transformation, respectively. $T_m$ is the measurement time). One can immediately notice that the ionic part contributes only as a low frequency noise since the ionic pulses strongly overlap already at low count rates as shown in Fig. 2.4. As such, it is often buried in the noise of the electronics and with the appropriate acquisition system it could be filtered out. Therefore, in the following analytic work, the ionic contribution is not considered. Nevertheless, the impact of it will be investigated in Chapter 4.
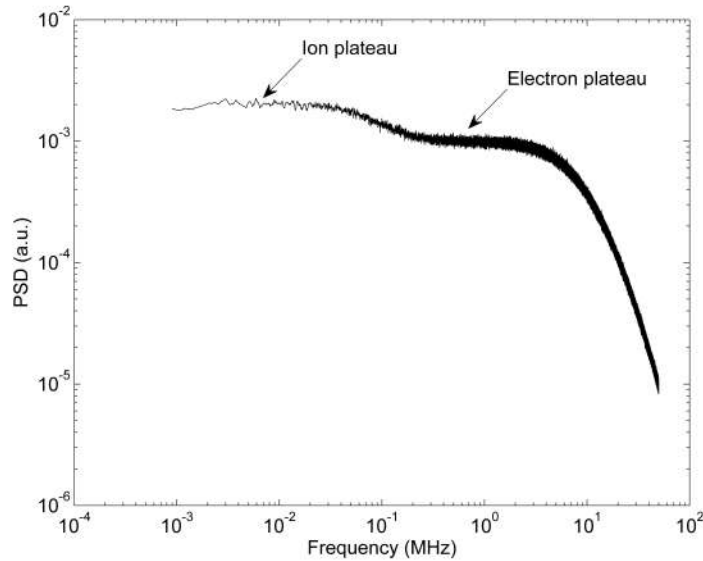


**Figure 2.5:** Illustration of the PSD of an idealised signal.

To verify the Poisson characteristics of the fission chamber signals, a measurement was performed at the MINERVE reactor (described in Sec. 2.3.3). During the measurement a fission chamber was located in the reflector of the reactor core. The time between the pulse arrivals was measured at low count rates (when the reactor already reached criticality). The probability density function of the time difference between the arrivals is shown in Fig. 2.6. The fit of an exponential distribution shows a good agreement with the empirical result (with 99% confidence). The filtered Poisson process model was accepted to describe the mathematical behavior of the fission chamber signal.

Since the fissile deposit is relatively thin, it can be assumed that the self-absorption in the layer is negligible [17]. Thus, nearly all of the heavy ions emerging from the fission event, and traveling towards the gas gap, will create a pulse. Therefore, the intensity, or count rate of the filtered Poisson process will be approximately equal to the fission rate defined in (2.1). If the count rate is time dependent, the process is inhomogeneous. If the count rate is constant in time ($s(t) = s_0$), the process is homogeneous. In the following, the inhomogeneous property due to the depletion of the deposit is neglected. But the time dependence of the count rate due to the change in the neutron flux will be considered in the numerical and experimental investigations.
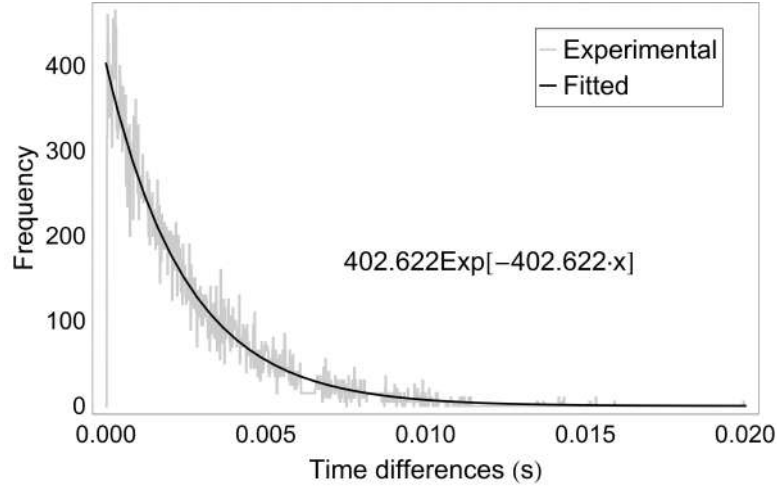
**Figure 2.6:** Verification of the Poisson nature of fission chamber signals.

## 2.2.1 General Campbell theorem

Campbell derived a linear relationship between the variance of a filtered Poisson process and its count rate [18]. It has been proposed that one can expand Campbell's theory for higher order cumulants of the signal in order to suppress the impact of unwanted minority components (such as gamma detections) [19]. The derivation of the general Campbell equations has been done previously in Refs. [20] and [21]. In this section, a recent, straightforward derivation, based on the master equation technique is summarized, which is detailed in Paper I.

In the following, the probability density function of a filtered Poisson process and the general Campbell equations are derived. The pulses in the process are considered having the shape defined in (2.2). The signal is assumed to be zero, when the measurement starts.

At the beginning, we consider that the process is an inhomogeneous Poisson-process. The probability that there are no arriving particles during the time interval $[t_0, t]$ (where $t_0 \leq t$) is given by (2.5), where $s(t)$ is the intensity of the process (should not be mistaken for the parameter $s$ of the Laplace transform which will be used later).

$$T(t_0, t) = \exp\left\{-\int_{t_0}^{t} s(t')\, dt'\right\}. \tag{2.5}$$

The probability that the detector response (with shape (2.2) and amplitude distribution $w(x)$) after the arrival of one single particle is not greater than $y$ at the time $t$ is given by the distribution function

$$H(y, t) = \int_{0}^{\infty} \Delta[y - x f(t)]\, w(x)\, dx \tag{2.6}$$

12

where $\Delta(x)$ is the Heaviside step function. The probability density function can be gained by the derivation of (2.6):

$$h(y,t) = \int_0^\infty \delta\left[y - xf(t)\right] w(x) \, dx. \tag{2.7}$$

The distribution function of the sum of detector responses (the signal) $\eta(t)$ is

$$\mathcal{P}\left\{\eta(t) \leq y | \eta(t_0) = 0\right\} \equiv P(y, t | 0, t_0) = \int_{-\infty}^y p(y', t | 0, t_0) \, dy' \tag{2.8}$$

A backward-type Chapman-Kolgomorov equation can be written for the probability density function $p(y', t | 0, t_0)$ by summing up the probabilities of the mutually exclusive events as

$$p(y, t | 0, t_0) = T(t_0, t) \, \delta(y) + \int_{t_0}^t T(t_0, t') s(t') \int_0^y h(y', t - t') \, p(y - y', t | 0, t') \, dy' \, dt'. \tag{2.9}$$

If the Laplace-transform of the amplitude distribution $w(x)$ is denoted as

$$\widetilde{w}(s) = \int_0^\infty e^{-sx} w(x) dx \tag{2.10}$$

then the Laplace-transform of the probability distribution (2.7) becomes

$$\widetilde{h}(s,t) = \int_0^\infty e^{-sy} h(y,t) dy = \int_0^\infty e^{-sxf(t)} w(x) dx = \widetilde{w}[sf(t)] \tag{2.11}$$

With these definitions, the Laplace transform of the Chapman-Kolgomorov equation (2.9) is

$$\widetilde{p}(s,t) = T(t_0, t) + \int_{t_0}^t T(t_0, t') s(t') \, \widetilde{h}(s, t - t') \, \widetilde{p}(s, t | 0, t') \, dt'. \tag{2.12}$$

where $t_0 = 0$ and $\widetilde{p}(s, t | 0, 0) = \widetilde{p}(s, t)$ The integral equation (2.12) can be rearranged as a differential equation and solved for homogeneous case ($s(t) = s_0$). The final form of the Laplace transform $\widetilde{p}(s, t)$ is then

$$\widetilde{p}(s,t) = exp\left\{-s_0 \int_0^t [1 - \widetilde{h}(s, t')] dt'\right\} = exp\left\{-s_0 \int_0^t [1 - \widetilde{w}[sf(t)]] dt'\right\} \tag{2.13}$$

If only the stationary case ($t \to \infty$) is considered, the Laplace transform reads as

$$\lim_{t \to \infty} \widetilde{p}(s,t) = \widetilde{p}_{st}(s) = exp\left\{-s_0 \int_0^\infty [1 - \widetilde{w}[sf(t)]] dt\right\} \tag{2.14}$$

13

The cumulants of the distribution function are given by definition [22] as

$$\kappa_n^{(st)} = (-1)^n \frac{d^n \ln(\widetilde{p}_{st}(s))}{ds^n} = (-1)^n \frac{d^n s_0 \int_0^\infty [\widetilde{w}[sf(t)] - 1]dt)}{ds^n} \qquad (2.15)$$

which finally results in the general form of the Campbell-equation

$$\kappa_n^{(st)} = s_0 \int\limits_{-\infty}^{+\infty} \left[ \int\limits_0^{+\infty} (xf(t))^n w(x)dx \right] dt = s_0 \langle x^n \rangle \int\limits_{-\infty}^{+\infty} f(t)^n dt \qquad (2.16)$$

Eq. (2.16) gives a relationship between the cumulants of the signal and the pulse characteristics. In this thesis, the goal of the derivation was to reach the general Campbell-equations, but the previous derivations also provide an opportunity to determine the probability density function of the process for specified pulse shape and amplitude distribution. Further results can be found in Paper I.

## 2.2.2 Campbelling for non-stationary signals

In Eq. (2.15) the stationarity of the signal was assumed. The term stationarity may be confusing for processes with a constant intensity. Stationarity means here that the time averaged cumulants of the process reach a constant value. Fig. 2.7a illustrates such behavior. The count rate of the illustrated process suffers a step change at 0 and at 300 ns. Although, the count rate becomes constant immediately after the changes, the time averaged mean of the signal needs time to reach a constant level. One should investigate how long time it takes after a step change in the flux before the stationary state is reached. To illustrate this, Eq. (2.13) was solved for a specific case: the intensity of the detection events follows a step change ($s_0 = 0$, when $t < 0$ and $s_0 = 10^7 \text{ s}^{-1}$, when $t \geq 0$), and the pulses have damped exponential shape with realistic parameters (resulting around 100 ns pulse width).

Fig. 2.7b illustrates the function $1 - \frac{\kappa_n(t)}{\kappa_n^{(st)}}$ to give an idea about the convergence time. The results show that the values of the theoretical cumulants converge quickly to their stationary values after the step change. The convergence time can be measured in tens of ns, which is comparable with the pulse width. Neither the pulse amplitude distribution, nor the count rate have any impact on the speed of the convergence.

The derivations in the previous section become elaborate if one tries to include a time dependent count rate (i.e. consider an inhomogeneous process). Nevertheless, the results for a step change imply that in practical situations (when the change of the count rate is slower than few thousand ns), the signal can be considered as a transition of quasi-homogeneous and quasi-stationary signals, therefore no special Campbell-equation has to be derived to measure transient events. Further remarks on the stationarity can be found in Paper II, and this assumption for transient signals is investigated with simulations and experiments in Chapter 4.
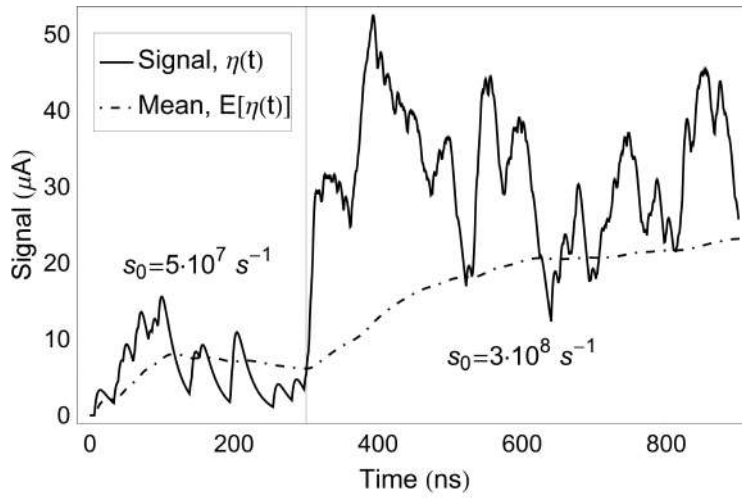
**(a)** Illustration of non-stationarity.
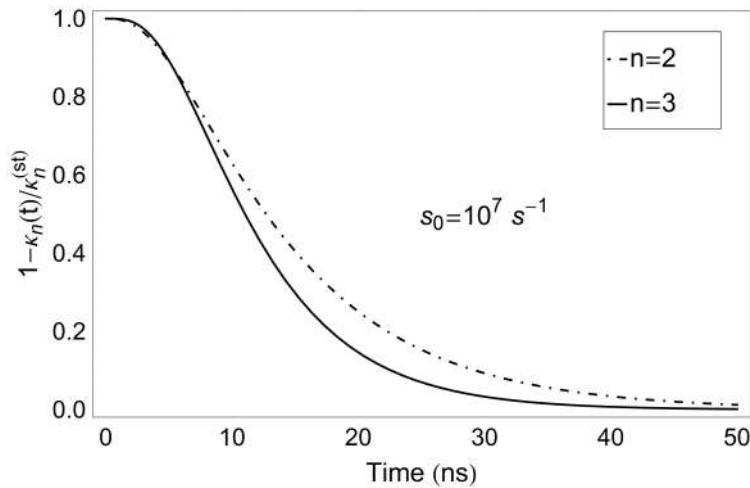


**(b)** Time dependence of cumulants after a step change in the detection intensity.

**Figure 2.7:** Non-stationarity of homogeneous processes.

## 2.3  Tools for the study

The analytic derivations provide important insights about the characteristics of filtered Poisson processes. Nevertheless, performing the inverse Laplace-transform of the probability density function (2.13) is possible only for a few specific pulse shapes and amplitude distributions. The real shape of the detector response function, and the amplitude distribution of the chamber are rather complicated, and usually cannot be described analytically. Also, the solution of Eq. (2.12) for inhomogeneous processes becomes cumbersome. In addition, the impact of the noise of the electronics, and other unwanted signal contributors cannot be considered in the analytic derivations.

Therefore, the investigation of fission chamber signals and the performance of

various signal processing methods requires to develop numerical simulations and to perform experiments. The following section summarizes the applied numerical tools and experimental setup in order to study the fission chamber response and signal.

### 2.3.1  pyFC

In order to simulate the current pulse creation in fission chambers, a code suite, named pyFC (*py*thon-based simulation of *F*ission *C*hambers) was developed. Although similar software tools already exist (such as described in Refs. [16, 23, 24]), pyFC aims to provide a straightforward, and fast computation route in order to facilitate the study of propagation of technological uncertainties to fission chamber signals.

The working scheme of pyFC is illustrated in Fig. 2.8. The suite first samples the fission products, then the trajectories of the fission fragments in the filling gas, and the spatial distribution of the created charges along the trajectories are computed with the TRIM code [25]. TRIM (Transport of Ions in Matter) is a collection of Monte Carlo based programs which determine the stopping power and range of ions and heavy ions in matter. Since TRIM defines the target material as a 3-dimensional bulk cuboid, and in fission chambers the target material (filling gas) usually has a cylindrical shape, some geometrical rotations are performed in the suite based on the initial incident angles of the ions. The parameters of the charge collection (such as the electron mobility in the gas) is calculated with the BOLSIG software [14]. The coupling of the codes is done in Python. The collection time of the charges is calculated in a numerical grid. The current pulse creation is based on the Shockley-Ramo theorem [26]. The suite outputs the time-resolved pulses created in each event, and allows to investigate the statistics of the pulses. The details of the implemented considerations behind the code system are described in [27].

The code does not consider any recombination events and avalanches, which means that the chamber is assumed to work in the saturation regime. The space charge effects are neglected (each fission product entering the inter-electrode space ionizes the gas independently). Only the current induced by the electrons is considered, since the mobility of the ions created by the fission fragment is much lower. The original version of the code suite neglects the self-absorption of the fission fragments, but the most recent version already includes the heavy ion transport within the fissile deposit.

Multi-electrode and multi-coating chambers can be investigated with superposition, i.e. combining the results of more runs, each corresponding to one fissile coating by assuming that the inter-electrode spaces are mutually independent.
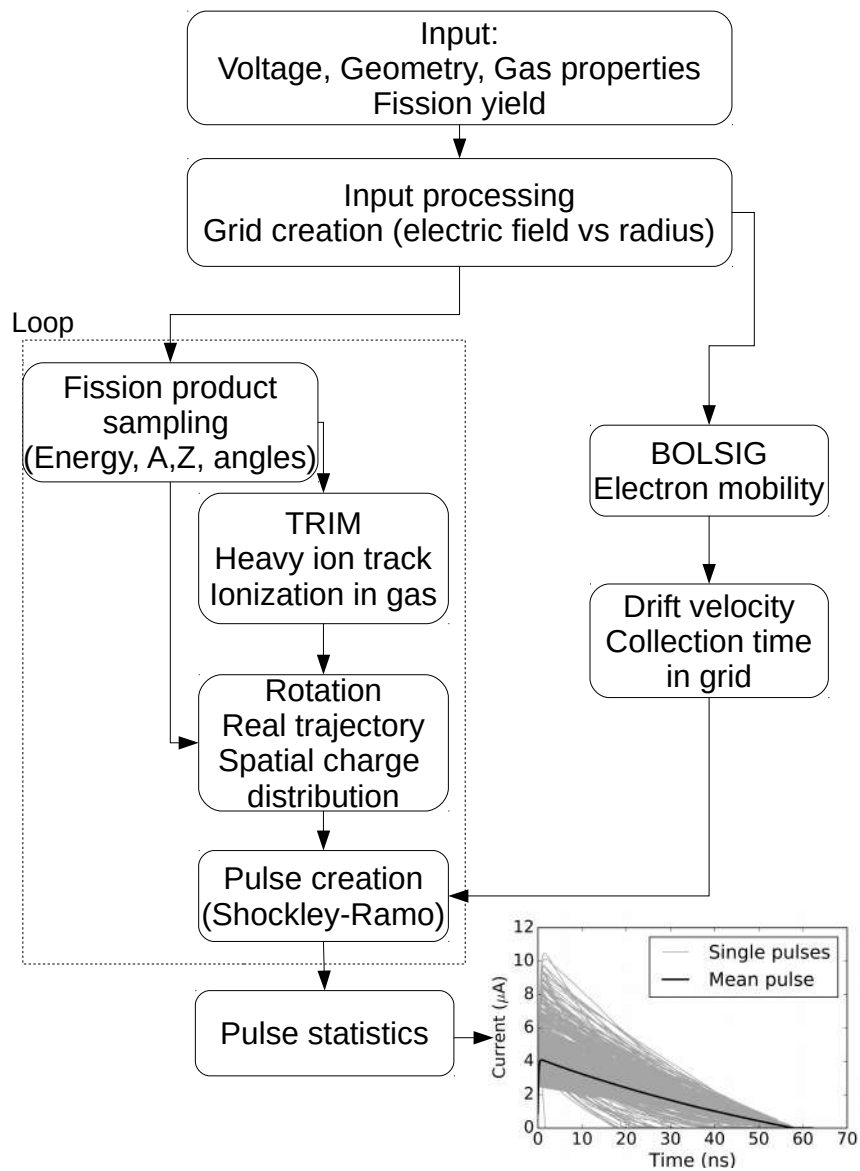
**Figure 2.8:** Flowchart of pyFC.

### 2.3.2   Matlab toolbox for filtered Poisson process

A MATLAB toolbox was implemented to simulate the fission chamber signal as a filtered Poisson process. The program generates the Poisson pulse train according to a pre-defined pulse shape, amplitude distribution and count rate. The generated signal is time-resolved like a real signal measured by an acquisition system, with a user-defined sampling frequency.

The pulse shape and the amplitude distribution can be defined as analytic functions (in order to provide comparison with theoretical results, as shown in Paper III) or may be defined by external data (e.g. from a measurement, in order to support the interpretation of measurements). The count rate may be defined as constant or as a time dependent function (in order to study transient events).

The user has the opportunity to define additional time signals, such as background noise or further Poisson trains and add these to the original pulse train. This way, the performance of signal processing methods can be investigated in the presence of unwanted signal contributors.

An important real detector-like feature of the simulation tool is the way how signals at high count rates are handled. If the order of count rate is comparable to the order of time resolution of the simulated signal, more than one pulse can appear within one time step. In this case those pulses will sum up, so the current delivered by the entirely overlapping pulses will not be lost.

The simulated signal is considered as a current signal, since in an industrial application the fission chambers are usually connected to current sensitive pre-amplifiers which can be located farther away from the core [28].

The toolbox includes a set of algorithms to estimate the count rate with various methods.

### 2.3.3   Experiment

During the work, two main experiment campaigns were done at CEA Cadarache. The first aimed to verify the applicability and the calibration of higher order Campbelling methods. The second focused on the test of a real-time measurement system, which is detailed in Chapter 6.

Both experimental setups consisted of a current-sensitive fission chamber placed in the reflector zone of the MINERVE reactor [29], which is a pool type zero-power, light water reactor, operated at CEA Cadarache with a maximum power of 80 W.

In the experiments, a CFUL01 fission chamber (manufactured by Photonis) [30] was studied. The CFUL01 is a multi-electrode and multi-coating detector, which means that the chamber contains three coaxial electrodes and four fissile coatings of enriched uranium. The sensitive length of the detector is 211 mm and the outer

radius of the first electrode is 14 mm, the inner and outer radii of the cathode is 16 and 17 mm, and the inner radius of the second anode is 19 mm. Therefore the gas gap is 2 mm wide for both the inner and the outer chambers. The nominal operating voltage is 600 V (and the maximum voltage is 800 V at 20 °C, while the limit is 1300 V with no radiation). The filling gas is Argon with 4 % Nitrogen at 250 kPa (at room temperature). The fissile deposit consists of $U_3O_8$, with the U-235 content enriched to 90 % with a surface density of 1.32 mg/cm$^2$. The thickness of the deposit is around 1.5 $\mu$m. The advantage of using multi-coating detectors is to increase the fissile mass in the chamber without increasing the surface mass and therefore the self-absorption of the deposit [17].

The fission chamber was connected to a fast broadband current pre-amplifier with a high immunity, 25 m long cable. The pre-amplifier acts as a high-pass filter in order to remove the DC part of the signal. It exhibits a sensitivity of $3.08 \cdot 10^{-5}$ A/V and its gain is $\pm 0.5$ dB in the 5 kHz - 50 MHz frequency band. During the first measurement campaign, the output signal of the pre-amplifier was digitized at a high sampling frequency (1 GHz) during a large time span with an advanced digital oscilloscope (Agilent Infiniium). The collected signals were post-processed with MATLAB. During the second measurement campaign the output signal was processed in real-time with a prototype, FPGA based measurement device (having 125 MHz sampling frequency), developed at CEA Cadarache.

# CHAPTER 3

## Traditional methods: Pulse and Campbelling mode

The generated current signal at the electrodes of the fission chamber is collected, amplified and processed. The main goal of the fission chamber signal processing is to estimate the count rate, i.e. the intensity $s_0$ of the signal, since this value is related directly to the neutron flux. Increasing intensity causes pile-ups of the pulses in the signal, whereas the electronic noise and the background level of the gamma and alpha radiation also pose challenges, thus the estimation of the count rate becomes a non-trivial task.

Depending on the count rate, the pulse shape and the signal sampling, the chamber is traditionally operated in three different modes: the pulse mode at low power levels, the Campbelling mode at medium and high power levels and the current mode at high power levels. All modes require a separate electronic acquisition system. Therefore, a traditional instrumentation based on fission chambers is a complex system which includes various processing electronics. This chapter introduces the traditional fission chamber modes, and investigates the performance of them through simulations. This chapter mainly summarizes Paper III. Similar results can be found in the literature [2, 31], nevertheless Paper III provides an extensive sensitivity study of the linearity of the traditional methods.

## 3.1 Discrete signal sample

In the previous chapter the fission chamber signal was considered as a continuous-time signal. In measurements (and in numerical simulations), after digitizing the signal, only a finite and discrete-time signal slice is available as shown in Fig. 3.1. The sampling rate is defined by the measurement device (by the Analog-to-Digital converter) or by the user in a simulation. Later on the following notation will be used to describe the sampled current quantities:

$$X_i = \eta(t_i) \quad \text{where} \quad i \in [1, N] \tag{3.1}$$

where $N$ is the size of the sample (defined by the length of the measurement and the sampling rate).
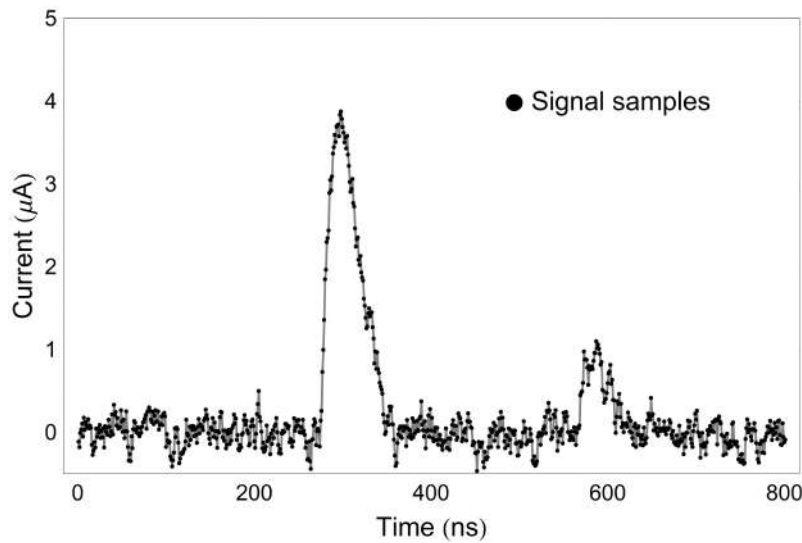
**Figure 3.1:** Sampled signal.

## 3.2 Pulse mode

The simplest way to estimate the intensity of the signal is through counting the pulses separately. The limitation of the separation between pulses is determined by the pulse width and the pulse intensity, as well as by the detector electronics.

In practice the counting process is achieved by a transistor-transistor logic (TTL). A discrimination level is set and when the chamber signal jumps from below to above this level, the electronics trigger a logic signal. The logical responses are counted in order to estimate the pulse count. This logic response has a certain time width and during this time the following jumps above the discrimination level are neglected. The application of such a counting system on a measured signal slice is illustrated in Fig. 3.2. The width of the TTL signal acts as a non-paralyzable dead-time (while the logical signal is on, the system will not count other pulses). The discrimination level has a paralyzable dead-time effect (meaning that if the signal stays above the level, then the electronics does not trigger more logic responses). Such a behavior can be observed in Fig. 3.2 (where a relatively high count rate was chosen in order to highlight the dead-time effect). The actual behavior depends on the TTL width, the pulse width, the pulse amplitude distribution and the discrimination level. In theory it is possible to perform dead-time corrections up to a certain extent [32].

Defining the optimal discrimination level is non-trivial. In case the pulse amplitudes are randomly distributed and the lower amplitudes are comparable with the amplitude of the noise, such a pulse counting method fails to estimate the pulse count properly. Fig. 3.3 shows the counted pulses in a 10 ms long measurement depending on the discrimination level: in case the discrimination level is too low, the noise triggers spurious counts; in case the level is too high, the method does not count low amplitude pulses. A possible option is to set the
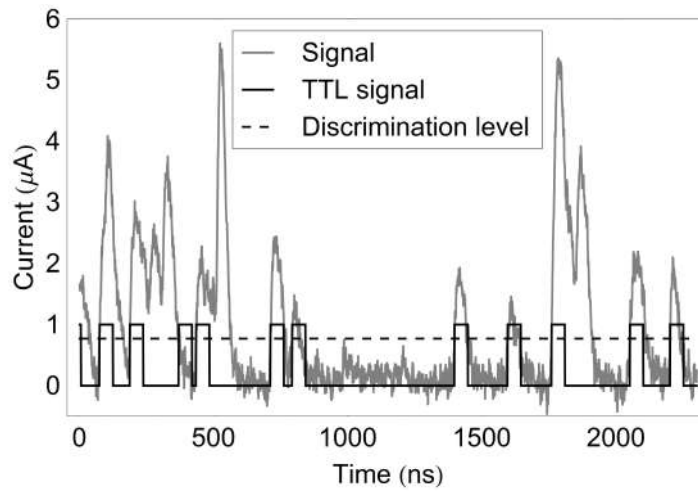
**Figure 3.2:** Illustration of a generated TTL signal.

discrimination level at the inflexion point of the curve (which is named integral bias curve in Ref. [33]).
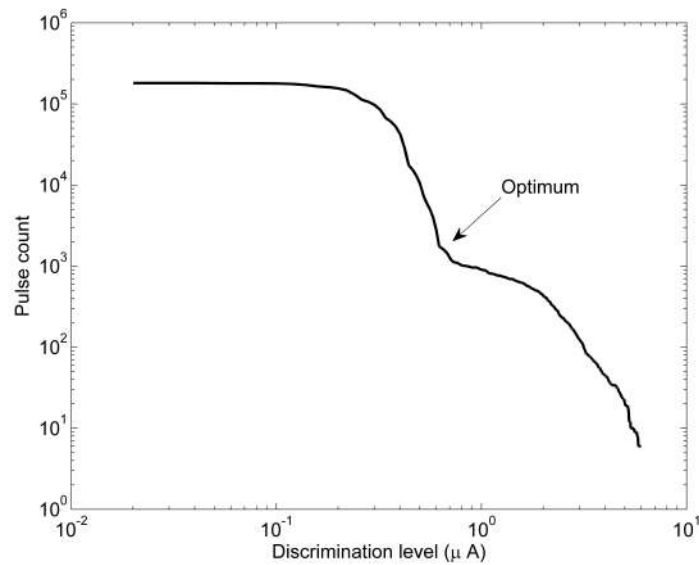


**Figure 3.3:** Estimated pulse count vs discrimination level.

In the simulations of the pulse mode included in the following sections, both dead-time phenomena inherently occur (the non-paralyzable due to the pulse shape, and the paralyzable due to the applied discrimination level). Nevertheless, corrections have not been applied, since we were interested in the limitations of the uncorrected pulse mode.

## 3.3   Campbell mode

In the Campbell, or fluctuation mode, the quantity of interest is the variance of the signal. Eq. (2.16) becomes

$$\mathbf{D}^2(\eta) = s_0 \langle x^2 \rangle \int\limits_{-\infty}^{+\infty} f(t)^2 dt \tag{3.2}$$

for the second order moment. The variance of the signal is approximated with the variance of the signal sample:

$$\mathbf{D}^2(\eta) = \frac{N \sum\limits_{i=1}^{N} X_i^2 - (\sum\limits_{i=1}^{N} X_i)^2}{N(N-1)} \tag{3.3}$$

The observed variance is a sum of the variance of the real fission chamber signal triggered by the incoming neutrons, of the noise, and of the gamma and alpha contribution. One may measure the variance directly based on the sample values, or determine the integrate of the power spectral density of the signal. The amplitude of the pulses triggered by gamma radiation is much lower than the pulses emerging from fission events. Therefore, the gamma contribution is largely suppressed, because the amplitude term is squared [34].

The fluctuation mode requires calibration, meaning that the pulse and amplitude terms have to be determined. In the following simulations these terms were considered as known.

Fig. 3.4 shows the probability density function of the amplitude of simulated signals with and without noise at different count rates. For this illustration, a rather high noise level (20 %) was set to highlight the general effects of noise on the probability density function. The probability density function was calculated by normalizing the histogram of the sampled current values of the simulated signals. One can see that at lower count rates the density function and the variance of the noisy signal is mostly dominated by the noise. Hence, when the count rate is estimated based on (3.2), the variance of the noise biases the estimated count rate. Conversely, at higher count rates the noise does not have a great effect on the probability density function.

## 3.4   Current mode

In the current mode the quantity of interest is the mean current. In fact, the current mode is based on the first order Campbell equation:
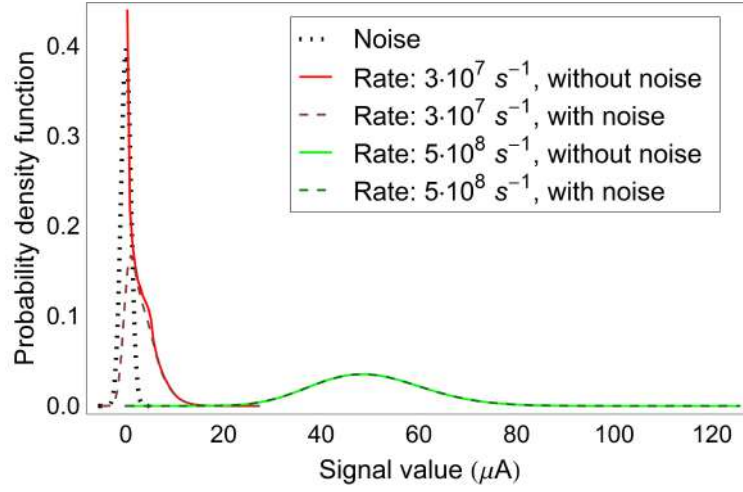
**Figure 3.4:** Probability density function of the signal.

$$\mathbf{E}(\eta) = s_0 \langle x \rangle \int\limits_{-\infty}^{+\infty} f(t)dt \tag{3.4}$$

Since the pulse shape in (3.4) is normalized, the integral becomes unity, therefore the knowledge of the pulse shape is not necessary to calibrate a fission chamber in current mode, which makes the calibration relatively simple. Although, measuring the mean of the current is simple and robust, this mode is extremely sensitive to any unwanted signal contributions. In this work the current mode is not considered, since according to earlier studies the current mode does not provide a wider application range than the Campbell mode [6].

## 3.5 Linearity gap

An extensive numerical comparison between the pulse mode and the second order Campbelling technique was performed. For the detailed results the reader is referred to Paper III.

In the simulations the pulses were considered as having an exponential decay shape with a width of around 90 ns. The performance studies were based on signal samples of 10 ms length with a sampling rate of 1 GHz. The signal was loaded with additional Gaussian white noise at various noise levels.

It was found that the pulse mode is nearly insensitive to the noise if the discrimination level is well set, whereas the Campbelling is significantly biased by the noise at low count rates. Nevertheless, already a relatively narrow pulse amplitude distribution results in a count rate underestimation in the pulse mode, whereas the Campbelling mode is not impacted by the stochastic amplitude if well

calibrated.

Fig. 3.5 shows the performance of the pulse and Campbelling modes for various pulse widths at a realistic noise level (the standard deviation of the noise is 5 % of the pulse amplitude). The pulse width change was considered through changing the nitrogen content of the filling gas, which would have an impact only on the electron and ion velocity (see Fig. 2.3), but not significantly on the amount of induced electron-ion pairs by the fission fragment. Therefore, the delivered charge of the pulses (i.e. their integrals) was kept fix in the simulations, while changing the pulse width, which results in a change of the pulse amplitude.
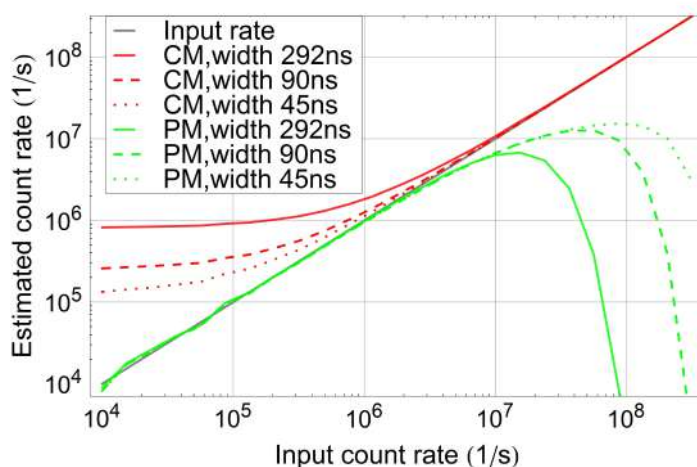


**Figure 3.5:** Impact of the pulse width on the pulse mode (PM) and the Campbelling (CM) (noise: 5%).

Fig. 3.5 shows that by increasing the count rate of the signal, the performance of the pulse mode gradually deteriorates, whereas the performance of the Campbelling improves (the reason for which is explained in Fig. 3.4). The pulse mode has a critical count rate, at which the dead-time saturates and the estimation breaks down. One can see that depending on the pulse width there will be a count rate region ($10^6 - 10^7 \, \text{s}^{-1}$), in which both methods fail to provide an accurate estimation. Although the literature of possible dead-time corrections is large and the research on correction methods is still active [35], most of the methods are cumbersome to be implemented in real-time systems and are limited to perform plausible corrections up to the breakdown point. Therefore, in order to guarantee the overlap of the applicability range of the pulse and the Campbell mode, the pulses have to be narrowed. As described in Chapter 2, this can be done by introducing nitrogen gas into the filling gas, but this solution would limit the lifetime of the chamber (due to the loss of nitrogen molecules under irradiation).

Thus there is a real need for unifying the two modes without altering the filling gas or the design of the chambers. A possible unifying solution is investigated in the following chapter.

# CHAPTER 4

## Performance of Higher order Campbelling

As the previous chapter highlighted, the traditional methods are vulnerable to the effect of various noises. The Campbell method is impacted by the parasitic noise of the electronic system. The gamma background and the ionic contribution results in a signal with rather high count rate, and low pulse amplitude, therefore it does not affect the pulse mode, but it has a moderate impact on the Campbell mode and a significant impact on the current mode. The alpha decay of the fissile layer induces relatively high pulses (the amplitude of pulses triggered by alpha particles is tenth of the amplitude of pulses triggered by the fission fragments) with a low count rate, therefore it impacts both the pulse, the Campbell and the current mode.

There are several solutions to reduce the impact of the various noises. The gamma and the alpha contributions can be compensated by introducing an additional ionization chamber in the measurement system with the same geometry, and containing an alpha decaying deposit instead of the fissile deposit (such as Ra-226), which emits an equivalent amount of alpha particles as the fissile deposit [36], and the measured mean and fluctuations of the compensating signal can be substracted from the mean and variance of the fission chamber signal. On the other hand, the impact of the ionic contribution and the parasitic noise can be filtered by investigating the spectral properties of the signal [37]. Nevertheless these methods are not perfect, and introduce additional complexity to the measurement system, therefore reduce the robustness to interpret the signal and to detect sensor failures.

To remedy this problem, the application of the Higher Order Campbelling (HOC) methods was proposed [20, 38]. These use the higher order statistics (cumulants) of the detector current to estimate the detection rate. Although the theoretical relationship between the higher order cumulants and the mean detection rate has long been known, the applicability and performance of these methods in practical applications and in transient scenarios has not been extensively tested, and the uncertainty related to applying high order methods has not been addressed. The available experimental results have large uncertainties, and the measurements need relatively long (a few s) signal samples [39], which is unfavorable for real-time applications. The rapid development of digital measurement devices (such as FPGAs) brings recent attention to these methods, since the reliable estimation of the higher order moments of the signal became achievable.

This chapter provides an introduction to and summary of the numerical and experimental performance studies of the HOC method detailed in Paper IV and Paper V.

## 4.1 Higher order Campbelling

Let us rewrite (2.16) in a general form:

$$\kappa_n^{(st)} = s_0 \langle x^n \rangle \int\limits_{-\infty}^{+\infty} f(t)^n dt = s_0 \cdot C_n \tag{4.1}$$

where commonly, the methods in which $n \geq 3$ are called higher order methods. Eq. (4.1) shows that if the pulse shape $f(t)$ and the amplitude distribution $w(x)$ are known (therefore the calibration coefficient $C_n$ is determined), and the cumulant $\kappa_n$ (of any order) of the signal is determined from measurement, then the count rate $s_0$ of the signal can be estimated.

### 4.1.1 Cumulant estimation

In practice, the empirical distribution of the signal is estimated from a finite, discrete sample, with an uncertainty depending on the length of the signal sample, as illustrated in Fig. 4.1. As a consequence, the cumulants of the signal have to be also estimated, and the estimations have uncertainties as well.
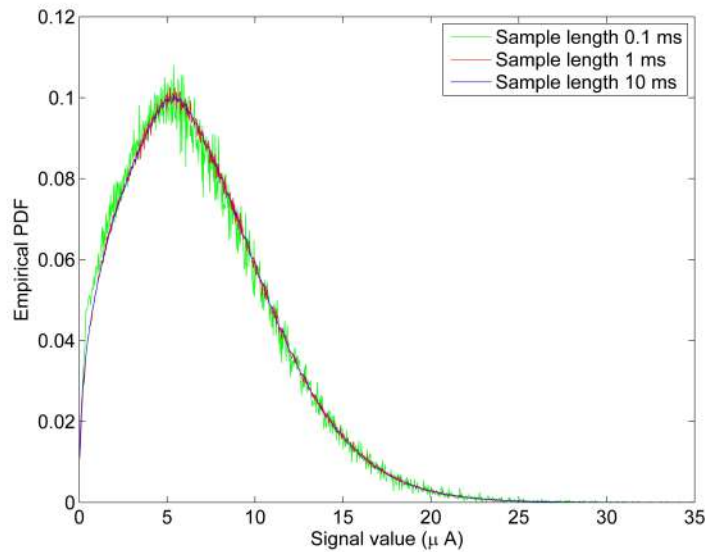


**Figure 4.1:** Empirical probability density function depending on the signal length (with identical sampling rate).

For the current work the k-statistics were applied to estimate the cumulants [40]. The $n$th k-statistic $k_n$ is a unique symmetric unbiased estimator of the cumulant $\kappa_n$, defined such that

$$\langle k_n \rangle = \kappa_n \tag{4.2}$$

If the sum of the $n$th powers of the data points $S_n$ is defined as

$$S_n = \sum_{i=1}^{N} X_i^n \tag{4.3}$$

where $N$ stands for the size of the sample as in the previous chapter, then the first two higher order k-statistics can be given in terms of these sums as

$$k_3 = \frac{2S_1^3 - 3S_1 S_2 + N^2 S_3}{N(N-1)(N-2)} \tag{4.4}$$

and

$$k_4 = \frac{12 N S_1^2 S_2 - 3N(N-1)S_2^2 - 4N(N+1)S_1 S_3 + N^2(N+1)S_4 - 6S_1^4}{N(N-1)(N-2)(N-3)} \tag{4.5}$$

The convergence of the cumulant estimation to the real value of the cumulant is the subject of Sec. 4.2.1.

## 4.2   Numerical studies

First, the performance of the higher order methods was investigated through numerical simulations. In this regard the convergence of the cumulant estimations was studied and the optimal measurement time was defined. Then, the impact of the ionic pulses, the parasitic noise of the electronics and the competitive shot noises were determined for the traditional and higher order Campbelling methods, in order to decide how large gain can be achieved by applying very high orders.

In the numerical study a normalized damped exponential pulse shape was considered for describing the electronic and ionic pulses:

$$f(t) \propto e^{-t/p_1} - e^{-t/p_2} \tag{4.6}$$

For the quantitative work, reference pulse parameters were chosen to describe both the electronic and the ionic pulses. The characteristics of the pulses are summarized in Table 4.1. The pulses were chosen to have deterministic length and shape: although, for a given pressure, there is some variation in the pulse shape (depending on the angles of the ionization tracks, and the kinetic energy of the

**Table 4.1:** The reference pulse characteristics

| type | $e^-$ | ion |
|---|---|---|
| time parameter $p_1$ | 20 ns | 2 $\mu$s |
| time parameter $p_2$ | 4 ns | 0.4 $\mu$s |
| mean charge $\langle q \rangle$ | 0.1 pC | 0.1 pC |
| amplitude $a$ | 3.34 $\mu A$ | 34 nA |
| pulse width | 100 ns | 10 $\mu s$ |
| resolution | 1 ns | 1 ns |

fission fragment), for simplicity, here only a mean shape is considered, since the reference fission chamber (CFUL01) is relatively small (the gas gap is only 2 mm), therefore, the pulse width is roughly independent of the track of heavy ions for this fission chamber.

For each investigation, 1000 signals with the same measurement time were generated in order to assess the random error of the estimated count rate. The expected value, or mean, of these estimations reflects the systematic error caused by the noise.

## 4.2.1 Convergence

Fig. 4.2a illustrates the count rate estimation of several order Campbell methods based on 10 ms long signal samples without noise (the second, third and fourth order estimations overlap each other). One can immediately see that at higher count rates the higher the order of the method is, the higher the uncertainty of the estimation is. The reason is the increase of the associated variance of the estimators

$$var(k_n) = \langle (k_n - \kappa_n)^2 \rangle \tag{4.7}$$

The analytic form of this variance and the unbiased estimators of the variance can be found in the literature [40]. Here only a illustrative term is highlighted.

$$var(k_n) \propto \frac{\kappa_2^n}{N} \tag{4.8}$$

Eq. (4.8) means that the variance of the estimator is proportional to the $n$th power of the variance of the signal. Since the variance of the signal increases with the count rate (which is expressed by the traditional Campbell equation introduced in Eq. (3.2) and illustrated in Fig. 3.4), the variance of the estimation increases exponentially with the count rate. This means that for accurate measurements with higher orders, one needs longer measurement times. Since for real-time monitoring one attempts to have as short measurement times as possible, this criterion limits the application of the very high order methods.
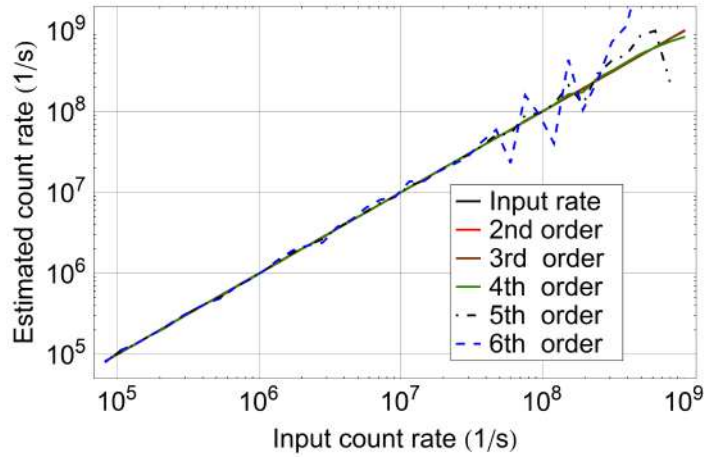
**(a)** Illustration of the estimation uncertainty.
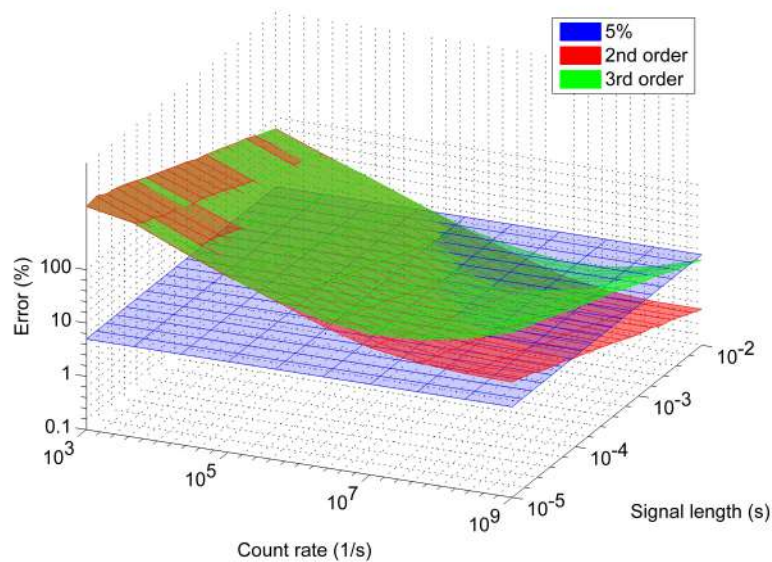


**(b)** Random error of the count rate estimation.

**Figure 4.2:** Error of the Campbell estimations.

Instead of evaluating the formulae of the variance of the estimators, a rather pragmatic approach was applied, which inherently includes the uncertainties due to the randomness of the process. Many signals were created at several count rates with several measurement lengths, and the relative difference of the estimated and the real count rate was determined. The random error of the estimation was defined as the standard deviation of this set of differences. The results are summarized in Fig. 4.2b for the second and the third order. One can see that at high count rates the random error indeed exponentially increases; and further, that at lower count rates, the error also increases, due to the randomness of the process. The plane related to 5 % error is also shown in the figure as a reference.

Based on these results it was concluded that for the third order methods a measurement time around $1 - 10$ ms provides reliable count rate estimation over a wide count rate range (above $10^4 - 10^5$ s$^{-1}$). Therefore, in the continuation, the computations were done for 10 ms.

Although, in the figure the fourth order estimate is not included, the calculations showed that the fourth order encounters more serious convergence problems. Nevertheless, in some of the following results the fourth order estimations are also included, to point out whether the application of higher than third order estimations has any practical advantage.

## 4.2.2 Noise suppression

This section investigates the impact of the ionic pulses, the parasitic noise of the electronics and the competitive shot noises (i.e. the gamma and the alpha contribution). These noises cause systematic measurement errors since the calibration coefficient in Eq. (4.1) takes into account only the most dominant part of the signal, the electronic pulses, because in an experimental calibration one determines the electronic pulse shape (as shown in Sec. 4.3). On the other hand, the measured cumulant is related to the compound signal (i.e. the fission chamber signal and the various noises). Hence, the systematic error may be estimated analytically (an example is given in Paper IV for the ionic contribution). Nevertheless, in the numerical simulations, the random errors due to the fluctuation of the number of pulses $N(t)$ arriving during the measurement time and the variance of the cumulant estimations are inherently included. Therefore, with simulations one gains more understanding about the significance of the impacts of the noise.

As was seen in Table 4.1, the ionic pulses carry the same amount of charge as their electronic counterparts, but their width is around two orders of magnitude longer, therefore the amplitude is two orders of magnitude lower. Figs. 2.4 and 2.5 have illustrated that such ionic contribution will introduce a low frequency noise.

Both analytic and numerical results (as presented in Paper IV) show that the traditional Campbell mode overestimates the count rate with about 1.2 % due to the ionic contribution, whereas the third order Campbell mode can reduce this bias to 0.2 %. Nevertheless, due to the larger random errors of the third order method, at count rates higher than $10^8$ s$^{-1}$ this reduction benefit vanishes.

The components of the electronics (such as the pre-amplifier, the cables and the connections) introduce a parasitic noise to the signal. Several simulations were carried out assuming different frequency dependence of this noise, since the experimental work shows that the noise is not white. From measurements, it was also verified that the noise distribution is close to Gaussian and its standard deviation is around 6-7 % of the mean pulse amplitude. It was shown that both the third and fourth order methods sufficiently suppress the impact of the noise, as the higher order cumulants of the Gaussian distribution are zero. The application

of the fourth order does not bring any advantage over the third order method. In contrast, the higher order methods are not entirely insensitive to the noise of the electronics: as shown in Eq. (4.8), a signal distribution with larger variance increases the variance of the estimator, therefore higher noise levels increase the random error of the higher order methods. For realistic noise levels this effect does not play a significant role, but it can be concluded that to suppress parasitic noise, it is favorable to limit the order of the method to avoid increasing the random error.

In the fission chamber other, not neutron-triggered ionizing radiations also induce pulses. These pulses also create a shot noise in the chamber, referred in this thesis as competitive shot noise. The main undesirable contribution originates from gamma radiation [41] and the alpha decay of the deposit. The assessment of the gamma contribution to the signal of a fission chamber, located in the reflector region of a sodium cooled reactor, lies beyond this work, nevertheless, the gamma triggered pulses are assumed to have at least 2 orders of magnitude lower pulse amplitude than the pulses of the fission fragments [41]. On the other hand, the alpha contribution of the reference fission chamber CFUL01 can be easily evaluated, hence the impact of the alpha background can be estimated. Since the deposit contains around 1 g of uranium (with a U-235 enrichment of 90 %), the alpha count rate is around $10^5 - 10^6 \, s^{-1}$. The mean pulse amplitude of the pulses triggered by the alpha particles was studied with the pyFC tool, and is around 10 % of the mean pulse amplitude of the pulses triggered by the fission products. Since both the gamma and the alpha pulses are mostly covered by the noise of the electronics, it is not possible to consider them in the calibration procedure.

With numerical simulations it was shown that, regarding the competitive noise, by increasing the order of the method, a significant suppression gain can be achieved (see Paper IV for further details). However, the random error of the fourth order exceeds its systematic error reduction compared to the third order. With the third order mode the competitive shot noise can be successfully suppressed even if the parasitic pulse amplitudes are 25 % of the neutron triggered pulse amplitudes and the intensity of the competitive process is comparable with the intensity of the neutron signal.

As a summary, Fig. 4.3 presents the results of the systematic and random errors for signals where all the above-mentioned noises appear simultaneously: Gaussian noise (with a standard deviation of 6 % of the mean pulse amplitude), ionic signal and competitive shot noise (with the same count rate as the fission rate - which is an underestimation for the alpha count rate at higher than $10^6 \, s^{-1}$ fission rates -, and the competitive pulse amplitudes are 1 % or 10 % of the mean pulse amplitude triggered by neutrons).

In case the count rate of the non-neutron triggered pulses is comparable with the count rate of the neutron-triggered pulses for the HTFCs applied in Astrid, and further if the data acquisition system can filter out low frequency noises (such as the ionic contribution), then at high count rates (above $10^8 \, s^{-1}$) still the application
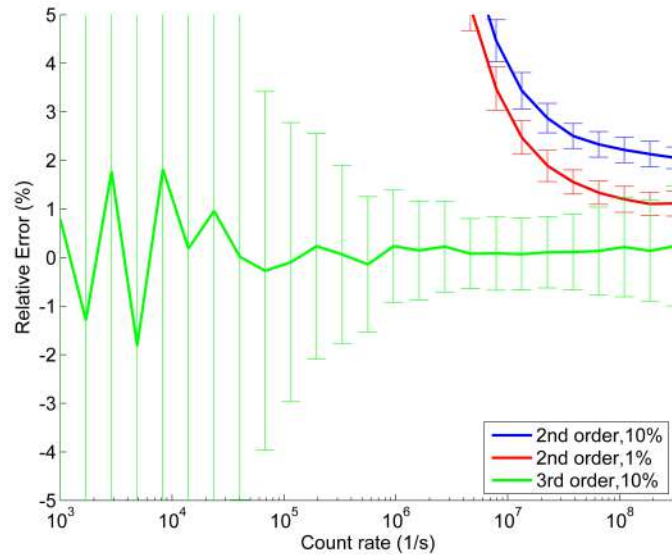
**Figure 4.3:** Cumulative impact of noise.

of the second order method may be advisable, considering the larger random error of the third order estimation.
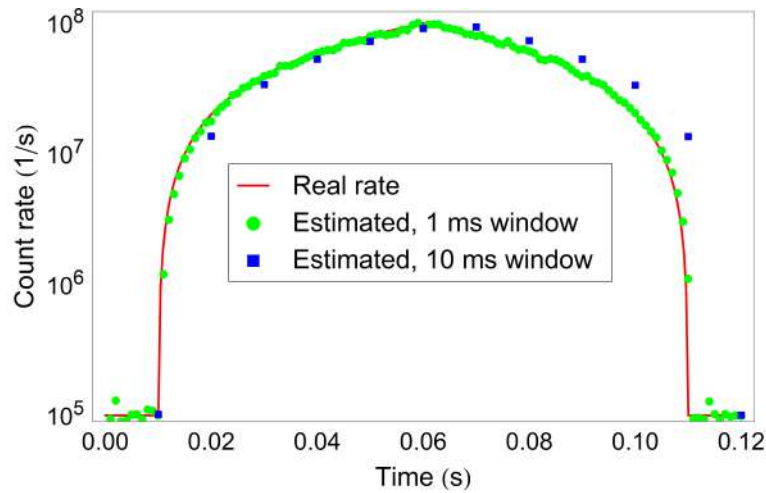
### 4.2.3 Transient

As detailed in Chapter 2, reactor transients result in an inhomogeneous signal, in which the count rate of the signal can be described as a time dependent function $s(t)$. The developed simulation toolbox has included the capability of describing such continuously changing count rates.

In order to assess the dynamic response of the higher order Campbelling, a test scenario was considered, which describes a heuristic, fast change in the count rate. The count rate was increased from $10^5 \, s^{-1}$ to $10^8 \, s^{-1}$ in 50 ms, and after reaching the maximum, it decreased to $10^5 \, s^{-1}$ in 50 ms (illustrated by the solid line in Fig. 4.4; note the logarithmic scale on the y-axis).

The simulation was performed as taking consecutive finite samples of the signal, and estimating the count rate of them with the Campbell equations for homogeneous processes (Eq. (4.1)). This implies that the inhomogeneous signal was approximated as a sequence of quasi-homogeneous signals. The length of the consecutive samples (the estimation window) was set to 1 ms or 10 ms.

Fig. 4.4 presents the count rate estimation over the transient event for the different estimation windows. The results show that there is a delay of the estimation due to the length of the sample size. If the window size is set too short then the accuracy of the measurement is going to be worse (due to the random error related to the stochastic characteristic of the signal and to the inaccuracy of the third order

**Figure 4.4:** Transient simulation: count rate estimation with window sizes 1 ms and 10 ms.

estimation), whereas with longer measurement times the exact shape of the transient may be lost, as in the example with longer measurement window, the peak is missed. This means that if the sample window is well optimized (meaning that it is sufficiently long to guarantee an accurate cumulant estimation, but sufficiently short to monitor the change in the count rate), then the inhomogeneous signal can be approximated as a sequence of homogeneous signals, and the homogeneous Campbell equations can be applied.

It can be concluded that the monitoring of transients is limited by the shortest reliable measurement time (in which the estimation is converged). As illustrated, with rather short, 1 ms long windows it is possible to reach a fair estimation even at high count rates, which means that one can be confident that transients slower than the ms scale can be followed with third order Campbelling methods.

## 4.3 Experimental studies

In order to verify experimentally the wide range linearity of the third order Campbell method, the possibility of calibration and the possibility to monitor transient events, a measurement campaign was carried out (the details of the experimental setup are described in Sec. 2.3.3).

At low reactor power levels when the pile-up of pulses is unlikely, pulses were collected separately (a sample of the recorded pulses are available in Fig. 4.5a). Although, at such low power levels the pile-up events are rare, during the post-processing the incidental pile-up events were eliminated from the data set.

At medium and high power levels, 10 ms long signal samples were collected (such a measurement at 30 W power level is illustrated in Fig. 4.5b). At medium levels the pulses overlap moderately. This provides an opportunity to estimate

the count rate accurately with pulse counting techniques and to compare it with the estimation obtained from the calibrated HOC mode.
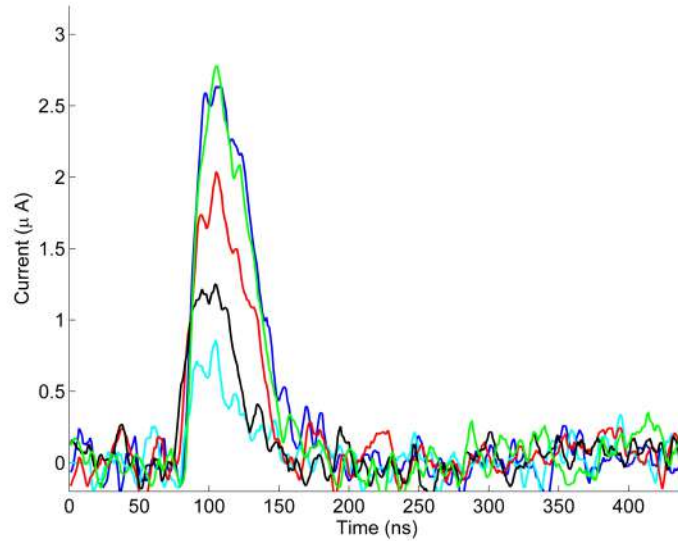


(a) Sample of recorded pulses.
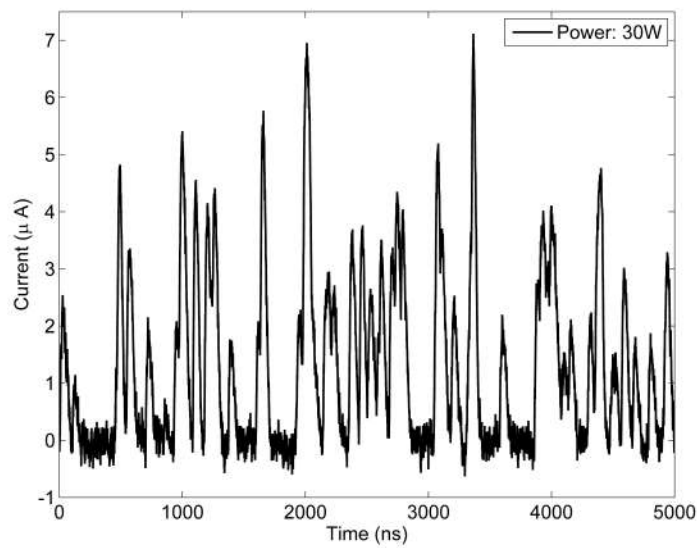


(b) Sample of recorded signal at 30 W.

**Figure 4.5:** Illustration of recorded data.

## 4.3.1  Calibration and linearity

The separated pulses recorded at low power were studied in order to determine the calibration coefficient $C_n$ (introduced in Eq. (4.1) as the product of the integral

of the $n$th power of the mean pulse shape and the $n$th order raw moment of the pulse amplitude distribution) for the second and the third order. The measured mean pulse shape and its standard deviation are shown in Fig. 4.6. A slight bump follows the main pulse, which is an artifact due to the current bouncing back on the cable.

The measured calibration coefficients of the second and third order Campbelling mode are summarized in Table 4.2. It has to be highlighted that these coefficients belong to the whole experimental setup (but are independent from the neutron spectra) and not only to the fission chamber. The random error of the coefficients was determined empirically (i.e. the coefficient was calculated for 10 set of 10000 pulses). The systematic error of the coefficient was estimated from the error of the amplitude measurement, since during the measurement, a discrimination level has to be introduced to separate the pulses from the noise. Therefore pulses lower than the discrimination level are not accounted for in the calibration procedure. Table. 4.2 also contains the empirical third order calibration coefficient $C_{3,empir}$, introduced later.

Since, as previously described in Chapter 2, the CFUL01 fission chamber is a multi-coated fission chamber, the impact of the variation in pulse shapes coming from the different coatings was addressed in Paper V. The overall error of the calibration coefficient due to assuming that all pulses have the same shape was estimated to be around 3 %.
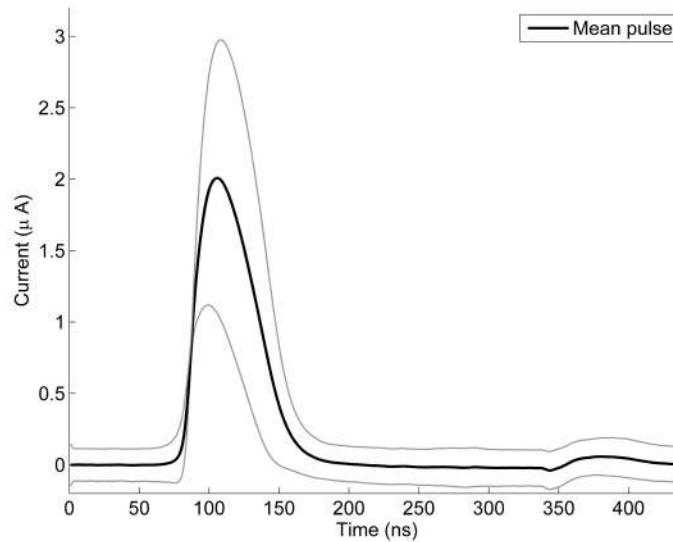


**Figure 4.6:** The recorded mean pulse shape and its standard deviation.

To assess the linearity of the third order Campbelling, several signal samples were recorded at 28 different power levels between 0.2 W and 80 W. This allowed to estimate the deviation of the cumulant estimation as well.

The count rates of the signals taken below 2 W were estimated with pulse count

**Table 4.2:** Calibration coefficients

|  | mean |
| --- | --- |
| $C_2\ (A^2 H z^{-1})$ | $(2.00 \pm 0.04) \cdot 10^{-19}$ |
| $C_3\ (A^3 H z^{-1})$ | $(5.32 \pm 0.3) \cdot 10^{-25}$ |
| $C_{3,empir}\ (A^3 H z^{-1})$ | $(5.19 \pm 0.2) \cdot 10^{-25}$ |

algorithms as well. These made it possible to compare the count rate estimations of the calibrated third order method to the estimations of the pulse counting (which can be considered as a reference at low count rates) and to determine an empirical calibration coefficient $C_{3,empir}$ by fitting a linear model between the empirical pulse count and the third order cumulant estimations. The empirical calibration coefficient is included in Table 4.2.

The count rate estimation results are summarized in Fig. 4.7. One immediately notices the failure of linearity for the traditional Campbelling at low count rates. However, the count rate estimated by the third order cumulant shows good agreement with the results of the pulse counting, and the third order Campbelling provides a linear estimation over the whole power range.
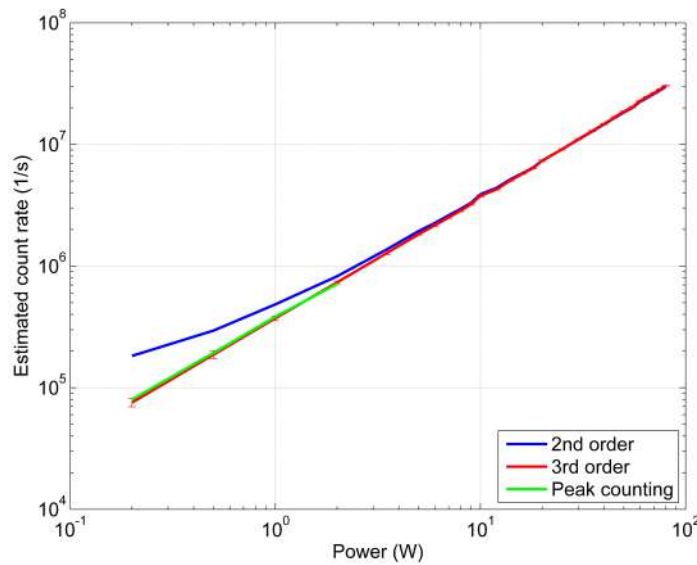


**Figure 4.7:** Count rate estimation with different methods.

The good agreement between the empirical and HOC calibration verifies the possibility to calibrate the fission chambers in HOC mode empirically. Thus, if one can perform a reliable pulse count estimation at low count rates, then the empirical calibration provides the simplest and most robust calibration methodology (i.e. the difference in pulse shape will not have any significance and the cumulant measuring system can be cross calibrated with a reliable pulse counting system, thus the system does not need to be capable of recording the signal). Such a calibration is not plausible for the traditional Campbelling method, due to the linearity gap

between the pulse counting method and the second order Campbelling.

## 4.3.2 Transient

The numerical studies showed that higher order Campbelling methods are limited only by the smallest reliable measurement time to monitor fast transients. In the frame of the measurement campaign, an experimental demonstration of the transient monitoring was performed.

The MINERVE reactor is not designed to induce transients, therefore the fastest transient which can be authorized by the operators is the control rod drop transient. For the current measurement, the reactor power was kept at a stationary 60 W power level, when the control rods were dropped. The fall of the control rods takes around 0.4-0.5 s.
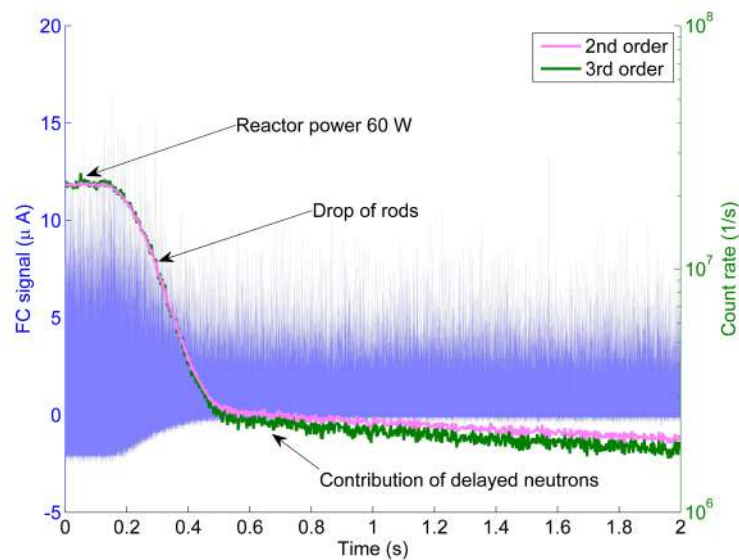


**Figure 4.8:** Transient measurement.

Fig. 4.8 shows the time evolution of the Campbell count rate estimations based on consecutive, 2 ms long signals (right axis, pink and green curves in the foreground) and the fission chamber signal (left axis, light blue curve in the background). Since the applied pre-amplifier removes the mean of the signal, one can observe the change of the offset during the measurement. At the beginning of the measurement the reactor was in stationary state, hence the estimated count rate is constant in time. The control rod was dropped 0.1 s after the recording started, which results a rapid, exponential decrease of the count rate. The control rod was fully inserted after a fall of 0.4 s, when the decrease of the count rate is turning slower, and the pulses in the signal are mostly triggered by the delayed neutrons. Both the traditional and the third order Campbell methods show a

sufficiently dynamic response during the fall of the control rod. However, at the end of the transient the count rate is overestimated by the traditional Campbelling.

## 4.4   Concluding remarks on the higher order Campbelling

It was shown through numerical studies that the uncertainty of the higher order cumulant estimations limits the applicable order.

Nevertheless, it was seen that already the third order method achieves significant noise suppression capabilities: it sufficiently eliminates the impact of the ionic signal contribution, the parasitic noises of the measurement system and possible competitive shot noises (such as the gamma background, and the alpha radiation of the fissile coating). Nevertheless, due to the large random error of the third order estimation at high count rates, it is advisable to apply a system, which makes use of the second order estimation at count rates above $10^9\,\mathrm{s}^{-1}$.

It was shown that with the currently available digital sampling rates it is possible to achieve accurate measurements above $10^4\,\mathrm{s}^{-1}$ based on signal samples of a few $\mathrm{ms}$. Monitoring lower count rates is still possible, but the measurement time needs to be longer (nevertheless, the pulse mode has the same drawback).

The wide range linearity and the transient following capability of the third order Campbell mode was verified through an experimental campaign.

Determining the theoretical calibration coefficient in high order mode may be problematic with cumulant measuring systems, which are not capable of recording the signal. For such systems, the pulse recording has to be done with a separate apparatus, which may have a different transfer function. In order to overcome this issue, it was verified that the calibration is possible empirically, based on pulse counting techniques.

# CHAPTER 5

## Self-monitoring

Eq. (4.1) shows that the cumulants of the signal may change not only due to the change in the count rate, but also due to the change in the mean pulse shape or the pulse amplitude distribution. The higher order methods are particularly sensitive to such changes due to the higher exponents in Eq. (4.1). These changes may occur due to the reduction of detector filling gas pressure or voltage. During measurements, only the change of the cumulant (therefore the change of the estimated count rate) will be detected, thus we have to be able to decide whether this change occurred due to the change of the neutron flux around the detector or due to the malfunction of the detector.

The current chapter explores the possibility of detecting the detector failure from the change of the shape $f(t)$ of the detector pulse. Namely, earlier work showed how the temporal auto-correlation of the detector signal depends on the detector pulse shape [42]. Hence, if the detector malfunction results in a change of the detector pulse shape, this latter can be discovered from the detector signal auto-correlation function, or from its power spectral density. Thus, this chapter investigates the alteration in the mean pulse shape due to failure of the detector and investigates the possibility to identify the malfunction from the changed characteristics of the detector signal PSD. In this thesis the capability of identifying such failures is called self-monitoring or smart detector capability.

Previously there have been attempts to perform regular tests to identify malfunctions of fission chambers. Ref. [43] proposed periodic testing (at least annual) of fission chambers installed in a reactor, and tests of newly-manufactured chambers and stored spare chambers. This pioneering technique was based on analog measurements of the power spectral density, and identifying changes in the amplitude of the spectra (therefore, the measurements had to be taken at steady flux level). An other proposition was to measure the transition frequency between the ion and electron plateau (i.e. the inflexion point in Fig. 2.5), which is not straightforward in case one wants to perform real time measurements (the change which has to be detected is a few kHz), and may be problematic if the instrumentation filters the frequencies lower than a few kHz, and if the measurements are not sufficiently long. To investigate these properties one needs dedicated offline measurements.

In contrast, Paper VI quantifies how the width of the spectra (i.e. the length of

the electron plateau) changes during a malfunction, and focuses on the possibility of real-time application, i.e. the possibility of performing spectral analysis during the operation. For this purpose the investigation of the amplitude of the spectrum is not adequate, since that may change due to the change in the reactor power as well.

## 5.1 Hypothetical malfunction

As mentioned before, the change of the fission chamber characteristics may have several causes. An illustration is given in Paper VI, where the chosen scenario was a pressure drop of the filling gas due to a crack on the wall of the fission chamber. Such a crack would not appear instantaneously, rather would develop during a longer period of time. Modeling the temporal development of such ruptures is beyond the scope of this thesis.

The sodium pressure in an Astrid-like core at the fission chamber location was calculated with Bernoulli's theorem and was found to be 72 kPa. This implies that the filling gas would leak from the chamber in case of a rupture. The characteristic time of this leakage strongly depends on the size of the crack, but for microscopic ruptures (a few tens of $\mu$m) the leakage progresses for a few hours. The goal of the present work was to quantify the minimum pressure drop which can be detected, in order to assess whether early fault detection is possible.

For this work the CFUL01 fission chamber was the reference fission chamber.

## 5.2 Impacts of pressure drop

First the pyFC suite was applied to simulate the change of the pulse shape during the pressure drop. The computation of the mean pulse shape and that of the pulse amplitude distribution was performed for several pressure values between 150 kPa and 250 kPa. As described before, although, for a given pressure, there is some variation in the pulse shape (depending on the angles of the ionization tracks), for simplicity, in the following only the mean shape is considered, because the most important characteristics of the pulse, its width, is roughly independent of the track (since the CFUL01 chamber is only few mm in diameter).

The results are summarized in Fig. 5.1. By decreasing the filling gas pressure (and therefore the number of gas atoms in the chamber) the pulse width and the carried charge (the integral of the current pulse) is decreasing as well. At lower pressure the heavy ion creates less electron-ion pairs and the mobility of the electrons becomes higher. The change in the mean pulse shape can be observed in Fig. 5.1a. The pulse width shows a saturation which is a consequence of the saturation in the drift velocity at low pressures (as shown in Fig. 2.3).
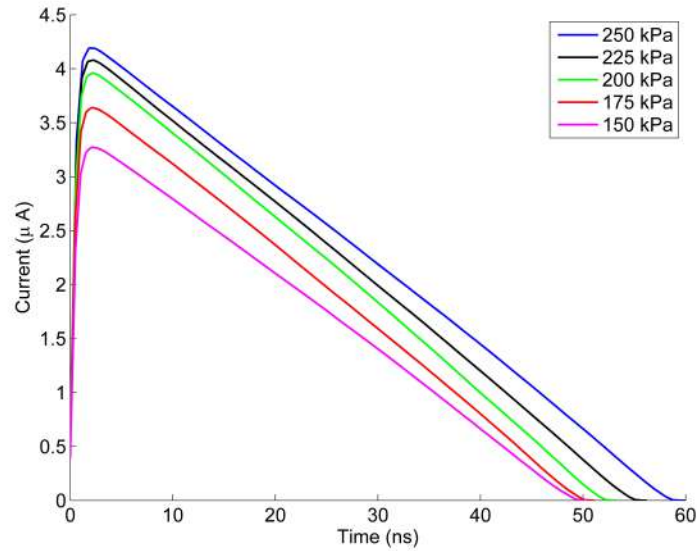
**(a)** Mean pulse shape.
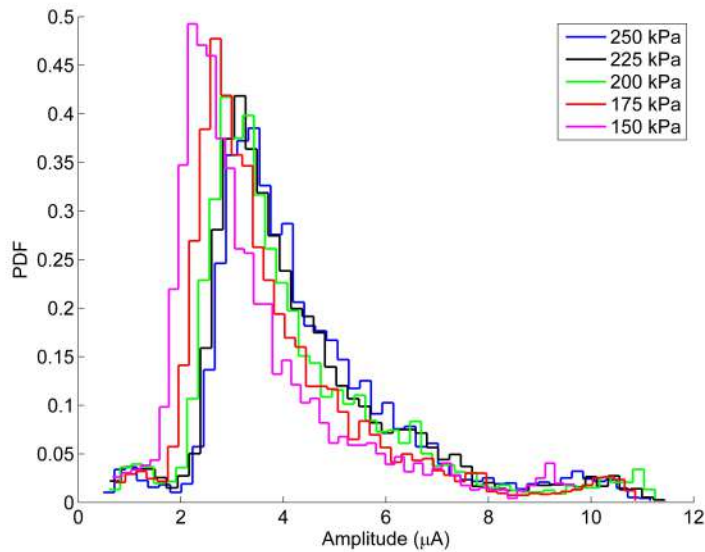


**(b)** Amplitude distribution.

**Figure 5.1:** Fission chamber pulse characteristics due to pressure drop.

Fig. 5.1b shows that the amplitude distribution of the created pulses is also affected by the pressure drop. The median of the distribution becomes lower and the raw moments of the distribution are decreasing during the pressure drop, since there is less gas to be ionized.

As a consequence, both terms of the calibration coefficient, introduced in Eq. (4.1), are decreasing during the pressure drop. The alteration in the second and third order coefficient is -15 % and -21 %, respectively, due to 25 kPa pressure change. Therefore the cumulants of the signal decrease significantly, even if the

real count rate is unchanged. This results in an underestimation of the count rate with the original calibration coefficient. As shown in Fig. 5.2, the count rate estimation drops during the pressure loss, even though the reactor is in a steady state.
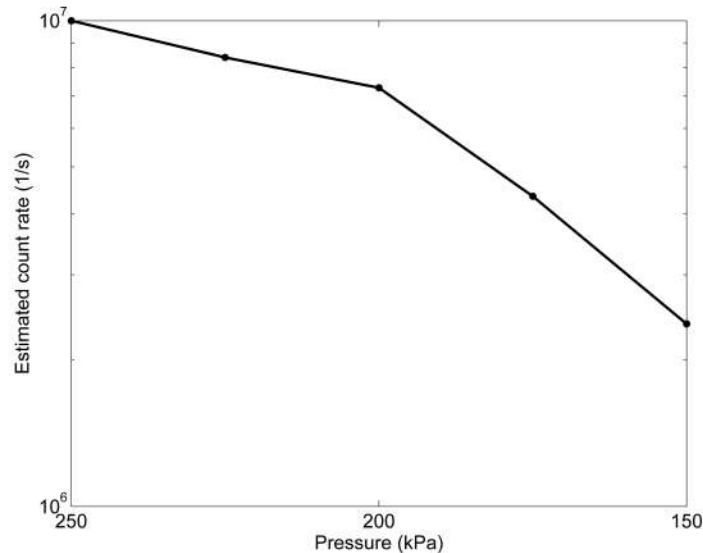


**Figure 5.2:** Estimated count rate at $s_0 = 10^7 \text{ s}^{-1}$.

## 5.3 Fault indicator

The task of a self-diagnosing detector is to identify whether the estimated count rate changed due to the change of the count rate or due to other reasons.

Therefore we have to define a measurable quantity of the fission chamber signal which is sensitive to the pulse shape change but not to the count rate change. The power spectral density of the detector signal satisfies this requirement. For a filtered Poisson process, it can be shown that the power spectral density has a breakdown at high frequencies which depends on the pulse shape [42].

To study the PSD of fission chamber signals, the same fission chamber signal simulator was used as in the previous chapters. With the software, various pulse trains, related to different filling gas pressures, were simulated.

First, it was verified that changing the count rate of the signal does not effect the shape and the breakdown frequency of the PSD, just the amplitude. Also the impact of the pulse amplitude distribution was studied separately. In accordance with our expectations, the pulse amplitude distribution has only an effect on the amplitude of the PSD.

Finally, the impact of the pulse shape was investigated. The results are shown in Fig. 5.3. Due to the alteration of the pulse shape, primarily of its width, the PSD
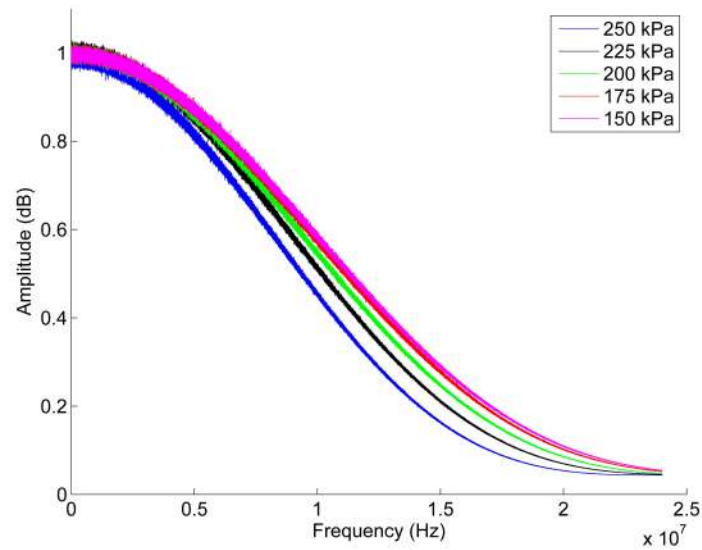
**Figure 5.3:** PSD of the signal at different filling gas pressures.

will extend to higher frequencies at lower filling gas pressures. This change was quantified by defining the PSD width as its full width at half maximum (FWHM) to provide a simple and measurable quantity to indicate gas leakage. The PSD width is contained in the 5-15 MHz band, which is an easily accessible frequency band with modern instrumentation.

One can notice that the spectral densities in Fig. 5.3 have some variance, therefore the estimation of the FWHM is not trivial. To guarantee reliable FWHM estimation and therefore reliable fault detection, the accuracy of the method had to be assessed. It was found that in case the FWHM estimation is based on 10 s long measurements, the error of the estimation is less than 1 %, which corresponds to a minimum detectable pressure drop of 5 kPa.

# CHAPTER 6

Implementation of the measurement techniques

In the previous chapters the signal processing was performed offline: after recording the signal, it was post-processed with a PC. Nevertheless, the ultimate goal of neutron monitoring is to realize a system, which is capable to work online.

Recently, neutron flux monitoring systems based on the traditional Campbelling technique make use of digital components, and FPGAs [31, 44]. Also the HOC methods were implemented on digital measurement devices with low sampling rate [39]. Nevertheless, there is still need to develop a neutron flux monitoring system, which is capable to work in real-time, and to provide count rate estimation based on ms long signals.

In case of higher order Campbelling, the online capability would mean that the higher order sums (introduced in Eq. (4.3)) are computed and the cumulants are estimated in real-time, while recording the signal. Therefore, the development of a prototype board, which implements the higher order Campbelling technique and the self-monitoring capability in real-time was started.

This chapter summarizes Paper VII, which covers the implementation of the real-time higher order Campbelling method on a the prototype measurement board. The requirements of an online neutron monitoring system, and the challenges of the implementation are summarized, and finally some of the experimental results are highlighted.

## 6.1 Requirements of real-time measurements and hardware selection

A recent trend to combine field-programmable gate arrays (FPGA) with embedded microprocessors and related peripherals in order to create a system on a programmable chip (SoC), made the development of digital measurement systems simpler and affordable. Currently several such systems are available on the market with varying complexity.

For the work the Red-Pitaya board [45] was chosen. The Red-Pitaya board was created in order to provide a customizable measurement system. The board comes

with a large amount of open source examples and tutorials, in order to facilitate implementing new modules. Its low price and a relatively large user community makes it an adequate tool to build a prototype system.

The requirements to build a real-time fission chamber signal processing system (and the characteristics of the board in relation to the requirements) are the following:

| Requirement | Red-Pitaya |
|---|---|
| Capability to convert and process the signal at the output of the available pre-amplifier which is typically a voltage between -10 V and 10 V. | Board provides two measurement ranges through jumper positions: $\pm 0.6$ V and $\pm 16$ V. |
| High sampling frequency in order to resolve the signal consisting of pulses with a width of a few tens of nanoseconds. | Board hosts ADC with 125 MHz sampling |
| Real-time computation of the first, second and third order sums of the signal. | FPGA on board |
| Ability to process a large amount of data in real-time (given that a time window of a few ms has to be applied for accurate estimations). | FPGA on board |

The Red-Pitaya board is built around a Xilinx Zync 7010 SoC which embeds an FPGA and a dual core Arm CPU. It hosts two Analog-to-Digital Converters (ADC) and two Digital-to-Analog Converters (DAC) which are directly connected to the FPGA. The ADCs have a sampling frequency of 125 MHz and a resolution of 14 bits. The board provides two measurement ranges through jumper positions: $\pm 0.6$ V and $\pm 16$ V. The great advantage of the FPGA is the possibility to design a circuit, which allows to process the data on-line, therefore reducing the time, and the memory storage needs for heavy computations. This makes FPGAs ideal to perform simple computing patterns on a vast amount of data in real-time. These characteristics of the Red-Pitaya fulfill all the above stated requirements to develop an online neutron monitoring system: the board is able to process the signal at the pre-amplifier output (which is $\pm 10$ V for the pre-amplifier applied in this work), to resolve the fission chamber pulses (with a length of few tens of ns), and to perform the real-time processing of a large amount of data.

## 6.2 Implementation of HOC

The main task of the system is to evaluate the third order cumulant estimator $k_3$ (Eq. (4.4)), which involves the computations of the sums $S_1$, $S_2$ and $S_3$ (Eq. (4.3)).

| Clock / Stages | $i-1$ | $i$ | $i+1$ | $i+2$ | $\cdots$ | $N+2$ |
|---|---|---|---|---|---|---|
| ADC in | $X_{i-1}$ | $X_i$ | $X_{i+1}$ | $X_{i+2}$ | . | . |
| $X$ | . | $X_{i-1}$ | $X_i$ | $X_{i+1}$ | . | . |
| $X^2$ | . | $X_{i-1} \cdot X_{i-1}$ | $X_i \cdot X_i$ | $X_{i+1} \cdot X_{i+1}$ | . | . |
| $S_1$ | . | $S_1 + X_{i-1}$ | $S_1 + X_i$ | $S_1 + X_{i+1}$ | . | . |
| $X^3$ | . | . | $X_{i-1}^2 \cdot X_{i-1}$ | $X_i^2 \cdot X_i$ | . | . |
| $S_2$ | . | . | $S_2 + X_{i-1}^2$ | $S_2 + X_i^2$ | . | . |
| $S_3$ | . | . | . | $S_3 + X_{i-1}^3$ | . | . |

**Figure 6.1:** Pipeline diagram to realize sum computation.

The most time consuming task is to compute these sums, since the higher order power of each signal sample is required in real-time. On the other hand, the further operations to compute the estimator $k_3$ based on the sums, has to be done only once at the end of each measurement window.

The real-time computation of the sum terms was realized on the FPGA (hence there is no need to store the sampled signal values), and, after the transfer of the sums to the CPU of the Red-Pitaya board, the final operations to compute the cumulant estimator were performed by a control software running on the CPU.

Although the computation of the sums may seem trivial, the FPGA introduces two constraints, since it is not possible to use procedural programming at the hardware level. The constraints, which have to be taken into account are the following: first, only one operand can be used in an operation, and second, every operation in an algorithmic block is performed in parallel during a clock tick, and their results will be available at the end of the clock tick. For example, to compute the sum of the third order powers of the signal, one first needs to compute the second order power of the signal. This cannot be done in the same clock tick (for the operation $x \cdot x \cdot x$, the result of $x \cdot x$ is needed, for which the result is not available immediately). Therefore, the computation of the powers and the sums have to be pipelined over several clock ticks. Fig. 6.1 illustrates the pipeline diagram of the computation of the sums.

A value measured by the ADC will be available for operations only in the following clock tick. Then, the FPGA is able to compute its square, and also the actual value of the first order sum can be evaluated. But the third power of the value and the second order sum can be computed only in the next clock tick. After the third power is available, the actual value of the third order sum can be computed during the following tick.

This introduces several inconveniences at the transfer of the sums, since they are not available at the same clock tick, but ideally the transfer should happen at the same time. By that time, the recording of the next time window (containing the next $N$ samples) has to begin in order to sustain continuous operation. The solution to these issues and the implementation of the precise data transfer is detailed in Paper VII.

## 6.3 Implementation of the smart detector module

To realize the self-monitoring system, which was named as the smart detector module, the FPGA recorded the raw signal values provided by the ADC. The raw signal was transferred then to the CPU of the board, and the complex data processing, such as computing the PSD and determining its width, was done on the CPU.

This solution is relatively slow (due to the large amount of data transfer), but as it was shown in the previous chapter, the time is not crucial for self-monitoring.

## 6.4 Experimental results

After various laboratory tests of the device (detailed in Paper VII), a measurement campaign at the MINERVE reactor was dedicated to test the reliability of the measurement prototype. During the measurements, two different types of fission chambers were used: a CFUL01 chamber (considered as the reference chamber for the previous chapters), and a CFUR chamber, which is a smaller chamber and contains only $10\,\mu g$ uranium. For the sake consistency with the cases earlier discussed in this thesis, here only some results related to the CFUL01 chamber are highlighted.

### 6.4.1 Higher order Campbelling results

During the measurement campaign, there was no opportunity to perform a transient measurement, hence the real time operation was tested at stationary power levels. Fig. 6.2 presents an example for the real time operation at 40 W reactor power. The third order cumulant was estimated at every 33 ms during almost a minute. The prototype performed well during the online measurement (the uncertainty of the estimation is due to the random errors, and the standard deviation of the mean of the estimated cumulant was less then 0.6 % with this time window).

In order to verify the linear behavior of the system, the third order cumulant has been estimated at reactor powers between 10 W and 80 W with the CFUL01, based on 33 ms time windows.
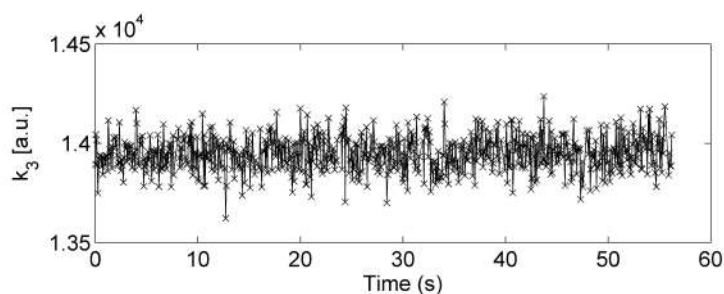
**Figure 6.2:** Real time cumulant measurement.
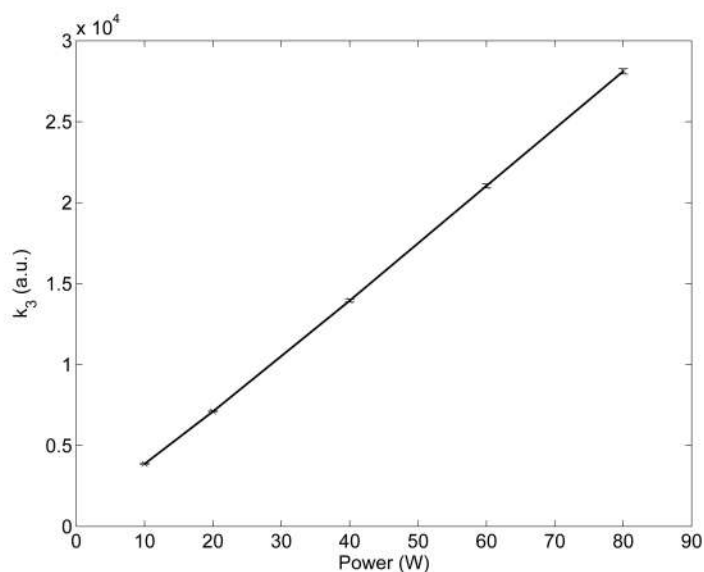


**Figure 6.3:** Cumulant estimation by the prototype device.

With the $\pm 16$ V input range the whole power range of the reactor was covered. The obtained cumulant estimations are presented in Fig. 6.3. The measured third order cumulant shows linearity with the reactor power. The departure from linearity is lower than 1.6 %.

### 6.4.2 Smart detector results

The previous chapter investigated the PSD change due to the loss of filling gas pressure. The experimental investigation of the pressure loss requires a fission chamber with variable filling gas pressure or a fission chamber which is already malfunctioning. In our measurements neither of these were available. Therefore a variable parameter, which has similar impact on the pulse width, had to be identified.

As Fig. 6.4 shows (the plotted values are obtained by pyFC simulations), the increase in the voltage between the electrodes has a similar impact on the pulse
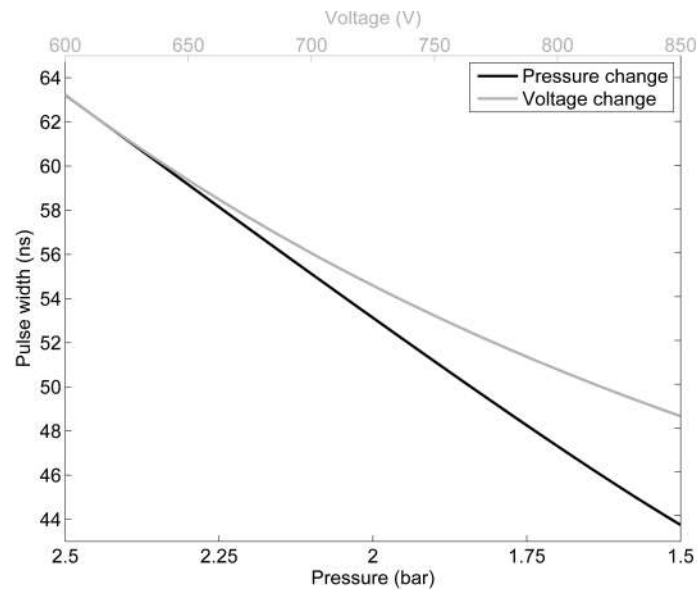
**Figure 6.4:** Simulated results of the pulse width vs the voltage and the gas pressure.

width as the decrease of the filling gas pressure. Since the voltage can be modified during the measurement, the PSD width was investigated at a constant reactor power of 20 W with the voltage changed between 600 V and 850 V (the CFUL01 chamber works in the saturation regime in this voltage range).

For each voltage, the PSD was calculated by averaging 4000 spectral densities of 0.52 ms long signals (i.e. the final PSD was based on a total measurement time of 2 seconds). With this signal length the uncertainty of the PSD already allowed to distinguish the change in the spectral width related to a change of 50 V. The measured PSD is shown in Fig. 6.5a, and the computed width is available in Fig. 6.5b. The small oscillation on the spectra is an artifact of the cable in the measurement.

Nevertheless, due to the slow data transfer between the FPGA and the CPU, the processing of this amount of data takes a few minutes (in this case the whole measured signal has to be transferred to the CPU). This means that the self-monitoring can be performed in every 2-3 minutes with the prototype.

The measurements with the prototype system proved the concept of the real-time self-monitoring capability based on the width of the PSD of fission chamber signals. However, by applying better performing devices, the time needed to measure the PSD width can be significantly reduced in the future.
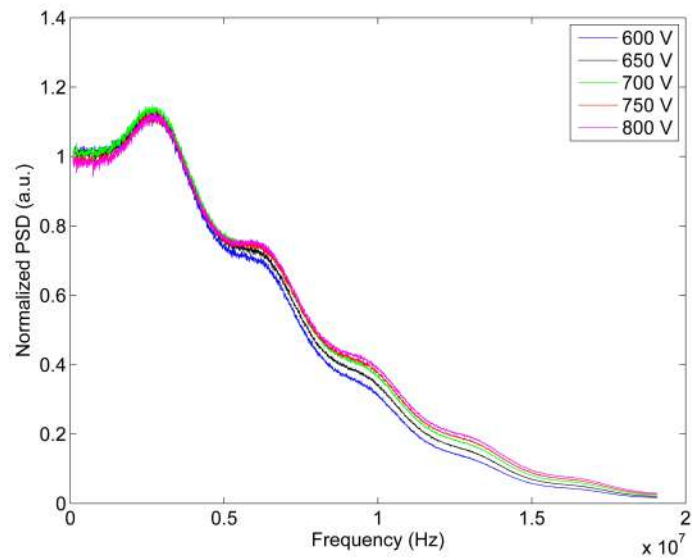
**(a)** Measured PSD.
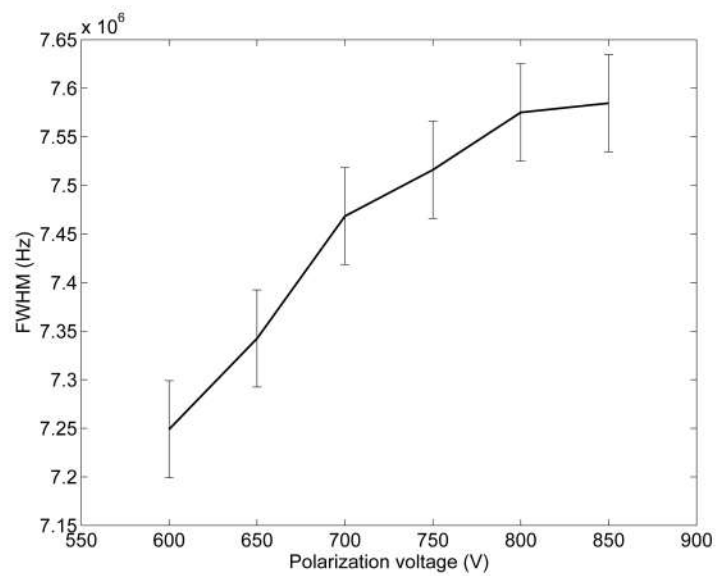


**(b)** Measured PSD width vs voltage.

**Figure 6.5:** Experimental results of the smart detector module.

# CHAPTER 7

## Concluding remarks

In this thesis three main areas were touched on: the limitations of the traditionally used fission chamber signal processing modes, the applicability of the higher order Campbell methods, and the self-monitoring capability of neutron monitoring systems. Here some of the conclusions are summarized, and also some further possible steps are mentioned.

- Concerning the traditional processing methods, sufficient overlap of the working regime of the pulse and Campbelling mode requires short pulse length. This could be achieved by increasing the nitrogen content in the filling gas. However, the nitrogen molecules disappear under irradiation at high temperature. Therefore, for applications such as Sodium cooled Fast Reactors, the development of the processing method is favored instead of changing the chamber design.

- By applying higher order Campbelling methods, it is possible to suppress the impact of the noise, the gamma (from the reactor) and the alpha (from the fissile deposit) background radiation. These methods provide an accurate count rate estimation at a wide count rate range. Nevertheless, the random uncertainties increase with the order of the method, and at really high count rates (above $10^9 \, s^{-1}$) the random errors tend to overcome the benefits of the method. Hence, the application of higher than third order methods is not feasible, nonetheless the even higher order methods do not provide significant advantages. With the use of third order mode, the real-time measurement can be based on a few ms long samples, which is sufficient to achieve real time monitoring. It was shown that the third order mode may work even at really low count rates (such as $10^3 \, s^{-1}$), but for that it requires a measurement length of a few seconds (nevertheless, the traditional pulse mode has the same drawback).

- The experimental calibration of the third order method is possible through investigating the pulse shape and the amplitude distribution of the pulses, therefore the count rate of the fission chamber signal can be estimated. But, at the moment the calibration is done off-line (by post-processing the recorded signal). This may be problematic, since the system measuring the third order cumulant is not necessarily capable of recording the signal. Therefore

the signal recording may be done with a separate system, which can have a different transfer function. A possible way to overcome this issue is to perform an empirical calibration, where the count rate is estimated with pulse counting techniques and compared to the measured cumulant. Such a calibration would not be plausible for the traditional Campbelling method, due to the linearity gap between the pulse counting methods and the second order Campbelling.

- In case the fission chamber is malfunctioning (for example the filling gas leaks through a crack), it is possible to detect this change from the PSD of the fission chamber signal. In order to achieve a low uncertainty on the spectral width measurements, a few seconds long samples are needed. Nevertheless, the estimated characteristic time for a filling gas pressure loss is in the order of magnitude of minutes, hence the early detection of malfunction is possible.

- Based on FPGAs the implementation of the third order Campbell mode for real time application is feasible. Using a relatively simple electronics device, which features an ADC, a CPU and an FPGA on board, a prototype measurement system was built and tested. The device proved the reliability and robustness of the concept. However, for the future industrial use, a better performing board may be favorable. It has to be highlighted again that the main drawback of the third order Campbell mode and of the device is the relatively challenging calibration. In order to perform the calibration, the developed device was capable to record the raw signal, which increased the complexity of the implementation. The calibration had to be done in the post-processing phase. As a further step an automatic, online calibration procedure is under development.

- Since the cumulant estimation was realized by pipelining the measured data through several clock cycles, the data transfer between the FPGA and the CPU is fast. On the contrary, for the self-monitoring module the device had to transfer larger amount of data between the FPGA and the CPU, therefore the PSD width measurement was possible only in every few minutes. This is already a remarkable achievement in regular monitoring, but with the use of higher performance devices in the future, this time can be significantly reduced.

- Fission chambers have some technological uncertainties (the size of the electrodes, the applied voltage, the nitrogen content of the filling gas, etc.). In the future, the impact of these uncertainties on the current pulses generated in the fission chamber will be investigated with the pyFC tool.

# Acknowledgements

First of all I would like to thank my supervisor, Professor Imre Pázsit for his endless mentoring, tutoring and support both in academic life and in life. He has an unbelievable knowledge about everything (stochastic processes, reactors, paprika growing, and even ulti!). Örök hálám.

My supervisors at CEA, Christian and Philippe. I received an incredible amount of help. Merci! From Philippe, I had the opportunity to learn about every possible details of fission chambers, pulses and simulations, but we had hilarious discussions about the dark side as well (of course I mean the SW universe). May the force be with you, Master!

Special thanks to Lénárd Pál, with whom I had the opportunity to work together for a short while. Meeting and "meditating about the stochastic signals" with him was one of the most memorable moments of this PhD period.

My present and former officemates during these four years, I am extremely lucky since you were so many and also because all of you are more easygoing than me. It was a great pleasure to share place and time with you inside and outside work: Florian, Micke, Fredrik, Manu, Vasu, Greg, Vlad, Klara and Alberto. With Greg, I even had the opportunity to work on some topics together, his knowledge on signal processing, programming, counting spectra and abusing English is fascinating, it was awesome to brainstorm with him so many times. I also would like to mention the other youngsters from Nephy, with whom I had the pleasure to share some fika, beers and conversations about life: Augi, Sebas and Victor. Thanks a lot guys, best times ever!

All my colleagues at Nephy, thank you so much for the great times, conversations and the infinite help: Anders' sense of humor was a real spice during fika in this spiceless Sweden. Lennart and Lasse are for sure the bests when it comes to computers. It was great to have Christophe and Paulo in this collaboration, their pragmatic views on how science works (or should work) was eye-opening. And Jóska is such a real Hungarian, he helped me a lot not to feel homesick.

Merci à tous mes collègues du LDCI. J'ai eu beaucoup des souvenirs inoubliables et aussi beaucoup de vins. Remerciement spécial pour Christelle, qui est très amiable et "chatty", et Jean-Michel, mon ami, qui a cru que je serai capable d'apprendre le français (et avec son aide, j'y suis un peu parvenu).

# BIBLIOGRAPHY

[1]  Richard G. Hewlett and Oscar E. Anderson. *The New World, 1939-1946*. University Park: Pennsylvania State University Press, 1962.

[2]  S. Normand. "Instrumentation Nucleaire pour les systemes industriels de mesure". Habilitation. Université de Caen, 2010.

[3]  F. Gauché. "Generation IV reactors and the ASTRID prototype: Lessons from the Fukushima accident". In: *Comptes Rendus Physique* 13 (2012), pp. 365–371.

[4]  C. Jammes, P. Filliatre, B. Geslot, T. Domenech, and S. Normand. "Assessment of the high temperature fission chamber technology for the French fast reactor program". In: *IEEE Transactions on Nuclear Science* 59 (2012), pp. 1351–1359.

[5]  M. A. Reichenberger, P. B. Ugorowski, J. A. Roberts, and D. S. McGregor. "First-order numerical optimization of fission-chamber coatings using natural uranium and thorium". In: *2014 IEEE Nuclear Science Symposium and Medical Imaging Conference (NSS/MIC)*. 2014.

[6]  B. Lescop et al. "A new system for in-core wide range neutron monitoring". In: *Nuclear Science Symposium Conference Record, 2004 IEEE*. Vol. 3. 2004, pp. 1567–1570.

[7]  G. F. Knoll. *Radiation Detection and Measurement*. 4th. John Wiley & Sons, 2010.

[8]  P. Filliatre, C. Jammes, B. Geslot, and L. Buiron. "In vessel neutron instrumentation for sodium-cooled fast reactors: Type, lifetime and location". In: *Annals of Nuclear Energy* 37 (2010), pp. 1435–1442.

[9]  Chang. J. *Table of Nuclides, KAERI(Korea Atomic Energy Research Institute)*. `http://atom.kaeri.re.kr/`. Accessed: 2016. August. 2016.

[10]  P. Filliatre, L. Oriol, C. Jammes, and L. Vermeeren. "Joint estimation of the fast and thermal components of a high neutron flux with a two on-line detector system". In: *Nuclear Instruments and Methods in Physics Research Section A: Accelerators, Spectrometers, Detectors and Associated Equipment* 603 (2009), pp. 415–420.

[11]  B. Geslot et al. "New measurement system for on line in core high-energy neutron flux monitoring in materials testing reactor conditions". In: *Review of Scientific Instruments* 82 (2011).

[12]   T. E. Bortner, G. S. Hurst, and W. G. Stone. "Drift velocities of electrons in some commonly used counting gases". In: *Rev. Sci. Instrum.* 28 (1957), pp. 103–108.

[13]   G. N. Haddad. "Drift Velocity of Electrons in Nitrogen-Argon Mixtures". In: *Aust. J. Phys.* 36 (1983), pp. 297–303.

[14]   G. J. M. Hagelaar and L. C. Pitchford. "Solving the Boltzmann equation to obtain electron transport coefficients and rate coefficients for fluid models". In: *Plasma Sources Sci. Technol.* 14 (2005), pp. 722–733.

[15]   S.F. Biagi. "Monte Carlo simulation of electron drift and diffusion in counting gases under the influence of electric and magnetic fields". In: *Nuclear Instruments & Methods in Physics Research, Section A: Accelerators, Spectrometers, Detectors, and Associated Equipment* 421 (1999), pp. 234–240.

[16]   P. Filliatre, C. Jammes, B. Geslot, and R. Veenhof. "A Monte Carlo simulation of the fission chambers neutron-induced pulse shape using the GARFIELD suite". In: *Nuclear Instruments and Methods in Physics Research Section A: Accelerators, Spectrometers, Detectors and Associated Equipment* 678 (2012), pp. 139–147.

[17]   C. Jammes, P. Filliatre, P. Loiseau, and B. Geslot. "On the impact of the fissile coating on the fission chamber signal". In: *Nuclear Instruments and Methods in Physics Research Section A: Accelerators, Spectrometers, Detectors and Associated Equipment* 681 (2012), pp. 101–109.

[18]   N. R. Campbell and V. J. Francis. "A Theory of Valve and Circuit Noise". In: *JIEE* 93 (1946), pp. 45–52.

[19]   R. A. DuBridge. "Campbell Theorem - System Concepts and Results". In: *IEEE Transactions on Nuclear Science* 14 (1967), pp. 241–246.

[20]   I. Lux and A. Baranyai. "Higher order campbell techniques for neutron flux measurement: I. Theory". In: *Nuclear Instruments and Methods in Physics Research* 202 (1982), pp. 469–475.

[21]   B. Bärs. "Variance and higher order signal moments in neutron flux measurements". In: *Nuclear Instruments and Methods in Physics Research Section A: Accelerators, Spectrometers, Detectors and Associated Equipment* 275 (1989), pp. 403–410.

[22]   R. A. Fisher. "Moments and Product Moments of Sampling Distributions". In: *Proceedings of the London Mathematical Society* 33 (1928), pp. 199–238.

[23]   P. Loiseau, B. Geslot, and J. Andre. "On the fission chamber pulse charge acquisition and interpretation at MINERVE". In: *Nuclear Instruments and Methods in Physics Research Section A: Accelerators, Spectrometers, Detectors and Associated Equipment* 707 (2013), pp. 58–63.

[24]   E. W. Pontes and A. Ferreira. "Using cumulants and spectra to model nuclear radiation detectors". In: *IEEE Transactions on Nuclear Science* 53 (2006), pp. 1292–1298.

[25] J. F. Ziegler, J. P. Biersack, and M. D. Ziegler. *The Stopping and Range of Ions in Matter*. 2008. URL: srim.org.

[26] W. Shockley. "Currents to Conductors Induced by a Moving Point Charge". In: *Journal of Applied Physics* 9 (1938), pp. 635–636.

[27] Zs. Elter. *pyFC: a TRIM-based fission chamber pulse shape simulator*. Tech. rep. CTH-NT-318. Chalmers University of Technology, 2015.

[28] S. N. Ahmed. *Physics and Engineering of Radiation Detection*. Academic Press, 2007.

[29] A. Gruel, P. Leconte, D. Bernard, P. Archier, and G. Noguère. "Interpretation of Fission Product Oscillations in the MINERVE Reactor, from Thermal to Epithermal Spectra". In: *Nuclear Science and Engineering* 169 (2011), pp. 229–244.

[30] *CFUL01 data sheet*. https://www.photonis.com/uploads/datasheet/ngd/CFUL01.pdf. Accessed: 2016. August.

[31] T. Rivero Gutiérrez, J. S. Benítez-Read, J. C. Palacios Hernández, A. Segovia-de-los-Ríos, and L. C. Longoria-Gándara. "Software-based Neuton Flux Measurement Channel (NFMC)". In: *Int. J. Nuclear Energy Science and Technology* 5 (2010), pp. 91–104.

[32] V. Bécares and J. Blázquez. "Detector Dead Time Determination and Optimal Counting Rate for a Detector Near a Spallation Source or a Subcritical Multiplying System". In: *Science and Technology of Nuclear Installations* 2012 (2012).

[33] M. A. Schultz. *Control of nuclear reactors and power plants*. McGraw-Hill, 1955.

[34] L. Vermeeren et al. "Experimental Verification of the Fission Chamber Gamma Signal Suppression by the Campbelling Mode". In: *IEEE Transactions on Nuclear Science* 58 (2011), pp. 362–369.

[35] C. Dubi et al. "Dead Time Corrections using the Backward Extrapolation Technique". In: *Physor conference*. 2016.

[36] C.T.I.I. Norman. "Gamma and alpha compensated fission chamber". US Patent 4,071,764. Jan. 1978. URL: https://www.google.com/patents/US4071764.

[37] B. Geslot et al. "Method to Calibrate Fission Chambers in Campbelling Mode". In: *IEEE Transactions on Nuclear Science* 59 (2012), pp. 1377–1381.

[38] I. Lux and A. Baranyai. "Higher order campbell techniques for neutron flux measurement: II. Correlated Campbelling". In: *Nuclear Instruments and Methods in Physics Research* 202 (1982), pp. 477–480.

[39] L. B. Baers, T. Rivero Gutierrez, R. A. Carrillo Mendoza, and Jimenez Santana G. "Use of Higher Order Signal Moments and High Speed Digital Sampling Technique for Neutron Flux Measurements". In: *IEEE Transactions on Nuclear Science* 40 (1993), pp. 832–839.

[40]    E. W. Weisstein. *k-Statistic - From MathWorld–A Wolfram Web Resource*. `http://mathworld.wolfram.com/k-Statistic.html`. Accessed: 2016. August. 2016.

[41]    P. Filliatre, L. Vermeeren, C. Jammes, B. Geslot, and D. Fourmentel. "Estimating the $\gamma$-ray contribution to the signal of fission chambers with Monte Carlo simulations". In: *Nuclear Instruments and Methods in Physics Research Section A: Accelerators, Spectrometers, Detectors and Associated Equipment* 648 (2011), pp. 228–237.

[42]    L. Pál and Pázsit. "Campbelling-type theory of fission chamber signals generated by neutron chains in a multiplying medium". In: *Nuclear Instruments and Methods in Physics Research Section A: Accelerators, Spectrometers, Detectors and Associated Equipment* 794 (2015), pp. 90–101.

[43]    R. Hunt. "Testing Fission Chambers". In: *Nuclear Engineering International magazine* (2011). URL: `http://www.neimagazine.com/features/featuretesting-fission-chambers/`.

[44]    M. Thevenin et al. "Digital Real-Time Multiple Channel Multiple Mode Neutron Flux Estimation on FPGA-based Device". In: *EPJ Web of Conferences* 106 (2016).

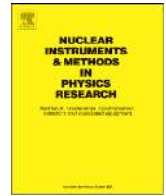[45]    *Red-Pitaya homepage*. `http://redpitaya.com/`. Accessed: 2016. August.

Papers I-VII

# Paper I

Comments on the Stochastic Characteristics of Fission Chamber Signals

L. Pál, I. Pázsit and Zs. Elter.

# Comments on the stochastic characteristics of fission chamber signals

L. Pál [a], I. Pázsit [b,*], Zs. Elter [b]

[a] Centre for Energy Research, Hungarian Academy of Sciences, H-1525 Budapest 114, POB 49, Hungary
[b] Chalmers University of Technology, Department of Applied Physics, Division of Nuclear Engineering, SE-412 96 Göteborg, Sweden

## ABSTRACT

This paper reports on theoretical investigations of the stochastic properties of the signal series of ionisation chambers, in particular fission chambers. First, a simple and transparent derivation is given of the higher order moments of the random detector signal for incoming pulses with a non-homogeneous Poisson distribution and random pulse heights and arbitrary shape. Exact relationships are derived for the higher order moments of the detector signal, which constitute a generalisation of the so-called higher order Campbelling techniques. The probability distribution of the number of time points when the signal exceeds a certain level is also derived. Then, a few simple pulse shapes and amplitude distributions are selected as idealised models of the detector signals. Assuming that the incoming particles form a homogeneous Poisson process, explicit expressions are given for the higher order moments of the signal and the number of level crossings in a given time interval for the selected pulse shapes.

© 2014 Elsevier B.V. All rights reserved.

## 1. Introduction

The recent interest in new reactor systems and in many other fields drew an increased attention to the development of neutron detectors which are particularly suitable for deployment in such systems, especially to the technical improvement of the fission chambers. The fission chamber is an ionisation chamber in which the electron–ion pairs are generated by fission fragments in the gaseous volume of the detector. These electron–ion pairs are collected to form a detector pulse of a certain shape, and the detector signal consists of a random sum of such pulse shapes, induced by the random primary events (impinging neutrons inducing fission).

Fission chambers have certain advantages over other type of detectors which are suitable for in-core neutron measurements [1,2]. One is that they have a large dynamic range, i.e. they can be used in both low, medium and high neutron fluxes. Unlike other detectors which can operate only either in pulse or current mode, fission chambers can be operated in both. At low neutron intensities, the fissions generate individual current signals, i.e. pulses, that are generally separated and can be counted with a given efficiency. At increasing neutron intensities, the pulses tend to overlap, which finally forms a randomly fluctuating continuous current. The expectation of this fluctuating signal, that is the direct current, is proportional to the neutron flux, which is the main quantity of interest.

Under the conditions that the continuous signal is formed as the superposition of constant pulse shapes induced by independent incoming events, the higher order moments inclusive the semiinvariants of the fluctuating signal are also proportional to the intensity of the primary incoming neutrons, and hence to the neutron flux. This is expressed by the so-called Campbell theorem [3,4], which shows the relationship of the first two moments of the detector signal to the primary event intensity in the form

$$\mathbf{E}\{\eta(t)\} = s_0 \int_{-\infty}^{+\infty} f(t)\, dt \quad \text{and} \quad \mathbf{D}^2\{\eta(t)\} = s_0 \int_{-\infty}^{+\infty} f(t)^2\, dt. \tag{1}$$

Here the random process $\eta(t)$ represents the fluctuating detector signal, which consists of a random sum of deterministic current signals $f(t)$ created according a homogenous Poisson process with intensity $s_0$.

Eq. (1) shows the second advantage of fission chambers in that instead of the first moment, the variance can also be used to estimate the neutron flux (which is also called "Campbelling techniques" or "Campbell-technique"). Then, even if the detector is sensitive to both neutrons and gamma photons, the gamma photons will produce less charge in the detector per incoming particle than the neutrons (through the fission products), and hence will be represented by a much smaller amplitude of the corresponding current signal shape $f(t)$. Hence the contribution of the unwanted minority component, i.e. that of the gamma detections, can be significantly reduced by the use of Campbelling techniques. One can extend the relationships (1) even to higher order moments (semiinvariants), leading to higher order Campbelling techniques [5–7], lending the possibility of even further reduction of the contributions from gamma detection and other unwanted components such as alpha particles.

---

*Corresponding author.
 E-mail address: imre@chalmers.se (I. Pázsit).

The complete process of neutron detection in a fission chamber, starting with the fission in the fissile deposit of the detector, the slowing down and escape of the fission products, the charge generation, collection and amplification is a complex process. All elements of this process will influence the pulse shape, the statistics of the pulse amplitude and finally the statistics of the detector current fluctuations and hence the form and validity of the Campbelling techniques. Many elements of this process can be simulated and modelled with advanced transport codes for charged particles. Such effects have been investigated by several authors [1,2,8,9]. The emphasis in these works is that by using the basic charge transport equations, to calculate both the mean shape of an individual signal and the mean value of the saturation current.

These questions are not touched on in the present paper, which will concentrate on the understanding of the information content in the temporal randomness of a detector signal composed by a random sum of pulses of a given fixed shape but with a random amplitude distribution. No attempt will be made to derive the signal shapes or the amplitude distributions from calculation from first principles; rather, two physically reasonable shapes and amplitude distributions will be postulated and investigated.

As a first step, the higher order Campbelling techniques will be derived for a non-homogeneous Poisson distribution, with random pulse height of arbitrary distribution and arbitrary signal shape. There exist derivations in the literature of the higher order Campbelling techniques, but these contain unnecessarily complicated and often incorrect calculations. The method used in this work is the backward form of the integral master equation for the probability distribution of the detector signal. Exact relationships will be derived for the higher order moments, which constitute a generalisation of the higher order Campbelling methods. These will, among others, reproduce the results published by Lux and Baranyai [5,6] and by Bärs in 1989 [7] in a simple and transparent way.

In addition to the moments of the signal, the number of cases when the signal is higher than a given level in a given time interval also gives information on the intensity of the primary events, and hence on the neutron flux. Such a measurement on a continuous signal show similarities with measurements in the pulse mode. Because of its information content, the intensity of events when the signal exceeds a certain level is also derived.

Although, as it will be seen, the higher order Campbelling techniques state that all higher order moments are proportional to the intensity of the incoming particles, the proportionality factor is a function of the signal shape and the amplitude distribution of the pulses. Hence, insight can be gained on the performance of the Campbelling techniques if explicit analytical results are available for some concrete characteristic pulse shapes and amplitude distributions. To this end, a few simple pulse shapes and amplitude distributions are selected as idealised models of the detector signals. Assuming that the incoming particles form a homogeneous Poisson process, explicit expressions are given for the higher order moments of the signal and the intensity of level crossings for the selected pulse shapes. The results for the different pulse shapes and amplitude distributions can be compared.

Regarding the analytical work, some of the calculations require extensive derivations. Apart from the derivation of the generalised higher order Campbell relations, which will be given in detail, in the concrete calculations with selected pulse shapes and amplitude distributions, most of the details of the calculations were omitted. Details of the derivations are described in a Chalmers internal report, available electronically [10] where even other pulse shapes are considered.

It can also be mentioned that regarding the assumption of independent primary incoming events, which are essential in the derivation of the Campbell theorems, can be relaxed. The treatment used in this paper can be extended to the case when detection events are related to neutrons arising in branching processes in a multiplying medium, and which hence are not independent events. The results of this extension will be published in a later communication [11].

## 2. General theory

### 2.1. Signal probability distribution

The objective of this work is to determine the probability distribution function of the sum of random response signals of randomly appearing particles in a simple detector model. We assume that the number of incoming particles within a given time period follows an inhomogeneous Poisson distribution, and that the detector counts all arriving particles. Also, the random response signals related to different particles are considered to be independent and identically distributed. Likewise, the question of correlated detection events, induced by incoming neutrons generated in a branching process, will be treated in a forthcoming publication.

The basic quantity, the "building brick" of the stochastic model of the detector signal is the current (or voltage) pulse form generated by each incoming particle arriving to the detector. This pulse shape can be considered as the response function of the detector. As mentioned, due to the statistical properties of the generation of such a pulse from the underlying physical processes, which also contain random elements, this response pulse form cannot be given by a deterministic function $f(t)$. In the general case it is described by a function $\varphi(\xi, t)$ which depends on the possible realisations of a random variable $\xi$. The continuously arriving particles generate the detector current as the aggregate of such response function current signals, each related to a different realisation of $\xi$.

In the treatment that follows we will restrict the study to cases in which the dependence of $\varphi(\xi, t)$ on its arguments is factorised into a form $\varphi(\xi, t) = a(\xi)f(t)$ where $a$ is the random amplitude of the pulse and $f(t)$ is the pulse shape. Although this assumption restricts somewhat the generality of the description, it will lead to a formalism which, for several basic signal shapes $f(t)$ is amenable to an analytical treatment, while still representing a realistic model of the detector signal. For signal shapes that are constant or monotonically decreasing for $t > 0$ (square and exponential) $\xi$ will be the (random) initial value of the response signal. For other, non-monotonically varying signal shape it can be identified with a given parameter of the signal pulse. We assume that $\xi \in \Re$, where $\Re$ is the set of real numbers, and it has a finite expected value and variance.

The derivation of the main quantity of interest, the probability density of the stochastic signal $\eta(t)$ at time $t$, given that at time $t = 0$ it was zero, needs the following definitions and considerations. We assume that the sequence of particle arrivals constitutes an inhomogeneous Poisson process. In this case the probability that no particle arrives at the detector during the time interval $[t_0, t]$, $t \geq t_0$ is given by

$$T(t_0, t) = \exp\left\{ -\int_{t_0}^{t} s_0(t')\, dt' \right\}. \tag{2.1}$$

Here $s_0(t)$ is the intensity of the particle arrivals at time $t$. Each particle will induce a pulse with shape $f(t)$ and a realisation $x$ of the random amplitude $\xi$. The cumulative probability distribution and the probability density of the amplitude distribution are

described by the functions $W(x)$ and $w(x)$, respectively, as

$$\mathcal{P}\{\xi \leq x\} \equiv W(x) = \int_{-\infty}^{x} w(x')\, dx' \tag{2.2}$$

The probability that the value of the response at time $t$ after the arrival of *one single* particle is not greater than $y$ is given by the degenerate distribution function

$$H(y,t) = \int_{-\infty}^{+\infty} \Delta[y - \varphi(x,t)]w(x)\, dx. \tag{2.3}$$

where $\Delta(x)$ is the unit step function. The probability density function $h(y,t)$ of $H(y,t)$ is given as

$$h(y,t) = \int_{-\infty}^{+\infty} \delta[y - \varphi(x,t)]w(x)\, dx. \tag{2.4}$$

Denoting the sum of the signals at $t \geq t_0$ as $\eta(t)$, we shall seek the probability of the event that $\eta(t)$ is less than or equal to $y$ with the condition that its value was zero at $t_0$, i.e. the quantity

$$\mathcal{P}\{\eta(t) \leq y | \eta(t_0) = 0\} = P(y,t|0,t_0) = \int_{-\infty}^{y} p(y',t|0,t_0)\, dy'. \tag{2.5}$$

Straightforward considerations yield the following backward-type integral Chapman–Kolmogorov equation for the probability density function $p(y,t|0,t_0)$:

$$p(y,t|0,t_0) = T(t_0,t)\delta(y) + \int_{t_0}^{t} T(t_0,t')s_0(t') \int_{-\infty}^{y} h(y',t-t')p(y-y',t|0,t')\, dy'\, dt'. \tag{2.6}$$

The r.h.s. of Eq. (2.6) consists of the sum of the probabilities of the mutually exclusive events that there will not, or there will be a first detection sometime between $t_0$ and $t$, respectively. The product of the probabilities in the last integral of the second term is due to the fact that the contribution to the total signal at terminal time $t$ from the first detection at time $t'$ is independent from that of the subsequent detections between $t'$ and $t$.

Eq. (2.6) shows that the probability density of the detector signal induced by the aggregate of pulses, generated by the sequence of incoming particles with an inhomogeneous Poisson distribution "source induced distribution", is expressed by the probability density of the detector signal induced by one single particle ("single-particle induced distribution"), in form of a convolution. In this respect it is a complete analogue of the backward master equation of neutron multiplication, connecting the source induced distribution with the single-particle distribution (the "Sevast'yanov formula" [12]; in many papers it is called the "Bartlett formula"). The arguments used in the derivation are also essentially the same in both cases.

As is known, in the case of the "Sevast'yanov formula", turning the probability balance equation for the discrete random variable representing the neutron number into an equation for the probability generation functions of the source and single-particle induced distributions, the arising equation can be solved by quadrature. This means that the sought source-induced generating function can be expressed as an exponential integral of the single-particle induced generating function and the source intensity. Hence, once the single-particle generation function, or at least its moments are known, the source-induced distribution (or its moments) can be obtained by integration, without solving any further equations.

It will be seen that the same is true for the master equation (2.6), if the characteristic functions of the source-induced and the single-particle induced distributions are introduced. One difference compared to the neutron number distribution is that for this latter, the single-particle induced distribution is not given in advance, rather it is obtained as the solution of the master equation of the branching process. However, the moments of the single induced distribution have a very simple form, and moreover

the first moment serves as the Green's function of the higher order moments. For the detector signal in our case, the single-particle induced distribution will be given in advance and hence known (through the model signal shapes and their amplitude distributions that we shall define); in turn these will be more complicated than in the case of the neutron transport and the arising integrals will be considerably more complicated to perform.

For continuous random variables that can take also negative values (which we shall assume for generality in this Section), the characteristic functions are defined by the Fourier transform in the signal value variable. Hence, the characteristic functions $\pi$ and $\chi$ of $p$ and $h$, respectively, are defined as

$$\pi(\omega,t|0,t_0) = \int_{-\infty}^{+\infty} e^{i\omega y} p(y,t|0,t_0)\, dy \tag{2.7}$$

and

$$\chi(\omega,t) = \int_{-\infty}^{+\infty} e^{i\omega y} h(y,t)\, dy$$

$$= \int_{-\infty}^{+\infty} \int_{-\infty}^{+\infty} e^{i\omega y} \delta[y - \varphi(x,t)]\, dy\, w(x)\, dx$$

$$= \int_{-\infty}^{+\infty} e^{i\omega\varphi(x,t)} w(x)\, dx. \tag{2.8}$$

Then, from Eq. (2.6) one obtains

$$\pi(\omega,t|0,t_0) = T(t_0,t) + \int_{t_0}^{t} T(t_0,t')s_0(t')\chi(\omega,t-t')\pi(\omega,t|0,t')\, dt'. \tag{2.9}$$

From this integral equation it is seen that

$$\lim_{t \downarrow t_0} \pi(\omega,t|0,t_0) = 1. \tag{2.10}$$

Derivation w.r.t. $t_0$ leads to the differential equation

$$\frac{\partial \pi(\omega,t|0,t_0)}{\partial t_0} = s_0(t_0)\pi(\omega,t|0,t_0)[1 - \chi(\omega,t-t_0)] \tag{2.11}$$

Accounting for the initial condition (2.10), the solution of (2.11) can be written as

$$\pi(\omega,t|0,t_0) = \exp\left\{ -\int_{0}^{t-t_0} s_0(t-t')[1 - \chi(\omega,t')]\, dt' \right\} \tag{2.12}$$

where $\chi(\omega,t')$ is defined in (2.8). Eq. (2.12) can be considered to be the characteristic function of the generalised non-homogeneous Poisson-process. Again, a close analogue is seen with the similar expression for the neutron multiplication process.

If the particle arrivals correspond to a homogeneous Poisson process with constant intensity $s_0$, then the characteristic function $\pi(\omega, +\infty|0, -\infty)$ is given by

$$\pi(\omega, +\infty|0, -\infty) = \pi_{st}(\omega) = \exp\left\{ -s_0 \int_{-\infty}^{+\infty} [1 - \chi(\omega,t)]\, dt \right\} \tag{2.13}$$

if the integral on the r.h.s. exists. Hence there exists an *asymptotically stationary signal level* $\eta^{(st)}$, with the probability density function

$$\pi_{st}(y) = \mathcal{L}^{-1}\{\pi_{st}(\omega)\}. \tag{2.14}$$

For the subsequent calculations it is also practical to introduce the logarithm $\gamma_{st}(\omega)$ of the characteristic function (2.13), i.e.

$$\gamma_{st}(\omega) = \ln \pi_{st}(\omega) = s_0 \int_{-\infty}^{+\infty} [\chi(\omega,t) - 1]\, dt. \tag{2.15}$$

## 2.2. Expectation, variance and cumulants

From (2.15) the expectation of the stationary signal $\eta^{(st)}$ can be easily calculated as

$$\mathbf{E}\{\eta^{(st)}\} = i_1^{(st)} = \frac{1}{i}\left[\frac{d\gamma_{st}(\omega)}{d\omega}\right]_{\omega=0} = s_0 \int_{-\infty}^{+\infty}\left[\int_{-\infty}^{+\infty}\varphi(x,t)w(x)\,dx\right]dt \tag{2.16}$$

and its variance as

$$\mathbf{D}^2\{\eta^{(st)}\} = \sigma_{st}^2 = -\left[\frac{d^2\gamma_{st}(\omega)}{d\omega^2}\right]_{\omega=0} = s_0 \int_{-\infty}^{+\infty}\left[\int_{-\infty}^{+\infty}\varphi(x,t)^2 w(x)\,dx\right]dt. \tag{2.17}$$

If the value of the signal amplitude $\xi$ is always unity, that is $w(x) = \delta(x-1)$, then (2.16) and (2.17) revert to the expressions of the Campbell's theorem, (1), in the form

$$\mathbf{E}\{\eta^{(st)}\} = s_0 \int_{-\infty}^{+\infty} f(t)\,dt \tag{2.18}$$

and

$$\mathbf{D}^2\{\eta^{(st)}\} = s_0 \int_{-\infty}^{+\infty} f(t)^2\,dt \tag{2.19}$$

with $f(t) = \varphi(1,t)$. After proper calibration, both of these forms are suitable to determine the particle intensity $s_0$.

As is known [13], the *cumulants* or *semiinvariants* $\kappa_n^{(st)}$ of $\eta^{(st)}$, which can be expressed by the moments of $\eta^{(st)}$, can be derived from the logarithmic characteristic function $\gamma_{st}(\omega)$ through the formula:

$$\kappa_n^{(st)} = \frac{1}{i^n}\left[\frac{d^n\gamma_{st}(\omega)}{d\omega^n}\right]_{\omega=0} = s_0 \int_{-\infty}^{+\infty}\left[\int_{-\infty}^{+\infty}\varphi(x,t)^n w(x)\,dx\right]dt.$$

This way one immediately arrives at the results referred to in the literature as *higher order Campbell techniques* [5,6]. It is readily seen that all cumulants are linearly proportional to the intensity $s_0$. A few cumulants are given below for illustration.

$$\kappa_1^{(st)} = i_1^{(st)},$$
$$\kappa_2^{(st)} = i_2^{(st)} - (i_1^{(st)})^2,$$
$$\kappa_3^{(st)} = i_3^{(st)} - 3i_2^{(st)}i_1^{(st)} + (i_1^{(st)})^3,$$
$$\kappa_4^{(st)} = i_4^{(st)} - 4i_3^{(st)}i_1^{(st)} - 3(i_2^{(st)})^2 + 12i_2^{(st)}(i_1^{(st)})^2 - 6(i_1^{(st)})^4$$

where

$$i_n^{(st)} = \mathbf{E}\{(\eta^{(st)})^n\}, \quad n = 1, 2, \ldots \quad.$$

## 2.3. Definition of the selected pulse shapes

In the rest of the paper we will only deal with processes of the form $\varphi(x,t) = x f(t)$ where $f(t)$ is a deterministic signal function. We will also assume that the realisations $x$ of the random variable $\xi$, as well as the signal function $f(t)$ itself take only non-negative real values. The signal forms considered all start with a jump, i.e. at time $t=0$, $f(t)$ jumps from zero to its maximum (equal to $x$), whereafter $f(t)$ will either monotonically decrease or remain constant during a period, after which it jumps back to zero. For the total detector signal, this means that the arrival of a particle to the detector incurs a jump of the signal level with the value $x$.

Since the detector signals are now non-negative, the Fourier transforms of the previous formulae will be replaced by Laplace transforms. Thus we shall consider the *Laplace-transform* of the density function $p(y,t|0,t_0)$, defined in (2.5) as

$$\tilde{p}(s,t|0,t_0) = \int_0^{\infty} e^{-sy} p(y,t|0,t_0)\,dy \tag{2.20}$$

as the characteristic function. Introducing the transforms

$$\tilde{h}(s,t) = \int_0^{\infty} e^{-sy} h(y,t)\,dy \quad \text{and} \quad \tilde{w}(s) = \int_0^{\infty} e^{-sx} w(x)\,dx \tag{2.21}$$

from (2.12) we obtain

$$\tilde{p}(s,t|0,t_0) = \exp\left\{-\int_0^{t-t_0} s_0(t-t')[1 - \tilde{h}(s,t')]\,dt'\right\} \tag{2.22}$$

where $\tilde{h}(s,t')$ is defined as

$$\tilde{h}(s,t') = \int_0^{\infty} \exp\{-s f(t')x\}w(x)\,dx = \tilde{w}[sf(t')]. \tag{2.23}$$

To simplify the further considerations let us choose

$$s_0(t-t') = s_0 \quad \text{and} \quad t_0 = 0$$

and use the notation

$$\tilde{p}(s,t|0,0) = \tilde{p}(s,t). \tag{2.24}$$

From Eq. (2.22) one immediately obtains

$$\tilde{p}(s,t) = \exp\left\{-s_0 \int_0^t [1 - \tilde{h}(s,t')]\,dt'\right\} = \exp\left\{-s_0 \int_0^t \{1 - \tilde{w}[sf(t')]\}\,dt'\right\}. \tag{2.25}$$

As in the previous case, the Laplace transform of the stationary case is defined by the Laplace-transform

$$\lim_{t\to\infty}\tilde{p}(s,t) = \tilde{p}_{st}(s) = \exp\left\{-s_0 \int_0^{\infty}[1 - \tilde{h}(s,t)]\,dt\right\}$$
$$= \exp\left\{-s_0 \int_0^{\infty}\{1 - \tilde{w}[sf(t)]\}\,dt\right\} \tag{2.26}$$

provided that the integral exists. From this it follows that there exists an asymptotically stationary signal level $\eta^{(st)}$ with the density function

$$p_{st}(y) = \mathcal{L}^{-1}\{\tilde{p}_{st}(s)\}. \tag{2.27}$$

In this case too, for the determination of the cumulants it is practical to use the logarithm of the Laplace-transform $\tilde{p}_{st}(s)$ of the density function $p_{st}(y)$:

$$\tilde{g}_{st}(s) = \ln \tilde{p}_{st}(s) = s_0 \int_0^{\infty}[\tilde{h}(s,t) - 1]\,dt \tag{2.28}$$

where

$$\tilde{h}(s,t) = \tilde{w}[sf(t)].$$

## 2.4. Level crossing intensity

The intensity $n_{st}(V)$ of the events when the signal level jumps above a certain level $V$ from a value $y \leq V$ is a measurable quantity. The level $V$ is usually called the *threshold*. Since it also contains information about the intensity of the incoming particle events, it is interesting to derive expressions for it. In the stationary case, it can be written in the following form:

$$n_{st}(V) = s_0 \int_0^V p_{st}(y)[1 - W(V-y)]\,dy \tag{2.29}$$

whose Laplace-transform is given as

$$\tilde{n}_{st}(s) = s_0 \frac{1 - \tilde{w}(s)}{s}\tilde{p}_{st}(s). \tag{2.30}$$

The expression for $n_{st}(V)$ in (2.29) consists of the product of the intensity of the particle arrivals and the probability that the signal level $y$ is under the threshold $V$ *and* the amplitude of the induced pulse is larger than $V-y$. Since these two latter events are independent, their probabilities are multiplied, and one has to integrate for all values of $y$ between zero and the threshold.

It can be expected that $n_{st}(V)$ is small for high threshold values, since the density function $p_{st}(y)$ is close to zero for such cases.

For small threshold values, the behaviour of $n_{st}(V)$ will sensitively depend on both the intensity of the incoming particles, as well as on the signal shape. For high intensities, $n_{st}(V)$ will be small for low threshold values. In most cases the intensity has a maximum at a threshold value $V_{max}$. The knowledge of this quantity can be useful when trying to eliminate by thresholding the background noise which contaminates the useful signal. The reduction of this component can only be achieved by using a threshold greater than the threshold $V_{max}$, corresponding to the maximum of the intensity $n_{st}(V)$.

In many cases the value of the jump $\xi$ can be assumed to be constant, i.e.

$$\mathcal{P}\{\xi \le x\} = W(x) = \Delta\left(x - \frac{1}{\mu}\right) \tag{2.31}$$

hence one has

$$n_{st}(V) = s_0[P_{st}(V) - P_{st}(V - 1/\mu)] \tag{2.32}$$

since

$$\int_0^V p_{st}(y)\Delta\left(V - y - \frac{1}{\mu}\right)dy = \int_0^{V-1/\mu} p_{st}(y)\,dy = P_{st}(V - 1/\mu).$$

It will be seen that in the case of a constant jump, the determination of the density function $p_{st}(y)$ from the Laplace-transform $\tilde{p}_{st}(s)$ is not an easy task. The problems encountered will be shown for the pulse shape $f(t) = e^{-\alpha t}$.

In order to study the characteristics of the detector signal functions in more detail, in the next section we perform detailed calculations for a few selected pulse shapes $f(t)$.

## 3. Results for concrete cases

### 3.1. Rectangular pulses

In this case the particles, arriving at the detector according to a Poisson process, generate a signal with a constant width $T_0$ and random height $\xi$. Two different realisations of such a pulse are shown in Fig. 1. For simplicity, an exponential distribution of the amplitudes will be assumed, i.e.

$$\mathcal{P}\{\xi \le x\} = W(x) = 1 - e^{-\mu x}. \tag{3.1}$$

where $1/\mu$ is expectation of the starting amplitude of a single signal. Since

$$f(t) = \Delta(T_0 - t) \tag{3.2}$$

from (2.25) one obtains

$$\tilde{p}(s,t) = \exp\left\{-s_0\int_0^t \frac{s\Delta(T_0 - t')}{s\Delta(T_0 - t') + \mu}dt'\right\}. \tag{3.3}$$
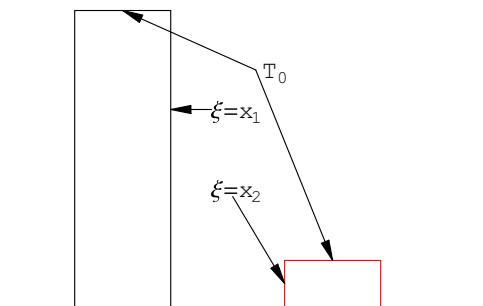


**Fig. 1.** Illustration of the rectangular pulses with random heights.

The integral in (3.3) can be performed analytically, leading to

$$\tilde{p}(s,t) = \begin{cases} \exp\left\{s_0 t\left(\dfrac{\mu}{s+\mu} - 1\right)\right\} & \text{if } t \le T_0 \\[2mm] \exp\left\{s_0 T_0\left(\dfrac{\mu}{s+\mu} - 1\right)\right\} & \text{if } t > T_0. \end{cases} \tag{3.4}$$

The resulting expressions can be inverted analytically, yielding the result as

$$p(y,t) = \begin{cases} e^{-s_0 t}\,e^{-\mu y}\left[\delta(y) + \sqrt{\dfrac{s_0 t\mu}{y}}I_1(2\sqrt{s_0 t\mu y})\right] & \text{if } t \le T_0 \\[3mm] e^{-s_0 T_0}\,e^{-\mu y}\left[\delta(y) + \sqrt{\dfrac{s_0 T_0\mu}{y}}I_1(2\sqrt{s_0 T_0\mu y})\right] & \text{if } t > T_0 \end{cases} \tag{3.5}$$

where $I_1(x)$ is the modified Bessel function of order one. It is worth noting that $p(y,t)$ converges rather fast to the asymptotically stationary density function $p_{st}(y)$ with increasing $t$. As the second part of (3.5) shows, the sum of the individual signals of particles arriving according to a homogeneous Poisson process with intensity $s_0$ has a stationary distribution already for $t > T_0$.

From the Laplace transform (3.4) we can get immediately the expected value of the sum of detector pulses at time $t$ as

$$\mathbf{E}\{\eta(t)\} = -\left[\frac{\partial \ln \tilde{p}(s,t)}{\partial s}\right]_{s=0} = \frac{s_0}{\mu}[t\Delta(T_0 - t) + T_0\Delta(t - T_0)] \tag{3.6}$$

and its variance as

$$\mathbf{D}^2\{\eta(t)\} = \left[\frac{\partial^2 \ln \tilde{p}(s,t)}{\partial s^2}\right]_{s=0} = 2\frac{s_0}{\mu^2}[t\Delta(T_0 - t) + T_0\Delta(t - T_0)]. \tag{3.7}$$

It is also worth noting that the *Fano factor* (variance to mean) for this case is equal to

$$\mathcal{F} = \frac{2}{\mu} \tag{3.8}$$

where $1/\mu$ is the expected value of the pulse jump. It is seen that the Fano factor does not depend on time.

For the illustration of the signal level crossing in the stationary case, we shall calculate the intensity $n_{st}(V)$ of particle arrivals which induce a jump of the signal from a level $y \le V$ to a signal level higher than $V$. Fig. 2. shows a possible realisation of the sum of pulses within a stationary time interval. The dots mark the particles which induce the jump of the signal level from a state $y \le V$ to above the threshold $V$. By using Eq. (2.29) we obtain

$$n_{st}(V) = s_0\int_{+0}^V e^{-\mu(V-y)}p_{st}(y)\,dy \tag{3.9}$$

where

$$p_{st}(y) = e^{-s_0 T_0}\,e^{-\mu y}\left[\delta(y) + \sqrt{\frac{s_0 T_0\mu}{y}}I_1(2\sqrt{s_0 T_0\mu y})\right].$$
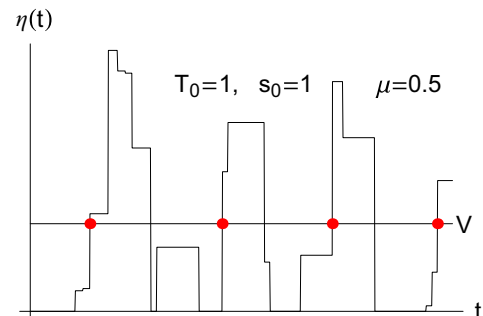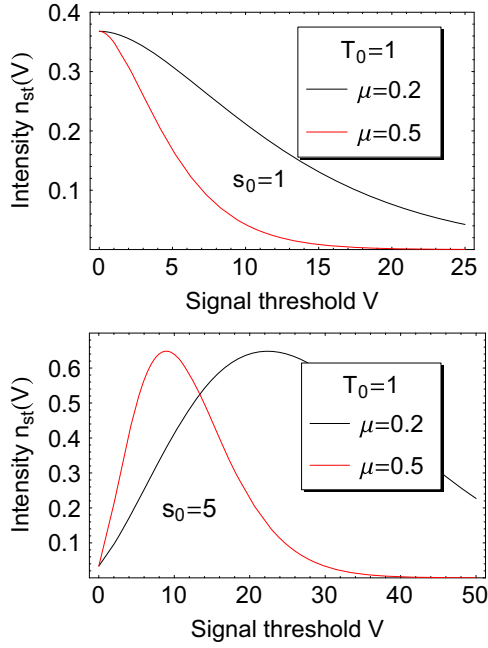


**Fig. 2.** A possible realisation of the sum of signals in an arbitrary time interval.

**Fig. 3.** Dependence of the intensity $n_{st}(V)$ on the signal threshold $V$ at two different input intensities $s_0$.



**Fig. 4.** Dependence of the output intensity $n_{st}(V)$ on the input intensity $s_0$ for two different values of $\mu$ and at two different threshold values $V$.

From this it follows that

$$n_{st}(V) = s_0\, e^{-s_0 T_0}\, e^{-\mu V} \int_0^V \left[ \delta(y) + \sqrt{\frac{s_0 T_0 \mu}{y}} I_1(2\sqrt{s_0 T_0 \mu y}) \right] dy$$
$$= s_0\, e^{-s_0 T_0}\, e^{-\mu V} I_0(2\sqrt{s_0 T_0 \mu V}), \tag{3.10}$$

where $I_0(x)$ is the modified Bessel function of order zero.

The dependence of the intensity $n_{st}(V)$ on the threshold $V$ is shown in Fig. 3 for two different values of $\mu$ and at two different input intensities $s_0$. It is seen how the values of $\mu$ and $s_0$ influence the dependence of the output intensity $n_{st}(V)$ on the threshold value $V$.

In order to show the influence of the input intensity $s_0$ on the output intensity $n_{st}(V)$, in Fig. 4 the dependence of $n_{st}(V)$ on $s_0$ is plotted for two threshold values $V$. One concludes that the mean amplitude $1/\mu$ of the rectangular signal must be chosen very carefully.

### 3.2. Exponential pulses

#### 3.2.1. Random amplitude

We will treat now the case when the pulses have an exponential decay shape

$$f(t) = e^{-\alpha t} \tag{3.11}$$

the initial values of which being the realisations of the random variable $\xi$. For simplicity, assume again exponential distribution of the amplitudes as in (3.1). Fig. 5. shows two possible pulses with $\alpha = 2$.

The probability density of the signal induced by one particle is given as

$$h(y,t) = \int_0^\infty \delta(y - xe^{-\alpha t}) w(x)\, dx \tag{3.12}$$

whose Laplace transform is obtained (for details, see [10]) as

$$\tilde{h}(s,t) = \frac{\mu}{\mu + s\, e^{-\alpha t}}. \tag{3.13}$$



**Fig. 5.** Exponential pulses generated by incoming particles.

Using (2.25) yields the Laplace transform of the density function $p(y,t)$ as

$$\tilde{p}(s,t) = \exp\left\{ -s_0 \int_0^t \left[ 1 - \frac{\mu}{\mu + s\, e^{-\alpha v}} \right] dv \right\}$$
$$= \exp\left\{ -s_0 \int_0^t \frac{s\, e^{-\alpha v}}{\mu + s\, e^{-\alpha v}}\, dv \right\}. \tag{3.14}$$

which leads to

$$\tilde{p}(s,t) = \exp\left\{ \frac{s_0}{\alpha} \ln \frac{\mu + s\, e^{-\alpha 1 t}}{\mu + s} \right\} = \left( \frac{\mu + s\, e^{-\alpha t}}{\mu + s} \right)^{s_0/\alpha}. \tag{3.15}$$

From (3.15) it is also obvious that a *stationary density function* exists with the Laplace transform

$$\lim_{t \to \infty} \tilde{p}(s,t) = \tilde{p}_{st}(s) = \left( \frac{\mu}{\mu + s} \right)^{s_0/\alpha}. \tag{3.16}$$

Eq. (3.15) can be rewritten as

$$\tilde{p}(s,t) = \left[ 1 - (1 - e^{-\alpha t}) \frac{s}{s + \mu} \right]^q \tag{3.17}$$

where

$$q = \frac{s_0}{\alpha} > 0. \tag{3.18}$$

The inversion of (3.17) will depend on the fact whether $q$ is an integer number or not. Details of the extensive calculations will be omitted here, these can be found in Ref. [10].
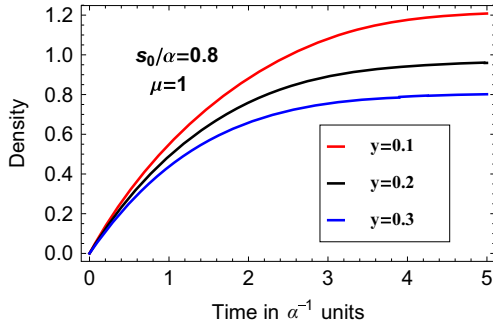
**Fig. 6.** Dependence of the density function $p(y,t)$ on the time parameter $\alpha t$ at three signal levels and at $q = s_0/\alpha = 0.8$.



**Fig. 7.** Dependence of the density function $p(y,t)$ on the time parameter $\alpha t$ at three signal levels for $q = s_0/\alpha = 2$.

If $q$ is not an integer and the following inequality holds

$$(1-e^{-\alpha t})\left|\frac{s}{s+\mu}\right| < q,$$

then, (3.17) can be written in the form

$$\tilde{p}(s,t) = 1 + \sum_{k=0}^{\infty}(-1)^k\frac{q(q-1)\cdots(q-k+1)}{k!}(1-e^{-\alpha t})^k\left(\frac{s}{s+\mu}\right)^k. \tag{3.19}$$

After considerable algebra, the inversion of (3.19), i.e that of (3.17), is obtained as

$$p(y,t) = \delta(y)\left[1 + \sum_{k=1}^{\infty}\frac{\Gamma(-s_0/\alpha+k)}{\Gamma(-s_0/\alpha)\Gamma(k+1)}(1-e^{-\alpha t})^k\right]$$
$$-\mu e^{-\mu y}\sum_{k=1}^{\infty}\frac{\Gamma(-s_0/\alpha)+k)}{\Gamma(-s_0/\alpha)\Gamma(k+1)}L_{k-1}^{(1)}(\mu y)(1-e^{-\alpha t})^k, \tag{3.20}$$

where $L_{k-1}^{(1)}(\mu y)$ is the generalised Laguerre polynomial.

Fig. 6. shows the dependence of the density function $p(y,t)$ on the parameter $\alpha t$ for $q = s_0/\alpha = 0.8$, for three different signal levels. It is interesting to note that the density function becomes constant relatively fast; in the present case the stationary behaviour is already reached for $\alpha t \approx 5$.

If $q = s_0/\alpha$ is a positive integer, expression (3.19) cannot be used. One has instead to return to Eq. (3.17) and use the rearrangement

$$\tilde{p}(s,t) = 1 - \sum_{k=1}^{q}\binom{q}{k}(-1)^{k-1}(1-e^{-\alpha t})^k\frac{s^k}{(s+\mu)^k}. \tag{3.21}$$

From this one obtains

$$p(y,t) = \delta(y)\left[1 - \sum_{k=1}^{q}\binom{q}{k}(-1)^{k-1}(1-e^{-\alpha t})^k\right]$$
$$+\mu e^{-\mu y}\sum_{k=1}^{q}\binom{q}{k}(-1)^{k-1}L_{k-1}^{(1)}(\mu y)(1-e^{-\alpha t})^k \tag{3.22}$$

which does not contain singular Gamma functions. Fig. 7 shows the dependence of the density function $p(y,t)$ on the parameter $\alpha t$ for $q = s_0/\alpha = 2$, for three different signal levels. One finds again that the density function is close to stationary already at $\alpha t \approx 5$.

We will now investigate the properties of the *stationary* signal sequence. The Laplace transform (3.16) of the density function $p_{st}(y)$ can easily be inverted. One obtains

$$p_{st}(y) = \frac{(\mu y)^{(s_0/\alpha)-1}}{\Gamma(s_0/\alpha)}e^{-\mu y}\mu \tag{3.23}$$

which shows that the stationary distribution of the sum of exponential pulses is given by

$$P_{st}(y) = \int_0^y p_{st}(y')\,dy' = \frac{\Gamma(s_0/\alpha)-\Gamma(\mu y, s_0/\alpha)}{\Gamma(s_0/\alpha)} \tag{3.24}$$
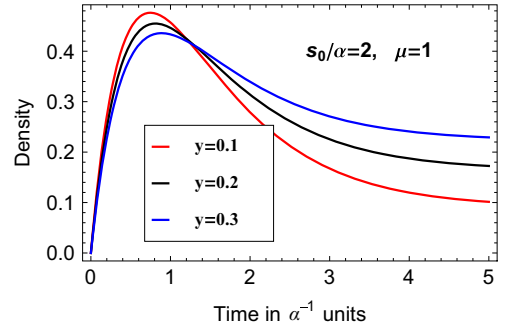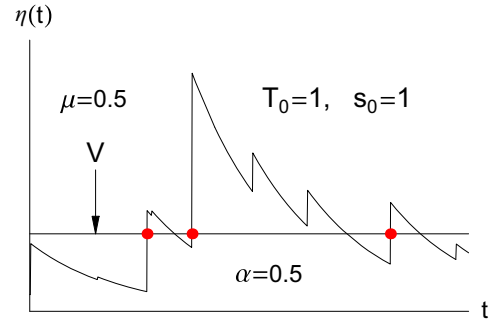
in which

$$\Gamma(\mu y, s_0/\alpha) = \int_{\mu y}^{\infty}\frac{v^{s_0/\alpha-1}}{\Gamma(s_0/\alpha)}e^{-v}\,dv$$

is the incomplete Gamma function.

Fig. 8 shows a possible realisation of the exponential pulse train in the stationary state. The dots mark the particles which induce a jump of the signal level to above the threshold $V$ from a level under $V$. By using (2.30) we obtain the Laplace transform

$$\tilde{n}_{st}(s) = s_0\frac{1-\tilde{w}(s)}{s}\tilde{p}_{st}(s) = s_0\frac{1}{\mu+s}\left(\frac{\mu}{\mu+s}\right)^{s_0/\alpha} \tag{3.25}$$

whose inverse is given as

$$n_{st}(V) = s_0\frac{(\mu V)^{s_0/\alpha}}{\Gamma(s_0/\alpha+1)}e^{-\mu V}. \tag{3.26}$$

Fig. 9 shows the dependence of the intensity $n_{st}(V)$ on the threshold $V$ for two different values of the parameter $\mu$. It is seen that the intensity $n_{st}(V)$ has a distinct maximum at the threshold

$$V_{max} = \frac{s_0}{\alpha\mu}.$$

The knowledge of this maximum could be important for the design of the detector electronics.

The expectation and the variance, important for practical applications, will now be calculated for both the non-stationary and the stationary case. From the logarithm of the Laplace transform (3.15) one obtains

$$-\left[\frac{d\ln\tilde{p}(s,t)}{ds}\right]_{s=0} = \mathbf{E}\{\eta(t)\} = \begin{cases}\frac{s_0}{\alpha\mu}(1-e^{-\alpha t}) & \text{if } t \leq \infty \\ \frac{s_0}{\alpha\mu} & \text{if } t = \infty\end{cases} \tag{3.27}$$



**Fig. 8.** A possible realisation of the sum of signals in stationary case in an arbitrary time interval.
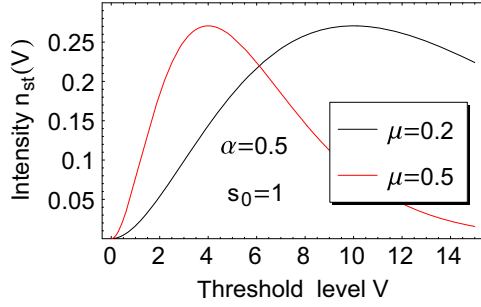
**Fig. 9.** Dependence of the intensity $n_{st}(V)$ on the signal threshold $V$.
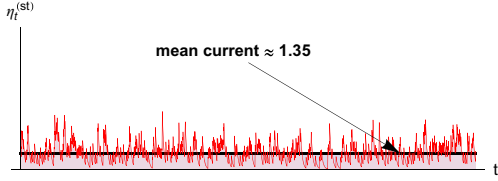


**Fig. 10.** Simulation of the stationary current $\eta_t^{(st)}$ of the ionisation chamber as a function of time, with exponentially decaying pulses of unit initial value (cf. Fig. 8).

and

$$\left[\frac{d^2 \ln \tilde{p}(s,t)}{ds^2}\right]_{s=0} = \mathbf{D}^2\{\eta(t)\} = \begin{cases} \frac{s_0}{\alpha\mu^2}(1-e^{-2\alpha t}) & \text{if } t \leq \infty \\ \frac{s_0}{\alpha\mu^2} & \text{if } t = \infty. \end{cases} \quad (3.28)$$

For illustration, the Fano factor for this case is also given. It reads as

$$\mathcal{F} = \begin{cases} \frac{1}{\mu}(1+e^{-\alpha t}) & \text{if } t \leq \infty \\ \frac{1}{\mu} & \text{if } t = \infty. \end{cases} \quad (3.29)$$

### 3.2.2. Constant amplitude

For more insight, the special case of constant pulse amplitudes, i.e. when the amplitude probability density function is given as $w(x) = \delta(x - x_0)$, will be calculated. From (3.12) one has

$$h(y,t) = \delta[y - x_0 \, e^{-\alpha t}] \quad (3.30)$$

whose Laplace transform is obtained as

$$\tilde{h}(s,t) = \exp[-s\,x_0\,e^{-\alpha t}]. \quad (3.31)$$

Substituting into (2.26) yields

$$\tilde{p}_{st}(s) = \exp\left\{-s_0 \int_0^\infty [1 - \exp[-s\,x_0\,e^{-\alpha t}]]\,dt\right\} \quad (3.32)$$

from which one obtains

$$\tilde{g}_{st}(s) = \ln \tilde{p}_{st}(s) = s_0 \int_0^\infty [\exp(-s\,x_0\,e^{-\alpha t}) - 1]\,dt. \quad (3.33)$$

From (3.33), one can immediately determine the expectation and the variance of $\eta^{(st)}$. One obtains

$$\mathbf{E}\{\eta^{(st)}\} = s_0\frac{x_0}{\alpha} \quad \text{and} \quad \mathbf{D}^2\{\eta^{(st)}\} = s_0\frac{x_0^2}{2\alpha} \quad (3.34)$$

whereas the Fano factor equals $\mathcal{F} = x_0/2$.

Fig. 10 shows the time dependence of the stationary current $\eta_t^{(st)}$ of the ionisation chamber, when the current is formed by exponentially decaying pulses of unit initial value. Except for the level crossing and the random amplitude of the pulses, this figure is analogous to Fig. 8, but shows a much longer time period of the

process. For this case one has

$$\mathbf{E}\{\eta_t^{(st)}\} \approx 1.35 \quad \text{and} \quad \mathbf{D}^2\{\eta_t^{(st)}\} \approx 0.58.$$

The inversion of (3.32) is a formidable task, and one way of performing it will be only outlined here. For the details we refer to Ref. [10]. With a change of variables the integration can be performed and (3.32) can be written as

$$\tilde{p}_{st}(s) = \exp\left[-\frac{s_0}{\alpha}\left(C + \ln x_0 s + \int_{x_0}^\infty \frac{e^{-su}}{u}\,du\right)\right] = \frac{\exp\left(-\frac{s_0}{\alpha}\int_{x_0}^\infty \frac{e^{-su}}{u}\,du\right)}{(x_0\,e^C s)^{s_0/\alpha}}. \quad (3.35)$$

Eq. (3.35) is written in the following, absolute convergent, infinite series:

$$\tilde{p}_{st}(s) = \frac{1}{(x_0\,e^C)^{s_0/\alpha}}\left\{\frac{1}{s^{s_0/\alpha}} + \sum_{n=1}^\infty (-1)^n \frac{1}{n!}\left(\frac{s_0}{\alpha}\right)^n \frac{1}{s^{s_0/\alpha}}\left(\int_{x_0}^\infty \frac{e^{-su}}{u}\,du\right)^n\right\}. \quad (3.36)$$

After a considerable algebra it can be shown that the inverse Laplace transform of (3.36) can be given by formula

$$p_{st}(y) = \frac{1}{(x_0\,e^C)^{s_0/\alpha}\Gamma(s_0/\alpha)}$$
$$\left\{y^{s_0/\alpha-1} + \sum_{n=1}^{[y/x_0]} \frac{(-1)^n(s_0/\alpha)^n}{n!}\int_{n\,x_0}^y (y-u)^{s_0/\alpha-1}h_n(u)\,du\right\} \quad (3.37)$$

where $[y/x_0]$ is the largest integer less or equal to $y/x_0$. The function $h_n(u)$ is defined by the recursive equation

$$h_n(u) = \int_{x_0}^{u-(n-1)x_0} \frac{h_{n-1}(u-v)}{v}\,dv \quad (3.38)$$

with the starting function

$$h_1(u) = \frac{1}{u}\Delta(u-x_0).$$

The next term is still simple to calculate with the result

$$h_2(u) = \int_{x_0}^{u-x_0} \frac{dv}{(u-v)v} = 2\frac{\ln\left(\frac{u}{x_0}-1\right)}{u}\Delta(u-2x_0) \quad (3.39)$$

However, calculation of the third term already shows that the complexity of the expressions increase drastically with the order of the terms:

$$h_3(u) = \frac{1}{6u}\left\{\pi^2 + 24\ln\frac{x_0}{u-2x_0}\ln\frac{x_0}{u-x_0}\right.$$
$$- 12\,\text{PolyLog}\left[2, 1+\frac{x_0}{x_0-u}\right]$$
$$\left.+ 12\,\text{PolyLog}\left[2, \frac{x_0}{u-x_0}\right] + 12\,\text{PolyLog}\left[2, 2-\frac{u}{x_0}\right]\right\}\Delta(u-3x_0) \quad (3.40)$$

where

$$\text{PolyLog}(n,x) = \text{Li}_n(x) = \sum_{k=1}^\infty x^k/k^n$$

is the Jonquiérés function.

The subsequent terms are still possible to calculate with *Mathematica*, but they are prohibitively long to reproduce in print.

By using the *Mathematica code* the dependence of the stationary density function $p_{st}(x)$ on $x$ has been calculated in the case of constant $x_0 = 1$ amplitude for three different $s_0/\alpha$ parameter values. In Fig. 11 one can see that the value of the ratio $s_0/\alpha$ sensitively influences the shape of $p_{st}(x)$. This sensitivity has to be taken into account by the construction of the detector electronics.
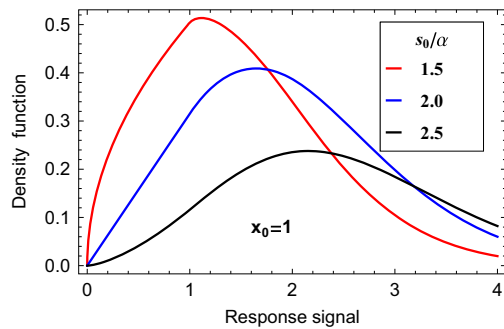
**Fig. 11.** Probability density function of the stationary current $\eta_t^{(st)}$ of the ionisation chamber with exponentially decaying pulses of constant $x_0 = 1$ amplitude with three different $s_0/\alpha$ parameter values.

## 4. Conclusions

In this report the theory of the Campbell method and that of the so-called higher order Campbelling techniques was revisited, as applied to the signals of ionisation chambers, with the fission chamber as the main interest of applications. First, a compact derivation was given of the higher order Campbell relationships for the case of an incoming particle sequence with a non-homogeneous Poisson distribution and with arbitrary signal amplitude distributions and signal shapes. The derivation is based on the integral form of the backward equation and it shows considerable resemblance to a similar formula in neutron branching processes, connecting the source-induced and single-particle induced distributions. For pulse forms which commence with a jump from zero to a maximum value after which they decay monotonically or remain constant for some time, a formula was given for the intensities of crossing a threshold level from below.

Concrete analytical solutions were given for the full probability distribution of the signal amplitudes, the first two moments and the level crossing intensities for two selected signal forms; a square and an exponential pulse form. In both cases an exponential amplitude distribution was assumed; for the exponential pulse, also the case of constant amplitude was considered.

In addition to giving insight, these results can also serve for benchmarking of Monte-Carlo codes. The explicit results presented in this report can serve to benchmark the accuracy of the higher order moments of the Monte Carlo simulation results. After benchmarking against the theoretical results presented in this papers, such codes can be used to calculate also other pulse forms (triangular, gamma-distribution-form, etc.) which are not amenable for analytical solutions.

It is a pre-requisite of applying the Campbell method that the particle arrivals to the detector constitute a Poisson process, and their responses are independent. In reality these conditions are usually not fulfilled. It appears therefore interesting to extend the theoretical model calculate the distribution function of the detector signal if the individual responses are not independent. This would give a possibility to determine higher order moments of the statistics of the neutron arrival times to the detector, to be used for diagnostic purposes. A further open question is whether interaction between the charges generated by the ionising particles, in the present case by the fission products, can be modelled by response functions, characterised by independent probability distributions.
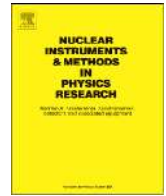
## References

[1] P. Filliatre, C. Jammes, B. Geslot, L. Buiron, Annals of Nuclear Energy 37 (11) (2010) 1435.
[2] P. Filliatre, L. Oriol, C. Jammes, L. Vermeeren, Nuclear Instruments and Methods in Physics Research Section A 593 (2008) 510.
[3] A. Papoulis, Probability, Random Variables and Stochastic Processes, 3rd Edition, McGraw-Hill Inc., New York, 1991.
[4] H.L. Pécseli, Fluctuations in Physical Systems, Cambridge University Press, Cambridge, 2000.
[5] I. Lux, A. Baranyai, Nuclear Instruments and Methods in Physics Research 202 (1982) 469.
[6] I. Lux, A. Baranyai, Nuclear Instruments and Methods in Physics Research 202 (1982) 477.
[7] B. Bärs, Nuclear Instruments and Methods in Physics Research Section A 275 (1989) 403.
[8] S. Chabod, G. Fioni, A. Letourneau, F. Marie, Nuclear Instruments and Methods in Physics Research Section A 566 (2006) 633.
[9] E.W. Pontes, A. Ferreira, IEEE Transactions on Nuclear Science NS-53 (2006) 1292.
[10] L. Pál, I. Pázsit, Comments on the Stochastic Characteristics of Fission Chamber Signals, Technical Report CTH-NT-284, Chalmers University of Technology, 2013.
[11] L. Pál, I. Pázsit, Ionization chamber signals in a fissile medium, 2014, to be submitted.
[12] I. Pázsit, L. Pál, Neutron Fluctuations: A Treatise on the Physics of Branching Processes, 1st Edition, Elsevier, New York, 2008.
[13] L. Pál, The foundations of probability theory and statistics, I., II., (in Hungarian) Akadémiai Kiadó, Budapest, 1995.

# Paper II

Remark on the applicability of Campbelling techniques for transient signals

Zs. Elter, I. Pázsit and C. Jammes

Contents lists available at ScienceDirect

# Nuclear Instruments and Methods in Physics Research A

journal homepage: www.elsevier.com/locate/nima

Technical Notes

# Remark on the applicability of Campbelling techniques for transient signals

Zs. Elter [a,b,*], I. Pázsit [a], C. Jammes [b]

[a] Chalmers University of Technology, Department of Applied Physics, Division of Nuclear Engineering, SE-412 96 Göteborg, Sweden
[b] CEA, DEN, DER, Instrumentation, Sensors and Dosimetry Laboratory, Cadarache, F-13108 Saint-Paul-lez-Durance, France

A B S T R A C T

The signals of fission chambers are traditionally evaluated with Campbelling methods at medium count rates. Lately there has been a growing interest in the extension of Campbelling methods to cover a wider range of count rates.

These methods are applied to measure the neutron flux in the stationary state of the reactor. However, there has not been any attempt to generalize these techniques for transient reactor states. This short note is devoted to a discussion of this question. It is shown through analytic and numerical calculations that for practical reasons the traditional, stationary Campbelling methods can be applied for transient scenarios as well.

© 2016 Elsevier B.V. All rights reserved.

## 1. Introduction

The signals of fission chambers are traditionally evaluated with different techniques for different count rates: pulse counting at low count rates, Campbelling methods at medium ($10^5$–$10^8$ $s^{-1}$) count rates and current mode at high count rates. Due to the fast development of hardware (such as Field Programmable Gate Arrays), there has been lately a growing interest in the extension of the Campbelling methods to extend their count rate applicability range. These methods will be implemented in the neutron flux monitoring system of sodium cooled fast reactors.

The most common application of fission chambers in a core monitoring system is to measure the neutron flux in the stationary state of the reactor [1]. As is well known, in such a case, it is advantageous to use the so-called Campbell relationships. Assuming that the detector signal $\eta(t)$ can be described as a filtered Poisson process or shot noise, (i.e. the signal is formed as the superposition of constant pulse shapes $f(t)$ with random amplitudes $\mathbf{q}$, induced by independent incoming events), the cumulants of the signals (i.e. the measurable quantity) are proportional to the count rate of the detection events (i.e. the quantity of interest). For the first two cumulants (or moments) this is expressed by the Campbell theorem. For a homogeneous, stationary signal $\eta(t)$ (and $\eta^{(st)} = \lim_{t \to +\infty} \eta(t)$), the general form of the Campbell relationships, including also higher order cumulants, is given as [2]

$$\kappa_n^{(st)} = s_0 \langle q^n \rangle \int_{-\infty}^{+\infty} f(t)^n \, dt \qquad (1)$$

where $\kappa_n$ is the $n$th order cumulant, $s_0$ is the count rate and $q$ is the random amplitude of the pulses (related to the collected charge). Commonly, the methods in which $n \geq 3$ are called as higher order Campbelling methods.

Although Eq. (1) might look as an expression of ergodicity, in which an ensemble average is replaced by a time average, it is actually not (although its validity assumes stationarity). Namely, (1) is not a prescription of the measurement (estimation) of the cumulants by time averaging; it merely expresses the theoretical values of the cumulants, defined by ensemble averaging, by parameters of the signal itself. Its only use is to show that all cumulants are proportional to the detection intensity, by also giving the proportionality factors. It also shows that, theoretically (with "clean", noiseless signals), minority (parasitic) components (such as unwanted contributions from gamma detection events) can be suppressed by higher order Campbelling methods.

The actual estimation of the stationary values of the cumulants is indeed based on time averaging methods, which assume ergodicity. These are based on the measured signal $\eta(t)$ itself and not on the pulse shape $f(t)$ of the individual detection events:

$$\mathbf{E}\{\eta\} = \frac{1}{T} \int_0^T \eta(t) \, dt \qquad (2)$$

* Corresponding author at: CEA, DEN, DER, Instrumentation, Sensors and Dosimetry Laboratory, Cadarache, F-13108 Saint-Paul-lez-Durance, France.
  Tel.: +33 4 4225 3926; fax: +33 4 4225 7876.
  E-mail address: zsolt@nephy.chalmers.se (Zs. Elter).

and

$$\mathbf{D}^2\{\eta\} = \frac{1}{T} \int_0^T (\eta(t) - \mathbf{E}\{\eta\})^2 \, dt, \tag{3}$$

or rather their discrete forms where the integrals are replaced by sums over the digitized sampled values of the signal. Due to the finiteness of the measurement duration $T$, the estimation procedures (2) and (3) are of course associated with errors. In order to have a sufficiently small statistical error, the sampling time $T$ must be long enough.

The question may arise how the accuracy of the estimation deteriorates in case that the measured neutron flux (i.e. the intensity of the primary detection events) changes, such as in case of a transient. It can be alternatively formulated such as how fast a transient can be detected and followed up with a given accuracy, or how long time it takes after a step change in the flux (intensity of the detection events) before the estimate, based on time averaging methods, supplies accurate enough values. This short note is devoted to the discussion of this question.

## 2. Ensemble averages

One notices that the deterioration of the estimate in a transient is due to two independent matters, and the main purpose of this note is to highlight and discuss these two different phenomena. The first one is the fact that after a step change of the intensity of the detection events (sudden increase or decrease of the neutron flux), it takes time for the detector signal itself to reach its stationary (asymptotic) value, such that Eq. (1) becomes valid. This behaviour is a purely theoretical effect, which has nothing to do with the estimation procedure. Due to the properties of the process, for all moments (cumulants), defined by ensemble averages, it will take time before they reach the stationary state. This transient is actually a consequence of the non-Markovian character of the filtered Poisson process: the evolution of the detector signal from a time instant $t_0$ is not uniquely determined by the value of the signal at $t = t_0$, but is also a function of all previous detection events which result in a non-zero contribution to the signal at time $t_0$. In other words, the transient is due to the memory of the process. In comparison, for a Markovian process, such as a Poisson point process, a step change of the event intensity incurs an immediate step change of all cumulants, since the process has no memory.

It may be surmized, however, that for the case of fission chamber signals, the transient period is rather short, since the filtered Poisson process has a rather short memory. For a pulse shape with a finite width (length) $\tau$, i.e. if $f(t) = 0$ for $t \geq \tau$, the memory length is equal to $\tau$, since no events for $t < t_0 - \tau$ can influence the signal for $t > t_0$. For an exponentially decaying pulse

shape, the memory is infinite in principle; however, roughly speaking, for an error less than e.g. 1%, the memory duration can be taken as the time it takes from the beginning of the pulse until the signal decreases to 1% of its maximum value. Since in the Campbelling mode the signal is always assumed to contain a large number of detection events, a memory whose length is comparable with the width of a single pulse will only have a minor effect.

As it was shown in [2], the time-dependence of the theoretical cumulants after a step change of the detection intensity from zero to a finite value $s_0$ at $t = 0$ can be calculated from a Chapman–Kolmogorov (master) equation, despite of the non-Markovian property of the process. This is possible only by using the integral form of the backward master equation with zero initial conditions. This is an enormous strength of the integral backward master equation, which is the reason why it is the preferred form of the master equation in the theory of branching processes [3], even in cases when its use is not necessary.

Qualitative and quantitative results can be given by using the general theoretical results obtained in [2] for any given pulse shape $f(t)$ and pulse amplitude distribution (or its expectations $\langle q^n \rangle$). For illustration, we will choose a normalized damped exponential pulse shape in the form

$$f(t) = \frac{e^{-t/p_1} - e^{-t/p_2}}{\int_0^\infty \left(e^{-t'/p_1} - e^{-t'/p_2}\right) dt'} \tag{4}$$

which is a fair representation of fission chamber pulses. For the amplitude distribution, we will choose either a deterministic case with a constant amplitude $q_0$, or an exponentially distributed amplitude with a mean equal to $\mu^{-1}$. Using the formulae obtained in [2], for the first case (constant amplitude) one has

$$\kappa_n[\eta(t)] = (-1)^n \left[ \frac{d^n \left( -s_0 \int_0^t [1 - e^{-sq_0 f(t')}] \, dt' \right)}{ds^n} \right]_{s=0}, \tag{5}$$

and for the exponentially distributed charge (amplitude) one has

$$\kappa_n[\eta(t)] = (-1)^n \left[ \frac{d^n \left( -s_0 \int_0^t \left[1 - \frac{\mu}{\mu + sf(t')}\right] dt' \right)}{ds^n} \right]_{s=0} \tag{6}$$

with $f(t)$ given in (4).

The above expressions can be evaluated analytically by using the symbolic manipulation code Mathematica. Since the analytic expressions are rather involved, instead of giving these, the results for a pulse shape defined with Eq. (4) are plotted in Fig. 1 with realistic parameters. The following parameter values were used: $p_1 = 20$ ns, $p_2 = 4$ ns, $q_0 = \mu^{-1} = 0.1$ pC which defines a pulse with around 100 ns width and amplitude with µA as order of magnitude.

Fig. 1a illustrates the function $1 - \frac{\kappa_n(t)}{\kappa_n^{(st)}}$ to give an idea about the convergence time. The results show that the values of the theoretical cumulants converge quickly to their stationary values. The
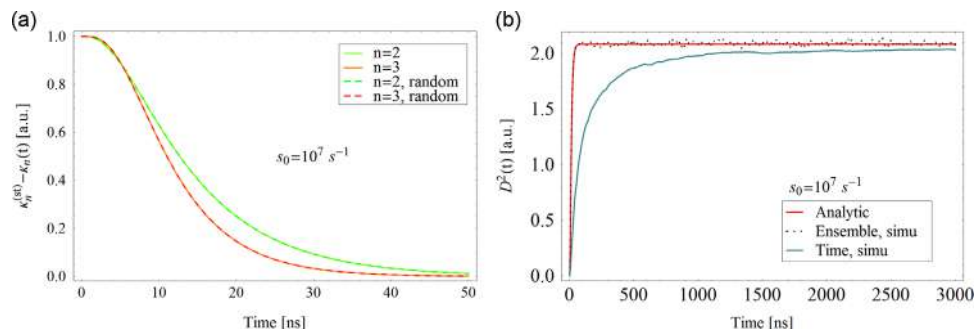


**Fig. 1.** Convergence of the cumulants to the stationary value. (a) Convergence for several orders ($s_0 = 10^7 \, s^{-1}$). (b) Convergence of sample and temporal moments by simulation.
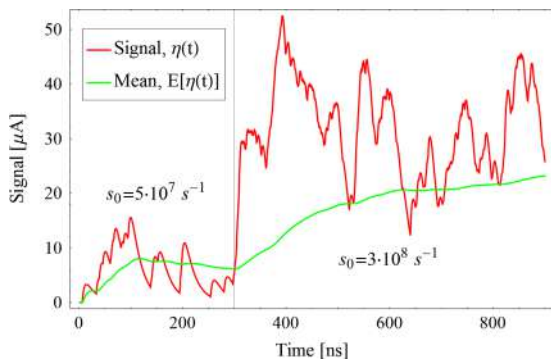
**Fig. 2.** Illustration of a non-stationary signal and its time-averaged mean.

convergence time can be measured in tens of *ns*, which is comparable with the pulse width. Neither the amplitude distribution, nor the count rate has any impact on the speed of the convergence, which is understandable from the considerations on the relationship between the convergence time and the pulse width, discussed previously. The independence of the duration of the transient from the count rate is also seen from Eqs. (5) and (6) where it appears as just a constant multiplier.

It is also seen that the higher the order of the cumulant, the faster the convergence is. This is also understandable if one relates the convergence time (the duration of the transient) to the time it takes for the signal to decrease to, say, 1% of its maximum value. Since in the *n*th order cumulant the expression $f^n(t)$ appears, it is the decay speed of $f^n(t)$ which determines the time of the transient. For monotonically decaying signals, the decrease of $f^n(t)$ to 1% of its maximum value will be the shorter, the larger $n$ is. Hence it is seen that the use of the higher order cumulants is useful not only for the suppression of the unwanted minority components, but also for a shorter transient time of the signal. However, it also has to be added that this refers to the true value (ensemble average) of the cumulants. In a measurement, only an estimate of these can be obtained by time averaging methods, as will be discussed below, for which such a conclusion cannot be drawn.

Although the quantitative results here refer to a particular pulse shape, the conclusions will be similar for other pulse shapes. The quantitative values may differ, but the results will be similar in the sense that the convergence time will be closely related to the pulse width.

## 3. Estimates by time averages

The second circumstance that affects the possibility of determining the detection intensity by Campbelling techniques, for transient signals is related to the estimation of the cumulants by time averaging methods over a finite time duration. This leads to a certain error even for stationary signals. For non-stationary signals, which are not ergodic, the errors will obviously become larger, since the time averages used for the estimation of the ensemble average will not hold even asymptotically. For such a case the stationary estimates (2) and (3) have to be replaced by

$$\mathbf{E}\{\eta\} = \frac{1}{2T} \int_{t-T}^{t+T} \eta(t')\, dt' \tag{7}$$

and

$$\mathbf{D}^2\{\eta\} = \frac{1}{2T} \int_{t-T}^{t+T} (\eta(t') - \mathbf{E}\{\eta(t')\})^2\, dt' \tag{8}$$

Obviously, (7) and (8) will not become exact even for $T \to \infty$. This

will induce a further error in the estimation, in addition to the error due to the finiteness of the time interval of the averaging. Besides, reconstructing the fast variation of the detection intensity would require a short time averaging, which, on the other hand, would deteriorate the statistical accuracy of the estimation.

Clearly, the accuracy of the time average estimation of the cumulants for non-stationary detection intensities cannot be investigated by analytical models and methods. Therefore, numerical simulations were carried out to estimate the convergence of the time cumulants. The simulations were performed with the toolbox described in [4]. For the current purpose several pulse trains were generated, and the quantities defined in Eqs. (7) and (8) were evaluated, and compared to the theoretical (ensemble based) moments. Fig. 2 shows such a simulation by showing the realisation of the signal together with its time-averaged mean value for the case of a step change in the count rate.

Results are shown in Fig. 1b for the second order moments, where both the time average and the ensemble average transient values are displayed after a step change of the detection intensity from zero to a finite value at $t=0$. It is seen that the ensemble and the time averaged cumulants converge to the same value, which is an expression of asymptotic ergodicity of the process, here not only for the expectation but also for the higher moments. It is also seen that, as expected, the convergence of the time averaged estimate is much slower (thousands of ns).

## 4. Conclusions

In practice the above-mentioned phenomena bear low importance. Except for very abrupt changes in the flux, the time averaging methods can follow moderate variations without delay and even a step change in the order of seconds. The study reported here was meant to give insight into the facts that govern the performance of the Campbelling methods for cases when the Campbell formulae are not valid, and to give some quantitative estimates.

It was shown that in practical situations (the change of the count rate is slower than few thousand ns) the signal can be considered as a transition of quasi-stationary signals, therefore no special Campbell-equation has to be derived to measure transient events.

## References

[1] C. Jammes, et al., Nuclear Engineering and Design 270 (2014) 273, http://dx.doi.org/10.1016/j.nucengdes.2013.12.057.
[2] L. Pál, I. Pázsit, Zs. Elter, Nuclear Instruments and Methods in Physics Research Section A: Accelerators, Spectrometers, Detectors and Associated Equipment 763 (2014) 44.
[3] I. Pázsit, L. Pál, Neutron Fluctuations: A Treatise on the Physics of Branching Processes, 1st ed., Elsevier, New York, 2008.
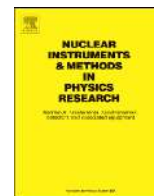[4] Zs. Elter, C. Jammes, I. Pázsit, P. Filliatre, Nuclear Instruments and Methods in Physics Research Section A: Accelerators, Spectrometers, Detectors and Associated Equipment 774 (2015) 60, http://dx.doi.org/10.1016/j.nima.2014.11.065.

# Paper III

Performance investigation of the pulse and Campbelling modes of a fission chamber using a Poisson pulse train simulation code

Zs. Elter, C. Jammes, I. Pázsit, L. Pál and P. Filliatre

# Performance investigation of the pulse and Campbelling modes of a fission chamber using a Poisson pulse train simulation code

CrossMark

Zs. Elter [a,b], C. Jammes [a,*], I. Pázsit [b], L. Pál [c], P. Filliatre [a]

[a] CEA, DEN, DER, Instrumentation, Sensors and Dosimetry Laboratory, Cadarache, F-13108 Saint-Paul-lez-Durance, France
[b] Chalmers University of Technology, Department of Applied Physics, Division of Nuclear Engineering, SE-412 96 Göteborg, Sweden
[c] Centre for Energy Research, Hungarian Academy of Sciences, H-1525 Budapest 114, POB 49, Hungary

## ABSTRACT

The detectors of the neutron flux monitoring system of the foreseen French GEN-IV sodium-cooled fast reactor (SFR) will be high temperature fission chambers placed in the reactor vessel in the vicinity of the core. The operation of a fission chamber over a wide-range neutron flux will be feasible provided that the overlap of the applicability of its pulse and Campbelling operational modes is ensured. This paper addresses the question of the linearity of these two modes and it also presents our recent efforts to develop a specific code for the simulation of fission chamber pulse trains. Our developed simulation code is described and its overall verification is shown.

An extensive quantitative investigation was performed to explore the applicability limits of these two standard modes. It was found that for short pulses the overlap between the pulse and Campbelling modes can be guaranteed if the standard deviation of the background noise is not higher than 5% of the pulse amplitude. It was also shown that the Campbelling mode is sensitive to parasitic noise, while the performance of the pulse mode is affected by the stochastic amplitude distributions.

© 2014 Elsevier B.V. All rights reserved.

## 1. Introduction

Sodium-cooled fast reactors (SFRs) are among the advanced reactors selected by the Generation IV International Forum. In order to meet needs of $CO_2$-zero-emission energy supply beyond 2030, the French government asked, in the year 2006, CEA, namely the French Alternative Energies and Atomic Energy Commission, to lead the development of an innovative GEN-IV nuclear-fission power demonstrator. The major objective is to improve the safety, reliability and availability of an SFR. The foreseen GEN-IV SFR is thus an innovative pool-type SFR featuring a negative sodium-void reactivity coefficient [1]. In addition, the instrumentation and more particularly the monitoring and online diagnostics will be enhanced.

The design of the neutron flux monitoring (NFM) system of the French GEN-IV SFR was discussed in Ref. [2]. As in any reactor, the NFM's main objectives are not only reactivity control and power level monitoring, but also the monitoring of flux distribution within the core regions in order to prevent any local melting accident. Given that the neutron shield of a pool-type SFR is contained in the reactor vessel, the neutron instrumentation is

planned to be installed in the vessel in order to monitor the neutron flux over a wide range, that is from startup to the full power of 1500 MW. High temperature fission chambers (HTFCs) were proved to be the most appropriate for this purpose [3,4]. An HTFC has to operate in an extreme environment. All the three prospective locations are in the vicinity of the core with a temperature from 400 °C to 550 °C at full power [4]. Although the development of the HTFCs had already been carried out at CEA from the early 1980s to the late 1990s, there is room for enhancing their robustness and capability [5,4]. All these activities are part of our research program in support of the French GEN-IV SFR nuclear instrumentation and take advantage of our past and recent experience in that domain.

The wide-range capability of a fission chamber requires a sufficient overlap of the signal processing modes in the so-called pulse and Campbelling regime [6] in order to ensure the linearity of the neutron flux measurement [4]. As will be described in more detail later, the processing of the detector signal is different for low and high detector event intensities, i.e. when the signal has the shape of individual "spikes" or consists of overlapping pulses that become a continuous signal for high event rates. The goal is in both cases to determine the detection event rate, which is proportional to the neutron flux. For low event rate the individual pulses are counted by a threshold counting technique (pulse mode) while for overlapping and

* Corresponding author. Tel.: +33 4 4225 3926; fax: +33 4 4225 7876.
  *E-mail address:* christian.jammes@cea.fr (C. Jammes).

continuous signals, i.e. high event intensity, the intensity is extracted by calculating the higher moments of the digitized detector signal (Campbelling technique). These two modes use different electronics and data processing. The term "linearity" or "mode overlapping" means that there is a region of intermediate event intensity when both methods work and supply the same result.

It has been claimed that the mode overlap could be achieved by lowering the electron collection time and hence the width of the individual fission pulses. A well-known solution to decrease the charge collection time is to add a few percents of polyatomic gas such as nitrogen [7,8]. However, it was observed that nitrogen molecules disappear under irradiation at high temperature of an SFR. In order to circumvent this loss, it was proposed to saturate all the chamber parts with nitrogen [4]. Given that the industrial qualification of this treatment is still uncertain, an alternative solution for the wide-range HTFC operation is sought.

In theory, the Campbelling technique could be used for both low and high detector event intensities, and the Campbelling techniques can be treated theoretically [9]. Therefore it might appear as if there is no need either for ensuring the linearity of the modes or for numerical simulations. However, in reality, electronic and other parasitic noise make the measurement inaccurate, and for low event rates application of the Campbelling technique becomes impractical and indeed impossible. Hence the existence of the mode linearity is not at all granted. Its validity cannot be investigated with pure theoretical methods either; concrete results for the moments of the signal can be obtained in a closed form only for certain signal shapes [9]. Even for these cases, the influence of parasitic noise cannot be assessed analytically, thus an analytical sensitivity and uncertainty analysis is not possible.

Hence, in order to address the question of the linearity of the pulse and Campbelling modes, a specific code was developed for the simulation of fission chamber pulse trains. The code can handle arbitrary signal shapes, amplitude distributions and the presence of added noise. With the help of the code, a quantitative analysis of the mode linearity was made. On the long run, this code aims at improving the signal processing of the future NFM system of the French GEN-IV SFR.

In this paper the principles of the code, its verification, and the results of the quantitative analysis of the mode linearity are described. First, a brief overview of the typical instrumentation based on a fission chamber is given. Second, the filtered Poisson process that permits to describe a conditioned signal of a fission chamber is discussed. Third, our developed simulation code is described and its overall verification is shown. Finally, the performances of the pulse and Campbelling modes are investigated.

## 2. Neutron monitoring instrumentation

### 2.1. Fission chamber

Fission chambers are nuclear detectors that are widely used to deliver online neutron flux measurements [6,5,10,11]. This type of detector is an ionization chamber containing fissile material in order to detect neutrons. The most common design consists of one or more coaxial electrode pairs, at least one electrode of which is coated with a fissile layer from a few micrograms to a few grams. The spacing between each anode and electrode goes from tens of microns to few millimeters. The chamber itself is filled with an argon-based gas pressurized at a few bars. When a neutron reaches the fissile coating, it is likely to induce a fission that generates two heavily charged ions, the fission products emitted in two nearly opposite directions. The one emitted out of the fissile layer ionizes the filling gas along its trajectory. Given that a DC-voltage of a few hundred volts is applied between the electrodes, the electrons and

positive ions drift across the filling gas in opposite direction, and generate a current signal. That DC-voltage must be high enough to collect all the charges, and low enough to prevent the production of secondary ionization pairs. If both conditions are fulfilled, the fission chamber operates in the so-called saturation regime [6,5], for which the neutron-induced current signal is proportional to the fission rate and nearly insensitive to the DC-voltage. In addition, one can note that the gamma particles that directly ionize the filling gas also generate a signal.

The proper operation of a fission chamber as well as its output signal chiefly depend on the following characteristics: (i) high voltage bias, (ii) inter-electrode distance, (iii) filling gas pressure and composition and (iv) nature and amount of fissile material.

### 2.2. Electronics

The conditioning electronics of a typical neutron flux-monitoring system consists of the detector itself, a high electromagnetic immunity cable and a current-sensitive pre-amplifier that converts the current flowing through the detector into a measurable voltage [12]. Such a pre-amplifier has to feature a very low input impedance compared to that of the fission chamber. As it will be hereafter described, a fission chamber can operate in three different modes: (i) pulse mode, (ii) Campbelling mode or (iii) current mode. Only the pulse and Campbelling modes, which allow for the neutron–gamma discrimination, will be addressed in this paper. In case of pulse mode, the acquisition system consists of a discriminator directly connected to a counter. The discriminator generates a logic signal if its analog input signal becomes larger than a predefined threshold. In case of Campbelling mode, the acquisition nowadays consists of a frequency band-pass filter, an analog-to-digital converter and a processing unit for variance calculation. The corresponding electronics is summarized in Fig. 1.

The signal was simulated as it arrives from the pre-amplifier. Since in the count rate range considered here the band-pass filter does not have an impact, it was not included into the simulation.

## 3. Signal modeling and processing

### 3.1. Filtered Poisson process

According to the previously described facts, the fission chamber signal can be idealized as a Poisson pulse train, or shot noise. In the literature the mathematical model behind these processes is often called a filtered Poisson process [13]. In such a stochastic process the time interval between each pair of consecutive events has an exponential distribution with an intensity parameter $s_0$ [14]. In the present case the intensity or the count rate is determined by the environment of the detector (e.g. reactor core) and is proportional to the neutron flux level. The consecutive events are pulses, hence the total signal is a superposition of pulses of the form:
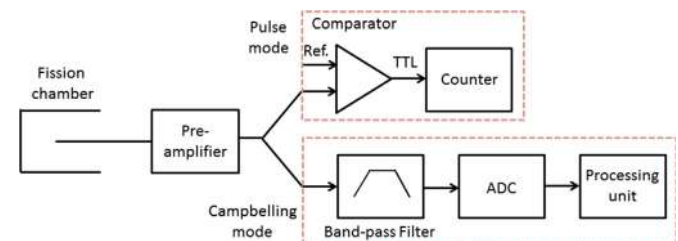
$$\varphi(x, t) = x \cdot f(t). \tag{1}$$



**Fig. 1.** Overall layout of a neutron monitoring system.

The form of the pulses can be considered as a function defined by Eq. (1). The constant shape function $f(t)$ in (1) is normalized to unity and is multiplied by a random amplitude $x$. In case of one pulse event it is assumed that the particle interaction with the detector took place at $t=0$. Every single pulse has an arrival time $t_k$ according to an exponential distribution and an amplitude $x_k$. The amplitude of the pulses can be considered as deterministic or randomly distributed:

$$\eta(t) = \sum_{k=0}^{N(t)} x_k \cdot f(t-t_k). \tag{2}$$

Hence the fission chamber signal can be described as a Poisson pulse train defined by (2). In the upper limit of the summation the function $N(t)$ is the cumulative number of counts in the detector which is a random variable following a Poisson distribution. If the measurement time converges to infinity then the number of hits also converges to infinity. A measurement or simulation of such a pulse train is limited by a measurement duration which implies that the summation is finite, since the number of collected pulses is finite.

A complete mathematical treatment of the statistics of such pulse train signals is provided in [9]. Nevertheless the analytic handling is only possible for a few specific pulse shapes and amplitude distributions. In addition, as was mentioned before, the effect of the electronic noise and background events cannot be included into the mathematical treatment.

Therefore, to investigate the fission chamber signals, a numerical simulation of the Poisson pulse train model, including the noise, is desirable. The features of this implementation are explained in the next section.

## 3.2. Operating modes

The main goal of the fission chamber signal processing is to estimate the count rate, the intensity $s_0$ of the process, since this value is related directly to the neutron flux. Increasing intensity causes pile-ups in the signal, meanwhile we also have to face electronic noises and the background level of the gamma radiation, thus the estimation of the intensity rate becomes a non-trivial task.

### 3.2.1. Pulse mode
The limitation of the separation between pulses is determined by the pulse width and the pulse intensity, as well as by the detector electronics. There will be a minimum time separation $\tau$ between two detection events, which is called the dead time [6].

Usually two different dead time models are used for counting systems: the paralyzable and the nonparalyzable dead time. The nonparalyzable model means that during the dead time no events can be recorded and no events will have an effect on the signal or on the detector. The paralyzable model means that the events occurring during the dead time will not be recorded, but will trigger a new dead time. Both models can be handled analytically, and the measured count rate $m$ can be easily calculated from the real count rate $n$ and the dead time $\tau$. For count rate, i.e. the first moment of the counting statistics, the derivations can be found in [6]. A deeper treatment of the effect of the dead time on the higher order moments of the counting statistics, with accounting for the random dead time is given in [15].

In practice the counting process is achieved by a transistor–transistor logic (TTL). A discrimination level is set and when the chamber signal jumps from below to above this level, the electronics triggers a logic signal. This logic response has a certain time width and during this time the following jumps above the discrimination level are neglected. This counting system is illustrated in Fig. 2.
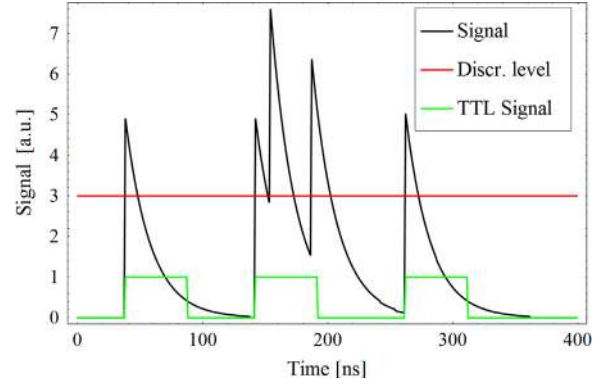




**Fig. 2.** Illustration of generated TTL signal.

Obviously none of the above mentioned dead time models can perfectly describe such a system, since the width of the TTL signal acts as a non-paralyzing dead time, whereas the pulse width and the pulse overlapping act like a paralyzing dead time (meaning that if the signal stays above the level then the electronics does not trigger more logic responses). The actual behavior depends on the TTL width, the pulse width and the discrimination level. In this work the paralyzing random dead time, arising from the pulse pile-up, is included. Also non-paralyzing dead time effects, due to electronics, were included into the simulations.

### 3.2.2. Campbelling mode
Campbell's theorem gives a relation between the cumulants and the intensity of a shot noise process. In the commonly used Campbelling mode the variance of the signal is measured. In this paper Campbelling refers to this second order method. Based on Ref. [9], the general form of the second order Campbelling equation for a signal $\eta(t)$ consisting of general pulses $\varphi(x,t)$ with a randomly distributed amplitude $x$ is given by (3), where $w(x)$ is the probability distribution function of the amplitude which is 0 for $x \le 0$:

$$\mathbf{D}^2(\eta) = s_0 \int_{-\infty}^{+\infty} \left[ \int_{-\infty}^{+\infty} \varphi(x,t)^2 w(x)\, dx \right] dt. \tag{3}$$

In real applications the lower limit of the integrals is zero both for the time and amplitude coordinates and the upper limit of the integrals are also finite for both dimensions. If we consider simple pulses defined in Eq. (1), then the integrals in Eq. (3) can be separated:

$$\mathbf{D}^2(\eta) = s_0 \int_{-\infty}^{+\infty} x^2 w(x)\, dx \int_{-\infty}^{+\infty} f(t)^2\, dt. \tag{4}$$

In Eq. (4) the first integral is the second raw moment of the amplitude distribution. Hence, for random amplitudes one has

$$\mathbf{D}^2(\eta) = s_0 \langle x^2 \rangle \int_{-\infty}^{+\infty} f(t)^2\, dt \tag{5}$$

whereas for constant amplitudes

$$\mathbf{D}^2(\eta) = s_0 x_0^2 \int_{-\infty}^{+\infty} f(t)^2\, dt. \tag{6}$$

In the deterministic case the probability distribution function $w(x)$ is interpreted as a Dirac delta function: $w(x) = \delta(x-x_0)$.

Eqs. (5) and (6) show that if the pulse shape $f(t)$ and the amplitude distribution $w(x)$ are known, and the variance of the signal is determined from measurement, then the count rate $s_0$ of the signal can be estimated. In a real application the shape and the amplitude distribution can be measured and considered as known information about the current fission chamber. However, this information is associated with uncertainties. The accuracy of the

estimation depends on the signal shape and its amplitude distribution. The required sensitivity and uncertainty analysis is not possible to achieve analytically.

## 4. Poisson pulse train simulation code

### 4.1. Description

The tool described above is a MATLAB implementation of the mathematical model of the signal including the discretization of the measurements and the simulation of electronic noise.

The program generates the Poisson pulse train according to the pre-defined pulse shape, amplitude distribution, count rate and time resolution. The pulse shape and the amplitude distribution can be defined to be analytic or can be taken from measurement or simulation results. The signal created is considered as a current signal since in an industrial application the fission chambers are usually connected to current sensitive pre-amplifiers which can be located farther from the core [12]. Any shape of finite pulse can be defined and applied in the program. The user can define the charge of the pulse (the integral value of the pulse) or the amplitude. The amplitude and the charge distribution are obviously related, this feature is only for convenience.

The user has the opportunity to define additional time signals, such as background noise or one or more further Poisson trains and add these to the original pulse train. This way the tolerance of the estimators can be investigated against electronic noises, or radiation backgrounds.

An important real detector-like feature of the simulation tool is the way how signals at high count rates are handled. If the order of count rate is comparable to the order of time resolution of the simulated signal, more than one pulse can appear within one time step. In this case those pulses will sum up, so the current delivered by the pulses will not be lost.

A limitation of the toolbox could have been mainly the computational memory size. For instance storing a pulse train of length $10^{-1}$ s with 1 GHz resolution will yield $10^8$ data, demanding about 1 Gb memory. In case of low intensities longer measurement times are needed to avoid the statistical error due to the randomness of the process. To overcome this potential memory issue we built in an opportunity to continue a pulse train exactly where it ended instead of generating a completely new process which would result that the process starts from zero again. It is useful because the fission chamber signal needs time to reach an asymptotically stationary state, when the moments of the signal are time independent [9]. Fig. 3 shows the statistical error of the simulation for several measurement times. The plotted statistical uncertainty was defined as the ratio of the standard deviation and the expected value of the number of pulses during the measurement time (which is a Poisson distributed random variable)
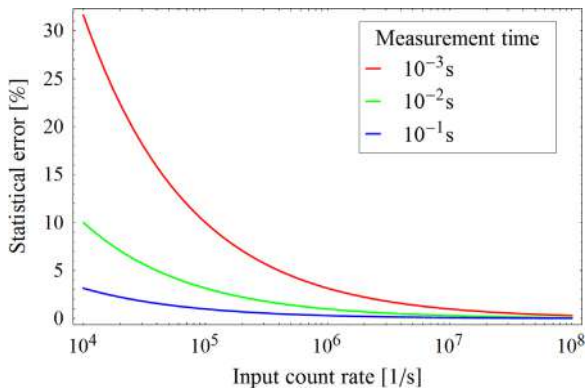
expressed as a percentage. Our goal is to keep the statistical error originating from the randomness under 10%, and our main focus is laid on count rates higher than $10^4$ s$^{-1}$. Thus, for the calculations a measurement time of $10^{-2}$ s was accepted.

### 4.2. Overall code verification

For obvious reasons, a full direct verification of the code with experiments is not possible. For the current work we chose an experimental check of the applied mathematical model and a theoretical verification for the implementation of the model.

The Poisson characteristics of the signal were checked with an experiment where the time delays were measured between the pulses. Based on this measurement the Poisson pulse train model was accepted as a valid mathematical model. After the implementation of the mathematical model, it was checked by comparing simulation results with analytic results.

#### 4.2.1. Experimental comparison

To investigate the Poisson characteristics of the fission chamber signals a measurement was performed at the MINERVE reactor [16]. During the measurement a CFUL01 fission chamber [4] was located in the reflector of the reactor core. The signal of the fission chamber was connected to a pre-amplifier and after that directly to an Agilent MSO9104A Infiniium oscilloscope. With the oscilloscope 20 μs long segments triggered by a pulse can be measured. The re-arm time of the oscilloscope was 5 μs. This means that the smallest detectable time difference between two pulses was 25 μs with the segmentation method. Hence the time between the particle arrivals was measured at low count rates (when the reactor already reached criticality). The probability density function of the arrivals is shown in Fig. 4. After fitting (with 99% confidence) an exponential distribution on the measured results, we found a good agreement. The Poisson pulse train model was accepted to describe the mathematical behavior of the fission chamber signal.

#### 4.2.2. Analytical comparison

To decide whether the mathematical model was implemented correctly, a comparison with the level crossing calculation was chosen from [9].

The intensity $n_{st}(A)$ of particle arrivals which induce a jump of the signal from level $y \leq A$ to a level higher than $A$ can be derived analytically for various pulse trains. For validation purposes we have chosen a case with an exponential pulse shape with a time constant $p$ in the form

$$f(t) = e^{-t/p} \tag{7}$$

and exponentially distributed random amplitudes with a mean $1/\mu$. As it was shown in [9], the intensity $n_{st}(A)$ in this case



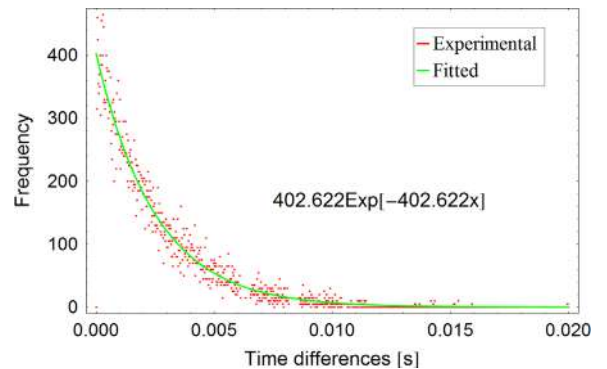Fig. 3. The statistical error of a pulse train simulation.



Fig. 4. Verification of the Poisson nature.

is given as

$$n_{st}(A) = s_0 \frac{(\mu A)^{s_0 p}}{\Gamma(s_0 p + 1)} e^{-\mu A} \qquad (8)$$

where $\Gamma$ indicates the Gamma-function. One can notice that the above definition of the level crossing intensity is identical of the pulse mode using a discrimination level and a TTL signal, the difference is that in this case the width of the TTL signal would be zero.

A level jumping algorithm was implemented to estimate the intensity $n_{st}(A)$. Fig. 5 shows that the numerical and analytic results are in a good agreement for this case as well, which means that the code gives an adequate handling of the pulse shapes and the shot noise as well as for the randomly distributed pulse amplitudes.

## 5. Performance of standard modes

In this section an extensive comparison between the recently applied pulse mode and the second order Campbelling technique is presented. Several calculations were been made for pulse trains containing pulses with both deterministic and stochastic amplitudes.

### 5.1. Pulse model

For the following calculations a reference pulse shape with reference parameters has been chosen based on previous simulation results with a Monte-Carlo based program suite [10]. The chosen pulse shape is an exponential decay shape defined by (7). This is a rather arbitrary choice, but it can be considered as an approximation of a pulse shape where the rising part of the pulse is rapid and is then followed by a damped exponential. The reference charge, shape parameter and other data are given in Table 1. The charge is the integral value of the pulse, hence the amplitude of the pulse can be calculated if the time parameter $p$ and the charge $Q$ are known (for

exponential shape the amplitude is $Q/p$). The pulse width was defined by $p \cdot \ln(90)$ rounded to ns precision. The pulse width alone does not play any role in the calculations, hence this definition is arbitrary and it was introduced only to give an insight of the effective length of the pulse. The resolution of the pulses was 1 ns. This resolution is an inherited parameter in the toolbox, hence the whole signal has the same resolution. Each pulse is followed for 10 μs, which is rather important for pulses longer than the reference as presented in Fig. 6. This parameter is important for the computation because if the pulse is given by the charge (hence by its integral), the pulse can be better approximated if the stored length is longer. A slightly larger length was chosen because this choice does not slow the calculation significantly and does not effect the results but can be used for a wide pulse width range. This length is limited by memory issues and also physically it is meaningless to follow a pulse infinitely. The impact of the longer and shorter pulses (plotted in Fig. 6) is assessed in Section 5.4.

### 5.2. Noise impact

As a first step, the impact of the electronic noise on the different methods was investigated. The noise was considered as a Gaussian white noise and the standard deviation of the noise was chosen as a percentage of the amplitude of the reference pulse shape for all cases. During a real experiment this noise is around 5–10%.

For the calculations, pulse trains of length $10^{-2}$ s were generated. During the calculations, for each count rate one pulse train was created and the noise was added. This way the results related to different noise strengths bear the same statistical uncertainty.

Fig. 7 shows the results for the sensitivity analysis. It is seen that the pulse mode is rather insensitive to noise. The Campbelling mode is affected by the noise at low count rates and the impact is
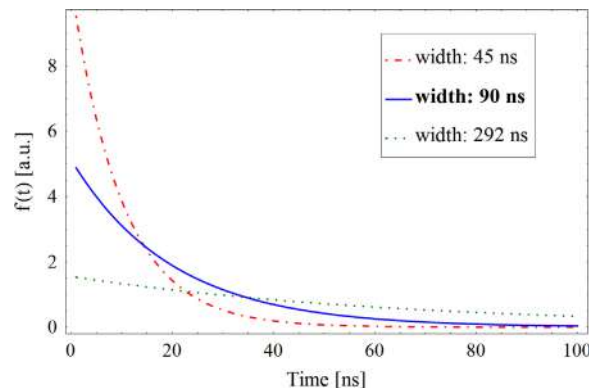


**Fig. 5.** Validation against the analytic level crossing results, $s_0 = 10^8$ s$^{-1}$, $p = 20$ ns, $\mu = 0.5$ μA$^{-1}$.

**Table 1**
The reference pulse.

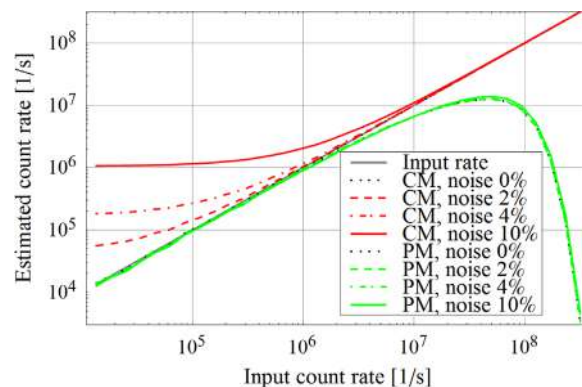| Shape | $\exp(-t/p)$ |
| --- | --- |
| Time parameter $p$ | 20 ns |
| Charge $Q$ | 0.1 pC |
| Amplitude $a$ | 5 μA |
| Pulse width | 90 ns |
| Resolution | 1 ns |
| Stored length | 10 μs |
| TTL width | 50 ns |



**Fig. 6.** The used pulses.



**Fig. 7.** The noise sensitivity of the pulse mode and the Campbelling mode.

significant. The higher the amplitude of the noise, the larger the bias in the estimation is. Hence the possible application of the Campbelling technique is limited to high count rates. At low count rates the inaccuracy of the estimation can become larger than 100% as it is seen in Fig. 8. This means that the overlap between the modes depends strongly on the amplitude of the noise. To reach less than 10% error with Campbelling mode the noise should be lower than 8% for count rates with an order of magnitude $10^6$ s$^{-1}$.

Fig. 9 represents the probability density function of the signal amplitude distribution with and without noise at different count rates. The probability density function was calculated by normalizing the histogram of the sampled current values of the simulated signal. One can see that at lower count rates the density function of the noisy signal is mostly dominated by the noise. Hence, when the variance of the noisy signal is calculated, the variance of the noise determines and hence also biases the estimated count rate. Conversely, at higher count rates the noise does not have any effect on the probability density function. For this investigation a rather high noise level (20%) was chosen to highlight the general effects of noise on the probability density function.

## 5.3. Pulse amplitude distribution impact

In the introduction it was already mentioned that the amplitude of the pulses (or equivalently, the charge of the pulses) can be considered as a random variable. As it was mentioned, the toolbox allows us to implement pulse amplitude distributions. A realistic distribution can be complicated since it depends on many parameters (the applied voltage, the pressure in the chamber, etc.). Thus in the prelim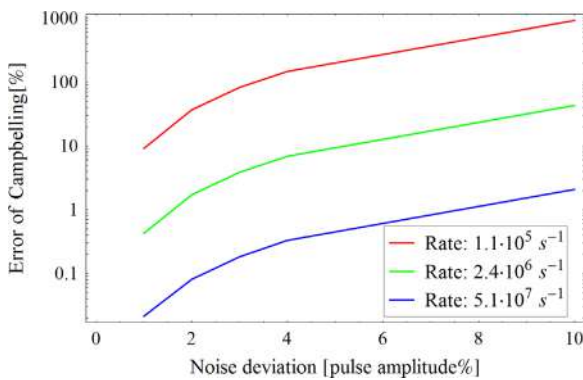inary calculations only a simple normal distribution was used to investigate the effect of the random amplitudes on the pulse and Campbell modes.

The mean of the amplitude distribution was considered as the amplitude of the reference pulse (5 μA), and the standard deviation was introduced as the mean multiplied by a factor $c$. In this case the raw moment $\langle x^2 \rangle$ in Eq. (5) can be described as the sum of the mean squared and the variance of the amplitude distribution as in the following equation:

$$\langle x^2 \rangle = Var(x) + \langle x \rangle^2 = (c^2 + 1)\langle x \rangle^2. \tag{9}$$

Such a normal distribution has a negative tail as well, which is non-physical. The use of truncated normal distributions could have been an alternative to overcome this issue. However, for this study the highest applied multiplier value $c$ was 0.4, in which case only 0.62% of the amplitudes would be negative. Hence, instead of overcomplicating a simple investigation, the negative amplitudes were rejected and new random amplitudes were sampled.

If a proper calibration is used (or one has a good knowledge about the amplitude distribution) then the Campbelling mode is unaffected by the amplitude distribution as it is presented in Fig. 10 in a noise-free case. The pulse mode is though biased regardless the order of the count rate since the discrimination level is fixed. This result shows that in case of wide amplitude distribution the pulse mode cannot be effective already at low count rates hence the overlap between the standard modes cannot be guaranteed.

## 5.4. Pulse width impact

The next investigation addressed the impact of the pulse width on the methods in case of deterministic amplitudes. For this
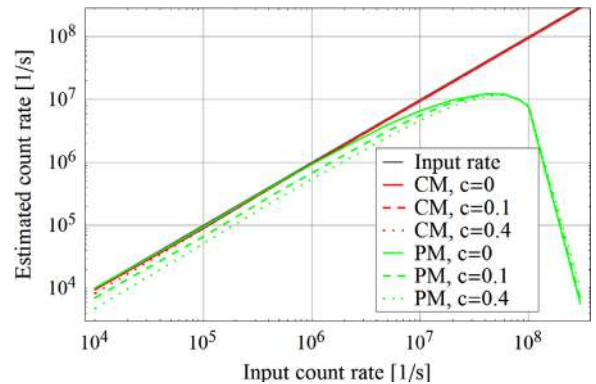


**Fig. 8.** Error of the Campbelling mode for several count rates.



**Fig. 10.** Impact of the amplitude distribution on the pulse mode and on the Campbelling mode.



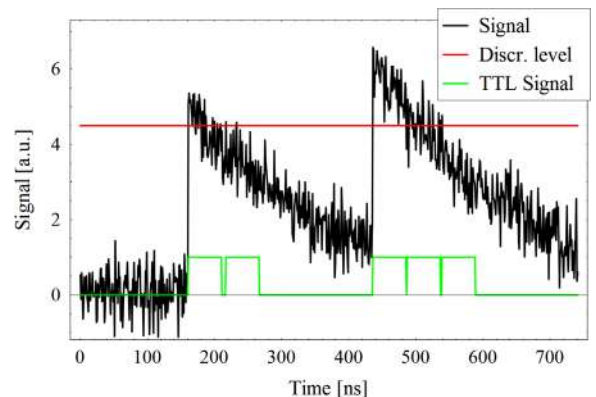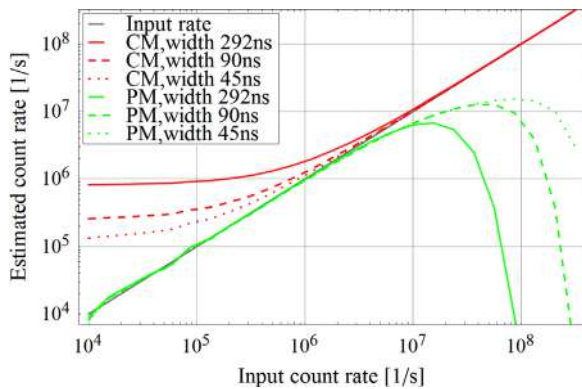**Fig. 9.** The probability density function of the noiseless and the noisy signal.



**Fig. 11.** Spurious counts triggered by the noise.

**Fig. 12.** Impact of the different pulse width on the pulse mode and the Campbelling (noise: 5%).

analysis, pulse widths with three different orders of magnitude were applied, as shown in Fig. 6. The pulse width was changed while the charge of the pulses were fixed (in this way the amplitude was modified). This is because we wanted to consider a pulse width change through changing the filling gas, which would have an impact only on the electron and ion velocity (hence the collecting time) but not the amount of induced electron–ion pairs by the fission fragment.

According to Fig. 6 it is obvious that for the different pulses, different discrimination levels have to be set. The need for such a calibration is a disadvantage of the pulse mode compared to the Campbelling mode.

The necessity of applying different TTL signal widths for different pulse widths is also an issue related to the pulse mode. Fig. 11 shows that in case of longer pulses, if the TTL signal width is 50 ns, the noise will trigger spurious logical signals, hence the estimated count rate would be increased. Thus, when using pulse mode, a calibration is also needed to set the adequate discrimination level and the TTL signal parameters. This need will not affect the robustness of the mode, but will affect its simplicity.

Fig. 12 shows that both modes perform better if the pulse is shorter. For pulse mode, the breakdown of the function is shifted to higher count rates when pulses are shorter. At the same time, Campbelling mode gives a more accurate estimation for lower count rates when pulses are shorter since it is more likely for short pulses to stick out from the background noise.

Both Figs. 7 and 12 show that for short pulses, the overlap between the two modes can be guaranteed. However for longer pulses there would be a serious need for a signal processing method which can be used over the whole count rate range and which is less sensitive to noise and pulse width.

## 6. Conclusion

In this paper a newly implemented simulation tool was introduced. The toolbox simulates fission chamber signals after the pre-amplifier. The code generates a shot noise or filtered Poisson process which is a superposition of pulses with arrival times following a Poisson point process. The main goal of the tool is to create pulse trains from arbitrary or real pulse shapes to aid the planning and the understanding of experiments and measurements. The toolbox also allows us to test several signal processing methods to retrieve the count rate information of the signal. Knowing the count rate of fission chamber signals is essential since it is proportional to the neutron flux of the environment.

The applied mathematical model was checked with a simple measurement performed at the MINERVE zero power research reactor. The measurement result shows that the filtered Poisson model can be accepted to describe the distribution of the time intervals between pulses in the fission chamber signals. The implementation of the mathematical model with MATLAB was verified by the level crossing method described in Ref. [9].

In addition to create such a toolbox the main purpose of the current work was to compare the recently used fission chamber modes for signal processing. The current interest focuses on the possibility of covering the low and medium flux ranges with pulse and Campbelling modes in case of short pulses. An extensive investigation was made to compare the performance of these modes in case of deterministic and stochastic pulse amplitude distributions. The efficiency of the pulse and Campbelling modes was also tested with different background noise levels. It was found that the pulse mode is insensitive to the noise level within reasonable limits, while the Campbelling mode is rather noise sensitive at low count rates. On the other hand the Campbelling mode is insensitive to the stochastic amplitude distributions, whereas the pulse mode is heavily affected if the distribution is rather wide.

One can conclude that in case of short pulses the overlap between the two modes can be guaranteed if the background noise is not too high. But for longer pulses the whole count rate range cannot be covered by the two modes. Thus there is a real need for unifying the different modes. In the continuation of this work it is planned to investigate the applications of the higher order Campbelling methods proposed by [17,18]. The expected bottleneck of the higher order methods is the lack of simplicity and robustness. In the future we have to investigate whether the use of higher order moments can cover the investigated count rate range in a feasible way.

## Acknowledgment

## References

[1] F. Gauché, Comptes Rendus Physique 13 (4) (2012) 365.
[2] C. Jammes, N. Chapoutier, P. Filliatre, J.P. Jeannot, F. Jadot, D. Verrier, A.-C. Scholer, B. Bernardin, Nuclear Engineering and Design 270 (0) (2014) 273.
[3] P. Filliatre, C. Jammes, B. Geslot, L. Buiron, Annals of Nuclear Energy 37 (11) (2010) 1435. http://dx.doi.org/10.1016/j.anucene.2010.06.023.
[4] C. Jammes, P. Filliatre, B. Geslot, T. Domenech, S. Normand, IEEE Transactions on Nuclear Science NS-59 (4) (2012) 1351.
[5] C. Jammes, P. Filliatre, B. Geslot, L. Oriol, F. Berhouet, J. Villard, L. Vermeeren, IEEE Transactions on Nuclear Science NS-57 (6) (2010) 3678. http://dx.doi.org/10.1109/TNS.2010.2075939.
[6] G.F. Knoll, Radiation Detection and Measurement, 4th ed., John Wiley & Sons, Hoboken, NJ, USA, 2010.
[7] T.E. Bortner, G.S. Hurst, W.G. Stone, Drift velocities in some commonly used counting gases, Rev. Sci. Instrum. 28 (2) (1957) 103.
[8] S.C. Brown, Basic Data of Plasma Physics: The Fundamental Data on Electrical Discharges in Gases, American Institute of Physics, Woodbury, NY, USA, 1997.
[9] L. Pál, I. Pázsit, Zs. Elter, Nuclear Instruments and Methods in Physics Research Section A: Accelerators, Spectrometers, Detectors and Associated Equipment 763 (2014) 44.
[10] P. Filliatre, C. Jammes, B. Geslot, R. Veenhof, Nuclear Instruments and Methods in Physics Research Section A: Accelerators, Spectrometers, Detectors and Associated Equipment 678 (0) (2012) 139. http://dx.doi.org/10.1016/j.nima.2012.03.020.
[11] C. Jammes, P. Filliatre, P. Loiseau, B. Geslot, Nuclear Instruments and Methods in Physics Research Section A: Accelerators, Spectrometers, Detectors and Associated Equipment 681 (0) (2012) 101. http://dx.doi.org/10.1016/j.nima.2012.03.032.
[12] S.N. Ahmed, Physics and Engineering of Radiation Detection, Academic Press, San Diego, CA, USA, 2007.

[13] E. Parzen, Stochastic Processes, Classics in Applied Mathematics, Society for Industrial and Applied Mathematics, Oakland, California, USA, 1999 ⟨http://books.google.fr/books?id=mwW-iODttSQC⟩.

[14] A. Papoulis, Probability Random Variables and Stochastic Processes, 3rd ed., McGraw-Hill, New York, NY, USA, 1991.

[15] L. Pál, I. Pázsit, Nuclear Instruments and Methods in Physics Research Section A: Accelerators, Spectrometers, Detectors and Associated Equipment 693 (0) (2012) 26. http://dx.doi.org/10.1016/j.nima.2012.07.036.

[16] A. Gruel, P. Leconte, D. Bernard, P. Archier, G. Noguère, Nuclear Science and Engineering 169 (3) (2011) 229.

[17] I. Lux, A. Baranyai, Nuclear Instruments and Methods in Physics Research 202 (3) (1982) 469.

[18] I. Lux, A. Baranyai, Nuclear Instruments and Methods in Physics Research 202 (3) (1982) 477.

# Paper IV

## Performance of Higher Order Campbell methods, Part I: review and numerical convergence study

Zs. Elter, M. Bakkali, C. Jammes and I. Pázsit

# Performance of Higher Order Campbell methods, Part I: review and numerical convergence study

Zs. Elter [a,b,*], M. Bakkali [c], C. Jammes [b], I. Pázsit [a]

[a] Chalmers University of Technology, Department of Physics, Division of Subatomic and Plasma Physics, SE-412 96 Göteborg, Sweden
[b] CEA, DEN, DER, Instrumentation, Sensors and Dosimetry Laboratory, Cadarache, F-13108 Saint-Paul-lez-Durance, France
[c] CEA, DRT, LIST, Sensors and Electronic Architecture Laboratory, Saclay, F-91191 Gif Sur Yvette, France

## ARTICLE INFO

## ABSTRACT

This paper investigates, through numerical simulations, the performance of a signal analysis method by which a high temperature fission chamber can be used over a wide range of count rates. Results reported in a previous paper (Elter et al., 2015 [1]) indicated that the traditional Campbell method and the pulse mode cannot provide a sufficient overlap at medium count rates. Hence the use of the so-called Higher Order Campbell (HOC) methods is proposed and their performance is investigated.

It is shown that the HOC methods can guarantee the linearity (i.e. correctness) of the neutron flux estimation over a wide count rate, even during transient conditions. The capabilities of these methods for suppressing parasitic noise (originating from various sources) are verified.

© 2016 Elsevier B.V. All rights reserved.

## 1. Introduction

Sodium-cooled fast reactors (SFRs) are among the advanced reactors selected by the Generation IV International Forum. In Europe, the development of an innovative pool-type SFR is under way, led by the French CEA and its industrial partners [2]. The development also concerns the neutron flux monitoring system, which is the subject of this paper.

As described in several publications in the literature [3–5], fission chambers capable of operating at high temperatures (high temperature fission chambers, HTFC) are the most promising candidates for neutron flux monitoring in SFRs. HTFCs have long been used for neutron flux monitoring [6,5]. However, a few aspects of their operation and use have not been solved satisfactorily. This paper attempts to solve some of these shortcomings.

One such point is that fission chambers operate in different modes, with corresponding different electronics and signal processing algorithms, at low (start-up) and high (full power) detection rates, respectively [7]. At low detection rates, when the signal has the shape of individual "spikes", a pulse counting technique, based on level crossing is applied. At higher count rates, when the detector pulses overlap, pulse counting becomes impossible and the detection rate is estimated from the detector current with the so-called Campbelling techniques. In its traditional form this

means that the mean count rate is determined from the variance of the detector current. This method has the advantage that it suppresses the (unwanted) contribution from minority components, such as counts from gamma photons.

In order to have a correct estimate of the neutron flux for all count rates, there should be a sufficiently wide overlap between the two operating regimes of the detector, where both methods supply correct results. Under ideal circumstances, the traditional Campbell method would provide a sufficient overlapping since, in principle, the Campbell formula is valid also for individual pulses. However, as the simulation studies of our previous work showed [1], at low count rates that the traditional Campbell method is vulnerable to the effect of parasitic noise (detection and electronic noise), and hence the overlap is not guaranteed.

To remedy this problem, the generalisation of the Campbelling technique was proposed through the application of the so-called Higher Order Campbelling (HOC) methods [8–10]. These use the higher order moments (cumulants) of the detector current to estimate the detection rate. Although the theoretical relationship between the higher order cumulants and the mean detection rate has long been known, the applicability and performance of these methods in practical applications has not been tested. The applicability concerns essentially two aspects. One is the sensitivity of the accuracy to parasitic (inherent) noise in the detection process and the electronics, which deteriorates the performance of all order Campbelling methods at low count rates. The other aspect is that the theoretical advantages of the use of higher order cumulants [11–13] are offset by the fact that in reality one only

uses an estimate of the theoretical cumulants, and the error of the estimate increases with the order of the moment to be estimated.

This paper addresses the question of linearity of HOC methods and the practical applicability of the cumulant estimators with the use of an advanced simulation package. In previous work, in order to investigate the question of the linearity of the pulse and the traditional Campbelling modes, a dedicated code was developed for the simulation of fission chamber pulse trains [1]. Recently the code was updated to be capable of simulating detector signals with time dependent count rate to study transient scenarios. The upgraded code was used in the recent study. The code can handle arbitrary signal shapes, charge distributions and the presence of added noise. With the help of the code, a quantitative analysis of the HOC methods was made.

As the continuation of this paper, a second part, describing the related experimental results, is planned to be published. Part II will introduce the calibration methodology to unfold the count rate and the reactor power information from the cumulants of the signal [22].

In this paper the principles of the HOC methods, their applications, and the results related to their performance study are described. First, the filtered Poisson process that permits us to describe a conditioned signal of a fission chamber and our developed simulation code is discussed briefly. Second, a brief overview of higher order methods, and the estimation of higher order cumulants is given. Finally, the performance of the higher order Campbelling modes is investigated for several cases, such as electronic noise, gamma background radiation and transient events. The investigations verify the expected advantages of HOC methods and explore the possible drawbacks of orders higher than 3 via computational simulations.

## 2. Physical processes in fission chambers

Fission chambers are nuclear detectors that are widely used for online neutron flux measurements. This type of detector is an ionisation chamber, containing fissile material in order to detect neutrons. The most common design consists of one or more electrode pairs, of which at least one electrode is coated with a fissile layer, ranging from a few micrograms to a few grams. The spacing between each anode and cathode goes from tens of microns to a few millimeters. The chamber itself is filled with an argon-based gas pressurised at a few bars. The processes leading to a current pulse after a neutron entering the chamber are the following:

(a) When a neutron reaches the fissile coating, it is likely to induce a fission event which generates (usually) two heavily charged ions, the fission products, emitted in two nearly opposite directions.

(b) The heavy ion which is emitted out of the fissile layer ionises the filling gas along its trajectory (therefore creates electron/ion pairs).

(c) A DC-voltage of a few hundred volts is applied between the electrodes, therefore the electrons and positive gas ions drift across the filling gas in opposite direction towards the anode and the cathode respectively

(d) During the drift both the electrons and the gas ions induce a current pulse (named in this document as electronic and ionic pulse) in the electrodes.

## 3. Simulation of the fission chamber signals

Since the basic principles and assumptions on the character of the fission chamber signals were already described in [1,10], only a

brief description will be given here. The fission chamber signal is described as a Poisson pulse train, or shot noise, also called a filtered Poisson process [14]. In such a stochastic process the time interval between each pair of consecutive events has an exponential distribution with an intensity parameter $s_0$ [15]. The intensity, or count rate, is proportional to the neutron flux level around the detector. In this section the signal is considered as the one induced by the electronic pulses (therefore the signal contains only one type of pulse), but later the impact of ionic pulses is also investigated. The form of an individual pulse is assumed to be

$$q \cdot f(t) \tag{1}$$

where $f(t)$ is the (deterministic) normalised pulse shape (the response function of the detector) and $q$ is a random variable representing the pulse charge, characterised with a charge distribution $w(q)$.

The detector signal $\eta(t)$ is a superposition of pulses of the form

$$\eta(t) = \sum_{k=0}^{N(t)} q_k \cdot f(t - t_k) \tag{2}$$

where $t_k$ are the exponentially distributed neutron arrival times at the detector, $q_k$ are the random pulse charges, and $N(t)$ is the number of pulses having arrived until time $t$ ($N(t)$ is a Poisson distributed random variable). The integral of the shape function $f(t)$ in (2) is normalised to unity. The simplest approximation is if the pulse charges are considered as deterministic (constant). This is the case which will be considered in the quantitative work in this paper too, since the simulation studies of our previous work [1] showed that the random character of the pulse charges did not have any influence on the detector signal characteristics that were studied.

The new features of the current simulation model, compared to that used in Ref. [1] are as follows. The first concerns the signal pulse shape $f(t)$. In the previous work [1], similar to the theoretical considerations [10], the pulse had a form of a step jump at $t=0$, followed by a monotonically decreasing (exponential) or non-increasing (rectangular/boxcar shape) behaviour, characterised by one single parameter. In the present work, the pulse shape was chosen to have the form of a damped exponential:

$$f(t) = \frac{e^{-t/p_1} - e^{-t/p_2}}{\int_0^\infty (e^{-t/p_1} - e^{-t/p_2}) \, dt}. \tag{3}$$

This form is more realistic, i.e. it avoids the discontinuity (jump) of the pulse at $t=0$, rather it is non-monotonic and it consists of a fast rising and a slowly decaying part. Hence it also allows a more varied pulse shape, due to the two different parameters $p_1$ and $p_2$. With the signal shape given by Eq. (3), the ionic and electronic components of the pulse can be modelled by suitable choice of the pulse parameters, i.e. the time constants $p_1$ and $p_2$ of the pulse shape $f(t)$ and the pulse charge $\langle q \rangle$.

For the quantitative work, reference pulse parameters were chosen to describe both the electronic and the ionic pulses. The characteristics of the pulses are summarised in Table 1, and Fig. 1 shows a graphical representation of the electronic pulse. The parameters have realistic orders of magnitudes and are based on

**Table 1**
The reference pulse.

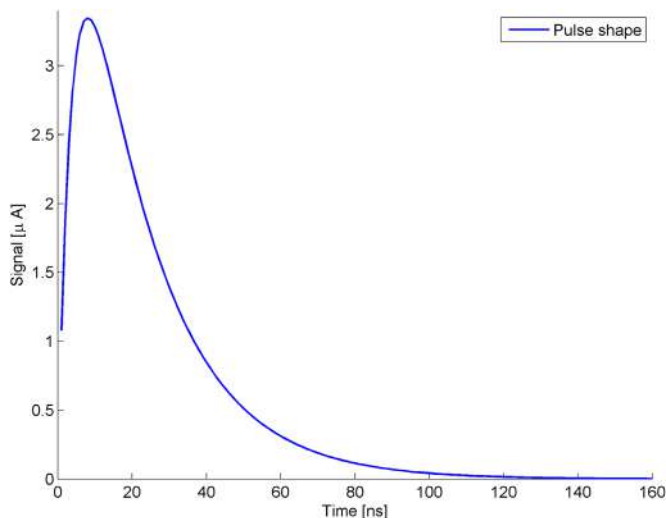| Type | e$^-$ | Ion |
|---|---|---|
| Time parameter $p_1$ | 20 ns | 2 μs |
| Time parameter $p_2$ | 4 ns | 0.4 μs |
| Mean charge $\langle q \rangle$ | 0.1 pC | 0.1 pC |
| Amplitude $a$ | 3.34 μA | 34 nA |
| Pulse width | 100 ns | 10 μs |
| Resolution | 1 ns | 1 ns |

**Fig. 1.** Electronic pulse shape.

simulation results described in [16] as well as on measurements performed at the Minerve reactor, which will be published later on [22]. The pulse widths in Table 1 are only provided to give insight, but the definition of the width is arbitrary. The time resolution of pulses (and all the simulations in this document) was 1 ns.

One can immediately see from Table 1 that the ionic pulses are two orders of magnitude longer while carrying the same charge as electronic pulses. Section 5.2 investigates the effect of the ionic signal on the estimation of the count rate.

One further novelty of the simulation code is that in order to test the properties of the detector signals in time-varying neutron fluxes, the simulation was extended to the case when the incoming primary event series (the neutron arrival times) constitutes an inhomogeneous Poisson process, i.e. a Poisson process with a time-dependent intensity $s(t)$. The conceptual questions arising when applying stationary Campbell techniques to non-stationary signals were discussed in a recent Technical Note [17]. Such scenarios will be quantitatively investigated and discussed in Section 5.6. The cases of the constant and the time-varying intensities will be referred to as homogeneous and inhomogeneous processes, respectively.

## 4. Higher order Campbelling

Campbell's theorem provides a relationship between the variance of the time-resolved detector signal and the intensity of the corresponding shot noise process [18]. Based on the linear relationship between the variance and the intensity, in the commonly used Campbelling mode the variance of the signal is measured in order to determine the intensity of the detection. In this paper "Campbelling" refers to this second order method. The generalisation of the Campbelling method for higher order moments of the detector signal was already proposed in [11]. The derivation was given only later in [9]. Recently an even more straightforward derivation, based on the master equation technique, was proposed in [10].

The general form of the Campbell relationships for a homogeneous, stationary signal ($\eta^{(st)} = \lim_{t \to +\infty} \eta(t)$) consisting of general pulses in the form defined by (1) and (2), is given as [10]

$$\kappa_n^{(st)} = s_0 \langle q^n \rangle \int_{-\infty}^{+\infty} f(t)^n \, dt = s_0 \cdot C_n \tag{4}$$

where $\kappa_n$ is the $n$th order cumulant. Cumulants or semi-invariants are moment-like quantities defined by the expansion coefficients

of the logarithm of the moment generating function. Commonly, the methods in which $n \geq 3$ are called higher order methods. Eq. (4) refers to stationary signals: in a related work the stationarity of fission chamber signals is discussed [17]. It was shown that in practical situations (the change of the count rate is slower than few thousand ns) the signal can be considered as a transition of quasi-stationary signals.

Eq. (4) shows that if the pulse shape $f(t)$ and the charge distribution $w(q)$ are known (therefore the calibration coefficient $C_n$ is determined), and the cumulant (of any order) of the signal is determined from measurement, then the count rate $s_0$ of the signal can be estimated. In a real application the shape and the charge distribution can be measured and thus can be considered as a priori information about the particular fission chamber and the experimental setup. However, this information is associated with uncertainties. The accuracy of the estimation depends on the accuracy of the knowledge about the signal shape and its charge distribution. The required sensitivity and uncertainty analysis is not possible to be achieved analytically.

Part II of this work will present the methodology to determine the calibration coefficient. The experimental study investigates the linearity of the HOC mode, and its performance during a control rod drop event [22].

## 5. Performance of the HOC methods

This section covers the sensitivity analysis of the HOC methods. In this regard first the optimal measurement time was defined, then the impact of the ionic pulses, the parasitic noise of the electronics and the competitive shot noises were determined for the traditional and higher order Campbelling methods. These noises cause systematic measurement errors since the calibration coefficient in Eq. (4) takes into account only the most dominant part of the signal, the electronic pulses, because in an experimental calibration one determines the electronic pulse shape. On the other hand, the measured cumulant is related to the compound signal (including the electronic pulse part and the additional noises). Hence the systematic error may be estimated analytically (this will be demonstrated for the case of ionic pulses but for the other cases the analytic handling is abandoned). Nevertheless, in the numerical simulations, the random errors due to the uncertainty of the number of pulses $N(t)$ (see in Eq. (2)) arriving during the measurement time and the variance of the cumulant estimations are inherently included. Therefore with simulations one gains more understanding about the significance of the impacts of the noise.

For each investigation, several signals with the same measurement time were generated in order to assess the random error of the estimated count rate. The expected value, or mean, of these estimations reflects the systematic error caused by the noise.

Finally the section presents results related to the performance of the higher order methods during transient scenarios.

### 5.1. Convergence of the estimator

The estimation of the cumulants was done with the $k$-statistics, which are the unique symmetric unbiased estimators of the cumulants ($\langle k_n \rangle = \kappa_n$ [19]). Here the convergence of these estimators is investigated briefly in order to define the optimal measurement length.

The variance of the estimators can be found in the literature [19], here only an illustrative term of these formulas is
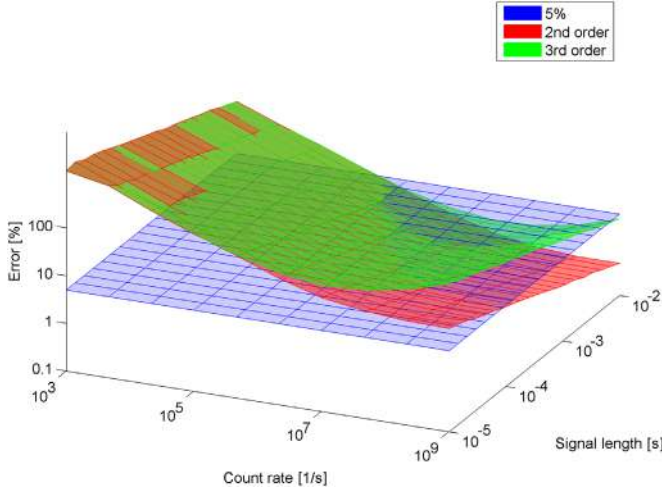
Fig. 2. Random error of the count rate estimation.



Fig. 3. Illustration of the electronic and the ionic part ($s_0 = 10^7$ s$^{-1}$).

highlighted:

$$var(k_n) \propto \frac{\kappa_2^n}{N} \tag{5}$$

where the number of samples is $N$. Eq. (5) means that the variance of the estimator is proportional to the $n$th power of the variance of the signal. Since the variance of the signal increases with the count rate (which is expressed by the Campbell theorem introduced in Eq. (4)), the variance of the estimation increases exponentially with the count rate. This means that for accurate measurements with higher orders, one needs longer measurement times. This limits the application of the very high order methods. The optimal measurement time was therefore estimated.

Instead of evaluating the formulae of the variance of the estimators, a rather pragmatic approach was applied here, which inherently includes the uncertainties due to the randomness of the process. Many signals were created at several count rates with several measurement lengths, and the relative difference of the estimated and the real count rate was determined. The random error of the estimation was defined as the standard deviation of this set of differences. The results are summarised in Fig. 2 for the second and the third order. One can see that at high count rates the random error indeed exponentially increases; and further, that at lower count rates, the error also increases, due to the randomness of the process. (The figure shows the plane related to 5% error as a reference.)

Based on these results it was concluded that for the third order methods a measurement time around 1–10 ms provides reliable count rate estimation over a wide count rate range. Therefore the following computations were done for 10 ms, which means $10^7$ samples at 1 GHz sampling frequency.

Although in the figure the fourth order estimation is not included, the calculations showed that the fourth order bears more serious convergence problems. Nevertheless in some of the following sections the fourth order results are also included to point out whether the application of higher than third order estimations has any practical advantage.

### 5.2. Impact of the ionic pulse

After the ionisation of the filling gas by the fission fragments, both the electrons and the ions induce a current pulse (as described in Section 2). The contribution of the ionic part may depend on the data acquisition system. Nevertheless it is important to quantify the impact of the ionic contribution.
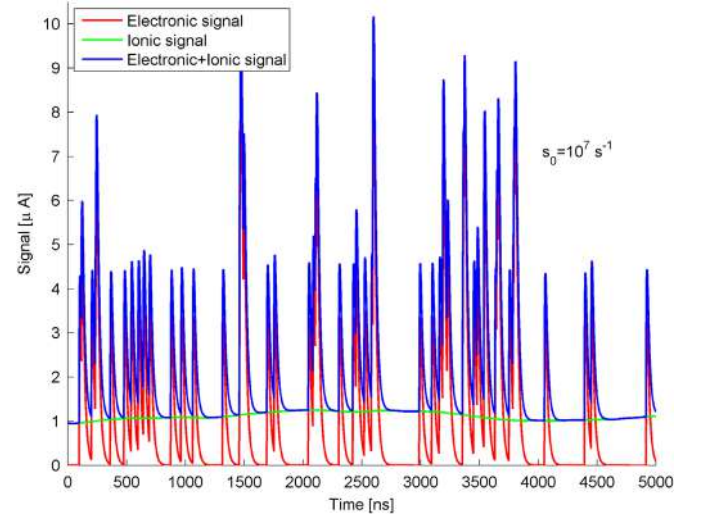
Table 1 shows that even though the ionic pulses convey the same order of magnitude charges as the electronic pulses, they are much wider and therefore their amplitude is small compared to the electronic pulses. By definition the ionic signal has the same count rate as the electronic signal, and the corresponding pulses arrive at the same time instant since the negative and positive charge creation is simultaneous.

Fig. 3 shows the composition of the two signals. One can immediately notice that the ionic part contributes only as a low frequency noise since the ionic pulses strongly overlap already at low count rates. As such, with the appropriate acquisition system it could be filtered out.

In the simulations the Campbelling modes were calibrated according to Eq. (4) only by taking into account the electronic pulse shape (which is the case in a real measurement [20]), whereas the appropriate underlying Campbell equation would be (for deterministic pulse charges)

$$\kappa_n^{(st)} = s_0 \int_{-\infty}^{+\infty} (f_e(t) + f_i(t))^n \, dt = s_0 \left[ \int_{-\infty}^{+\infty} f_e(t)^n \, dt + \int_{-\infty}^{+\infty} f_i(t)^n \, dt \right.$$
$$\left. + \int_{-\infty}^{+\infty} \left( \sum_{k=1}^{n-1} \binom{n}{k} f_e(t)^{n-k} f_i(t)^k \right) dt \right]$$
$$= s_0 (C_{n,e} + C_{n,i} + C_{n,ei}) = s_0 \cdot C_{n,real} \tag{6}$$

with the assumption that the ionic and electronic processes are totally dependent. Hence the real count rate is

$$s_0 = \frac{\kappa_n^{(st)}}{C_{n,real}} \tag{7}$$

while the measured count rate with the calibration coefficient containing only the electronic pulses is

$$\hat{s_0} = \frac{\kappa_n^{(st)}}{C_{n,e}}. \tag{8}$$

Therefore the systematic error of the measurement is

$$\epsilon_n = 100 \cdot \frac{\hat{s_0} - s_0}{s_0} = 100 \cdot \left( \frac{C_{n,real}}{C_{n,e}} - 1 \right) [\%]. \tag{9}$$

After calculating $C_{n,real}$ and $C_{n,i}$ with the pulse parameters summarised in Table 1, the systematic error $\epsilon_n$ appears to be around 1.2% for the second order and 0.2% for the third order method.

These results show that similarly to how the effect/contribution of "minority components", such as gamma counts, is suppressed by the use of the higher order Campbelling methods (as it will be
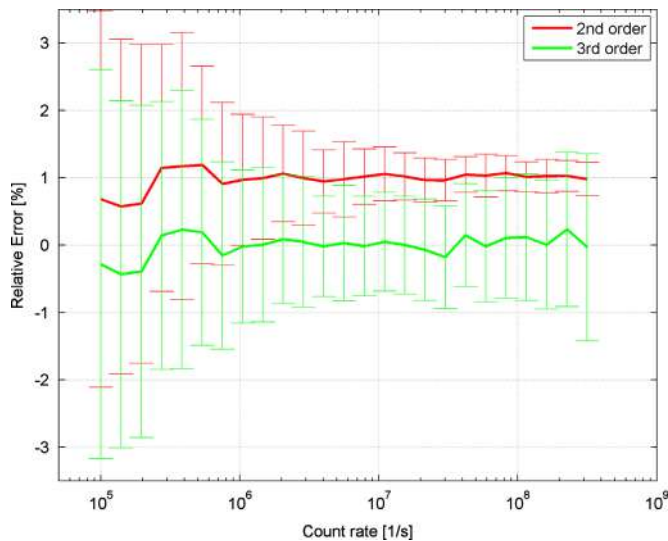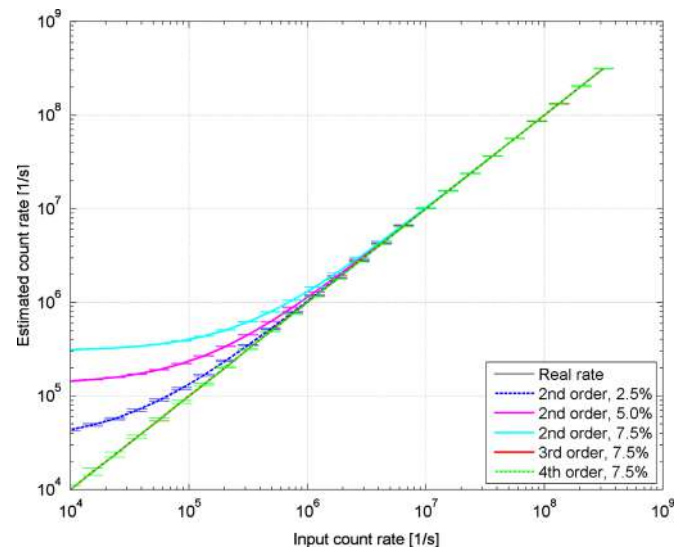
Fig. 4. The impact of the ionic signal.



Fig. 5. Electronic noise effect.

discussed in more detail later in Section 5.4), the contribution of the ionic component is also suppressed by the higher order methods. However, the reasons are different, which is worth a short discussion. In case of the detector pulse due to a gamma photon, the pulse shape $f(t)$ is rather similar to that induced by a neutron detection. As Eq. (4) shows, the reason of the suppression is the factor $\langle q^n \rangle$, which is much smaller for gamma pulses than for neutron pulses (much less charges created). In addition, the neutron and gamma detections are independent from each other, hence the Campbell relationships can be considered for these two components separately. For the case of the electronic and ionic pulses, the factor $\langle q^n \rangle$ is the same for both components; the difference is in the pulse shapes. Since the longer pulse (i.e. the ionic one) has inevitably a smaller amplitude, raising each component to higher powers will lead to the diminishing of the integral of the $f_i(t)^n$ term as compared to that of the $f_e(t)^n$ term. However, in contrast to the neutron and gamma counts, the ionic and electronic pulses are not independent; in each detection event both an electronic and an ionic pulse is generated simultaneously. This leads to the appearance of "cross-terms", i.e. the last term on the r. h.s. of the first line of Eq. (6). At a first glance, one might expect that this would decrease the suppressing power of the higher order methods, since there will be e.g. a term $f_e(t)^{n-1} f_i(t)$ in the $n$th order cumulant. However, any cross term, even without raising to any power, will be small because of the different shape of the two signals. For instance the integral of $f_e(t) \cdot f_i(t)$ will be much smaller than unity (both terms are normalised to unity) because they overlap very weakly. For the $t$ values around the maximum of $f_e(t)$, the values of $f_i(t)$ will be very small, and vice versa. This is even more so for higher powers of the pulses. Hence, despite the non-independent character of the electronic and ionic pulses, still the contribution of the ionic component will be increasingly suppressed by the higher order Campbelling methods.

The numerical results of the difference between the real and the estimated count rate, presented in Fig. 4 are consistent with the theoretical prediction. Clearly, at count rates higher than $10^8 \, \mathrm{s}^{-1}$ the performance of the third order is poorer than that of the second order, since the random errors related to the higher orders exceed the systematic error of the second order. However the bias is less than 1.5% at high count rates and less than 3% at low count rates (where the deviation due to the randomness of the process dominates) for both methods.

### 5.3. Parasitic noise suppression

The fission chamber signal is loaded with parasitic noise originating from the cables and the pre-amplifier included in the data acquisition system. A simple measurement was performed to estimate the distribution and in particular the amplitude of the noise. This measurements and the characteristics of the noise will be described in Part II in more detail [22]. The polarisation voltage of the fission chamber was set to 0 V, therefore only the parasitic noise of the system was collected. It was verified that the noise distribution is close to Gaussian and its standard deviation is around 6–7% of the pulse amplitudes [22].

The measurement of the parasitic noise showed that the noise was not white. Therefore simulations were performed with coloured noise. It was verified through simulations that the frequency content of the noise does not affect the performance of the Campbelling methods.

Fig. 5 shows the count rate estimation for signals loaded with Gaussian white noise. The traditional Campbelling method cannot be used at low count rates, because it significantly overestimates the count rate. However, the HOC methods provide linearity on the whole count rate range, since they sufficiently suppress the impact of the noise, as the higher order cumulants of the Gaussian distribution are zero. Nevertheless it has to be mentioned that the higher order methods are not totally insensitive to the noise: as it is shown in Eq. (5), the wider signal distribution increases the variance of the estimation, therefore higher noise levels increase the random error of the higher order methods. For realistic noise levels this effect does not play a significant role.

The simulations also showed that at count rates above $10^8 \, \mathrm{s}^{-1}$ the random error of the third order estimation exceeds the systematic error of the second order estimation, therefore at high count rates the application of the traditional Campbelling mode is advised.

### 5.4. Competitive shot noise suppress

In the fission chamber other, not neutron triggered ionising radiations also induce pulses. These pulses also create a shot noise in the chamber. The main undesirable contribution is originating from gamma radiation [21]. The assessment of the gamma contribution to the signal of a fission chamber, located in the reflector region of a sodium cooled reactor, lies beyond this work.
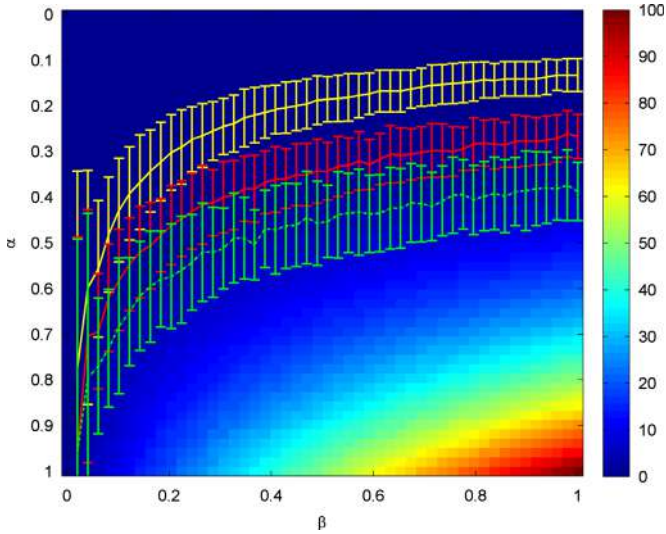
Fig. 6. Bias due to the competitive shot noise for the third order method. The coloured contour lines (visible in the on-line version) correspond to 2% error of the different order HOC methods. Yellow (uppermost): second order; red (middle): third order; green (lowermost): fourth order. (For interpretation of the references to colour in this figure caption, the reader is referred to the web version of this paper.)

Therefore in this paper we intend to illustrate the shot noise suppression capabilities of the HOC methods via a simple model: competitive shot noise was added to the original, neutron triggered shot noise. Both the pulse charge and the count rates of the competitive signal were considered as a fraction of the neutron pulse charge and count rate:

$$s_c = \alpha s_0 \quad \text{and} \quad q_c = \beta q_0 \quad (\alpha, \beta \in [0, 1]) \tag{10}$$

where $s_0$ and $s_c$ are the count rates of the neutron and competitive signal respectively, and $q_0$ and $q_c$ are the charges of the neutron and competitive pulses respectively. The pulse shape and width of the competitive pulses was chosen to be the same as that of the neutron triggered electronic pulses.

The difference between the estimated count rate of the compound signal and the original neutron signal was determined for several $\alpha$ and $\beta$ values. Fig. 6 presents the results for the third order Campbelling method at count rate $s_0 = 10^6 \, \text{s}^{-1}$. The red curve[1] (in the middle, between the yellow and green) gives the margin of 2% error which was considered as acceptable. The yellow (uppermost) and green (lowermost) curves show the same margin for the second and fourth order Campbelling methods. One can conclude that by increasing the order of the method, a significant suppression gain can be achieved. However, the random error of the fourth order exceeds its systematic error reduction compared to the third order. With the third order mode the competitive shot noise can be successfully suppressed even if the parasitic pulse charges are 25% of the neutron charges and the intensity of the parasitic process is comparable with the neutron signal's intensity. Nevertheless in the future we have to address the question of parasitic pulses in a sodium cooled fast reactor to justify that the third order methods are adequate.

[1] These curves are simply contour plots corresponding to a given error, and the different colours are used to distinguish between the different orders of the HOC methods. Hence they have nothing to do with the colour scheme of the colour bar to the right of the figure.
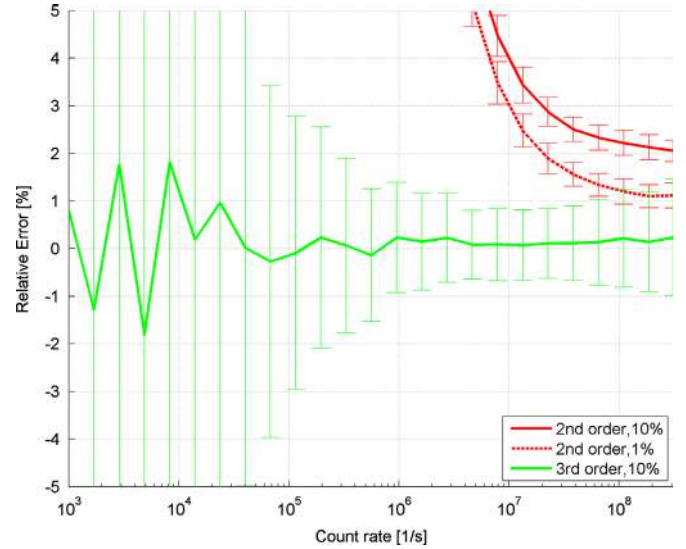


Fig. 7. Cumulative impact of noise.
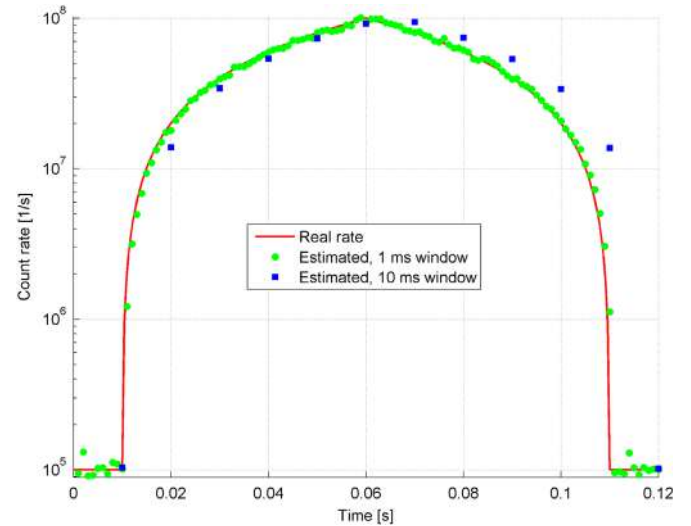


Fig. 8. Transient simulation: count rate estimation with window sizes 1 ms and 10 ms.

### 5.5. Compound signal

As a summary, Fig. 7 presents the results of the systematic and random errors for signals where all the above-mentioned noises appear simultaneously: Gaussian noise (with 6% amplitude), ionic signal and competitive shot noise (with $\alpha = 1$ and $\beta = 0.01$ or 0.1).

In case the amplitude of the non-neutron triggered pulses is rather small in the HTFCs applied in ASTRID (which is highly probable according to [21]), and further if the data acquisition system can filter out low frequency noises (such as the ionic contribution), then at high count rates (above $10^8 \, \text{s}^{-1}$) still the application of the second order method is advisable.

### 5.6. Inhomogeneous process

The final study included in this work shows the performance of the third order Campbelling method during a transient event.

Transients result in an inhomogeneous signal, in which the count rate of the signal can be described as a time dependent function $s(t)$. Our simulation code was extended with the possibility to describe continuously changing count rates.

The test scenario was a simple transient event; Fig. 8 shows the results. The count rate increased from $10^5\,\mathrm{s}^{-1}$ to $10^8\,\mathrm{s}^{-1}$ in 50 ms and after reaching the maximum, it decreased to $10^5\,\mathrm{s}^{-1}$ in 50 ms (illustrated by the solid line in Fig. 8; note the logarithmic scale on the *y*-axis). This test describes a fast transient, with a significant count rate change. The measurement is considered as taking consecutive finite samples of the signal, and estimating the count rate of them with the Campbell equations for homogeneous processes (Eq. (4)). This implies that the inhomogeneous signal is approximated as a sequence of quasi-homogeneous signals. The length of the consecutive samples (the estimation window) was set to 1 ms or 10 ms.

One can see that there is a delay of the estimation due to the length of the sample size. If the window size is set too short then the accuracy of the measurement is going to be worse (due to the random error related to the stochastic characteristic of the signal and to the inaccuracy of the third order estimation), whereas with longer measurement times the exact shape of the transient may be lost, as in the example with longer measurement window, the peak is missed. Which means that if the sample window is well optimised (meaning that it is sufficiently long to guarantee an accurate cumulant estimation, but sufficiently short to monitor the change in the count rate), then the inhomogeneous signal can be approximated as a sequence of homogeneous signals, and the homogeneous Campbell equations can be applied.

It can be concluded that the monitoring of transients is limited by the shortest reliable measurement time (in which the estimation is converged). As it was illustrated, with rather short, 1 ms long windows it is possible to reach a fair estimation even at high count rates, which means that one can be confident that transients slower than the ms scale can be followed with third order Campbelling methods.

## 6. Conclusion

In this paper some aspects of the application of the higher order Campbelling methods were investigated and reviewed. The application of such methods was proposed to guarantee a wide count range monitoring in neutron detection.

To investigate the applicability of the HOC methods a Matlab toolbox, emulating the generation of a fission chamber signal, was applied. The main purpose of the current work was to investigate the robustness of the higher order methods. Here the linearity of the HOC method was assessed.

The noise sensitivity of the higher order methods was investigated for several cases. It was shown that any kind of Gaussian noise, regardless of its frequency characteristics, can be efficiently filtered out already with the third order Campbelling method. The higher order methods are also able to suppress any competitive shot noise. Although the suppression can be improved by increasing the order of the method, due to the related random error of higher order methods, the third order method was chosen for later applications.

It was also concluded that transient events slower than few millisecond can be sufficiently well monitored with third order methods. Although, due to the limitation of the measurement window length, there will be a short delay between the real event and the monitoring.

It was shown that at count rates above $10^8\,\mathrm{s}^{-1}$ the random error of the third order estimation exceeds the systematic error of the second order estimation, therefore at high count rates the application of the traditional Campbelling mode is advised. Hence, in the future, implementation of an adaptive Campbelling mode is planned. This way it can be guaranteed that the error (both systematic and random) of the estimations is less than 2% over the whole count rate range.

In Part II of this work the calibration of a fission chamber in HOC mode will be demonstrated in measurements, and finally the real-time application of the method has to be verified.

## References

[1] Zs. Elter, C. Jammes, I. Pázsit, L. Pál, P. Filliatre, Nucl. Instrum. Methods Phys. Res. Sect. A: Accel. Spectrom. Detect. Assoc. Equip. 774 (2015) 60, http://dx.doi.org/10.1016/j.nima.2014.11.065.
[2] F. Gauché, C. R. Phys. 13 (4) (2012) 365.
[3] C. Jammes, N. Chapoutier, P. Filliatre, J.P. Jeannot, F. Jadot, D. Verrier, A.-C. Scholer, B. Bernardin, Nucl. Eng. Des. 270 (2014) 273.
[4] P. Filliatre, C. Jammes, B. Geslot, L. Buiron, Ann. Nucl. Energy 37 (11) (2010) 1435, http://dx.doi.org/10.1016/j.anucene.2010.06.023.
[5] C. Jammes, P. Filliatre, B. Geslot, T. Domenech, S. Normand, IEEE Trans. Nucl. Sci. NS-59 (4) (2012) 1351.
[6] C. Jammes, P. Filliatre, B. Geslot, L. Oriol, F. Berhouet, J. Villard, L. Vermeeren, IEEE Trans. Nucl. Sci. NS-57 (6) (2010) 3678, http://dx.doi.org/10.1109/TNS.2010.2075939.
[7] G.F. Knoll, Radiation Detection and Measurement, 4th edition, John Wiley & Sons, New York, 2010.
[8] I. Lux, A. Baranyai, Nucl. Instrum. Methods Phys. Res. 202 (3) (1982) 477.
[9] I. Lux, A. Baranyai, Nucl. Instrum. Methods Phys. Res. 202 (3) (1982) 469.
[10] L. Pál, I. Pázsit, Zs. Elter, Nucl. Instrum. Methods Phys. Res. Sect. A: Accel. Spectrom. Detect. Assoc. Equip. 763 (2014) 44.
[11] R.A. DuBridge, IEEE Trans. Nucl. Sci. NS-14 (1967) 241.
[12] B. Bars, Nucl. Instrum. Methods Phys. Res. Sect. A: Accel. Spectrom. Detect. Assoc. Equip. 275 (2) (1989) 403.
[13] L.B. Baers, T. Rivero Gutierrez, R.A. Carrillo Mendoza, G. Jimenez Santana, Use of higher order signal moments and high speed digital sampling technique for neutron flux measurements, IEEE Trans. Nucl. Sci. NS-40 (1993) 832–839.
[14] E. Parzen, Stochastic Processes, Classics in Applied Mathematics, Society for Industrial and Applied Mathematics, Oakland, Canada, 1999. ⟨http://books.google.fr/books?id=mwW-iODttSQC⟩.
[15] A. Papoulis, Probability, Random Variables and Stochastic Processes, 3rd edition, McGraw-Hill, New York, 1991.
[16] P. Filliatre, C. Jammes, B. Geslot, R. Veenhof, Nucl. Instrum. Methods Phys. Res. Sect. A: Accel. Spectrom. Detect. Assoc. Equip. 678 (2012) 139, http://dx.doi.org/10.1016/j.nima.2012.03.020.
[17] Zs. Elter, I. Pázsit, C. Jammes, Remark on the applicability of Campbelling techniques for transient signals, Nucl. Instrum. Methods Phys. Res. Sect. A: Accel. Spectrom. Detect. Assoc. Equip.. 813, 2016, 10, http://dx.doi.org/10.1016/j.nima.2015.12.061.
[18] N.R. Campbell, V.J. Francis, A theory of valve and circuit noise, J. Inst. Electr. Eng. 93 (1946) 45.
[19] E.W. Weisstein, "k-statistic" from MathWorld—a Wolfram Web Resource. ⟨http://mathworld.wolfram.com/k-Statistic.html⟩.
[20] B. Geslot, T.C. Unruh, P. Filliatre, C. Jammes, J. Di Salvo, S. Breaud, J. Villard, IEEE Trans. Nucl. Sci. NS-59 (4) (2012) 1377, http://dx.doi.org/10.1109/TNS.2012.2198669.
[21] P. Filliatre, L. Vermeeren, C. Jammes, B. Geslot, D. Fourmentel, Nucl. Instrum. Methods Phys. Res. Sect. A: Accel. Spectrom. Detect. Assoc. Equip. 648 (1) (2011) 228.
[22] G. Zs. Elter, P. deIzarra, C. Filliatre, I. Jammes, Pázsit: Performance of Higher Order Campbell methods, Part II: calibration and experimental application, To be submitted to Nuclear Instruments and Methods A, 2016.

# Paper V

Performance of Higher Order Campbell methods, Part II: calibration and experimental application

Zs. Elter, G. de Izarra, P. Filliatre, C. Jammes and I. Pázsit

# Performance of Higher Order Campbell methods, Part II: calibration and experimental application

Zs. Elter [a,b,*], G. de Izarra [b], P. Filliatre [b], C. Jammes [b], I. Pázsit [a]

[a] *Chalmers University of Technology, Department of Physics, Division of Subatomic and Plasma Physics, SE-412 96 Göteborg, Sweden*
[b] *CEA, DEN, DER, Instrumentation, Sensors and Dosimetry Laboratory, Cadarache, F-13108 Saint-Paul-lez-Durance, France*

A B S T R A C T

Applying Higher Order Campbelling methods in neutron flux monitoring with fission chambers is advantageous due to their capabilities to suppress the impact of unwanted noises and signal contributions (such as gamma radiation). This work aims to verify through experimental results that the basic assumptions behind the Higher Order Campbelling methods are valid in critical reactors.

The experiments, reported in this work, were performed at the MINERVE reactor in Cadarache. It is shown that the calibration of a fission chamber and the associated electronic system is possible in higher order mode. With the use of unbiased cumulant estimators and with digital processing, it is shown that over a wide count rate range, accurate count rate estimation can be achieved based on signal samples of a few *ms*, which is a significant progress compared to similar experimental results in the literature. The difference between the count rate estimated by pulse counting and by the Higher Order Campelling is less than 4%.

The work also investigates the possibility of monitoring transient events. For this purpose, a control rod drop event was followed in Higher Order Campbelling mode.

© 2016 Elsevier B.V. All rights reserved.

## 1. Introduction

Sodium-cooled fast reactors (SFRs) are among the advanced reactors selected by the Generation IV International Forum [1]. In Europe, the development of an innovative pool-type SFR is under way, led by the French CEA and its industrial partners [2]. The development also concerns the neutron flux monitoring system, which is the subject of this paper.

Fission chambers are the most promising candidates for neutron monitoring in SFRs. Such detectors traditionally operate in three modes: pulse mode at low flux levels, Campbelling or fluctuation mode at medium flux levels, and current mode at high flux levels. Recently it was shown that to guarantee the overlap of the pulse and Campbelling mode, one needs to design dedicated fission chambers [3]. A design independent alternative can be the operation of the fission chambers in Higher Order Campbell (HOC) mode [4,5]. As detailed in Part I of this work [6], the application of higher order methods is limited by the fact that the error of the estimation increases with the order of the method, therefore larger signal samples are needed. The rapid development

of digital measurement devices (such as FPGAs, field programmable gate arrays) brings recent attention to these methods, since the reliable estimation of the higher order moments of the signal became achievable.

In Part I of this work, the performance of the higher order methods was extensively investigated through numerical simulations [6]. In the same work, it was shown that higher order methods are capable to suppress the disadvantageous impact of various noises and unwanted signal contributions. It was found that the application of the third order method is reliable, and that it is redundant to apply higher than third orders.

As a continuation of that work, this paper investigates experimentally the application of the third order Campbelling method. A simple approach is proposed to make use of the third order cumulants of the signal in the time-domain, instead of dealing with the third order spectra of the signal as [7]. With the use of unbiased cumulant estimators and with digital processing, it is shown that accurate count rate estimation can be achieved based on signal samples of a few *ms*, which is a significant progress compared to similar experimental results in the literature [8]. This paper presents the methodology of the calibration to link the cumulants of the signal to the power of the reactor and to the fission rate of the chamber. The disadvantages of the calibration are discussed. A rather involved calibration methodology based on the spectral properties of the signal can be found in [9] for the traditional Campbelling mode.

* Corresponding author at: Chalmers University of Technology, Department of Physics, Division of Subatomic and Plasma Physics, SE-412 96 Göteborg, Sweden.
  E-mail address: zsolt@nephy.chalmers.se (Zs. Elter).

The current work is a step towards the implementation of an FPGA-based Campbelling measurement system, which is capable of real-time flux monitoring.

First, the Higher Order Campbell theorem is briefly discussed. Second, Section 3 presents the experimental setup, the noise of the system and addresses the general applicability of Campbell's theorem in critical reactors. Section 4 summarizes the measurement results during stationary and transient reactor states, and the methodology to calibrate fission chambers in higher order mode. The accuracy of the calibration is assessed with the help of pulse counting techniques, and an empirical calibration, based on the pulse counted results, is proposed.

## 2. Higher Order Campbell method

In Part I [6], the general form of the Campbell relationships [10,11] for a homogeneous (i.e. having a constant count rate) shot noise signal $y(t)$ consisting of general pulses $f(t)$ with a charge distribution, and count rate $s_0$ (such signal is an appropriate approximation of the fission chamber signals [3]), was given. Similarly, the general Campbell equations can be given by introducing the pulse amplitude distribution instead of the charge distribution as [12]

$$\kappa_n(y(t)) = s_0 \langle a^n \rangle \int_{-\infty}^{+\infty} f(t)^n dt = s_0 \cdot C_{a,n} \tag{1}$$

where $\kappa_n(y(t))$ is the $n$th order cumulant of the distribution of the signal $y(t)$ and $\langle a^n \rangle$ stands for the $n$th raw moment of the pulse distribution. Commonly, the methods in which $n \geq 3$ are called higher order methods. The pulse function $f(t)$ is normalized to the amplitude.

Eq. (1) shows that if the pulse shape $f(t)$ and the charge or amplitude distribution are known (therefore the calibration coefficient $C_{a,n}$ – later referred to only as $C_n$ – is determined), and the cumulant (of any order) of the signal is measured, then the mean count rate $s_0$ of the signal can be estimated. Eq. (1) assumes that the signal contains pulses with the same shape. It is shown later, that this assumption is not valid in multi-coating chambers. Section 4.2 addresses the bias of considering the pulse shape as constant. For this investigation the pulse shape will be considered as bimodal.

The coefficient $C_n$ links the signal statistics to the fission rate directly, which means that such a calibration is independent of the neutron environment or neutron spectra. The present work aims to estimate the calibration coefficient by investigating the mean shape and the amplitude distribution of the pulses (see Section 4.3), and also by performing an empirical calibration through estimating the count rate with pulse counting technique.

It was shown previously in [6] that the application of higher order methods sufficiently suppresses the impact of various noises: the parasitic noise of the system, the unwanted signal contributions of ionization processes not originating from the fission events, and the ionic contribution of the charge creation in the filling gas.

In this work the cumulants are estimated during the post-processing of the measured and recorded signals. The unbiased cumulant estimators, or $k$-statistics, are applied [14], for which the calculation of the $n$th order sums of the signal values are needed. This allows a simple estimation in the time-domain with a relatively fast convergence. Practically, estimating the cumulant means, that a finite and discrete-time signal slice is recorded, and the cumulants of the distribution of these sampled values are computed. Fig. 1 shows an example of the recorded signal (the details of the system for recording are given in the next section), its probability density function and the related cumulant estimations.
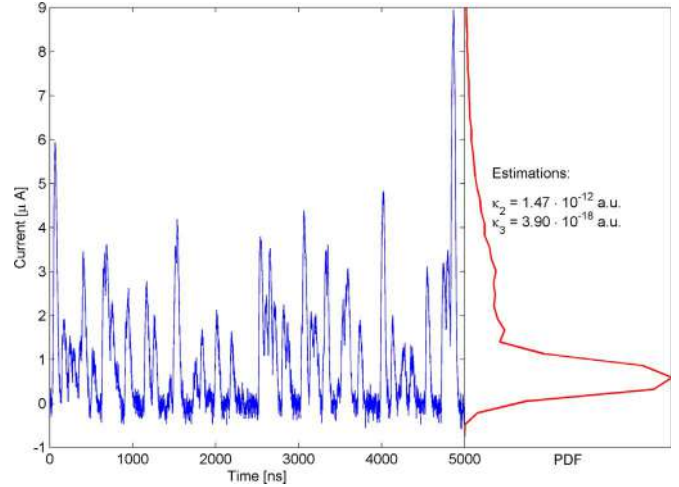


**Fig. 1.** An example of a recorded signal slice and its distribution at 20 W.

## 3. Experimental setup

The experimental setup consisted of a current-sensitive fission chamber placed in the reflector zone of the MINERVE reactor. MINERVE is a pool type zero-power, light water reactor, operated at CEA Cadarache with a maximum power of 80 W.

In the experiment a CFUL01 fission chamber (manufactured by Photonis) was studied. The CFUL01 is a multi-electrode and multi-coating detector, which means that the chamber contains three coaxial electrodes and four fissile coatings of enriched uranium, as illustrated in the schematic radial cross section of the chamber, Fig. 2. The sensitive length of the detector is 211 mm, the outer radius of the first anode is 14 mm, the inner and outer radii of the cathode are 16 and 17 mm, and the inner radius of the second anode is 19 mm. Therefore the gas gap is 2 mm wide for both the inner and outer chambers. The nominal operating voltage is 600 V (and the maximum voltage is 800 V at 20 °C, while the limit is 1300 V with no radiation). The filling gas is argon with 4% nitrogen at 250 kPa (at room temperature). The fissile deposit consists of $U_3O_8$, with the U235 content enriched to 90%, with a surface density of 1.32 mg/cm². The thickness of the deposit is around 1.5 μm (in Fig. 2 the thickness of the circles referring to the deposit was enlarged only for the illustration purpose). The advantage of using detectors with multiple coatings is to increase the fissile
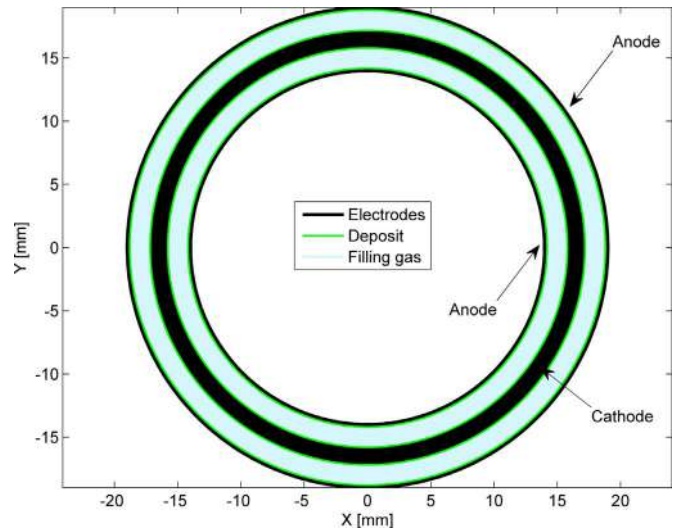


**Fig. 2.** Illustration of the radial cross section of the CFUL01 chamber.

mass in the chamber without increasing the surface mass and therefore the self-absorption of the deposit [15].

The fission chamber was connected to a fast broadband current pre-amplifier with a high immunity, 25 m long Fileca 1209-38 cable. The pre-amplifier acts as a high-pass filter in order to remove the DC part of the signal. It exhibits a sensitivity of $3.08 \cdot 10^{-5}$ A/V and its gain is $\pm 0.5$ dB in the 5 kHz to 50 MHz frequency band. The output signal of the pre-amplifier was digitized at a high sampling frequency (1 GHz) during a large time span with an advanced digital oscilloscope (Agilent Infiniium). The collected signals were post-processed with MATLAB.

## 3.1. Saturation curve

In theory, Campbelling measurements could be performed outside of the saturation regime of an ionization chamber, since the pulse arrivals are independent of the applied voltage, therefore the Campbell theorem stays valid. But the pulse shape and amplitude distribution (hence the calibration coefficient $C_n$) is more sensitive to the change of the voltage outside of the saturation regime, meaning that a small perturbation in the bias voltage causes a large change in the calibration coefficient and in the measured cumulant. This change is amplified for higher order methods due to the higher order powers of the amplitude distribution and the pulse shape. Therefore in Campelling measurements it is advisable to guarantee that the fission chamber operates in the saturation regime.

The measured saturation curve of the CFUL01 chamber is shown in Fig. 3. Due to the limitations of the fission chamber, it was not possible to set a higher voltage than 800 V. At 600 V the current still slightly increases with the voltage, but due to safety requirements, in the following measurements the chamber was operated with a bias voltage of 600 V. The error associated with this choice is less than 1%.

## 3.2. Noise of the measurement

The numerical simulations in Part I showed that the key advantage of applying higher order methods is to suppress the impact of the parasitic noise of the system, since in case the amplitude distribution of the noise is Gaussian, the higher than second order cumulants of the noise become zero. It was also shown that the suppression does not depend on the frequency content of the
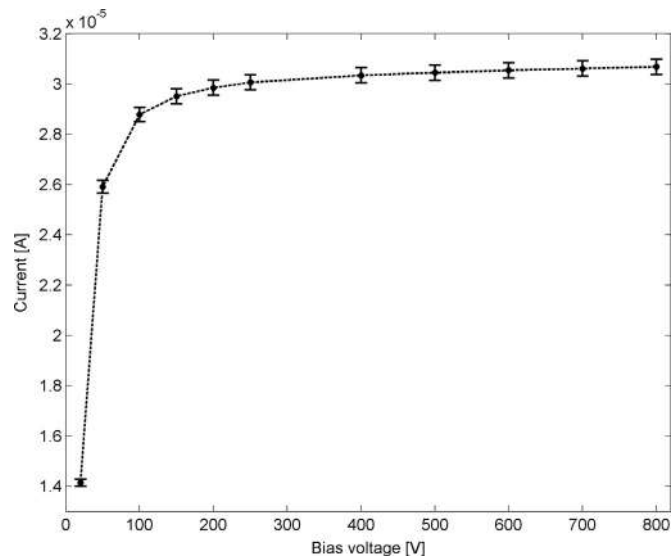
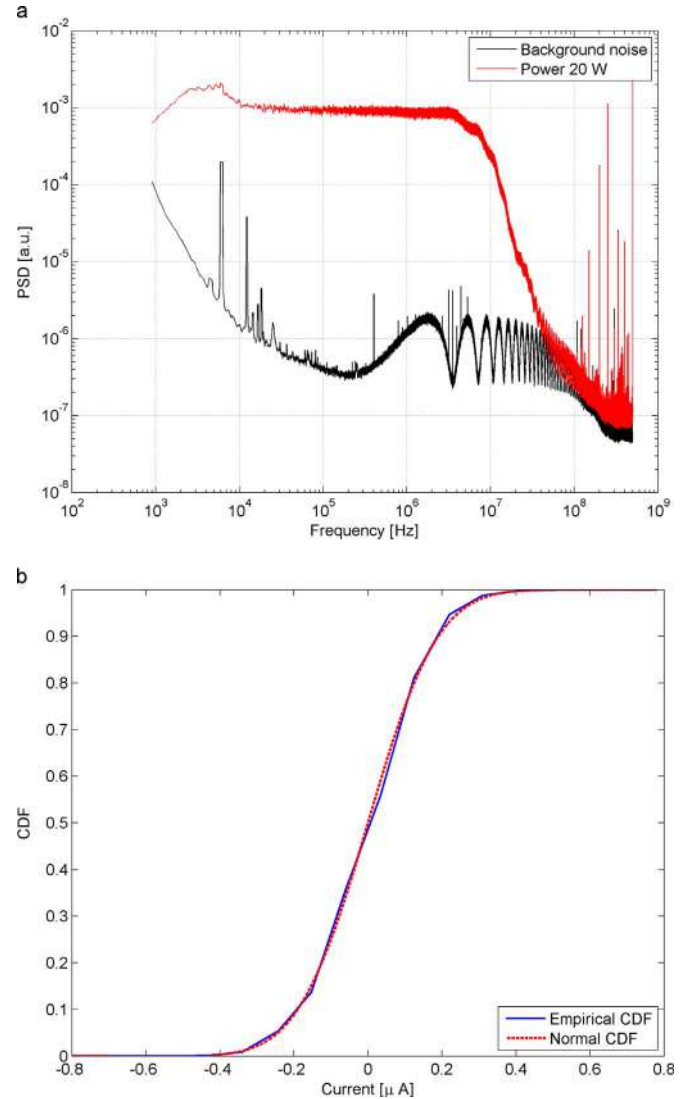Fig. 3. Saturation curve of CFUL01.

Fig. 4. Noise characteristics. Top: Power spectral density of the noise and the signal at 20 W. Bottom: Cumulative distribution function.

noise. The noise of the applied measurement system is briefly described below.

A measurement was performed while the voltage of the fission chamber was set to 0 V. In this case the signal consists only the parasitic noise of the electronic system (the pre-amplifier, the cables, and the oscilloscope). The study of the power spectral density shows that the noise level on the frequency domain of interest ($10^4$–$10^8$ Hz) is relatively low but not negligible compared to the real level of the signal as shown in Fig. 4 (the real signal corresponds to 20 W reactor power, and the nominal voltage of 600 V). The noticeable peaks on the PSD of the noise below 30 kHz are suspected to be caused by electromagnetic pollution, nevertheless their impact is negligible on the signal. Above $10^8$ Hz both PSDs exhibit almost the same amplitude which means that no useful signal is carried at those frequencies in the pulse train. The appearing peaks in this high frequency range are artifacts of the amplifier. The noise has pink frequency characteristics, with an oscillation in the spectra. The oscillation is caused by the cable (the period of the oscillation is around 4 MHz, which corresponds to the 25 m cable length). One can see also that the pre-amplifier removes the low frequency part of the signal hence the amplitude of the PSD of the pulse train at this frequency band is just an order of magnitude higher than that of the noise. This means that a

possible way to suppress the noise in traditional Campbelling is to compute the variance by integrating the PSD only in a certain frequency, as it was attempted in [9].

When computing the cumulants, spectral analysis is computationally more expensive. Therefore, working in the time domain is simpler and more suitable for real-time, digital applications.

The study of the amplitude of the recorded noise shows that although it is not Gaussian, its characteristics show similarities with the Gaussian distribution. The cumulative distribution function of the amplitude is compared to the normal CDF of the same standard deviation in Fig. 4. The standard deviation of the noise is around 7% of the amplitude of the mean pulse. The noise distribution is slightly skewed, but the third order cumulant of the noise distribution is three orders of magnitude lower than the third order cumulant of the signal at the lowest measurable power level, therefore its impact is negligible.

### 3.3. Applicability of Campbelling methods

In case the neutron source is a multiplying medium, the independence of the pulse arrival times is not a valid assumption anymore and the Campbelling results will be biased, especially around the critical reactor state, as it was shown for a system with only prompt neutrons [16]. However, one may assume that due to the low detection efficiency of fission chambers (around every ten thousandth neutrons) the detected neutrons over a short, few ms scale (i.e. the current pulses contributing to the signal) do not belong to the same neutron chain, hence the information about the neutron correlations is lost. In fact, the neutron chains are infinite in a critical reactor, but the prompt chains die out quickly. The chains become infinite only due to the delayed neutrons, but this would have an impact only at longer time scales (few seconds).

The auto-correlation function

$$ACF(\tau) = \lim_{T \to \infty} \frac{1}{2T} \int_{-T}^{T} y(t)y(t+\tau)dt \qquad (2)$$

of the fission chamber signal $y(t)$ was calculated numerically (since the recorded signal slice is a time-discrete signal) at a critical reactor state, 40 W power, for a measurement time ($T$) of 10 ms. The normalized (to the maximum) ACF is shown in Fig. 5. The same ACF is presented with a long, 10 ms (bottom, black) and a short, 500 ns (top, red) time scale. The ACF does not show any short or long term correlations in the signal. The shape of the function reflects only the average pulse shape of the fission chamber. The small bump around 250 ns is due to the current bouncing on the cable (which corresponds to the 25 m length of the cable with around 0.66 relative speed). Hence, if the Campbell measurements are based on sample sizes of few ms, the signal can be considered as uncorrelated, hence the Campbelling equations stay applicable at critical reactor state.

## 4. Results

At low reactor power levels when the pileup of pulses is unlikely, pulses were collected separately. During the post-processing the incidental pileups were eliminated. These measurements allow us to determine the calibration coefficient $C_n$, introduced in Eq. (1). At medium and high power levels longer signals were collected. At medium levels the pulses overlap moderately hence counting them separately is still possible to estimate the count rate of the signal. This provides an opportunity to estimate the count rate accurately and to compare it with the estimation coming from the calibrated HOC mode, and also allows us to perform an empirical calibration.
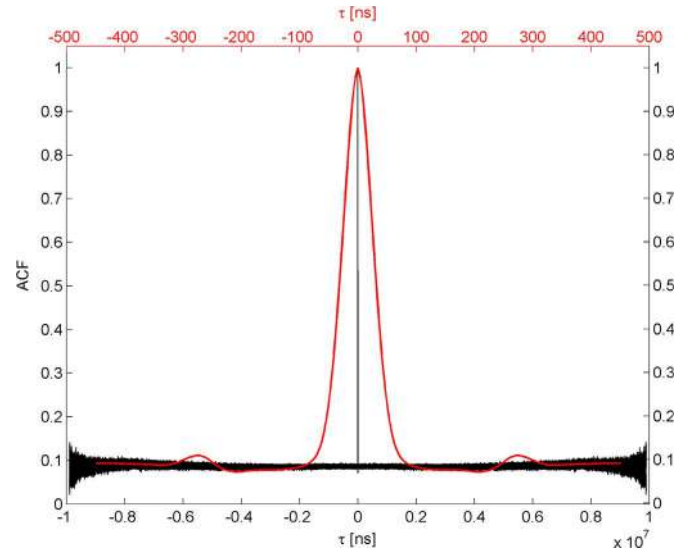


**Fig. 5.** Normalized autocorrelation function. (For interpretation of the references to color in this figure caption, the reader is referred to the web version of this paper).

It was shown in Part I that the third order Campbell methods provide an acceptable uncertainty for sample length of few ms. Therefore during this experiment the collected signal slices were 10 ms long.

In Section 4.1, first the linearity of the HOC mode is verified and the calibration against the reactor power is given. In Sections 4.2 and 4.3, the pulses contained in the signal are studied: the possible need of pulse classification is discussed and the calibration against the count rate is determined. Finally, in Section 4.4 the accuracy of the count rate estimation is investigated.

### 4.1. Calibration to power, linearity

To assess the linearity of the third order cumulant estimation against the power, the cumulants of the signal were estimated at several power levels. At each power level a set of 10 ms long samples were recorded in order to estimate the deviation of the cumulant estimation as well. The results, presented in Fig. 6, show a good agreement with the linear model fitted on the data. The power is also an estimated value (by a pre-calibrated measurement system), but at higher levels, the uncertainty of this estimation is negligible (around 0.1 W), therefore Fig. 6 does not show the horizontal error bars.

Based on the linear fit, it is possible to give an empirical calibration between the reactor power and the cumulants. But as it was mentioned, our main goal is to calibrate the chamber signal against its count rate. In the subsequent sections, the same cumulant values are used to verify the accuracy of that calibration.

### 4.2. Pulse discrimination

The CFUL01 fission chamber is a multi-coated fission chamber, as previously described in Section 3. The variation in pulse shapes coming from the different coatings has to be addressed, since (as discussed earlier) the Campbell-equation (1) based on one pulse shape may become inaccurate to describe the cumulant of the signal.

With the aid of the recently developed pyFC (python-based Fission Chamber simulator) code suite [17], the diversity of the pulse shape was illustrated. The suite simulates realistic heavy ion transport in 3-D. An illustrative sample of simulated heavy ion trajectories and the corresponding pulse shapes are presented in Fig. 7 (the geometry belongs to the inner chamber of the CFUL01,
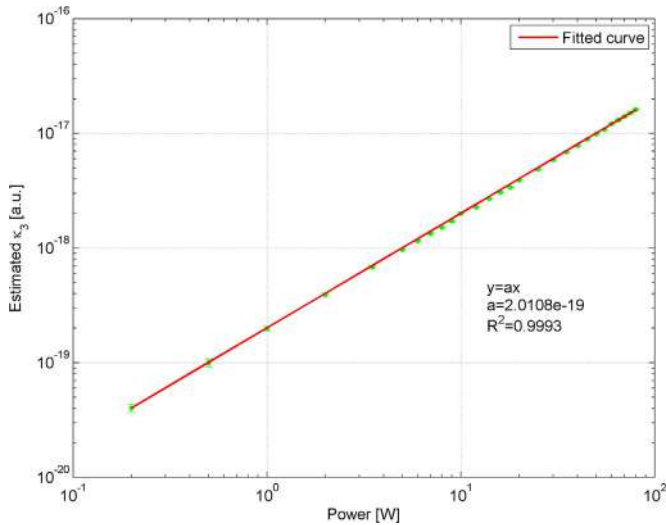
**Fig. 6.** Linearity of third order cumulant.

and only the radial coordinates of the trajectories are shown; the suite simulates the pulse creation before the pre-amplifier). The trajectories originating from the anode result in mostly quasi-triangular pulse shapes (and some exponentially decaying, shorter than average pulse shapes created by the heavy ions leaving axially the chamber before hitting the opposite electrode; due to the relatively small fraction of this kind, in the following they will be neglected). However, the trajectories originating from the cathode result in quasi-triangular pulses if the trajectory ends at the anode and quasi-trapezoidal pulses if the trajectory ends at the cathode. Therefore the fission chamber pulse shapes can be approximated as bimodal.

As a consequence, with the assumption that the creation of quasi-triangular and quasi-trapezoidal pulse shapes are independent (this independence is discussed in [18]), in the

Campbell-equation (1), a mixed, weighted calibration coefficient ($C_{n,mix} = p_{trap}C_{n,trap} + (1 - p_{trap})C_{n,tri}$) can be assumed. Here, $C_{n,trap}$ and $C_{n,tri}$ are the associated coefficients of the mean quasi-trapezoidal and quasi-triangular shapes, respectively, whereas $p_{trap}$ is the probability of observing a quasi-trapezoidal pulse, which is around 6% based on the simulations for the CFUL01. The mixed calibration coefficient necessarily differs from the one based on the mean pulse shape $\left(f = p_{trap}f_{trap} + \left(1 - p_{trap}f_{tri}\right)\right)$, since due to the $n$th power in the integral, cross terms of the quasi-trapezoidal and quasi-triangular pulses would appear.

Nevertheless, due to the band-pass filtering, in the experiments the difference in the shape is significantly mitigated, because both the quasi-trapezoidal and quasi-triangular pulses are distorted towards a Gaussian-shape, which makes their classification difficult. Based on the simulations, it was decided to estimate the impact of the pulse shape difference. The measured pulses were classified by measuring the distances of the left and right half maxima from the maximum of the pulse. Based on these distances, the pulses were classified as positively or negatively skewed.

Based on the simulations, around 6% of the CFUL01 pulses are expected to be quasi-trapezoidal shaped. With this simple discrimination method, around 4% of the measured pulses were classified as quasi-trapezoidal shaped during the experiment (the mean pulse shape of these pulses is shown in Fig. 8). As it will be seen in Section 4.3, the impact of the classification is less than 2% on the calibration coefficient. Therefore, the pulse classification method was not further improved, and it is advised to neglect this impact, in order to keep the simplicity of the calibration methodology. The overall error due to considering all pulses as having the same shape is estimated to be around 3%.

### 4.3. Calibration coefficient

As shown in Eq. (1) the calibration coefficient links the count rate of the signal to its cumulants. In this work the calibration
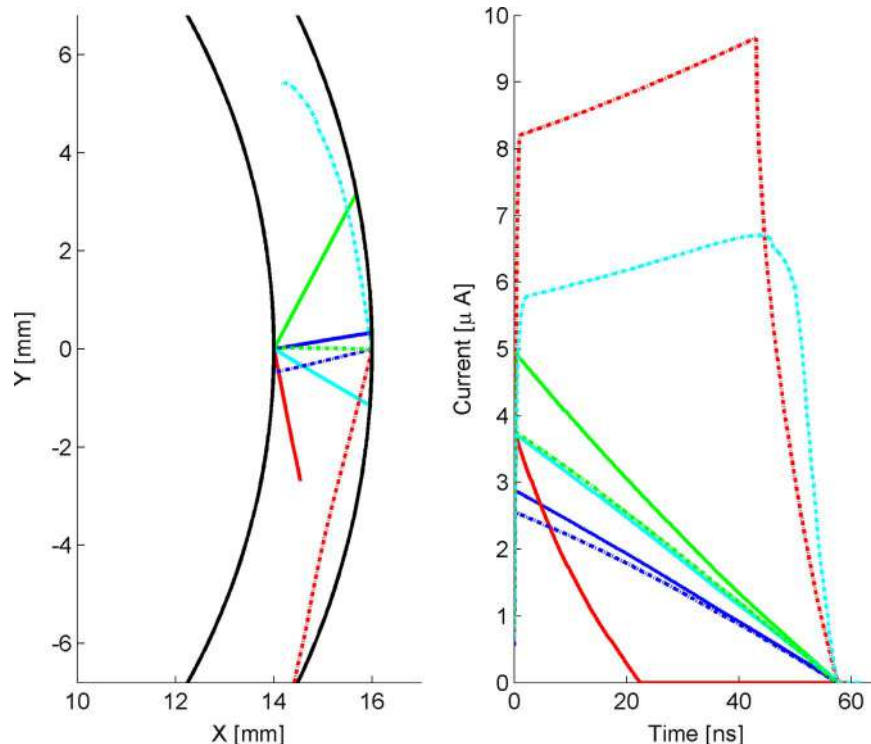


**Fig. 7.** Simulated heavy ion trajectories (left) and corresponding pulses (right) (straight line: anodic source, dotted line: cathodic source, same colors belong to the same event). (For interpretation of the references to color in this figure caption, the reader is referred to the web version of this paper).
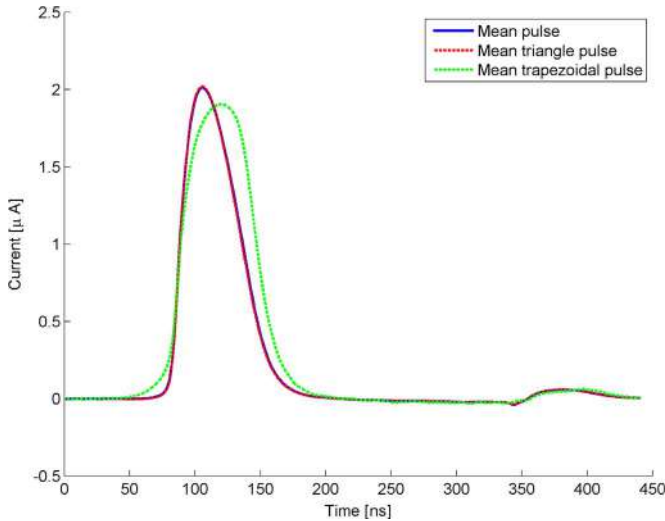
**Fig. 8.** Mean pulse shapes.

based on the amplitude distribution approach was followed, since a current-sensitive pre-amplifier was used for the measurements. In order to estimate the parameters needed to determine the coefficient, the statistical properties of the pulses were studied.

Fig. 8 presents the mean pulse shape and the mean shape of the classified trapezoidal and triangular pulses. Since only a few percent of the pulses are trapezoidal, the overall mean pulse shape is close to the triangular mean. A slight bump follows the main pulse events due to the cable, as discussed earlier. While calculating the time integral of the pulses, the boundaries of the integration covered these bumps as well.

For the determination of the maximum distribution, the pulses were smoothed with moving averaging method, because measuring the amplitude of pulses loaded with noise shifts the distribution towards larger values, which results in an overestimation of the raw moments. The moving average smoothing reduces this overestimation, without reshaping the pulses, and without suppressing the real amplitudes. Nevertheless, such smoothing reduces the robustness of the calibration.

The calibration coefficients of the second and third order Campbelling modes are summarized in Table 1. The random error of the coefficients was determined empirically (i.e. the coefficient was calculated for 10 set of 10 000 pulses), and the systematic error was estimated from the error of the amplitude measurement and the uncertainty of the measured current. Table 1 also contains the empirical third order calibration coefficient $C_{3,empir}$, introduced and discussed in Section 4.4. It has to be highlighted that the Campbell coefficients belong to the whole experimental setup (but are independent from the neutron spectra) and not only to the fission chamber. This shows the main disadvantage of the calibration procedure through investigating the pulse shape and its statistics. Such calibration may be problematic in case the system, which measures the third order cumulant, is not capable of recording the signal. In such case, the signal recording for calibration purpose may be done with a separate system, which can have a

different transfer function than the cumulant measuring system, and the pulse shape (and therefore the calibration coefficient) is sensitive to the transfer function. A possible way to overcome this issue is to perform an empirical calibration (as shown in the following section), where the count rate is estimated with pulse counting techniques (which are less sensitive to the transfer function) and compared to the measured cumulant.

### 4.4. Verification of the count rate estimation

After determining the calibration coefficient $C_n$, the count rate of the signal can be estimated. This has been done with both the calibrated traditional and the third order Campbelling methods. In order to verify the correctness of the estimated count rate and therefore the accuracy of the calibration procedure, the estimations at medium count rates were compared with the estimation provided by pulse counting. At these count rates (below $10^6$ s$^{-1}$), pulse mode measurements still can be performed accurately, because the signal mostly consists of not overlapping pulses.

The pulse counting (or pulse mode measurement) could be done in several ways, both with analog and digital systems. Since, for this work, the pulse counting was also performed during the post-processing phase, a simple algorithm, implemented in Matlab was used: when the recorded signal crossed a pre-defined discrimination level, a logical signal with a certain width (comparable to the pulse width) was triggered, and these logical pulses were counted. As reported in Ref. [3], in case the pulse amplitudes are randomly distributed and the low amplitudes are comparable with the amplitude of the noise, such pulse counting method fails to estimate the pulse count properly: in case the discrimination level is too low, the noise triggers spurious counts; in case the level is too high, the method does not count low amplitude pulses. Therefore, before counting the pulses, a second order Savitzky–Golay smoothing filter was applied to suppress the noise of the signal. Such a method is computationally expensive to be implemented in a real-time application, but for the purpose of this verification this was not a drawback. After smoothing the signal, the choice of the discrimination level is still not trivial. The pulse count was determined with several discrimination levels, in order to find the optimum discrimination level. The dependence of the pulse count on the discrimination level at 0.2 W power is shown in Fig. 9. The optimum was chosen at the inflexion point of this curve, as shown. Although, after smoothing the determination of the inflexion point becomes simpler, the pulse count is lower than without smoothing, which may mean that the pulse count is slightly underestimated.

The efficiency of the applied pulse counting method and its underestimation was investigated with the pulse train simulator described in [3]. In the simulation, the exact number of pulses contained in the simulated signal (containing the measured pulse shapes and amplitude distribution) is known, and it was compared with the counted number. For count rates in the order of $10^5$ s$^{-1}$ and lower, the error of the estimation is lower than 5%, when the optimum discrimination level is applied.

The count rate estimation results by the pulse counting and the Campbelling methods are summarized in Fig. 10. One immediately notices the linearity defect for the traditional Campbelling at low count rates. The overestimation is due to the noise (as described in [3,6]). However, the count rate estimated by the third order cumulant shows good agreement with the results of the pulse counting. It was found that the pulse counting already underestimates the count rate at 2 W due to the pileup events (hence the sign change in the relative difference between the empirical and the HOC estimation, presented in the bottom figure of Fig. 10).

An empirical calibration coefficient $C_{3,empir}$ was determined from the linear regression between the pulse counted count rate
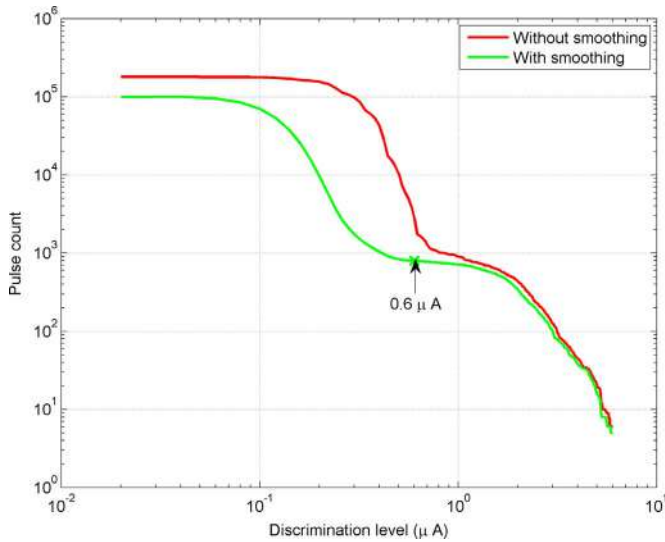
**Table 1**
Calibration coefficients.

| | |
|---|---|
| $C_2$ (A$^2$ Hz$^{-1}$) | $(2.00 \pm 0.04) \cdot 10^{-19}$ |
| $C_{2,mix}$ (A$^2$ Hz$^{-1}$) | $(2.00 \pm 0.03) \cdot 10^{-19}$ |
| $C_3$ (A$^3$ Hz$^{-1}$) | $(5.32 \pm 0.32) \cdot 10^{-25}$ |
| $C_{3,mix}$ (A$^3$ Hz$^{-1}$) | $(5.41 \pm 0.29) \cdot 10^{-25}$ |
| $C_{3,empir}$ (A$^3$ Hz$^{-1}$) | $(5.19 \pm 0.19) \cdot 10^{-25}$ |

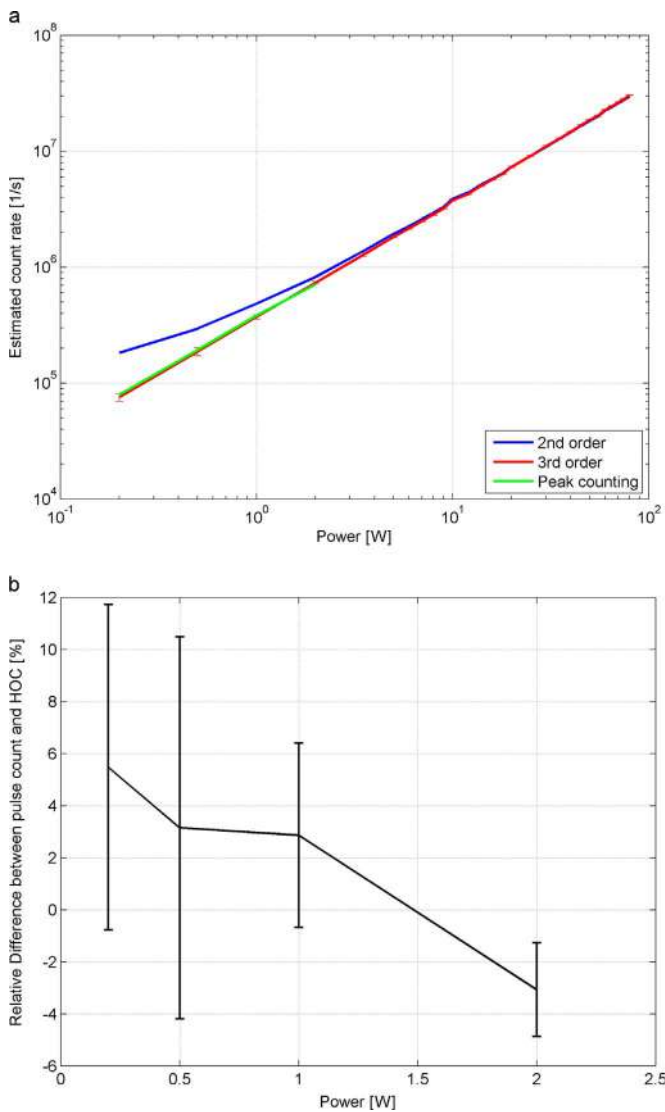**Fig. 9.** Pulse count dependence of the discrimination level.



**Fig. 10.** Top: Count rate estimation with different methods Bottom: Relative difference between pulse counting and HOC.

and the third order cumulant estimations. The empirical coefficient is included in Table 1. The empirical calibration was based on longer, 100 ms long signal slices, therefore the empirical coefficient has a rather small random error, and its standard deviation was dominated by the propagation of the systematic error of the pulse count (detailed earlier). The difference of the empirical and the HOC calibration is less than 4%.

The good agreement between the empirical and HOC calibration verifies the possibility to calibrate the fission chambers in HOC mode empirically. Thus if one can perform a reliable pulse count estimation at low count rates, then the empirical calibration provides the simplest and most robust calibration methodology (i.e. the difference in pulse shape will not have any significance, and the cumulant measuring system can be cross calibrated with a reliable pulse counting system, since the difference in the transfer function will not have a significant impact on the pulse count). Such calibration is not plausible for the traditional Campbelling method, due to the linearity gap between the pulse counting method and the Campbelling.

### 4.5. Transient events

A key requirement for online flux monitoring systems is the capability of following changes in the flux, and to provide reliable information even if the reactor is in a non-stationary state. It was argued [13] and investigated numerically [6] that the Campbelling and higher order Campbelling methods are limited only by the smallest reliable measurement time to monitor fast transients. In the frame of the current work an experimental demonstration of the transient monitoring was performed.

The MINERVE reactor is not designed to induce transients, therefore the fastest transient which can be authorized by the operators is the control rod drop transient. For the current measurement the reactor power was kept at stationary 60 W power level, when the control rods were dropped. The fall of the control rods takes around 0.4–0.5 s.

Fig. 11 presents the time evolution of the Campbell count rate estimations based on 2 ms long signal slices (right axis, pink and green curves in the foreground) and the fission chamber signal (left axis, light blue curve in the background). At the beginning of the measurement, the reactor was in stationary state at 60 W, the estimated count rate is constant in time. The control rod was
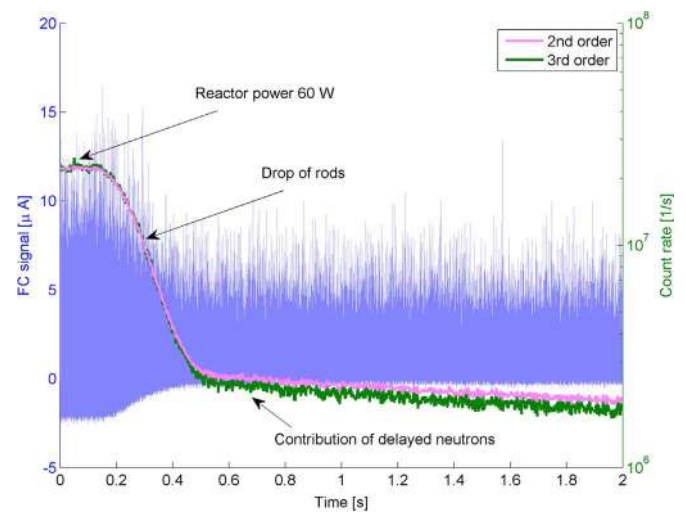


**Fig. 11.** Transient measurement. (For interpretation of the references to color in this figure caption, the reader is referred to the web version of this paper).

dropped 0.1 s after the measurement was started, which can be observed from the rapid, exponential decrease of the estimated count rate (the semi-logarithmic plot is linear). During this time period, one can observe the change in the offset of the signal, which is caused by the applied pre-amplifier, which removes the mean of the signal. By definition, a constant offset does not impact the Campbell methods (i.e. the second and third order cumulants are not sensitive to constant shifts), but it has to be highlighted that in the current situation, the offset changes with time. Nevertheless, due to the short sampling length, the offset of each sample is approximately constant, hence its impact is negligible. The control rod was fully inserted after a fall of 0.4 s, when the decrease of the count rate is turning slower. From 0.5 s, a slow decrease of the count rate can be observed as a result of the delayed neutrons. Both the traditional and the third order Campbell method show sufficiently dynamic response at the beginning of the transient (during the fall of the rod). However, at the end of the transient, the count rate is overestimated by the traditional Campbelling mode.

## 5. Conclusion

In this paper a method to calibrate fission chambers in Higher Order Campbelling mode was presented. For the calibration the statistical properties of the fission chamber pulses were measured.

The measurements were performed at the MINERVE reactor with a CFUL01 fission chamber. The cumulant estimation of the acquired signals was done during post-processing the data.

During the experiments, the linearity of the High Order Campbelling methods was verified, and the accuracy of the count rate estimation was tested. The dynamics of the Campbelling method during a transient event were assessed.

The experimental calibration of the third order method was done through investigating the pulse shape and the amplitude distribution of the pulses. The work points out that this procedure may be problematic for third order cumulant measuring systems, which are not capable of recording the signal. For such cases the signal recording has to be done with a separate system, which can have a different transfer function, for which the calibration coefficient is sensitive.

Since the third order cumulant shows good linearity even at low count rates ($10^4$–$10^5$ s$^{-1}$), where accurate count rate estimation is possible with pulse counting techniques, a possible way to overcome this issue, is to perform an empirical calibration, where the count rate is estimated with pulse counting and compared to the measured cumulant. Such empirical calibration could be performed with dedicated pulse mode systems as a cross-calibration, because the difference in the transfer function would not affect the applied pulse count technique.

In the current work, the difference between the count rate estimated by the calibrated higher order Campbelling and the count rate estimated by the empirical pulse counting is less than 5%.

This work is a step towards the implementation of an FPGA-based real-time digital measurement system. The realization of such system and its testing is under progress.

## References

[1] OECD/NEA, Technology Roadmap Update for Generation IV Nuclear Energy Systems, Technical Report, OECD/NEA, January 2014.

[2] F. Gauché, Generation IV reactors and the ASTRID prototype: lessons from the Fukushima accident, C. R. Phys. 13 (4) (2012) 365–371.

[3] Zs. Elter, C. Jammes, I. Pázsit, L. Pál, P. Filliatre, Performance investigation of the pulse and Campbelling modes of a fission chamber using a Poisson pulse train simulation code, Nucl. Instrum. Methods Phys. Res. Sect. A: Accel. Spectrom. Detect. Assoc. Equip. 774 (2015) 60–67, http://dx.doi.org/10.1016/j.nima.2014.11.065.

[4] I. Lux, A. Baranyai, Higher order campbell techniques for neutron flux measurement: I. Theory, Nucl. Instrum. Methods Phys. Res. 202 (3) (1982) 469–475.

[5] I. Lux, A. Baranyai, Higher order campbell techniques for neutron flux measurement: II. Correlated Campbelling, Nucl. Instrum. Methods Phys. Res. 202 (3) (1982) 477–480.

[6] Zs. Elter, M. Bakkali, C. Jammes, I. Pázsit, Performance of higher order campbell methods, part I: review and numerical convergence study, Nucl. Instrum. Methods Phys. Res. Sect. A: Accel. Spectrom. Detect. Assoc. Equip. 821 (2016) 66–72, http://dx.doi.org/10.1016/j.nima.2016.03.023, URL 〈http://www.sciencedirect.com/science/article/pii/S0168900216300420〉.

[7] E.W. Pontes, A. Ferreira, Using cumulants and spectra to model nuclear radiation detectors, IEEE Trans. Nucl. Sci. 53 (3) (2006) 1292–1298, http://dx.doi.org/10.1109/TNS.2006.875200.

[8] L.B. Baers, T. Rivero Gutierrez, R.A. Carrillo Mendoza, G. Jimenez Santana, Use of higher order signal moments and high speed digital sampling technique for neutron flux measurements, IEEE Trans. Nucl. Sci. 40 (4) (1993) 832–839.

[9] B. Geslot, T.C. Unruh, P. Filliatre, C. Jammes, J. Di Salvo, S. Breaud, J. Villard, Method to calibrate fission chambers in Campbelling mode, IEEE Trans. Nucl. Sci. 59 (4) (2012) 1377–1381, http://dx.doi.org/10.1109/TNS.2012.2198669.

[10] N.R. Campbell, V.J. Francis, A theory of valve and circuit noise, JIEE 93 (1946) 45.

[11] R.A. DuBridge, Campbell theorem – system concepts and results, IEEE Trans. Nucl. Sci. NS-14 (1967) 241.

[12] L. Pál, I. Pázsit, Zs. Elter, Comments on the stochastic characteristics of fission chamber signals, Nucl. Instrum. Methods Phys. Res. Sect. A: Accel. Spectrom. Detect. Assoc. Equip. 763 (2014) 44–52.

[13] Zs. Elter, I. Pázsit, C. Jammes, Remark on the applicability of Campbelling techniques for transient signals, Nucl. Instrum. Methods Phys. Res. Sect. A: Accel. Spectrom. Detect. Assoc. Equip. 813 (2016) 10–12.

[14] E.W. Weisstein, "k-statistic." From Mathworld – A Wolfram Web Resource. URL 〈http://mathworld.wolfram.com/k-Statistic.html〉.

[15] C. Jammes, P. Filliatre, P. Loiseau, B. Geslot, On the impact of the fissile coating on the fission chamber signal, Nucl. Instrum. Methods Phys. Res. Sect. A: Accel. Spectrom. Detect. Assoc. Equip. 681 (0) (2012) 101–109, http://dx.doi.org/10.1016/j.nima.2012.03.032.

[16] L. Pál, Pázsit, Campbelling-type theory of fission chamber signals generated by neutron chains in a multiplying medium, Nucl. Instrum. Methods Phys. Res. Sect. A: Accel. Spectrom. Detect. Assoc. Equip. 794 (1) (2015) 90–101.

[17] Zs. Elter, pyFC: A TRIM-based Fission Chamber Pulse Shape Simulator, Technical Report, CTH-NT-318, Chalmers University of Technology, 2015.

[18] P. Filliatre, C. Jammes, B. Geslot, R. Veenhof, A. Monte, Carlo simulation of the fission chambers neutron-induced pulse shape using the GARFIELD suite, Nucl. Instrum. Methods Phys. Res. Sect. A: Accel. Spectrom. Detect. Assoc. Equip. 678 (0) (2012) 139–147, http://dx.doi.org/10.1016/j.nima.2012.03.020.

# Paper VI

## Self-monitoring fission chamber: theoretical ground-work

Zs. Elter, P. Filliatre, G. de Izarra, I. Pázsit and C. Jammes

# Self-monitoring fission chamber: theoretical groundwork

**Zsolt Elter and Imre Pázsit**
Department of Physics, Division of Subatomic and Plasma Physics
Chalmers University of Technology, SE-412 96 Göteborg, Sweden
zsolt@nephy.chalmers.se
imre@nephy.chalmers.se


**Philippe Filliatre, Grégoire de Izarra and Christian Jammes**
CEA, DEN, DER, Instrumentation, Sensors and Dosimetry Laboratory
Cadarache, F-13108 Saint-Paul-lez-Durance, France
philippe.filliatre@cea.fr
gregoire.deizarra@cea.fr
christian.jammes@cea.fr

### ABSTRACT


The most common application of fission chambers in a core monitoring system is to measure the neutron flux. As is well known, in such a case, it is advantageous to use the so-called Campbell relationships. However, the application of of the Campbell methods requires some calibration of the chamber. Due to certain events, such as crack of the chamber wall, the calibration might become obsolete, and the system would underestimate the count rate and therefore the flux.

This paper investigates the possible application of a simple method to identify whether the measured count rate change is due to the malfunction of the detector or due to the change of neutron flux. The method is based on the change of the frequency dependence of the power spectral density of the fission chamber signal, due to the malfunction. For the current work the filling gas pressure drop due to cracking was considered as the malfunction. In theory the method enables an early failure detection. The experimental verification is under progress.


*Key Words:* **Fission chamber, Neutron flux monitoring, Self-monitoring, Campbelling**

## 1. INTRODUCTION


The application of the higher order Campbelling methods (HOC) for neutron flux monitoring is an active research topic at CEA Cadarache. Assuming that the detector signal $\eta(t)$ can be described as a filtered Poisson process also known as shot noise, (i.e. the signal is formed as the superposition of constant pulse shapes $f(t)$ with random amplitudes $\mathbf{q}$, induced by independent incoming events), the cumulants of the signal (i.e. the measurable quantity) are proportional to the count rate of the detection events (i.e. the quantity of interest). The higher order Campbelling methods are based on the higher

order Campbell theorem, which gives this proportionality between the higher order cumulants of the detector signal and its count rate [1]:

$$\kappa_n = s_0 \langle q^n \rangle \int\limits_{-\infty}^{+\infty} f(t)^n dt = s_0 \cdot C_n \tag{1}$$

where $\kappa_n$ stands for the $n$th order cumulant of the fission chamber signal (the quantity we can measure) and $s_0$ denotes the count rate (the quantity we would like to determine). The proportionality coefficient $C_n$ contains the raw moment of the pulse charge distribution $q$ and the normalized mean pulse shape $f(t)$. The application of the HOC method is limited by the proper calibration of the proportionality coefficient.

Eq. (1) shows that any cumulant of the signal may change not only due to the change in the count rate, but also due to the change in the mean pulse shape or the charge distribution. And the higher order methods are particularly sensitive to these changes due to the higher exponents in Eq. (1). These changes may occur due to the reduction of detector pressure or voltage. During the measurement only the change of the cumulant (therefore the change of the estimated count rate) will be detected thus we have to be able to decide whether this change occurred due to the change of the neutron flux around the detector or due to the malfunction of the detector.

Previously there have been attempts to perform regular tests to identify malfunctions of fission chambers [2]. Due to the fast development of digital hardware (such as field programmable gate arrays), the Campbell techniques can be realized with digital processing and the fault detection may be implemented in the same system in real-time.

The current work explores the possibility of detecting the detector failure from the change of the shape $f(t)$ of the detector pulse. Namely, earlier work showed that the temporal auto-correlation of the detector signal depends on the detector pulse shape [1]. Hence, if the detector malfunction results in a change of the detector pulse shape, this latter can be discovered from the detector signal auto-correlation function, or from its power spectral density (PSD). Thus, this work investigates the alteration in the mean pulse shape due to failure of the detector and investigates the possibility to identify the malfunction from the changed characteristics of the detector signal PSD.

The hypothetical malfunction scenario is considered as the loss of filling gas from the chamber. First we model the change of the pulse shape characteristics in a CFUL01 fission chamber during a pressure drop of the filling gas. Second, the impact of the altered pulse shape on the auto power spectral density of the signal is evaluated. Finally, the implementation of the method on an experimental FPGA board is briefly described. The work is the first step towards a self-diagnosing detector in order to increase the neutron monitoring system preventive maintenance.

## 2. FISSION CHAMBER PULSE SIMULATION

### 2.1. Description of the Fission Chamber

For this work a CFUL01 fission chamber (manufactured by Photonis) was studied, which has a very similar geometry to the high temperature fission chambers designed for the Astrid reactor. The CFUL01 is a multi-electrode and multi-coating detector, which means that the chamber contains four coaxial electrodes and four fissile coatings of enriched uranium. The sensitive length of the detector is 211 mm and the electrode radii are 14, 16, 17, 19 mm. The nominal operating voltage is 600 V. The filling gas is Argon with 4 % Nitrogen at 250 kPa (at room temperature).

### 2.2. The pyFC Pulse Shape Simulator

The current pulses in a fission chamber come from the ionization of the filling gas by the heavy ion emitted from the neutron induced fission in the fissile deposit. Recently a new fission chamber pulse shape simulator, the pyFC suite (*py*thon-based simulation of *F*ission *C*hambers) was developed to compute the pulses of a fission chamber. In pyFC the path of the heavy ion and the spatial distribution of the charges emerging from the ionization process are simulated with the TRIM code [3], and the parameters of the charge collection between the electrodes are computed with the BOLSIG software [4]. The coupling of the codes is done in Python. The details of the code system are described in [7].

The code does not consider any recombination events and avalanches, which means that the chamber is assumed to work in the saturation regime. The space charge effects are neglected (each fission product entering the inter-electrode space ionizes the gas independently). Only the current induced by the electrons is considered, since the mobility of the ions created by the fission fragment is much lower, therefore with a high-pass filter the ionic signal can be filtered out. The self-absorption of the fission fragments within the coating is neglected.

Multi-electrode and multi-coating chambers can be investigated with superposition, i.e. combining the results of more runs, each corresponding to one fissile coating by assuming that the inter-electrode spaces are mutually independent. Therefore the simulations of the CFUL01 chambers consisted of four independent runs.

## 3. IMPACT OF PRESSURE DROP

As mentioned before, the change of the fission chamber characteristics may have several causes. For illustration in this work the chosen scenario was a pressure drop of the filling gas due to a crack on the

wall of the fission chamber. Such a crack would not appear instantaneously, but rather would develop during a longer period of time. Modeling the development of such ruptures is beyond this work.

Instead, a simple model was derived to describe the pressure drop in a fission chamber. For simplicity the filling gas was considered as pure argon and the crack was assumed to be cylindrical through the wall. The sodium pressure in an Astrid-like core at the fission chamber location was calculated with Bernoulli's theorem and is around $72$ kPa. Given the scope of the article, the derivation of the flow model is not included here. It was shown that for crack diameters less than $1~\mu$m the pressure drop is negligible. While for crack diameter larger than $100~\mu$m the drop is almost instantaneous. The method presented in this work is applicable in case of intermediate crack diameters. Such a pressure drop is presented in Fig. 1, which is related to $25~\mu$m diameter.
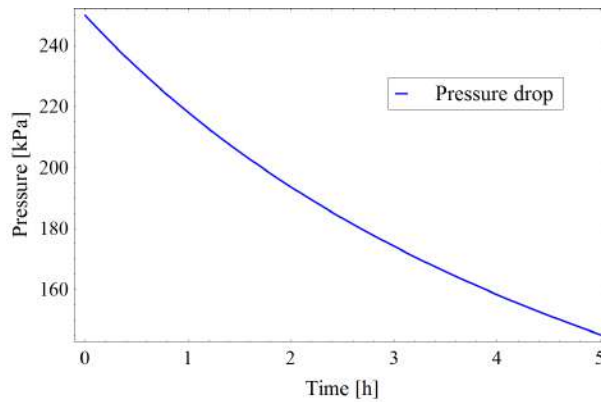


**Figure 1.** Pressure drop in the fission chamber

### 3.1. Pulse Shape Change

The computation of the mean pulse shape and the charge distribution was performed for several pressure values between $150$ and $250$ kPa. Only the pulses generated by the electron tracks were considered. Although, for a given pressure, there is some variation in the pulse shape (depending on the angles of the ionization tracks), for simplicity, in the following only the mean shape is considered, because the most important characteristics of the pulse, its width, is roughly independent of the track. The results are summarized in Fig. 2. By decreasing the filling gas pressure (and therefore the number of gas atoms in the chamber) the pulse width and the carried charge (the integral of the current pulse) is decreasing as well. At lower pressure the heavy ion creates less electron-ion pairs and the mobility of the electrons becomes higher. The pulse width shows a saturation which is a consequence of the saturation in the drift velocity at low pressures.

Fig. 2 shows that the charge distribution of the created pulses is also affected by the pressure drop. The median of the distribution becomes lower and the raw moments of the distribution are decreasing during the pressure drop.
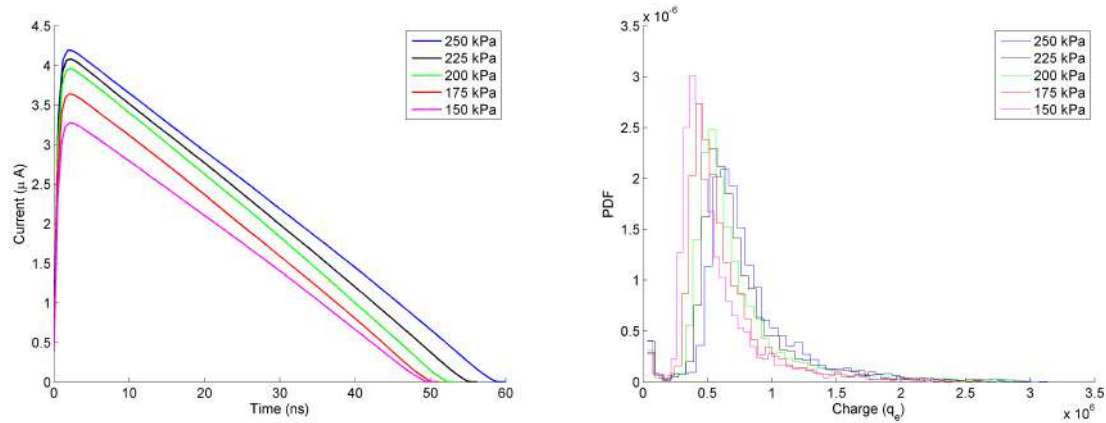
**Figure 2.** Fission chamber pulse characteristics due to pressure drop; Left: Mean pulse shape Right: Charge distribution

As a consequence, both terms of the calibration coefficient, introduced in Eq. (1) are decreasing during the pressure drop. The alteration in the second and third order coefficient is $-15\%$ and $-21\%$ due to $25\,\text{kPa}$ pressure change. Therefore the cumulants of the signal decrease significantly, even if the real count rate is unchanged. This results in an underestimation of the count rate with the original calibration coefficient.

## 4. MALFUNCTION DETECTION THROUGH POWER SPECTRAL DENSITY

### 4.1. Theory

The previous section showed that in case of detector failure during neutron flux monitoring one can experience diminishing count rate estimation without an actual change in the neutron flux. The task of a self-diagnosing detector is to identify whether the estimated count rate changed due to the change of the count rate or due to other reasons.

Therefore we have to define a measurable quantity of the fission chamber signal which is sensitive to the pulse shape change but not to the count rate change. The power spectral density (PSD) of the detector signal satisfies this requirement. It can be shown for a filtered Poisson process (which describes the fission chamber signals) that the power spectral density has a breakdown at high frequencies which depends on the pulse shape [5].

To study the PSD of the fission chamber signals, an in-house fission chamber signal simulator was used (the software and its verification are described in detail in [6]). With the software, various pulse trains were simulated.

First it was verified that changing the count rate of the signal does not effect the shape and the breakdown frequency of the PSD, just the amplitude. Also the impact of the charge distribution was studied separately. In accordance with our expectations the charge distribution has only an effect on the amplitude of the PSD.

Finally, the impact of the pulse shape was investigated. The results are shown in Fig. 3. Due to the alteration of the pulse shape, primarily its width, the PSD will extend to higher frequencies at lower filling gas pressures. This change can be quantified by considering the PSD as half of a Gaussian-like peak, and use its full width at half maximum (FWHM) to provide a simply measurable quantity to indicate gas leakage.
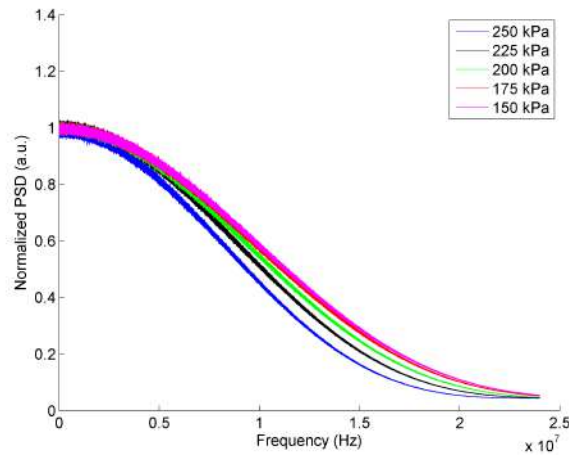


**Figure 3.** PSD of the signal for different pulses

### 4.2. Accuracy

One can notice that the spectral densities in Fig. 3 have some variance, therefore the estimation of the FWHM is not trivial. To guarantee reliable FWHM estimation and therefore reliable fault detection, the accuracy of the method has to be assessed.

Three methods were evaluated to determine the FWHM. In all cases, first the maximum was computed after filtering out the frequency range under $2\,\mathrm{kHz}$ with a high-pass filter. Thereafter the FWHM was determined by either searching for the half maximum of the PSD from low frequencies towards high frequencies, or from high to low frequencies. The third estimate was represented by averaging the other two. Fig. 4 shows the convergence of the FWHM estimations. The best convergence can be reached by the estimation which scans the spectra from high to low frequencies. The reason is that the variance of the spectra is higher at lower frequencies, therefore by increasing the measurement time the estimated value of the FWHM is increasing with the other methods. This also implies that the "real" value of the FWHM is closer to the one estimated by scanning from higher to lower frequencies.
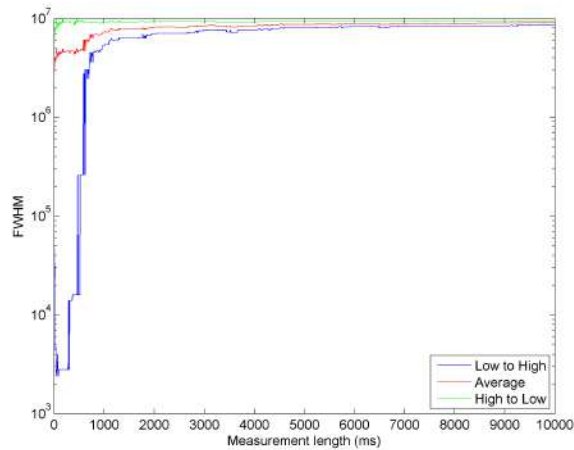
**Figure 4.** Convergence of FWHM estimation ($P = 250$kPa)

If the FWHM estimation is based on $10$ s long signals, then the error of the estimation is less than $1\%$, which corresponds to a minimum detectable pressure drop of $5$ kPa.

## 4.3. Semi-Experimental Verification

The real time performance of the PSD FWHM estimation was investigated by implementing the algorithm on a CPU/FPGA System on a Chip (SoC) board. For convenience, the Red-Pitaya board was chosen since it carries a Xilinx Zync 7010 SOC as well as two 14 bits, 125 MHz ADC (LTC2145CUP-14 from Linear Technology). As input, the simulated signals, generated by the pyFC suite of codes were used.

The implementation was made as simple and versatile as possible; the FPGA is responsible for gathering data and storing them into a 65356 samples buffer on the order of the CPU. Once the buffer is full, a flag alerts the control software running on the CPU that data is ready to be transferred. The data transfer is serialized and performed on demand in order to keep computing power and bandwidth for other measurements like the Campbelling mode. The computation of fast Fourier transform is done on the CPU with dedicated functions of the Gnu Scientific Libraries. The Bartlett Method (averaged periodogram) was chosen to retrieve the PSD. At last, the estimation of the FWHM of the PSD is done, while the FPGA is gathering new data.

The experimental FPGA board is in early testing stage. It was already tested in laboratory with the help of signal generators. Poisson pulse trains of 0.16 second duration with a count rate of 1 MHz were created with the simulation software and played with a 1 GHz arbitrary waveform generator while the experimental board was recording. The trains contained Gaussian shaped pulses with $50$ns mean width and standard deviation of $5$, $10$ and $15$ ns in order to show the effect of pulse shape duration

on the spectrum. The normalized PSDs, averaged on 100 spectra are shown in Fig. 5. The peak at 1 MHz frequency and its harmonics are "deliberate" artifacts due to the cyclic play of the pulse trains. This way the correctness of the measurement was tested. The spectrum is clearly broadening with the reduction of pulse width, which is in accordance with the expectations. The working principle of the experimental FPGA board is demonstrated; however, a large amount of work remains to optimise and validate it. This will be made soon through an experimental campaign in the MINERVE reactor.
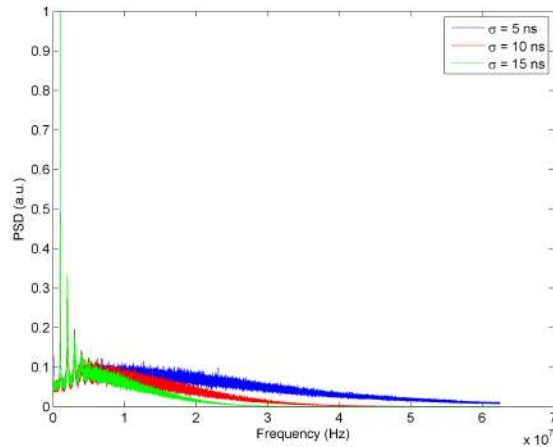


**Figure 5.** PSD measurement test performed with an FPGA board

## 5. CONCLUSIONS

It was shown that the FWHM measurement of the PSD of a fission chamber signal provides an opportunity to detect the change of the mean pulse shape, which indicates malfunctioning. For the current work the leakage of the filling gas was considered as a possible malfunction. It was shown through simulations that the filling gas pressure drop has a significant impact on the pulses generated in the fission chamber, and therefore on the PSD of the signal. According to the preliminary analysis the minimum detectable pressure drop is $5$ kPa.

It has to be verified that the PSD widening due to the pressure drop does not vanish in a real measurement system due to the frequency filtering effects of the electronics.

The development of an FPGA based measurement tool which determines the PSD of the fission chamber signal during flux monitoring is under progress. In the near future a measurement campaign is planned in the MINERVE reactor to test the FPGA tool. The PSD measurements will be carried out while continuously changing the voltage, since during the measurement one can only control the bias voltage of the fission chamber, and not the filling gas pressure.

# ACKNOWLEDGMENTS

# REFERENCES

[1] L. Pál, I. Pázsit, Zs. Elter, "Comments on the stochastic characteristics of fission chamber signals", *Nuclear Instruments and Methods in Physics Research Section A: Accelerators, Spectrometers, Detectors and Associated Equipment* **763**: pp. 44-52. (2014)

[2] R. Hunt, "Testing fission chambers", *Nuclear Engineering International magazine* (2011) URL http://www.neimagazine.com/features/featuretesting-fission-chambers/

[3] J. F. Ziegler, J. P. Biersack, M. D. Ziegler, "The Stopping and Range of Ions in Matter", http://SRIM.org (2008)

[4] G. J. M. Hagelaar, L. C. Pitchford, "Solving the Boltzmann equation to obtain electron transport coefficients and rate coefficients for fluid models", *Plasma Sources Sci. Technol.* **14**: pp. 722-733 (2005)

[5] L. Pál, I. Pázsit, "Campbelling-type theory of fission chamber signals generated by neutron chains in a multiplying medium", *Nuclear Instruments and Methods in Physics Research Section A: Accelerators, Spectrometers, Detectors and Associated Equipment* **794**: pp. 90-101. (2015)

[6] Zs. Elter, C. Jammes, I. Pázsit, L. Pál, P. Filliatre, "Performance investigation of the pulse and Campbelling modes of a fission chamber using a Poisson pulse train simulation code", *Nuclear Instruments and Methods in Physics Research Section A: Accelerators, Spectrometers, Detectors and Associated Equipment* **774**: pp. 60-67. (2015)

[7] Zs. Elter, "pyFC: a TRIM-based fission chamber pulse shape simulator", *Chalmers University of Technology technical note* **CTH-NT-318** (2015)

# Paper VII

Design of a higher order Campbelling mode measurement system using open source hardware

G. de Izarra, Zs. Elter and C. Jammes

# Design of a high order Campbelling mode measurement system using open source hardware

G. de Izarra[a], Zs. Elter[b,c], C. Jammes[b]

[a] *CEA, DEN,DER, Experimental Programs Laboratory, Cadarache,*
*F-13108 Saint-Paul-lez-Durance, France*
[b] *CEA, DEN,DER, Instrumentation, Sensors and Dosymetry Laboratory, Cadarache,*
*F-13108 Saint-Paul-lez-Durance, France*
[c] *Chalmers University of Technology, Department of Physics, Division of Subatomic and Plasma Physics,*
*SE-412 96 Göteborg, Sweden*

## Abstract

This paper reviews a new, real-time measurement instrument dedicated for online neutron monitoring in nuclear reactors. The instrument implements the higher order Campbelling methods and self-monitoring fission chamber capabilities on an open source development board. The board includes an CPU/FPGA System On a Chip.

The feasibility of the measurement instrument was tested both in laboratory with a signal generator and in the Minerve reactor. It is shown that the instrument provides reliable and robust count rate estimation over a wide reactor power range.

The fission chamber failure detection ability is also verified, the system is able to identify whether the measured count rate change is due to the malfunction of the detector or due to the change of neutron flux. The applied method is based on the change of the frequency dependence of the fission chamber signal power spectral density, due to the malfunction. During the experimental verification, the considered malfunction was the change of the polarization voltage.

*Keywords:* High order Campbelling, FPGA, Measurement system, Count rate estimation
*PACS:* 29.85.-c, 28.50.Dr, 28.41.Rc

# 1. Introduction

The recent development of French Sodium-cooled Fast Reactor (SFR) induces the need for new neutron flux monitoring systems in order to enhance the safety features. Given the configuration of the pool type SFR, the neutron instrumentation is planned to be set up in the reactor vessel in order to monitor the neutron flux over a few orders of magnitude [1]. The high temperature fission chambers are the best candidates for this purpose since the typical temperature in the vicinity of the core is around 500 $^o$C [2]. This detector type was extensively studied in the CEA during the nineties and is still under active development. In addition, a research effort is currently done in order to exploit the wide flux range monitoring capability of fission chambers: it was previously shown that the use of high order Campbelling mode (HOC) provides a linear estimation of the neutron flux over a wide range of count rate by suppressing the impact of parasitic noises.

In this framework, a HOC measurement system prototype was developed at the Instrumentation, Sensors and Dosimetry Laboratory (LDCI) of CEA Cadarache. The main goal of the work is to assess the feasibility and the industrial use of such measurement system. To complete the measurement device, a fission chamber malfunction detection module (referred later as "smart-detector" capability) was included.

In this paper, the implementation of HOC method on an open source hardware development board is detailed. First, the general theory of HOC is discussed briefly and the most important advantages of its application are highlighted. The theoretical basis of the fission chamber malfunction detection is also reviewed. Second, the design of the Campbell measurement system is presented: the preference of using a open source hardware with a CPU/FPGA chip at the prototype phase are summarized; The HOC computation algorithm is explained through diagrams and clocking figures; The software dedicated to control the FPGA module is introduced. The last part of the paper is dedicated to the validation of the measurement system through laboratory measurements and in-core experimental campaigns performed at the Minerve reactor.

# 2. Theoretical background

## 2.1. High order Campbelling theoretical background

Campbell derived a theorem [3] that links the intensity of a shot noise process consisting of general pulses $f(t)$ with an amplitude distribution to

37 the variance of the process. The generalisation of this theorem was proposed
38 and its complete derivation has been performed in [4, 5]:

$$s_0 = \frac{\kappa_n}{\langle x^n \rangle \int f^n(t)dt} = \frac{k_n}{C_n}. \tag{1}$$

39 where $\kappa_n$ is the $n$th order cumulant of the signal, $s_0$ is the count rate and
40 $\langle x^n \rangle$ stands for the $n$th order raw moment of the amplitude distribution.
41 Commonly, the methods in which $n \geq 3$ are called higher order methods.
42 Eq. (1) shows that if the pulse shape and the amplitude distribution are
43 known (therefore the calibration coefficient $C_n$ is determined), and the cu-
44 mulant (of any order) of the signal is measured, then the mean count rate
45 $s_0$ of the signal can be estimated.
46    In the current work, the estimation of the cumulants is performed by
47 applying unbiased cumulant estimators, called k-statistics [6]. If the mea-
48 sured signal consists of $N$ discretely sampled values $Y_i$, then the third order
49 cumulant estimator is given as:

$$k_3 = \frac{2S_1^3 - 3NS_1S_2 + N^2S_3}{N(N-1)(N-2)}, \tag{2}$$

50 where $S_1$, $S_2$, $S_3$ are the first, second and third order sums of the data points
51 defined as:

$$S_n = \sum_{i=1}^{N} Y_i^n \tag{3}$$

52 The performance of high order Campbelling methods have been intensively
53 studied in [7]; it was shown that the application of higher order methods
54 sufficiently suppresses the impact of various noises. The linearity of the
55 count rate estimation over a wide count rate range (from $10^4$ to $10^9$ cps)
56 have been verified both numerically and experimentally. It was highlighted
57 that the application of higher than third order methods do not bring any
58 practical advantage and accurate count rate estimation can be achieved with
59 the third order Campbelling based on signal samples of a few ms.

60 *2.2. Smart detector theoretical background*

61    Eq. (1) shows that any cumulant of the signal may change not only due
62 to the change in the count rate, but also due to the change in the mean
63 pulse shape or in the amplitude distribution. The higher order methods are
64 particularly sensitive to these changes because of the higher exponents in
65 Eq. (1). The change of the pulse shape and its amplitude may occur due
66 to a malfunction, such as the reduction of detector pressure or voltage since

3

these result a change in the electron drift velocity. During the measurement only the change of the cumulant (therefore the change of the estimated count rate) will be detected, thus we have to be able to decide whether this change occurred due to the change of the neutron flux around the detector or due to the malfunction of the detector.

Therefore we have to define a measurable quantity of the fission chamber signal which is sensitive to the pulse shape change but not to the count rate change. As a previous study shows [?], the width of the power spectral density (PSD) of the detector signal satisfies this requirement. In this work the PSD of a signal $y(t)$ is defined as:

$$PSD(f) = \frac{FT(y)FT^*(y)}{T_m} \tag{4}$$

where FT stands for the Fourier transform, and $T_m$ is the measurement time

It was shown that by measuring the width of the PSD, one can detect the change of the pulse shape due to the leakage of the filling gas. The spectral width was defined as the width at the half maximum of the PSD, it is usually contained in the 0-20 MHz band, which is an easily accessible frequency band with the modern instrumentation.

## 3. Design of high order Campbelling measurement system

The development of an on-line neutron monitoring system, which makes use of fission chamber signals and works in higher order Campbell mode, requires:

- Capability to convert and process the signal at the output of the available pre-amplifier (between -10 and 10 V for the typical nuclear instrumentation).

- Real-time computation of the first, second and third order sum of the signal (see Eq. (3)).

- High sampling frequency in order to resolve the signal consisting of pulses with a width of a few tens of nanoseconds.

- Ability to process a large amount of data in real-time (given that a time window of a few ms has to be applied for accurate estimations).

Since this work aims to develop a prototype system and provide proof of concept, two additional requirements have to be considered:

4

- Versatility in order to modify the prototype easily and test new implementations.

- Large user community and preferably open source philosophy in order to facilitate the learning and to get fast technical support.

*3.1. Hardware selection*

Recently several single board computers and system on a chip (SoC) boards revolutionized and facilitated the development of digital measurement instruments. Based on the above defined criteria, the Red-Pitaya board was chosen; it was created to provide a customizable measurement system with a generous amount of examples according to the open source philosophy. Due to its low footprint, low price and relatively large user community, it fulfills all the requirements which were expected at the prototype stage.

The Red-Pitaya board is built around a Xilinx Zync 7010 SoC which embeds an FPGA and a dual core Arm CPU clocked at 668 MHz. The Red-Pitaya board hosts two Analog-to-Digital Converters (ADC) and two Digital-to-Analog Converters (DAC) which are directly connected to the FPGA. The ADCs have a sampling frequency of 125 MHz and a resolution of 14 bits. The board provides two measurement ranges through jumper positions: $\pm 0.6$ V and $\pm 16$ V. The great strength of the FPGA is letting to design a circuit, which allows to process the data in line, therefore reducing the time, and the memory storage for heavy computations. This makes FPGAs ideal to perform simple computing patterns on a vast amount of data in real time. These characteristics fulfill all the above stated requirements to develop an online neutron monitoring system: the board is able to process the signal at output of the most common pre-amplifier(0,10 V for the CEA PADF and -10,0 V for the Canberra ADS pre-amplifiers applied in this work), to resolve the fission chamber pulses (with a length of few tens of ns), and to perform the real-time processing of large amount of data.

It has to be mentioned, that although it may seem that the CPU could handle all the data processing needed to calculate the high order sums of the signal, the real time computation with the CPU couldn't be realized due to the huge amount of data transfer and operations ($\approx 750$[Mop/s]) it implies. Therefore, in the neutron monitoring instrument, the FPGA was dedicated to the low level, time critical, redundant operations (namely computing the power sums of the signal values), whereas more complicated operations were performed on the CPU.

The FPGA of the board is configured using Verilog, a low level Hardware Description Language (HDL), and the softwares running on the CPU are developed in C language. It has to be recognized that development with a

hardware description language is more cumbersome than with a normal procedural language (the main constraints are detailed in the following section). Thus, during the design of the instrument the use of the low level computing was kept to a reasonable minimum, in order to facilitate the development and the maintainability of the device while keeping CPU computing power for prospective data processing. The following sections are devoted to explain the inner design of the new measurement system.

## 3.2. Third order cumulant measurement system

The most time consuming operations, while computing the third order cumulant estimator $k_3$ (Eq. 2), are the computations of the sums $S_1$, $S_2$ and $S_3$ (Eq. 3), since the higher order power of each signal sample is required in real-time. On the other hand, the further operations to compute the estimator $k_3$ based on the sums, has to be done only once at the end of the measurement time and don't exhibit any simple computational patterns. Consequently, the real-time computation of the sum terms were realized on the FPGA, and, after the transfer of the sums to the CPU, the final operations to compute the cumulant estimator were performed by a control software running on the CPU.

The developed FPGA module of the measurement system is composed of five algorithmic blocks. Two blocks are dedicated to read and write data for the Processing System (PS, i.e. the computer part of the SOC). One block is in control of the measurement soft reset. Two blocks are directly related to computation of the third order cumulant estimator terms. The function and the realisation of the last two blocks are detailed below.

### 3.2.1. Unbiased cumulant estimation FPGA module

The algorithm design starts with the definition of registers (variables used to store data): s1, s2 and s3 contain respectively the sum of single, square and cubic power of the samples for N number of samples. It is favorable to limit the number of samples to a power of 2 to simplify division by N into bit shifting operation. It was shown previously that the proper measurement time for the cumulant was between a hundred of micro-seconds and a few tens of millisecond [7], in terms of number of samples, this corresponds to $N$ between $2^{22}$ (33.5 ms) and $2^{14}$ (131 $\mu$s) if the sampling frequency is 125 MHz; Register N size was set to 23 bits.

The sizes of s1, s2 and s3 have to be carefully defined as well, since their sizes have to be adequately large in order to avoid overflows. The development board provides two's complement signed 14 bits samples, an addition of two samples has to be stored on 15 bits, where as their multiplication is

6

stored on 28 bits. This implies that `S1`, which contains up to `N` summed data
has to be 36 bits wide because of the maximum value of `N`, which is $2^{22}$. `S2`
and `S3` must be 50 and 64 bits wide in order to contain respectively the sum
of square and cubic power of samples.

Once each used register has the proper size, the algorithm can be de-
signed. Two important constraints have to be taken into account at the low
level computing. First, every operation in an algorithmic block is performed
in parallel during a clock tick; the results of the operations will be available
at the end of the clock tick which prohibits the use of regular procedural
programming. However, branching (i.e. conditional tests) does not consume
any computation time. Second, only one operand can be used in an opera-
tion; it implies to pipeline the computation of square and cubic power over
several clock ticks.

Fig. 1 summarizes the implemented algorithm: the main algorithmic
block contains a loop dedicated to the computation of the sums. To provide a
better understanding of the time operation of the algorithm, Fig. 2 illustrates
is clocking diagram for $N = 4$.

At each clock tick, the data stream coming from the ADC (`adc_a`) is stored
into two temporary registers (`single` contains the ADC value and `double`↩
 contains the square of the ADC value), which are used to pipeline the power
computation. In the same time, `adc_a` is added to `S1`, `double` to `S2` and `triple`
to `S3` (`triple` is also a temporary register dedicated to store the cubic power
of samples, it is fed with the result of the multiplication `single*double`).

A sample counter (`sample`) is incremented at each cycle to keep track of
the amount of samples processed since the start of the current measurement.
When `sample` is equal to `N`, the completion process and the transfer of `S1`, `S2`,
`S3` to registers accessible by the PS (namely `S1mem`, `S2mem`, `S3mem`) begins. To
transfer the sums to the area from which the data transfer towards the CPU
takes place, intermediate registers (namely `S1inter`, `S2inter`, `S3inter`) have to
be used to store the sums due to the pipelining. The reason is that the final
values of `S2` and `S3` will be available respectively one and two clock ticks after
`S1`, however, the data transfer has to be done in one clock cycle in order not
to mix old and new data in registers where the CPU has access.

To achieve the transfer, first the flag `data_transfer` responsible for data
transfer from intermediate registers to the memory area accessible by CPUs
is set to false. In the same clock tick when the `sample` is equal to $N$, the
flag specifying the availability of `S1` (`S1ready`) is set to true, while the flags
indicating the availability of `S2` and `S3` (`S2ready` and `S3ready`) are set to `false`.

In the next clock tick, a test `S1ready==true` allows `S1` to be transferred
to the intermediate register `S1inter`, while the computation of `S1` restarts.

7

At the same time, `S2ready` is set to true since `S2` will be ready for the next tick. During the following tick, a test `S2ready==true` allows `S2` to be copied to `S2inter` and its computation restarts, while `S3ready` is also set to `true`. In the next clock tick, the test `S3ready==true` is verified and the copy of `S3`↩ to `S3interm` is performed; a register which keeps track of measurement time (`time_stamp`) is also incremented and the flag `data_transfer` is reset to `true`↩. All the sums can now be copied from intermediate registers to the ones accessible by the PS (the algorithmic block responsible for this transfer is summarized in Fig.3)), while the registers containing the sums, `S1`, `S2`, `S3` are already filled with the data of the new measurement.

*3.2.2. Control software of the High Order Campbelling module*

A software was written in a high level programming language to control the FPGA module. Its main task is to read the data provided by the FPGA at the designated memory addresses, to construct the estimator $k3$ and to make it available for further processing. At this phase, two constraints have to be considered to fulfill the requirements of real-time monitoring: first, the software must be capable to construct the estimator in a time window shorter than the duration of the measurement without being slowed down by the post-processing of data. Second, it should not miss any measurement and should store each result produced in the memory for further processing.

In order to fulfill these requirements, the software design uses two threads, which allow to take advantage of the dual core architecture. One transfers the available measurement into the memory of the PS: it reads the time stamp computed by the FPGA, and if this time is larger than the one stored in computer memory, $S1$, $S2$ and $S3$ are transferred and $k3$ estimation is constructed. The second thread is responsible for heavy and slow processes such as printing and saving the cumulant estimator. It has only access to the data provided by the measurement thread. In order not to lose data, a FIFO (First In First Out) pile can be used by the measurement thread to store the terms of the cumulant. Both threads are detailed through diagrams available in Fig. 4 and Fig. 5.
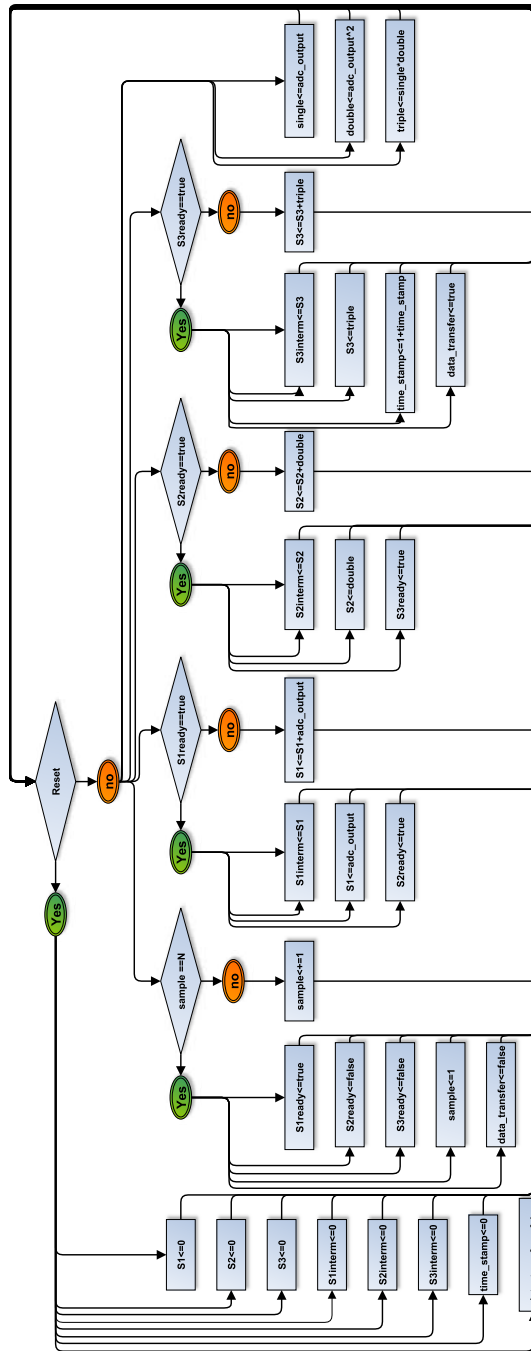
Figure 1: The algorithm for the computation of the terms of the estimator $k3$: $S1$, $S2$ and $S3$.
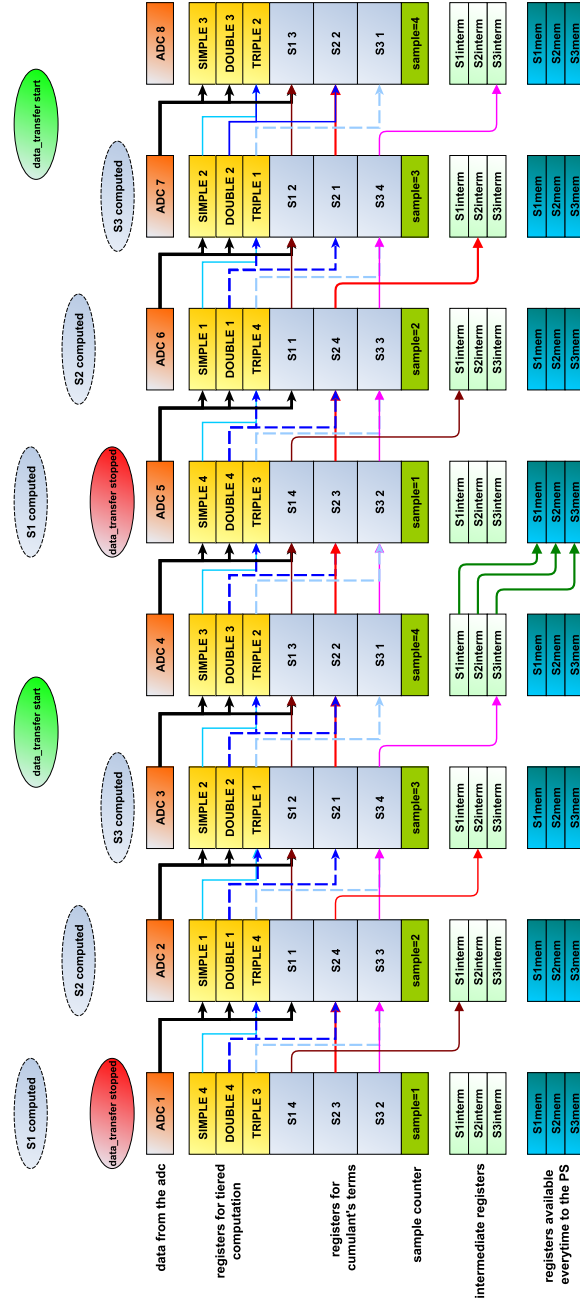
Figure 2: Clocking diagram of the algorithm for computation of the cumulant terms. For the sake of simplicity, the number of samples per measurement is set to $N = 4$. The squares represent the state of registers at each tick while the arrows summarize the operation performed during the tick. Bubbles at the top of the diagram are related to flags for finishing the computation and initiating memory transfer.
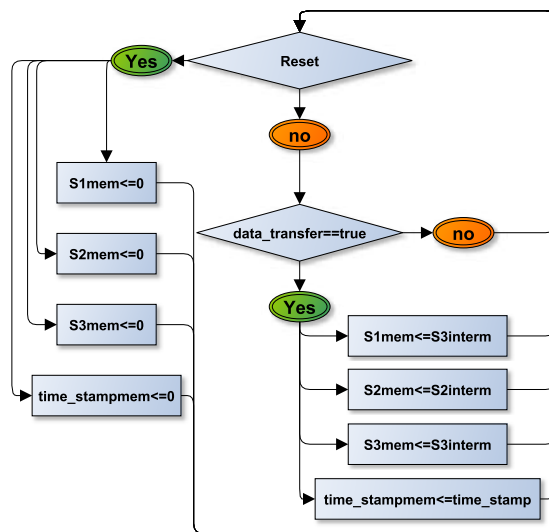
10

Figure 3: Diagram of the algorithmic block dedicated to transfer data from the computing block to the block in charge of communication between the FPGA and the PS.
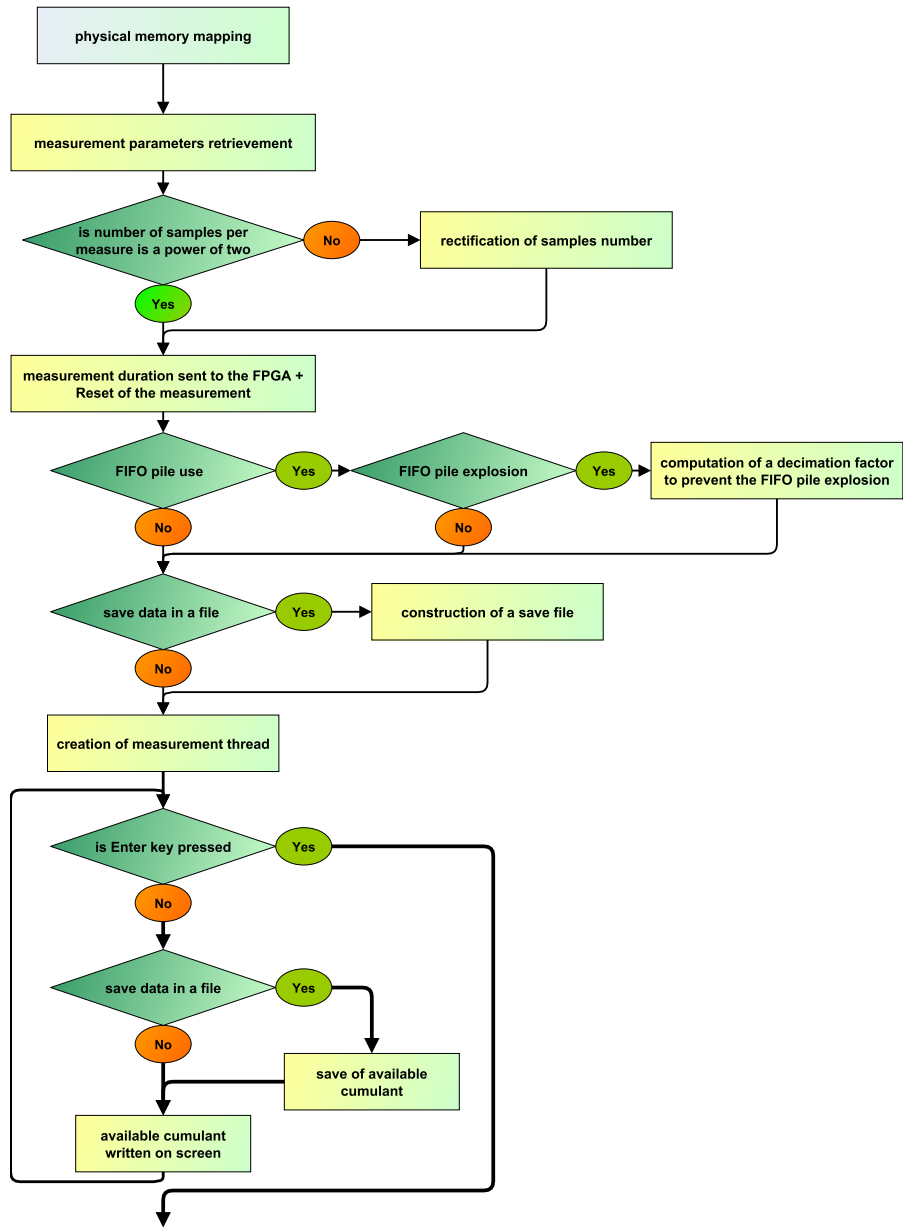
Figure 4: Diagram of the HOC measurement system control software.
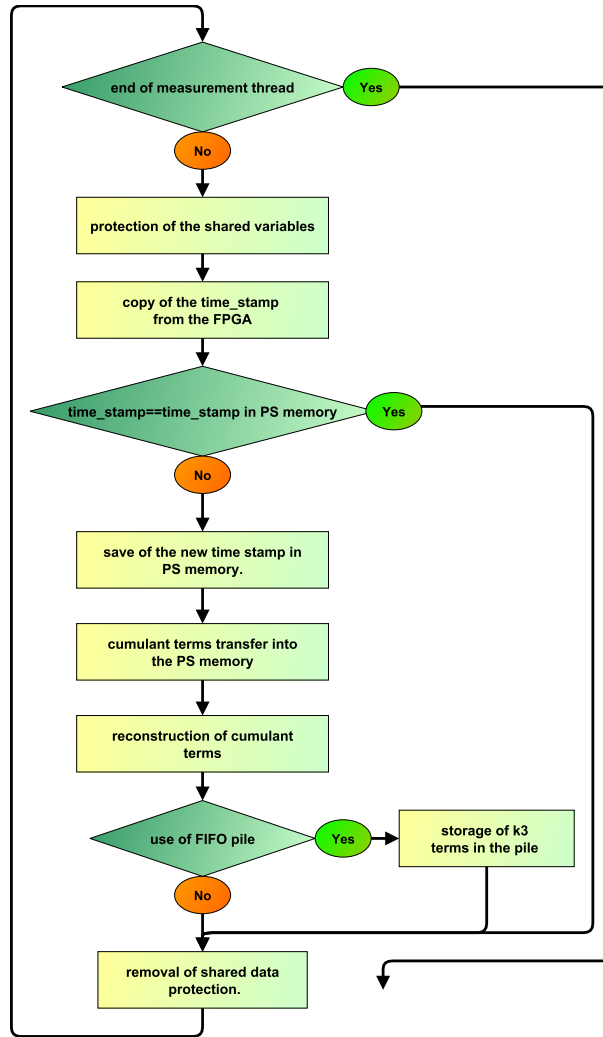
Figure 5: The measurement loop schematized here is called by the measurement thread independently from the main software.

*3.3. Smart detector system*

The measurement prototype was completed with smart detector capabilities in order to detect the change in the width of the power spectral density, which indicates a possible malfunction during operation.

As it was shown previously [8], it is satisfactory to monitor the power spectral density on the s time scale. In order to minimize the necessary change in the FPGA modules developed for the higher order cumulant computations, in the smart detector module, the FPGA (controlled by the PS) is responsible only for recording the raw data. The complex data processing, such as computing the PSD and determining its width, is done on the CPU with specific C routines from the GSL (GNU Scientific Library) [9].

*3.3.1. Smart detector FPGA module*

The hardware part of the smart detector module consist of a punctual raw data recorder which makes use of the block RAM available on the FPGA; the Artix-7 have 60 blocks of 36 kB RAM which can have a limited set of configuration [10]: Since the data coming from the ADC are 14 bits wide, only $2^{16}$ data points (0.524 ms) can be stored in the memory.

The FPGA module is constructed from three algorithmic blocks available in Fig. 6: the first one stores ADC data into a memory buffer, while the second and third one deal respectively with data transfer to the PS and with message dispatching through the smart detector module.

For the sake of simplicity, it was decided to use the memory transfer algorithm included in the Red-Pitaya project and a serialised architecture to move data buffer from the FPGA to the PS: The PS sends the memory address to be read and the memory transfer code block makes ready the related data (`buff[yraw_read_addr]`) for an eventual read command.

Even with a limited signal length and slow memory transfer ($\approx 12.5$ Mdata/s), this architecture is suitable for the fission chamber failure detection. Nevertheless, in the future, it is possible to improve this module: since the granularity of memory transfer is 32 bits, transferring more than one 14 bits of useful data in a clock tick could speed up the transfer to the PS by a factor 2.

*3.3.2. Control software of the smart detector module*

The control software of the campbell measurement system was extended in order to include the smart detector capabilities. The general architecture remains the same: two threads are running on the two cores of the CPU. One is dedicated to the measurement and only does lightweight processing while the other is related to heavy data processing (as shown in Fig.7). A
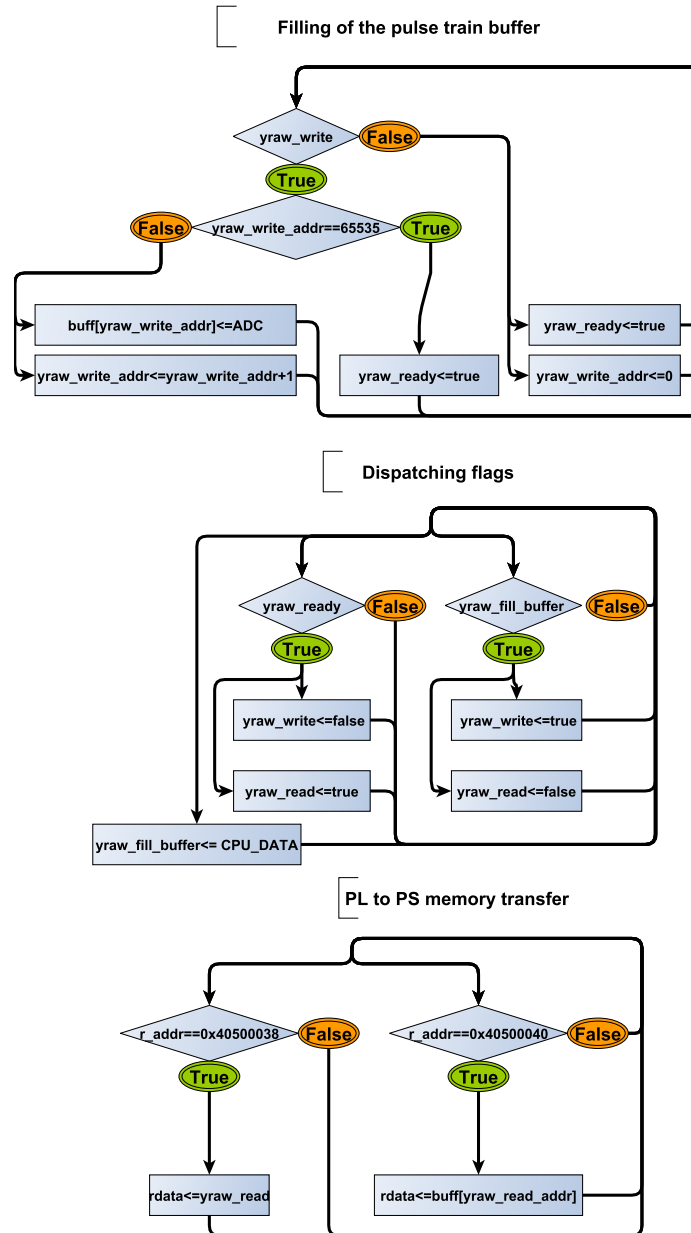
14

Figure 6: Smart detector algorithm implemented on the FPGA. The register `ADC` represents a raw sample.

flag set by the user at the program start-up (`compute_psd`) allows to enable
the smart detector module.

The measurement thread was adapted to transfer signal segments: one
flag is shared with the data processing thread, `psd_compute_flag` is used to no-
tify the FPGA that the signal buffer has to be filled. Then, the measurement
thread checks periodically if the data buffer is ready. Once it is ready, the
data is transferred. When a complete signal segment has been transferred,
the measurement thread indicates it with `psd_compute_flag`.

The data processing thread is in charge of PSD computation. When the
buffer data is ready to be processed, the thread proceeds to the PSD com-
putation after requesting a new signal segment. The spectrum is computed
using the Bartlett's method. When the the amount of computed spectra
reaches `MAX_PSD`, the average spectrum is computed, and the width of the
spectrum is estimated. Finally, the mean spectrum is saved on the disk.

## 4. Experimental validation

The measurement system prototype was tested through several experi-
ments. During the development phase, experiments in laboratory were per-
formed to check whether the FPGA modules are well implemented. Finally,
the measurement system was connected to fission chambers and tested in
the Minerve reactor under real working conditions. The measurements and
the obtained results are detailed in the following sections.

### 4.1. Laboratory validation

### 4.1.1. Validation of the HOC measurement system

The validation of the HOC measurement system was done in two steps.
In the first step, the proper computation and transfer of $S1$, $S2$ and $S3$ was
checked by replacing the ADC input data by a constant value of 2. It was
verified that for N samples, the computed sums $S_1$, $S_2$ and $S_3$ are equal to
$2N$, $4N$ and $8N$ respectively.

In the second step, the accuracy of the third order cumulant estimation
was tested with Poisson pulse trains simulated by a pulse train generator.
The pulse trains consisted of exponential damped pulses with a width of
around 100 ns and a random normally distributed amplitude. The count
rates were varying between $4 \cdot 10^5$ to $4 \cdot 10^7$ c/s. The pulse trains were
loaded (in the proper format) and played by a Tektronix AWG 5012 signal
generator. The datasets were 0.128 second long, with a sampling time of 8 ns
and the pulse amplitude selected to be consistent with the output of a typical
fission chamber measurement chain (3% of the ±16 V range were used). For
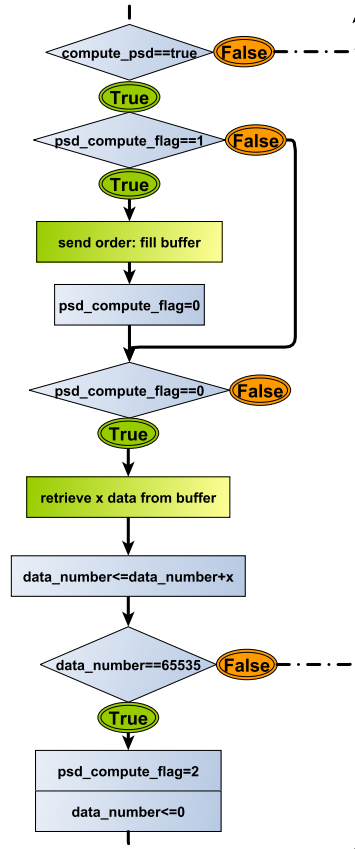
**Data processing**
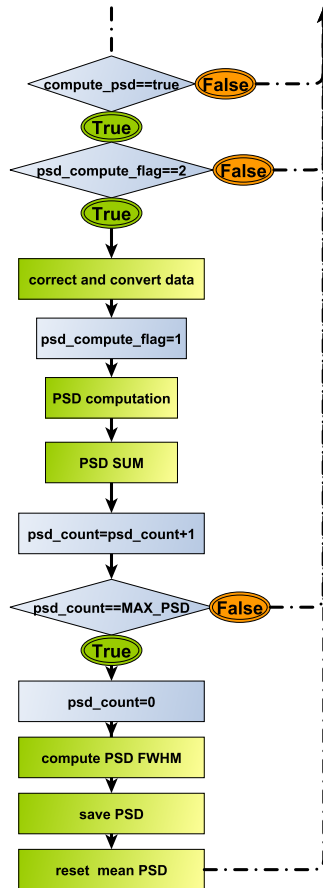
**Measurement**



Figure 7: The control software dedicated to the smart detector module. (Only the measurement thread communicates with the FPGA smart detector module, even if the request for a new measurment is sent through the shared variable `psd_compute_flag` by the data processing thread.)

17

each pulse train, the third order cumulant estimator was computed before
uploading to the signal generator and compared with the estimation of the
measurement system. The results are summarized in the Table 1.

The measured third order cumulants are close to the computed ones. A
maximum of 3.5 % of relative overestimation was found during these tests.
The discrepancy is most probably due to the electronics transfer function and
the truncation made by the ADC. Investigations has shown that the trans-
fer function results a slight reshaping, therefore the measured estimation is
slightly higher then the computed cumulant. Nevertheless, in practical sit-
uations the calibration methodology will inherently take into account the
reshaping, hence the count rate will not be overestimated.

| c. rate (c/s) | $k3$ (computed) | $k3_a$ (measurement) | $k3_b$ (measurement) $\mu$s |
|---|---|---|---|
| $4 \cdot 10^6$ | $2.84 \cdot 10^{-5}$ | $(2.90 \pm 0.01) \cdot 10^{-5}$ | $(2.91 \pm 0.19) \cdot 10^{-5}$ |
| $4 \cdot 10^7$ | $5.70 \cdot 10^{-5}$ | $(5.85 \pm 0.02) \cdot 10^{-5}$ | $(5.86 \pm 0.36) \cdot 10^{-5}$ |
| $4 \cdot 10^6$ | $3.22\text{e} \cdot 10^{-5}$ | $(3.33 \pm 0.02) \cdot 10^{-5}$ | $(3.37 \pm 0.27) \cdot 10^{-5}$ |
| $4 \cdot 10^5$ | $1.15 \cdot 10^{-5}$ | $(1.19 \pm 0.02) \cdot 10^{-5}$ | $(1.27 \pm 0.27) \cdot 10^{-5}$ |

Table 1: Computed and measured third order estimators for pulse trains at various count
rates. $k3_a$ refers to the estimation based on 34 ms samples and $k3_b$ refers to the estimation
based on 262 $\mu$s samples.

### 4.1.2. Smart detector module validation

In order to test the smart detector module, and the PSD measurement
capabilities of the system, several pulse trains with a length of 0.128 s were
simulated, and played with the signal generator. The trains contained Gaus-
sian shaped pulses with a mean count rate of $10^6$ c/s. The width (i.e. the
standard deviation of the Gaussian) of the pulses were changed (5 ns, 10 ns
and 15 ns were considered).

The obtained power spectral densities are available in Fig.8. As it can
be seen, the spectrum shape is characteristic of the pulse shape. The line
centered around 1 MHz and its harmonics are artifacts due to the fact the
same 0.128 s signal was played periodically. The functioning of the smart
detector module was appropriate.

### 4.2. In reactor validation

Finally, the measurement device was tested during an experimental cam-
paign at the Minerve facility of CEA [11].

Several setups were realized in order to assess the compatibility of the
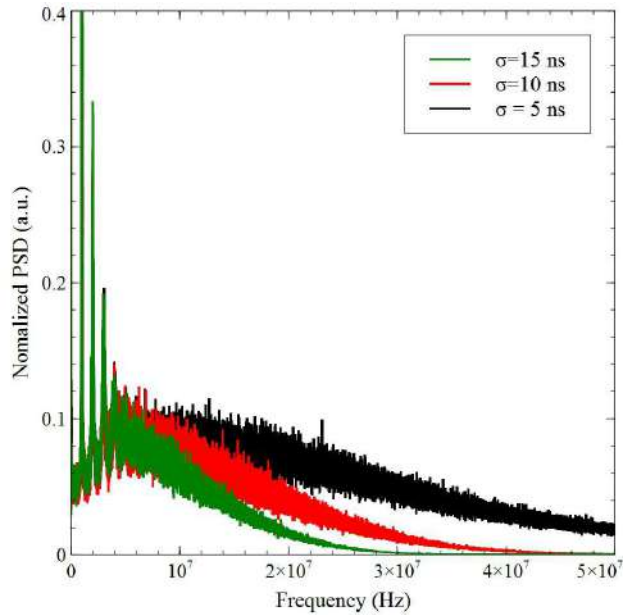device with the standard nuclear instrumentation. During the campaign,

Figure 8: PSD obtained with simulated pulse trains.

two pre-amplifiers were used: the ADS, manufactured by Canberra and the PADF designed by the CEA instrumentation and electronics laboratory. These pre-amplifiers are different in their output voltage and transfer function.

In order to cover a wide count rate range, two type of fission chambers were tested during the experiments: the CFUL01 (a relatively large chamber, which contains 1g of U235; its pulse shape is around 80 ns wide) and the CFUR (a rather small chamber, which contains $10\mu g$ of U235; its pulse shape is around 20 ns wide). At the same neutron flux, the CFUR chamber results 5 orders of magnitude lower count rate than the CFUL01.

The CFUL01 chamber was located in the surrounding of the driver zone, whereas the CFUR was installed in the center of the reactor.

During the campaign, the following experiments were performed in order to assess various aspects of the measurement device:

- Cumulant estimation with the CFUL01 and the PADF at various power levels: to assess the linearity of the measurement system.

- Cumulant estimation with the CFUR and the PADF at various power

19

levels: to assess the limits of the system at low count rates.

- Pulse train recording with the CFUR and the PADF at various power levels: to calibrate the HOC system (in order to retrieve the count rate with the higher order method), and to estimate the count rate with pulse counting algorithms.

- PSD measurement with the CFUL01 and the ADS pre-amplifier with various bias voltages: to simulate a detector failure and to measure the change of the spectral width.

*4.2.1. Third order cumulant measurements, CFUL01/PADF*

The third order cumulant has been estimated at reactor powers between 10 W and 80 W with the CFUL01, based on 33 ms time windows. Both the $\pm 0.6$ V and the $\pm 16$ V input ranges have been used, in order to assess the linearity with both ranges.

The signal saturates at 30 W reactor power, when measured with low voltage range. Therefore, only two measurements were done with this range (at 10 W and 20 W). The cumulant over power ratios are $(4.04 \pm 0.36)\ 10^6$ (a.u.).W$^{-1}$ and $(4.11 \pm 0.28)\ 10^6$ (a.u.).W$^{-1}$ for the 10 W and 20 W power, respectively. Although, in the future a better resolution of the power is needed to draw deeper conclusion, the good agreement of the ratios implies that the behavior is linear.

With the $\pm 16$ V range the whole power range was covered. The obtained cumulant estimations are presented in Fig.9. The measured third order cumulant shows linearity with the reactor power. The departure from linearity is lower than 1.6 %, which is the result of the random error of the estimation. In order to estimate the count rate, the measurement chain has to be calibrated. The calibration, through applying the methodology described in [12] (namely, to evaluate the coefficient $C_n$ in Eq. (1) by measuring the mean pulse and the pulse amplitude distribution at low power), was planned to be done during the post-processing of recorded signal samples. Unfortunately, for this purpose the signal was recorded with the high voltage range, which was not appropriate to discriminate properly the single pulses from the noise. In the future, when further reactor time can be obtained for similar measurement purpose, the calibration is going to be repeated with the low voltage range as well. In order to avoid similar problems, also a new calibration procedure is under development, which can be performed during the real-time operation, and does not require post-processing. Nevertheless, the measurement with the CFUL01 was still valuable to assess the linear cumulant estimation of the measurement device.
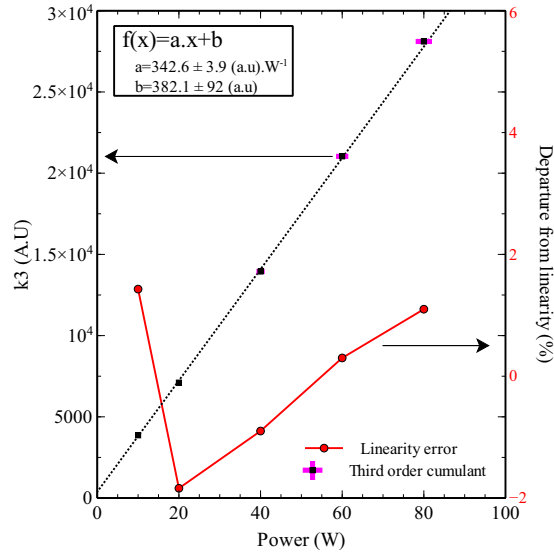
Figure 9: Third order cumulant recorded with the ±16V range as a function of the reactor power.

### 4.2.2. Third order cumulant measurements, CFUR/PADF

Measurements with the CFUR chamber were performed only with the low voltage range, since the count rate of the signal was expected to be rather low on the power range of Minerve.

The measurements were done at 40 W and 80 W power level. The results are summarized in Table 2. The cumulant estimation based on one 33 ms long sample results a high standard deviation, which is expected since at these count rates only few pulses appear during one sample, and the number of observed pulses is uncertain. Nevertheless, the expected value of the cumulant estimator was based on 1900, 33 ms long signal samples, therefore the overall deviation of the estimated mean cumulant is less then 2.3%. (In comparison, when the reactor was all control rods down, was not connected and estimation was based only on the noise in the system, the estimated third order cumulant appeared to be $350 \pm 50$, which is less than the deviation of the cumulant estimation for the fission chamber signal). The mean cumulant over the power ratios show good agreement, which implies linear behaviour. For the estimated count rates (discussed later), the deviation refers to the $400 \cdot 0.52$ ms sample, not only to one sample.

To calibrate the fission chamber through the methodology presented

Table 2: Cumulant and count rate estimations with the HOC module and with pulse counting.

| Power (W) | $k_3$ (a.u.) | $\langle k_3 \rangle / P$ (a.u.).W$^{-1}$ | HOC count rate c.s$^{-1}$ | Ref. count rate c.s$^{-1}$ |
|---|---|---|---|---|
| 40 | $(1.18 \pm 0.39)10^4$ | 295±12 | 3430± 354 | (2861±118) |
| 80 | $(2.38 \pm 0.56) 10^4$ | 297±10 | 6918± 686 | (6103± 171) |

in Ref. [12], the raw signal recorder module dedicated to smart detector was used, with a minimalist control software. Several signal segments were recorded at 80 W and the pulses were isolated during post-processing in order to determine the calibration coefficient in (1). From the measurements nearly 2700 pulses were isolated, which allows to have acceptable statistics. The mean pulse shape and the amplitude distribution of the pulses is illustrated in Fig. 10. As one can see, the dynamic of the measurement system allows to discriminate the pulses from the noise and the resolution is fine enough to observe even the current bouncing back from the cable (a small bump following the main pulse). The prototype is capable of working as a raw signal recorder as well. The estimated calibration coefficient for the third order is:

$$C_{clas} = 3.44 \pm 0.3 \ (a.u.).s/c \qquad (5)$$

The calibration has large uncertainty, which shows the disadvantage of this methodology. As it was highlighted in Ref. [12] as well, for the high order methods an empirical calibration may be favorable. Such calibration is not plausible for the traditional Campbelling method, due to the linearity gap between pulse counting methods and the second order Campbelling.

In order to obtain a reference count rate, 400 signal segments recorded at a reactor power of 80W and 400 recorded at a power of 40 W were analyzed with pulse counting method as well. The estimated count rates obtained by pulse counting, and the ones computed from the calibrated higher order Campbelling are included in Table 2. It has to be highlighted again that the standard deviation refers to the $400 \cdot 0.52$ms long signal samples for the counting algorithm result while it is related to the $1800 \cdot 33$ ms long signal for the calibrated HOC. The standard deviation of an estimation based on one $0.52$ ms sample is much higher for the pulse count, but the goal was to define the reference (i.e. the real) count rate of the chamber at these powers. The good agreement of the estimated count rates show that the results measured
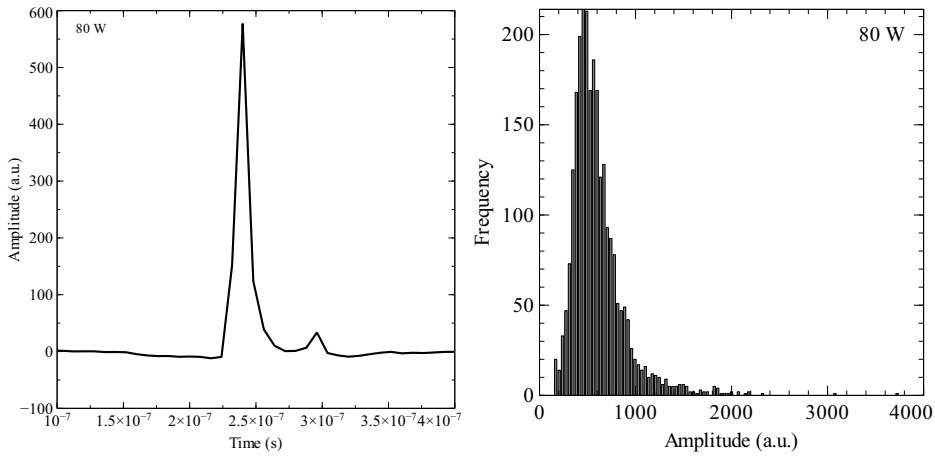
22

Figure 10: Left: mean pulse shape computed with single pulses coming from the 80 W measurement data. Right: amplitude distribution of pulses computed on datasets recorded at 80 W.

by the system are physically correct. The results also imply that monitoring at really low count rates (in the order of $10^3$ cps) is possible with higher order Campbelling, but longer measurements are necessary (nevertheless, the same holds for pulse mode measurements as well).

### 4.2.3. PSD measurements, CFUL01/ADS

When the tests of the smart detector module were performed, only the ADS preamplifier were available, which allowed to verify that the device is capable to work with other instruments as well.

The ADS pre-amplifier and a CFUL01 chamber were used to test the smart detector module. Using the CFUL01 was advantageous for this purpose, since it has a higher count rate, therefore its power spectral density can measured more accurately during real time operation.

In the current experimental work, the change of the pulse shape was achieved by changing the fission chamber voltage in the saturation regime. The increase of the voltage has similar effects on the pulse width as the decrease of the gas pressure, but it is simpler to achieve during the measurement.

Measurements were taken at a constant reactor power of 20 W with the voltage changed between 600 V and 850 V. For each applied voltage, the PSD was constructed by using 4000 datasets of 0.52 ms long signals. The low vari-

23
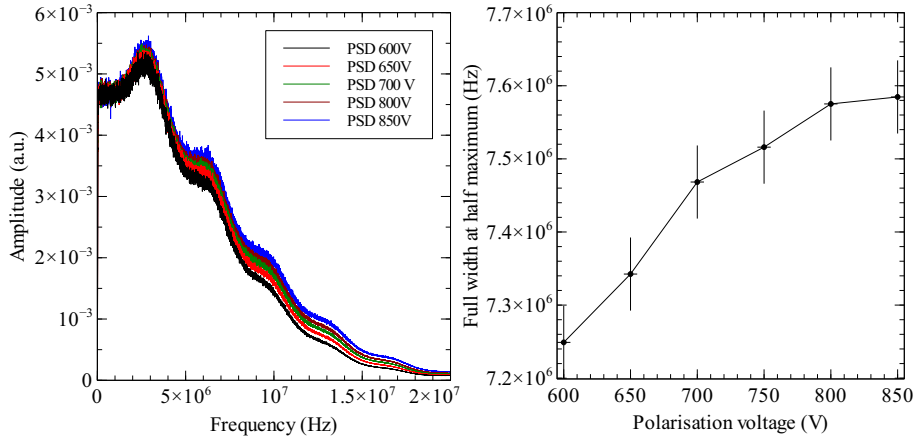
Figure 11: Left: PSD as a function of the applied voltage. Right: Spectral width as a function of the polarisation voltage.

ance of the spectra estimated from this amount of data, allows to distinguish change in the spectral as small as 50 kHz. The measured PSD and the estimated spectral width are presented in Fig.11. The slight oscillation of the PSD is an artifact due to the applied cable. As expected, the spectral width increases with the increase of the applied voltage, and it saturates at high voltages. The reason of the saturation of the spectral width is the saturation of electron drift velocity in argon-nitrogen mixtures at high reduced electric fields [13].

Therefore, the proof of concept of the smart detector is validated: it is possible to detect a change of mean pulse shape from investigating the power spectral density, whereas the measurement noise and the low frequency filtering of the system have negligible influence on the determination of the spectral width.

Although, in the current experiment, the time needed to record and process the 4000 datasets is approximately 300 s due to the slow data transfer, this already allows to test in every 5 minutes whether the chamber malfunctions. However, the processing time of the smart detector prototype could be reduced by a factor of 3 by using optimised FFT routines, and in the future even faster tests can be achieved for the industrial application by implementing the same method on board with higher performance.

## 5. Conclusion

An innovative measurement system prototype for real time neutron monitoring was presented and validated through this paper. The prototype was built using an open source CPU/FPGA device with ADC on board. Such architecture has a several advantages: time critical, simple operations can be performed on the FPGA, immediately after recording the data, whereas complex and heavy data processing can be performed on the CPU. The simplicity of the chosen board (Red-Pitaya) allowed fast and straightforward development.

The main purpose was to prove the feasibility of a real time neutron flux monitoring system using the third order Campbell mode. This method suppresses the impact of noise and provides wide range of operation. In this work it was shown that the method is even capable to work at count rates as low as $10^3$ cps.

In the work, the concept of fission chamber failure detection was also included. The self monitoring capability of the system is based on detected the change in the width of the power spectral density of the signal.

The paper provides detailed description of the implemented FPGA algorithms and the control software running on the CPU. All the challenges and solutions were highlighted in order to serve as a tutorial for similar developments.

The reliability of the concepts and the robustness of the device was tested through an experimental campaign at the Minerve reactor. The linear response and the real time operation of the device was verified over a wide power range. Through the calibration of the system the physical validity of the measured results was assessed. The self monitoring capability was also tested, the system is capable to detect the change in the voltage set between the electrodes of the chamber.

Since the calibration of the system is rather elaborate, a simpler, automatic and real time calibration procedure is under development.

For industrial usage, the next step is going to be the implementation of the same concepts on a board which has higher performance in order to achieve faster self monitoring capability.

## Acknowledgment

25

part of an on-going collaboration project on the instrumentation and safety of sodium cooled fast reactors between Chalmers and CEA.

[1] C. Jammes, N. Chapoutier, P. Filliatre, J. P. Jeannot, F. Jadot, D. Verrier, A.-C. Scholer, B. Bernardin, Neutron flux monitoring system of the French GEN-IV SFR: Assessment of diverse solutions for in-vessel detector installation, Nuclear Engineering and Design 270 (2014) 272–282.

[2] C. Jammes, P. Filliatre, B. Geslot, T. Domenech, S. Normand, Assessment of the high temperature fission chamber technology for the french fast reactor program, IEEE Transactions on Nuclear Science 59 (2012) 1351–1359.

[3] N. R. Campbell, V. J. Francis, A theory of valve and circuit noise, Journal of the Institution of Electrical Engineers-Part III: Radio and Communication Engineering.

[4] I. Lux, A. Baranyai, Higher order campbell techniques for neutron flux measurement, Nuclear Instruments and Methods in Physics Research 202.

[5] L. Pál, I. Pázsit, Zs. Elter, Comments on the stochastic characteristics of fission chamber signals, Nuclear Instruments and Methods in Physics Research Section A: Accelerators, Spectrometers, Detectors and Associated Equipment 763 (2014) 44–52.

[6] E. Parzen, Stochastic Processes, Classics in Applied Mathematics, 1999.

[7] Zs. Elter, M. Bakkali, C. Jammes, I. Pázsit, Performance of Higher Order Campbell methods, Part I: review and numerical convergence study, Nuclear Instruments and Methods in Physics Research Section A: Accelerators, Spectrometers, Detectors and Associated Equipment 821 (2016) 66 – 72. doi:http://dx.doi.org/10.1016/j.nima.2016.03.023.

[8] Zs. Elter, P. Filliatre, G. de Izarra, I. Pázsit, C. Jammes, Self-monitoring fission chamber: theoretical groundwork, in: Physor conference, 2016.

[9] M. Galassi, J. Davies, J. Theiler, B. Gough, al., GNU Scientific Library Reference Manual (3rd Ed.).

[10] Xilinx, 7 Series FPGAs Memory Resources, 2014.

[11] G. Bignan, P. Fougeras, P. Blaise, J.-P. Hudelot, F. Mellier, Reactor physics experiments on zero power reactors, in: D. Cacuci (Ed.), Handbook of Nuclear Engineering, Springer US, 2010, pp. 2053–2184.

[12] Zs. Elter, G. de Izarra, P. F. C. Jammes, I. Pázsit, Performance of Higher Order Campbell methods, Part II: calibration and experimental application, Nuclear Instruments & Methods in Physics Research, Section A: Accelerators, Spectrometers, Detectors, and Associated EquipmentBeen submitted.

[13] G. Haddad, Drift velocity of electrons in nitrogen-argon mixtures, Aust. J. Phys. 36 (1983) 297–303.